Design of Roadside Barrier Systems Placed on MSE Retaining Walls

DETAILS

184 pages | | PAPERBACK

ISBN 978-0-309-15499-4 | DOI 10.17226/22924

AUTHORS

NATIONAL COOPERATIVE HIGHWAY RESEARCH PROGRAM

NCHRP REPORT 663

Design of Roadside Barrier Systems Placed on MSE Retaining Walls

Roger P. Bligh
Jean-Louis Briaud
Kang Mi Kim
Akram Abu-Odeh
TEXAS TRANSPORTATION INSTITUTE
TEXAS A&M UNIVERSITY SYSTEM
College Station, TX

Subscriber Categories
Bridges and Other Structures

Research sponsored by the American Association of State Highway and Transportation Officials
in cooperation with the Federal Highway Administration

TRANSPORTATION RESEARCH BOARD

WASHINGTON, D.C.
2010
www.TRB.org

NATIONAL COOPERATIVE HIGHWAY RESEARCH PROGRAM

Systematic, well-designed research provides the most effective approach to the solution of many problems facing highway administrators and engineers. Often, highway problems are of local interest and can best be studied by highway departments individually or in cooperation with their state universities and others. However, the accelerating growth of highway transportation develops increasingly complex problems of wide interest to highway authorities. These problems are best studied through a coordinated program of cooperative research.

In recognition of these needs, the highway administrators of the American Association of State Highway and Transportation Officials initiated in 1962 an objective national highway research program employing modern scientific techniques. This program is supported on a continuing basis by funds from participating member states of the Association and it receives the full cooperation and support of the Federal Highway Administration, United States Department of Transportation.

The Transportation Research Board of the National Academies was requested by the Association to administer the research program because of the Board's recognized objectivity and understanding of modern research practices. The Board is uniquely suited for this purpose as it maintains an extensive committee structure from which authorities on any highway transportation subject may be drawn; it possesses avenues of communications and cooperation with federal, state and local governmental agencies, universities, and industry; its relationship to the National Research Council is an insurance of objectivity; it maintains a full-time research correlation staff of specialists in highway transportation matters to bring the findings of research directly to those who are in a position to use them.

The program is developed on the basis of research needs identified by chief administrators of the highway and transportation departments and by committees of AASHTO. Each year, specific areas of research needs to be included in the program are proposed to the National Research Council and the Board by the American Association of State Highway and Transportation Officials. Research projects to fulfill these needs are defined by the Board, and qualified research agencies are selected from those that have submitted proposals. Administration and surveillance of research contracts are the responsibilities of the National Research Council and the Transportation Research Board.

The needs for highway research are many, and the National Cooperative Highway Research Program can make significant contributions to the solution of highway transportation problems of mutual concern to many responsible groups. The program, however, is intended to complement rather than to substitute for or duplicate other highway research programs.

NCHRP REPORT 663

Project 22-20
ISSN 0077-5614
ISBN 978-0-309-15499-4
Library of Congress Control Number 2010935293

COPYRIGHT INFORMATION

NOTICE

The project that is the subject of this report was a part of the National Cooperative Highway Research Program, conducted by the Transportation Research Board with the approval of the Governing Board of the National Research Council.

The members of the technical panel selected to monitor this project and to review this report were chosen for their special competencies and with regard for appropriate balance. The report was reviewed by the technical panel and accepted for publication according to procedures established and overseen by the Transportation Research Board and approved by the Governing Board of the National Research Council.

The opinions and conclusions expressed or implied in this report are those of the researchers who performed the research and are not necessarily those of the Transportation Research Board, the National Research Council, or the program sponsors.

The Transportation Research Board of the National Academies, the National Research Council, and the sponsors of the National Cooperative Highway Research Program do not endorse products or manufacturers. Trade or manufacturers' names appear herein solely because they are considered essential to the object of the report.

Published reports of the

NATIONAL COOPERATIVE HIGHWAY RESEARCH PROGRAM

are available from:

Transportation Research Board
Business Office
500 Fifth Street, NW
Washington, DC 20001

and can be ordered through the Internet at:

http://www.national-academies.org/trb/bookstore

Printed in the United States of America

THE NATIONAL ACADEMIES

Advisers to the Nation on Science, Engineering, and Medicine

The **National Academy of Sciences** is a private, nonprofit, self-perpetuating society of distinguished scholars engaged in scientific and engineering research, dedicated to the furtherance of science and technology and to their use for the general welfare. On the authority of the charter granted to it by the Congress in 1863, the Academy has a mandate that requires it to advise the federal government on scientific and technical matters. Dr. Ralph J. Cicerone is president of the National Academy of Sciences.

The **National Academy of Engineering** was established in 1964, under the charter of the National Academy of Sciences, as a parallel organization of outstanding engineers. It is autonomous in its administration and in the selection of its members, sharing with the National Academy of Sciences the responsibility for advising the federal government. The National Academy of Engineering also sponsors engineering programs aimed at meeting national needs, encourages education and research, and recognizes the superior achievements of engineers. Dr. Charles M. Vest is president of the National Academy of Engineering.

The **Institute of Medicine** was established in 1970 by the National Academy of Sciences to secure the services of eminent members of appropriate professions in the examination of policy matters pertaining to the health of the public. The Institute acts under the responsibility given to the National Academy of Sciences by its congressional charter to be an adviser to the federal government and, on its own initiative, to identify issues of medical care, research, and education. Dr. Harvey V. Fineberg is president of the Institute of Medicine.

The **National Research Council** was organized by the National Academy of Sciences in 1916 to associate the broad community of science and technology with the Academy's purposes of furthering knowledge and advising the federal government. Functioning in accordance with general policies determined by the Academy, the Council has become the principal operating agency of both the National Academy of Sciences and the National Academy of Engineering in providing services to the government, the public, and the scientific and engineering communities. The Council is administered jointly by both the Academies and the Institute of Medicine. Dr. Ralph J. Cicerone and Dr. Charles M. Vest are chair and vice chair, respectively, of the National Research Council.

The **Transportation Research Board** is one of six major divisions of the National Research Council. The mission of the Transportation Research Board is to provide leadership in transportation innovation and progress through research and information exchange, conducted within a setting that is objective, interdisciplinary, and multimodal. The Board's varied activities annually engage about 7,000 engineers, scientists, and other transportation researchers and practitioners from the public and private sectors and academia, all of whom contribute their expertise in the public interest. The program is supported by state transportation departments, federal agencies including the component administrations of the U.S. Department of Transportation, and other organizations and individuals interested in the development of transportation. **www.TRB.org**

www.national-academies.org

CRP STAFF FOR NCHRP REPORT 663

Christopher W. Jenks, *Director, Cooperative Research Programs*
Crawford F. Jencks, *Deputy Director, Cooperative Research Programs*
Charles W. Niessner, *Senior Program Officer*
Emily R. Greenwood, *Senior Program Assistant*
Eileen P. Delaney, *Director of Publications*
Natalie Barnes, *Editor*

NCHRP PROJECT 22-20 PANEL
Field of Design—Area of Vehicle Barrier Systems

Mark P. McClelland, *Texas DOT, Austin, TX* (Chair)
Alexander K. Bardow, *Massachusetts DOT, Boston, MA*
Robert L. Chen, *Parsons Brinckerhoff, Irvine, CA*
Ronald K. Faller, *University of Nebraska–Lincoln, Lincoln, NE*
Grant Gummow, *Utah DOT, Salt Lake City, UT*
Ramesh C. Gupta, *Virginia DOT, Richmond, VA*
Christopher Hahin, *Illinois DOT, Springfield, IL*
Michael L. McMullen, *Denver, CO*
Silas Nichols, *FHWA Liaison*
Stephen F. Maher, *TRB Liaison*

FOREWORD

By Charles W. Niessner
Staff Officer
Transportation Research Board

This report presents a design procedure for roadside barrier systems mounted on the edge of a mechanically stabilized earth (MSE) wall. The procedures were developed following AASHTO Load Resistant Factor Design (LRFD) practices. The report will be of particular interest to personnel responsible for the structural design of MSE walls.

It is estimated that 10 million square feet of mechanically stabilized earth (MSE) retaining wall is constructed annually in the United States. Most MSE retaining walls used in highway fill applications are constructed with a roadside barrier system consisting of a traffic barrier placed on a structural footing (moment slab). The footing is intended to provide stability for the barrier to resist impact loads and to reduce the influence of those impact loads on the retaining wall system by distributing the load over a wide area. The proper design of the roadside barrier, the structural slab, and the MSE wall system requires a good understanding of how barrier impact loads are transferred through the structural slab and into the wall system.

The move from the *AASHTO Standard Specifications for Highway Bridges* (ASD) to the *AASHTO LRFD Bridge Design Specifications* has made evident the need for a rational, reliable procedure for designing roadside barrier systems placed on MSE retaining walls. Current procedures and design details for roadside barriers placed on retaining walls vary widely among state highway agencies. Most designs currently used are overly conservative because of inadequate understanding of how barrier impact loads are distributed through the barrier and transferred to the structural slab and the wall system. There is a need to develop procedures for use by state highway agencies in designing roadside barrier systems placed on MSE retaining walls.

Under NCHRP Project 22-20, "Design of Roadside Barrier Systems Placed on MSE Retaining Walls," Texas A&M Research Foundation reviewed the current design practice for roadside barriers, conducted a survey of state transportation agencies, performed finite element simulations, conducted static and dynamic tests using a bogie vehicle and a full-scale Test Level 3 crash test following the AASHTO *Manual for Assessing Safety Hardware* (MASH). Based on these evaluations, recommended design procedures were developed following AASHTO LRFD design practices.

The design procedures for the barrier system address sliding, overturning, and structural adequacy of the coping and wall panel. The reinforcement design procedure considers pull-out and rupture of the reinforcement. The dynamic design loads are specified using both a pressure distribution approach and a line load approach.

CONTENTS

Note: Many of the photographs, figures, and tables in this report have been converted from color to grayscale for printing. The electronic version of the report (posted on the web at www.trb.org) retains the color versions.

CHAPTER 1

Introduction

1.1 Research Problem Statement

Millions of square feet of mechanically stabilized earth (MSE) retaining wall are constructed annually in the United States. When used in highway fill applications in conjunction with bridges, these MSE walls are typically constructed with a roadside barrier system supported on the edge of the wall. This barrier system generally consists of a traffic barrier or bridge rail placed on a continuous footing or structural slab. The footing is intended to reduce the influence of barrier impact loads on the retaining wall system by distributing the load over a wide area. The proper design of the roadside barrier, the structural slab, and the MSE wall system requires a good understanding of relevant failure modes, how barrier impact loads are transferred through the structural slab into the wall system, and the magnitude and distribution of these loads.

Current design procedures and standard details for placement of roadside barriers on retaining walls vary widely among state highway agencies. Most current designs are believed by engineers to be overly conservative. This conservative design is in part due to an inadequate understanding of how barrier impact loads are transferred and distributed to the slab and wall system. There is a need to develop standardized procedures for use by state highway agencies in designing economical roadside barrier systems placed on MSE retaining walls.

1.2 Research Objective

The objective of this research is to develop, in a format suitable for adoption by American Association of State Highway and Transportation Officials (AASHTO), procedures for designing roadside barrier systems placed on MSE retaining structures.

1.3 Research Approach

The research plan for accomplishing the project objective to develop procedures for designing roadside barrier systems placed on MSE retaining structures consisted of 10 tasks divided into three distinct phases:

- **Phase I**
  - *Task 1. Conduct literature review.* Analyze, describe, and critique pertinent domestic and international research, on the basis of applicability, conclusiveness of findings, and usefulness in developing a methodology for the design of roadside barrier systems placed on MSE retaining walls. Critically review the *AASHTO Standard Specifications for Highway Bridges* (*1*) and the *AASHTO Load and Resistance Factor Design (LRFD) Bridge Design Specifications* (*2*) and relevant interim updates.
  - *Task 2. Conduct survey.* Survey state highway agencies, federal agencies, crash testing facilities, and retaining wall manufacturers to determine existing methodologies and details used in designing roadside barrier systems placed on MSE retaining walls. Identify the barrier impact loads and crash-test level [as defined in *NCHRP Report 350* (*3*)] associated with particular barrier systems. Find and document lessons learned from known failures of existing systems.
  - *Task 3. Summarize state of practice.* Summarize the state of practice for roadside barrier systems placed on MSE retaining walls. Identify successful design procedures and details that warrant further investigation. In addition, identify promising design procedures and details for further investigation that are not necessarily used in current practice.
  - *Task 4. Develop detailed work plan.* Based on the information developed in Tasks 1, 2, and 3:
    - Propose design procedures for further investigation that address barrier impact loads and the transfer of these loads to the MSE retaining wall.
    - Prepare a detailed plan for developing a recommended design procedure. The plan shall include proposed analytical methods, component testing, and full-scale

crash testing needed for development and validation of the design procedure.
    - Update and elaborate on the work plan.
  - *Task 5. Submit first interim report.* Submit an interim report documenting the results of Phase I. The interim report shall include as a separate appendix the updated work plan for completing Phases II and III. Meet with the NCHRP 22-20 panel to discuss the interim report and the updated work plan. Work on Phase II will not begin without prior approval of NCHRP.
- **Phase II**
  - *Task 6. Develop preliminary design procedures.* Develop preliminary procedures for the design of roadside barrier systems placed on MSE retaining structures. Evaluate the preliminary procedures using the analytical methods and component testing. Modify and re-evaluate the preliminary procedures as necessary.
  - *Task 7. Develop full-scale crash test plan.* Develop the justification for and the details of a full-scale crash testing plan for validating the preliminary procedures. The testing plan shall include a detailed description of the instrumentation to be used in the barrier, the load transfer system, and the MSE retaining wall system.
  - *Task 8. Submit second interim report.* Submit the procedures, modeling results, and full-scale crash test plan for review by the NCHRP 22-20 panel. Meet with the NCHRP 22-20 panel to discuss the procedures and crash testing plan.
- **Phase III**
  - *Task 9. Validate procedures.* Validate the procedures by executing the full-scale crash testing plan agreed on during the Task 8 interim meeting. Modify the procedures as necessary.
  - *Task 10. Submit final report.* Submit a final report documenting the entire research effort. Include the procedures in a stand-alone appendix, in a format suitable for adoption by AASHTO.

1.4 Report Scope

This report documents the research efforts, findings, and recommendations of this project. The report includes details of the state-of-practice survey, the engineering analyses, finite element modeling, and full-scale testing conducted in support of the guideline development process, and presents guidelines for designing barriers supported on the edge of MSE walls.

CHAPTER 2

State of the Practice

2.1 Design of MSE Wall

MSE walls are made of alternating layers of soil (fill) and reinforcement (Figure 2.1) (*4*). The fill must satisfy specifications (e.g., plasticity index limits, percentage passing #200 limits) and are generally sandy or rocky fills. The reinforcement is tied to panels erected vertically at the front of the wall. The reinforcement can be made of steel strips, bar mats, or geosynthetics. Each layer between reinforcement is compacted to the required compaction level (Figure 2.2).

The idea of an MSE wall is to create a reinforced earth mass that is equivalent to a gravity wall. As such, the basic design consists of two parts: external stability design and internal stability design.

2.1.1 External Stability

The external stability ensures that the wall is safe against sliding, overturning, bearing capacity failure, and slope stability failure (see Figure 2.3):

- Sliding design consists of ensuring that the active force developing behind the wall does not represent an unreasonable risk of overcoming the friction resistance at the base of the wall.
- Overturning design consists of ensuring that the moment created by the active force around the bottom of the front of the wall does not represent an unreasonable risk of overcoming the resisting moment due to the weight of the wall mass.
- Bearing capacity design consists of ensuring that the pressure due to the wall mass does not represent an unreasonable risk of overcoming the ultimate bearing capacity of the soil.
- Slope stability design consists of ensuring that the overall wall configuration does not represent an unreasonable risk of failing by general deep seated rotation.

2.1.2 Internal Stability

The internal stability ensures that the wall mass is a coherent solid block with tensile resistance. This design addresses the issues of the load on the reinforcement, the required length of the reinforcement, and the stress in the reinforcement (see Figure 2.4).

- The load on the reinforcement is obtained by using a semi-empirical equation developed from experience. This equation expresses that the reinforcement must safely resist the pressure on the panel that would develop in the soil if the reinforcement were not there.
- The length of the reinforcement is equal to the sum of the length required to safely resist in friction the load calculated in the previous step plus the length in the failing zone behind the wall. This length is usually calculated by a prescriptive approach, L = 0.7H (height of the wall).
- The stress in the reinforcement is the load divided by the reinforcement area after discounting the corrosion thickness and other factors if appropriate. This stress is checked to ensure that it is safely below the yield stress of the material used.

In AASHTO LRFD (*2*), to satisfy the internal stability, the static factored resistance (ϕP) to pullout of the reinforcement should be at least equal to the static factored load (γT) due to the earth pressure.

The static resistance (P) per unit of reinforcement width is calculated using the following equation (LRFD Equation 11.10.6.3.2-1):

$$P = F^{*}\alpha\sigma_{v}CL_{e} \qquad (2\text{-}1)$$

where

F^{*} = Pullout friction factor as shown in Figure 2.5
α = Scale effect correction factor (LRFD Table 11.10.6.3.2-1)

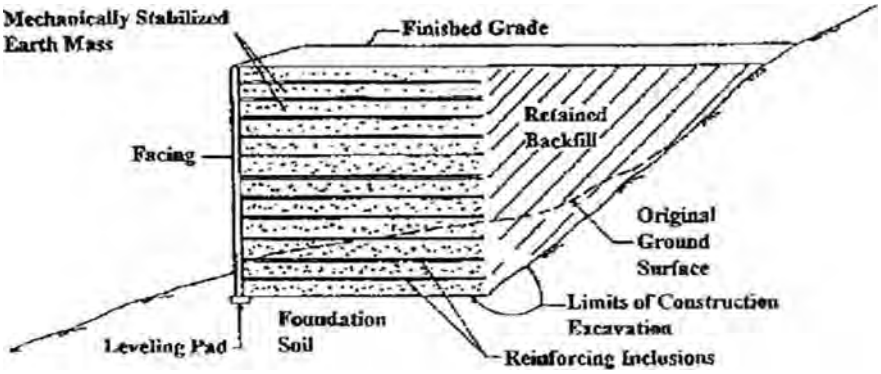

Source: Elias et al. (*4*)

Figure 2.1. Principal elements of MSE wall.

$\sigma_v = \gamma \times h$, where γ = Soil unit weight, h = Height of the strip from the roadside
C = Overall reinforcement surface area geometry factor based on the gross perimeter of the reinforcement and equal to 2 for strip-, grid-, and sheet-type reinforcements
L_e = Length of reinforcement in resisting zone

To obtain the static load (T) expected per unit of wall width due to the soil, the following equation in AASHTO LRFD is used (LRFD Equation 11.10.6.2.1-2)

$$T = \sigma_h S_v \quad (2\text{-}2)$$

where

σ_h = Horizontal stress due to the soil, $\sigma_h = K_r \times \sigma_v$, where K_r = lateral earth pressure coefficient
S_v = Vertical spacing of the reinforcement

Example applications of the AASHTO LRFD MSE wall design procedures are presented in Appendix A, which is available from the *NCHRP Report 663* summary web page on the TRB website (www.trb.org) by searching for "NCHRP Report 663".

2.2 Design of Barrier

This section includes background regarding roadside barrier crash testing criteria, a history of the design loads, and design practice of roadside barriers.

2.2.1 Background of Barrier Crash Testing Guidelines

Guidelines for testing roadside appurtenances originated in 1962 with a one-page document—"Proposed Full-Scale Testing Procedures for Guardrails" (*5*). This document included four specifications on test article installation, one test vehicle, six test conditions, and three evaluation criteria. *NCHRP Report 153* (*6*), published in 1974, provided the first complete test matrix. Parameters to be measured were specified along with methods and limiting values, and limited guidance on

Source: Elias et al. (*4*)

Figure 2.2. Construction of MSE wall.

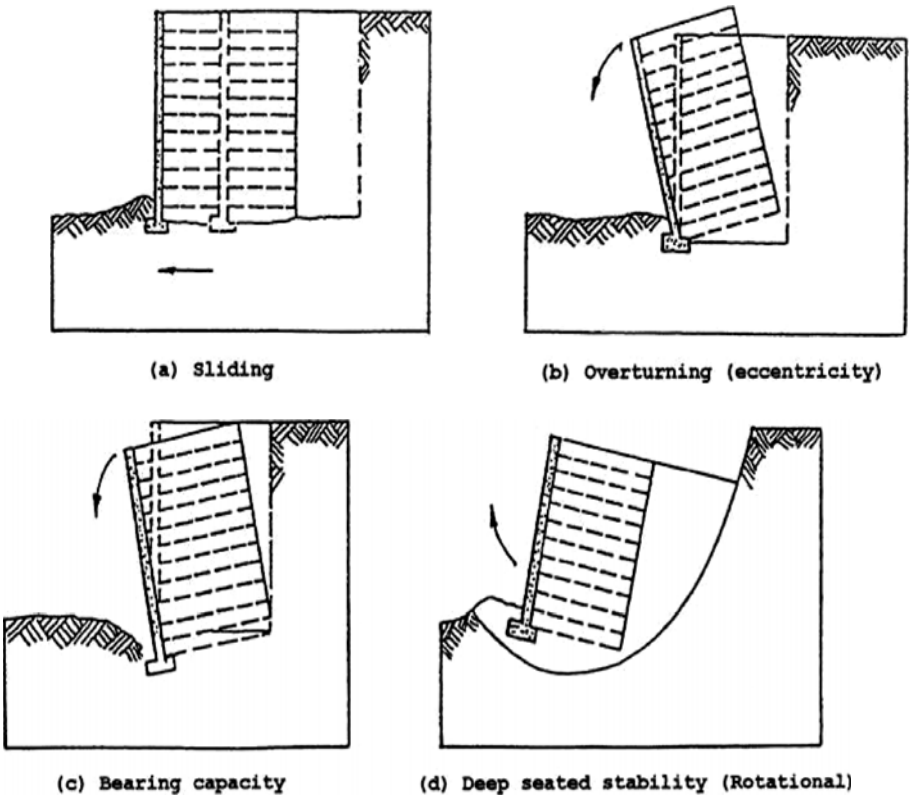

Source: Elias et al. (*4*)

Figure 2.3. External stability considerations.

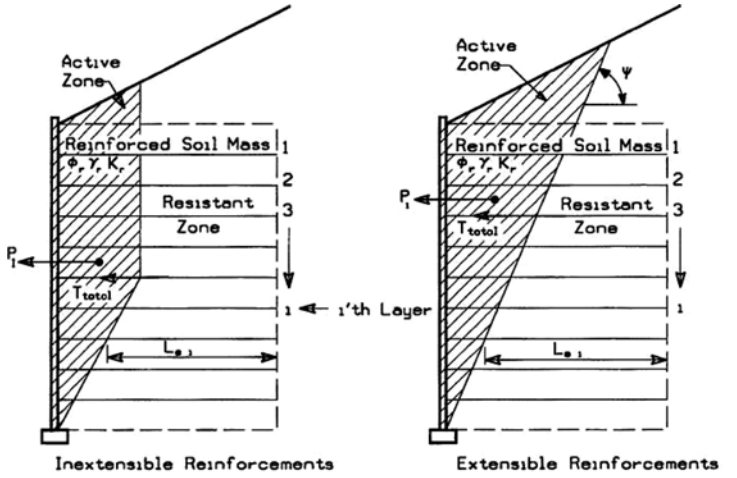

P_i = Internal inertial force due to the weight of the backfill within the active zone.

L_{ei} = The length of reinforcement in the resistant zone of the i'th layer.

T_{max} = The load per unit wall width applied to each reinforcement due to static forces.

T_{ad} = The load per unit wall width applied to each reinforcement due to dynamic forces.

The total load per unit wall width applied to each layer, $T_{total} = T_{max} + T_{ad}$

Source: AASHTO (*2*)

Figure 2.4. Internal stability considerations.

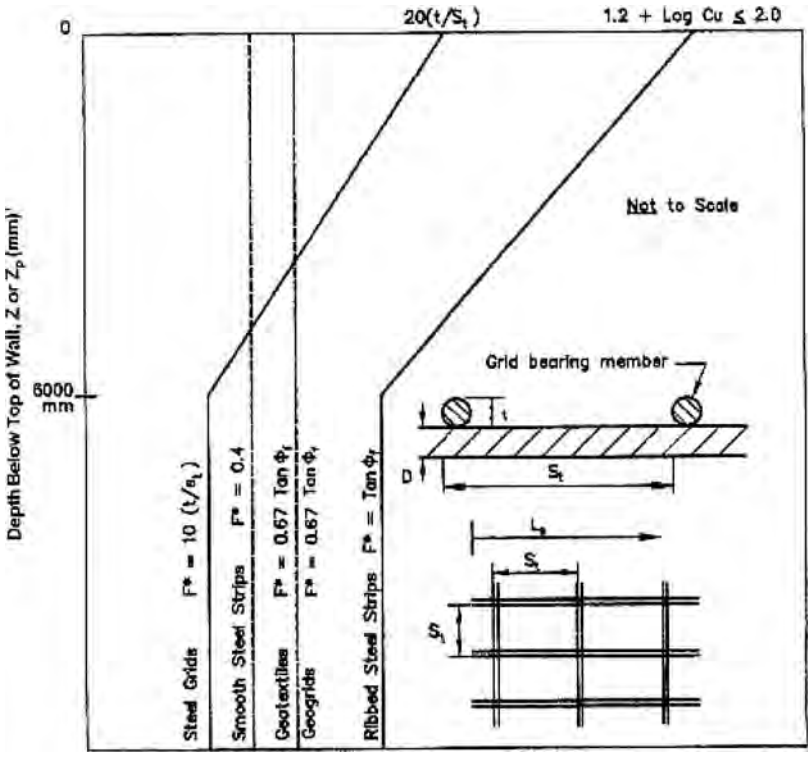

Source: AASHTO LRFD Figure 11.10.6.3.2-1 (*2*)

Figure 2.5. Default values for the pullout friction factor, F*.

reporting formats was included. These procedures gained wide acceptance following their publication, but it was recognized at that time that periodic updating would be needed.

In 1978, *Transportation Research Circular 191* (*7*) was published to provide limited interim changes to *NCHRP Report 153*. An extensive revision and update was made in 1981 with the publication of *NCHRP Report 230* (*8*). This document specified different service levels for evaluating longitudinal barriers whose test matrices included vehicles ranging from small passenger cars to intercity buses.

NCHRP Report 350 (*3*), which was published in 1993, provides current guidance on testing and evaluating roadside safety features. This 132-page document represented a comprehensive update to crash test and evaluation procedures. It incorporated significant changes and additions to procedures for safety performance evaluation, and updates reflecting the changing character of the highway network and the vehicles using it.

NCHRP Report 350 selected a 2,000 kg (4,409 lb) pickup truck as the design test vehicle to reflect the fact that over one half of new passenger vehicles sales in the United States were in the light truck category. This change was made recognizing the differences in wheel bases, bumper heights, body stiffness and structure, front overhang, and other vehicular design factors associated with light trucks. *NCHRP Report 350* further defines other supplemental test vehicles including an 8,000 kg (17,637 lb) single-unit cargo truck and 36,000 kg (79,366 lb) tractor-trailer vehicles to provide the basis for optional testing to meet higher performance levels.

Six test levels are defined for longitudinal barriers (e.g., bridge rails, median barriers, guardrails) that place an increasing level of demand on the structural capacity of a barrier system. The basic test level is Test Level 3 (TL-3). The structural adequacy test for this test level consists of a 2,000 kg (4,409 lb) pickup truck impacting a barrier at 100 km/h (62 mph) and 25 degrees. At a minimum, all barriers on high-speed roadways on the National Highway System (NHS) are required to meet TL-3 requirements. Many state transportation departments require that their bridge railings meet TL-4, which requires accommodation of an 8,000 kg (17,637 lb) single-unit truck hitting a barrier at 80 km/h (50 mph) and 15 degrees. Higher containment barriers are sometimes used when conditions such as a high percentage of truck traffic warrant. Such barriers are necessarily taller, stronger, and more expensive to construct.

Since publication of *NCHRP Report 350,* changes have occurred in vehicle fleet characteristics and testing technology. NCHRP Project 22-14(2) (*9*), "Improved Procedures for the Safety-Performance Evaluation of Roadside Features," was initiated to take the next step in the continued advancement and evolution of roadside safety testing and evaluation. The results of this research effort culminated in the new document

Manual for Assessing Safety Hardware (MASH) (*10*) that was published by AASHTO and supersedes *NCHRP Report 350.* Changes in the new guidelines include new design test vehicles, revised test matrices, and revised impact conditions. The weight and body style of the pickup truck changed from a 2,000 kg (4,409 lb), 0.75-ton, standard cab pickup to a 2,270 kg (5,000 lb), 0.5-ton, four-door pickup. For TL-4, the weight of the single-unit truck increased from 8,000 kg (17,637 lb) to 10,000 kg (22,000 lb) and the speed increased from 80.47 km/h (50 mph) to 90.12 km/h (56 mph). Although still a draft, many user agencies have already begun applying the MASH criteria in their crash test programs.

2.2.2 Background of Barrier Design Loads

Historically, the design of bridge rails has followed guidance contained in the AASHTO Standard Specifications. Prior to 1965, the AASHTO Standard Specifications required very simply that "Substantial railings along each side of the bridge shall be provided for the protection of traffic." It was specified that the top members of bridge railings be designed to simultaneously resist a lateral horizontal force of 2.19 kN/m (150 lb/ft) and a vertical force of 1.46 kN/m (100 lb/ft) applied at the top of the railing. The design load on lower rail members varied inversely with curb height, ranging from 7.3 kN/m (500 lb/ft) for no curb to 4.4 kN/m (300 lb/ft) for curb heights of 0.23 m (9 in.) or greater. It was further specified that the railing have a minimum height of 0.69 m (27 in.) and a maximum height of 1.07 m (42 in.) above the roadway surface.

These loads are only a fraction of what is used today. Based on a poor accident history, accentuated by increased exposure due to dramatically increasing travel volumes, the engineering community came to realize that these criteria were inadequate. There was a recognized need (and, in the words of some, an "urgent necessity") for a railing specification that established loading requirements more in line with the weights and increased speeds of vehicles of that day.

In 1962, the U.S. Department of Commerce, Bureau of Public Roads (BPR), now the Federal Highway Administration (FHWA), developed proposed revisions to the specifications for bridge railings. It was proposed that bridge railings and parapets be designed for a transverse load of 133.4 kN (30 kips) using plastic design procedures. This load was distributed among the horizontal railing members. A figure with 10 different railing types/configurations was provided to assist with distribution of the load. The difficulty of defining a static load that would be equivalent in effect to a vehicle impact on a railing was recognized. As part of the rationale for selecting the load of 133.4 kN (30 kips), reference was made to designs that met the proposed specification and which experience indicated would be adequate to resist the usual anticipated forces of impact.

Based on information received from a retired Texas Department of Transportation (TxDOT) bridge engineer involved in review of this proposal, many AASHTO members were unfamiliar with plastic design procedures and there was "great objection" to using it. Ultimately, after considerable discussion, comment, and revision, the AASHTO Committee on Bridges and Structures approved a revision to the railing specification in 1964.

The revised railing specifications were subsequently published in 1965 in the ninth edition of the *AASHTO Standard Specifications for Highway Bridges* (*11*). It required that rails and parapets be designed for a transverse load of 44.5 kN (10 kips) divided among the various rail members using an elastic analysis. The force was applied as a concentrated load at mid-span of a rail panel with the height and distribution of the load based on rail type and geometry as provided in an accompanying figure. Posts were designed for the transverse loading applied to each rail element plus a longitudinal load of half the transverse load. The transverse force on concrete parapet walls was distributed over a longitudinal length of 1.52 m (5 ft). Guidance on the effective length of slab resisting post loadings was provided for rail designs with and without a parapet. The height of the railing was required to be no less than 0.69 m (27 in.). It was noted that railing configurations successfully crash tested were exempt from the design provisions.

The rationale for changing the 133.4 kN (30 kips) force proposed by the BPR to the 44.5 kN (10 kips) force ultimately adopted by AASHTO is not fully known. However, it can be shown that a 44.5 kN (10 kips) load with the rail resistance defined by elastic analysis is roughly equivalent to a 133.4 kN (30 kips) load with the rail resistance defined by plastic analysis following the BPR procedure. Such an equivalency may have been established to permit more familiar design procedures to be followed. The provisions in the 17th edition of the *AASHTO Standard Specifications for Highway Bridges* (*1*), published in 2002, are essentially the same as the revised specification adopted in 1965.

These requirements are intended to produce bridge rails that will function adequately for passenger cars for a reasonable range of impact conditions. The reserve load capacity of the rail, beyond its elastic strength, offers some degree of protection for more severe impact conditions or for heavier vehicles. Several catastrophic crashes involving large vehicles increased awareness of design requirements for bridge rails and the need to extend protection beyond passenger cars.

In the first of two such studies, an instrumented concrete wall (shown in Figure 2.6) was designed to, for the first time, measure the magnitude and location of vehicle impact forces (*12*). The wall consisted of four 3.05 m (10 ft) long panels laterally supported by four load cells. Each of the 1.07 m (42 in.) tall × 0.61 m (24 in.) thick panels was also instrumented with an accelerometer to account for inertia effects. Surfaces in

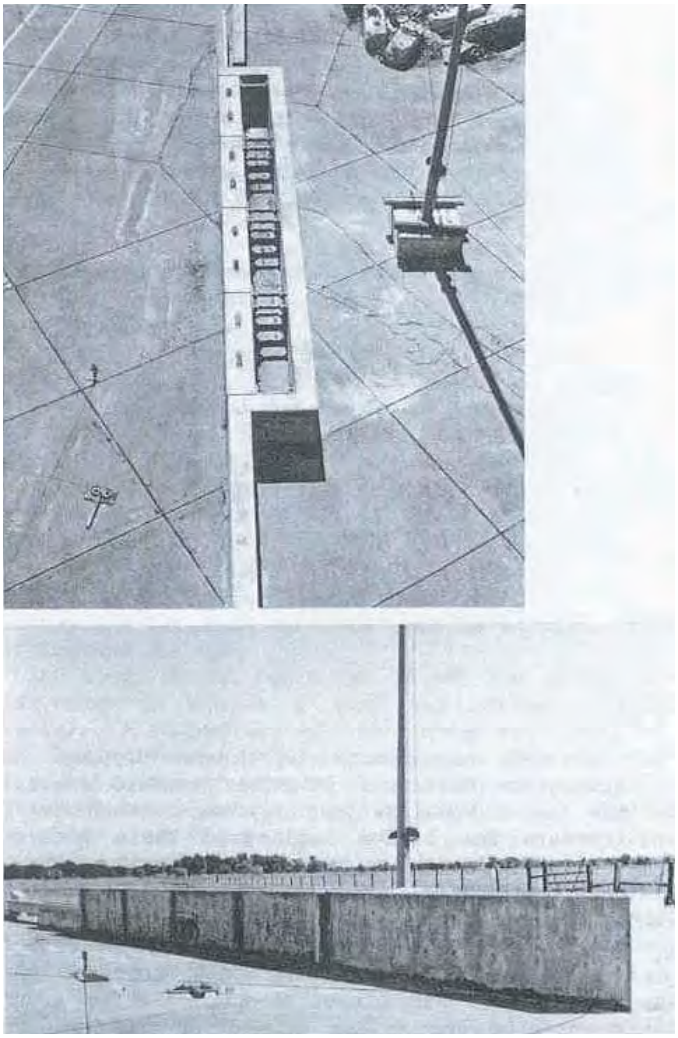

Source: Noel et al. (*12*)

Figure 2.6. Instrumented wall.

contact with the supporting foundation and adjacent panels were Teflon coated to minimize friction. In this first study, eight full-scale crash tests were conducted using various sizes of passenger cars and buses. In the second such study (*13*), a new wall with a height of 2.29 m (90 in.) was constructed using similar design details, and crash tests with a variety of trucks (up to and including a 36,300 kg (80,000 lb) tractor with tank-type trailer) were conducted. Speeds in these tests ranged from 80.5 km/h (50 mph) to 69.6 km/h (60 mph) and the impact angles ranged from 15 degrees to 25 degrees.

The data from the instrumented wall tests were analyzed to determine the resultant magnitudes, locations, and distributions of the contact forces. Maximum forces were obtained by averaging the data over 0.05-second (sec) intervals to reduce the effect of force "spikes" in the data that were believed to have little consequence to the required structural integrity of the bridge railings due to their short duration. Two forces were determined for each test—one associated with the initial impact of the front corner of the vehicle, and one associated with the second impact or "backslap" as the rear of the vehicle rotates (yaws) into the rail as it is redirected. An example is shown in Figure 2.7.

The pressure of these resultant forces was assumed to be distributed as half a sine wave in both the horizontal and vertical directions (see Figure 2.8). The length of the contact area was measured from high-speed film. An example of the longitudinal distribution obtained in this manner is shown in Figure 2.9. Because the force measurements were obtained from a nearly rigid barrier, they are considered to represent the upper bound of forces that would be expected on an actual bridge railing. Any deformation of the bridge rail during impact will tend to reduce the magnitude of the impact forces below those obtained on the "nearly rigid" instrumented concrete wall.

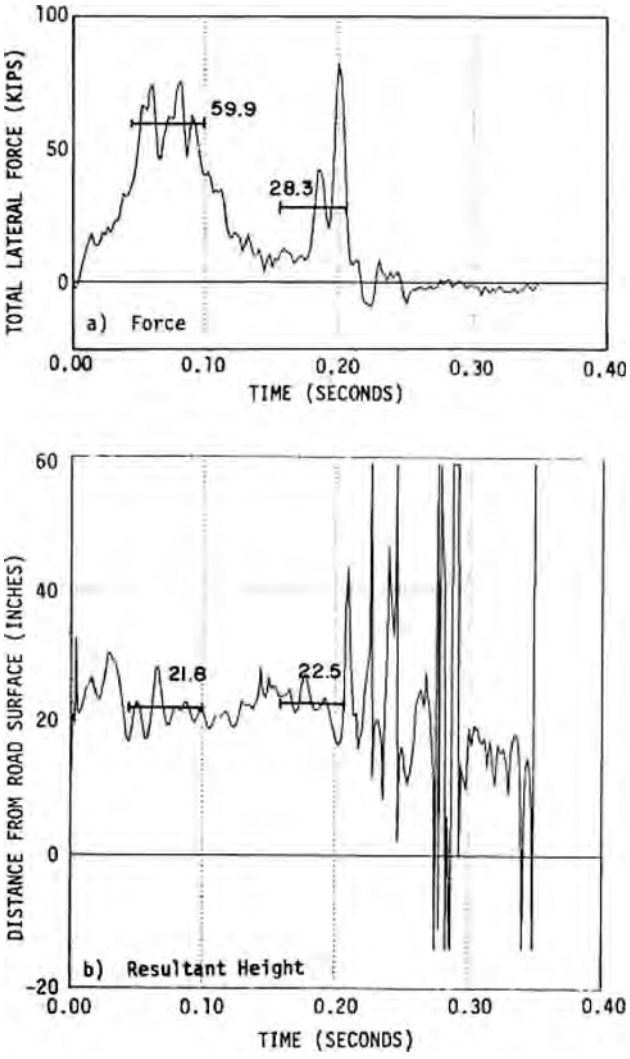

Source: Noel et al. (*12*)

Figure 2.7. Magnitude and location of average resultant force (4,740 lb vehicle, 60 mph, 24 degrees).

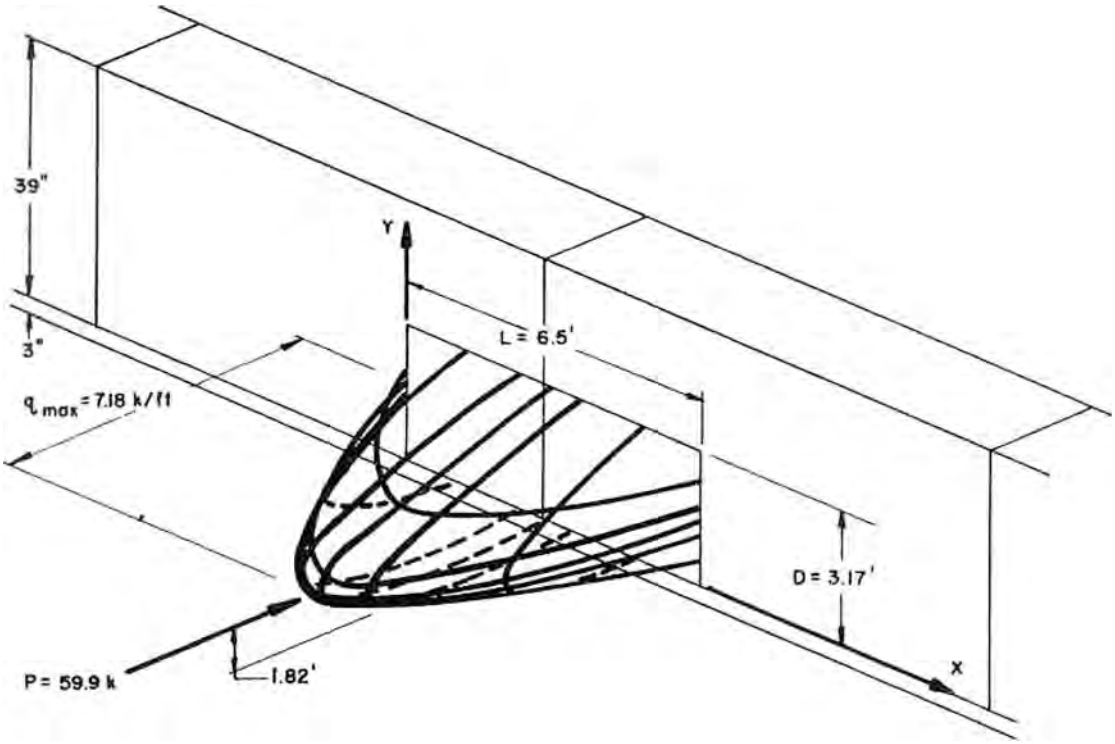

Source: Noel et al. (*12*)

Figure 2.8. Distribution of contact pressure.

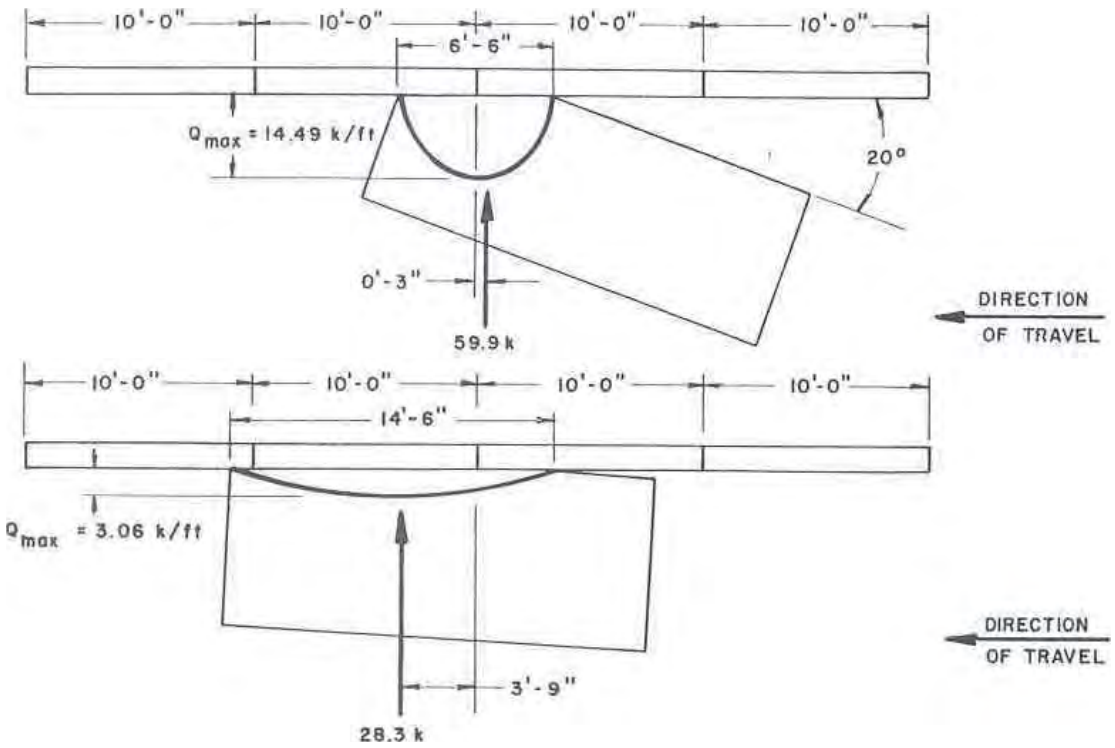

Source: Noel et al. **(***12***)**

Figure 2.9. Longitudinal distribution for initial and final impacts (4,740 lb vehicle, 60 mph, 24 degrees).

Data from the instrumented wall studies were used to derive barrier design loads for various impact conditions included in the *AASHTO Guide Specifications for Bridge Railings* (*14*) and subsequently, the *AASHTO LRFD Bridge Design Specifications:* Section 13, Railings (*2*).

2.2.3 Barrier Design Practice

As previously mentioned, the *AASHTO Standard Specifications for Highway Bridges* (*1*) specifies an elastic, allowable stress analysis methodology for designing bridge rails using a static load of 4,536 kg (10,000 lb) distributed among the various rail elements. These requirements have existed since their adoption in the ninth edition of the *AASHTO Standard Specifications for Highway Bridges* (*11*) in 1965.

It can be observed that measured dynamic impact forces obtained from full-scale vehicle crash tests into an instrumented concrete wall are significantly higher than static loads used in the design of bridge rails for passenger cars. Yet, this observation does not necessarily mean that railings designed for a static load of 4,536 kg (10,000 lb) following the *AASHTO Standard Specifications for Highway Bridges* are inadequate, because a railing system will generally have an ultimate strength well above that indicated by allowable stress design procedures. However, the amount of reserve capacity will vary depending on materials and design details and is not predicted when allowable stress design methods are used. Ultimate strength design procedures provide a more accurate indication of the actual strength of a rail.

In 1984, Buth et al. (*15*) recommended that bridge rails be designed based on ultimate strength procedures using yield strength of the material with a factor of safety equal to 1.0. The capacity determined in this manner is compared to the dynamic impact loads determined from data measured in the instrumented wall testing programs. Such a design procedure is intended to produce yielding, but not ultimate failure/fracture, when a design impact collision occurs. This premise should hold true provided the materials and structural elements have sufficient ductility and ultimate strength substantially greater than yield strength.

Such analyses are based on bending moments induced in the structure and the formation of plastic hinges at points of high bending moment. Thus, the failure mechanism of the rail must be known or assumed. The failure mechanism and the number of posts involved in the mechanism are dependent on how the load applied by the vehicle is distributed to the system. Investigation of several different failure mechanisms for a given rail system is typically required to determine the controlling mechanism (i.e., the mechanism that develops at the lowest load). One-span, two-span, and three-span failure mechanisms are idealized in Figure 2.10. The validity of an ultimate strength failure mechanism requires the structure to be able to deform enough to actually develop the failure mechanism.

Ultimate strength design procedures were widely used by roadside safety researchers in the 1980s to develop bridge rails capable of containing buses and trucks. In most cases, the impact performance of the rails was verified through full-scale crash testing. In 1989, these procedures were incorporated into the *AASHTO Guide Specifications for Bridge Railings.* This specification prescribed three performance levels for bridge rails and warrants for their use. The test matrices associated with these performance levels included tests with trucks which, up to this time, had not been given consideration in testing documents such as *NCHRP Report 230.*

Impact conditions associated with Performance Level 1 (PL-1) included a 2,500 kg (5,400 lb) pickup truck hitting at a speed of 72.4 km/h (45 mph) and an angle of 20 degrees. For PL-2, the speed of the pickup truck test was increased to

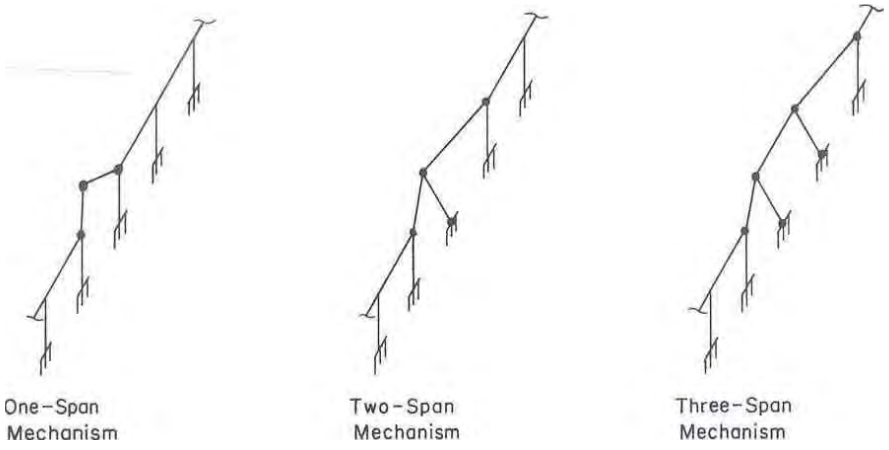

Source: Buth et al. (*15*)

Figure 2.10. Idealized span-based failure mechanisms.

96.5 km/h (60 mph) and a test with an 8,165 kg (18,000 lb) single-unit truck impacting the barrier at a speed of 80.5 km/h (50 mph) and an angle of 15 degrees was added to the test matrix. The highest performance level, PL-3, incorporates a test with a 22,680 kg (50,000 lb) van-type tractor trailer impacting the barrier at a speed of 80.5 km/h (50 mph) and an angle of 15 degrees. The design impact loads prescribed for each performance level were determined based on data measured in the previously described instrumented wall crash tests (*12, 13*).

In 1993, *NCHRP Report 350* was published. This report contains six test levels for longitudinal barriers. Test Levels 1 through 3 relate to passenger vehicles and vary by impact speed. Test Levels 4 through 6 retain consideration of passenger cars, but also incorporate consideration of trucks. The impact conditions of TL-4 in *NCHRP Report 350* are similar to those associated with PL-2 in the 1989 *AASHTO Guide Specifications for Bridge Railings.* TL-4 is the test level used by most states to qualify the impact performance of their bridge rails—a fact that may be a holdover from prior use of the 1989 *AASHTO Guide Specifications for Bridge Railings.*

Ultimate strength design procedures were subsequently adopted in the first edition of the *AASHTO LRFD Bridge Design Specifications* published in 1996 (*16*). Rather than perpetuate two sets of impact performance criteria, the test levels of *NCHRP Report 350* were adopted over the performance levels of the 1989 AASHTO Guide Specifications.

Section 13, Railings, of the *AASHTO LRFD Bridge Design Specifications* applies to the design of railings for bridges. Yield line theory considers the plastic strength of all the railing system components with consideration given to barrier geometry, material strengths, applied loading, and strength of the supporting bridge structure. Steel rail systems, concrete rail systems, or a combination rail composed of a steel rail on a concrete parapet can be evaluated using these design procedures. Based on the yield line theory, the limiting ultimate capacity of the railing system is calculated. This ultimate capacity is then compared to design forces derived from vehicular loads measured in actual crash testing.

Typically, capacities of the railing system are calculated at both mid-span of the railing system and at a joint or end of the rail system. The controlling yield line failure mechanism for a vertical concrete parapet loaded at mid-span is shown in Figure 2.11. The failure mechanism for loading at a joint or end is theoretically similar but involves only a single "hinge" as shown in the illustration presented in Figure 2.12. For safety-shaped barriers, such as the New Jersey (N.J.) and F-shape barriers, the hinges or failure planes are often isolated in the upper, narrower portion of the barrier as shown in Figure 2.13. (*17*)

Post-and-beam types of bridge parapets are fabricated from concrete, structural steel, or aluminum components, or a combination of these materials. Failure mechanisms in post-and-beam parapets can occur in several different modes. As the name implies, the impact loads must be transferred to the deck through discrete posts rather than through a continuous rail section. This can result in higher concentrations of load that can result in severe localized damage to the deck or slab if not properly designed.

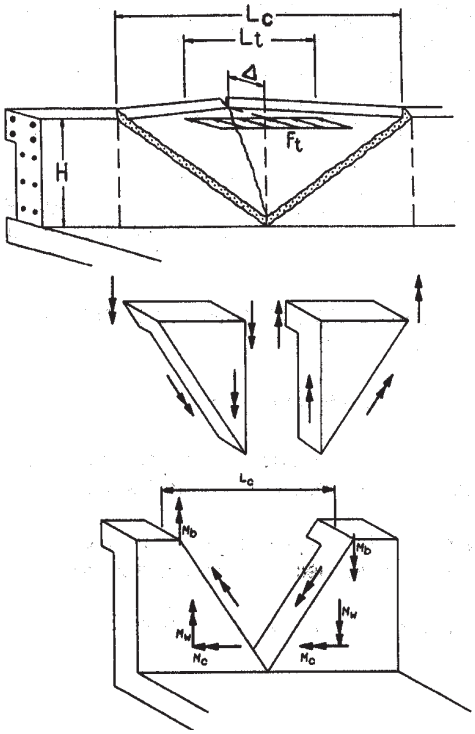

Source: AASHTO (*2*)

Figure 2.11. Idealized mid-span failure mechanism.

The calculated ultimate strength or capacity of the rail is then compared to applicable design forces to assess its structural adequacy. The prescribed impact loads for different test levels are presented in Table A13.2-1, Section 13 of the *AASHTO LRFD Bridge Design Specifications.* The loads are considered to be short duration, one-time loads. The barrier is sized such that it will have an ultimate strength, based on a yield line analysis, that is equal to or greater than the specified load with no "factor of safety."

2.3 Design of the Barrier on Top of the MSE Wall

AASHTO allowable stress design (ASD) (*1*) and LRFD (*2*) use the same basic procedure to design a barrier on top of an MSE wall even though the impact specification was increased from 44.5 kN (10 kips) to 240 kN (54 kips) for the design of the traffic barrier. This section summarizes the current AASHTO LRFD design procedure for barriers mounted on

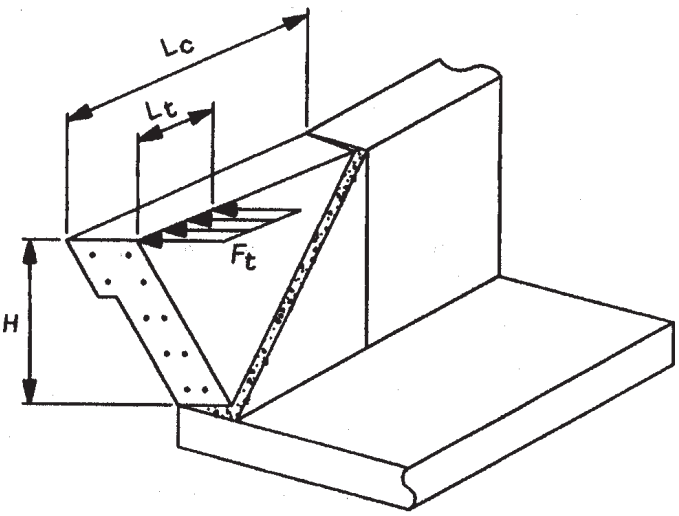

Source: AASHTO (*2*) and Alberson et al. (*17*)

Figure 2.12. Failure mechanism at barrier joint or end.

Source: Alberson et al. (*17*)

Figure 2.13. Typical failure pattern for safety-shaped barriers.

the edge of MSE walls, compares the AASHTO ASD and LRFD procedures, and describes previous test results.

2.3.1 Design of MSE Wall for Barrier Impact

In *AASHTO LRFD Bridge Design Specifications* Section 11.10.6.2.1, the following equation is presented to calculate horizontal stress due to the soil weight and the impact load:

$$\sigma^H = \sigma_h + \Delta\sigma_{h,\max} \quad (2\text{-}3)$$

where

σ_h = horizontal stress due to the soil weight = $k_r \times \sigma_v$, k_r is the horizontal earth pressure coefficient given by 1.7 k_a, σ_v is vertical stress due to the soil weight

$\Delta\sigma_{h,\max}$ = horizontal stress due to the impact load (P_{h1}) on the barrier = $2P_{h1}/l_1$, l_1 is the depth of influence of the impact load down the wall face as shown in Figure 2.14.

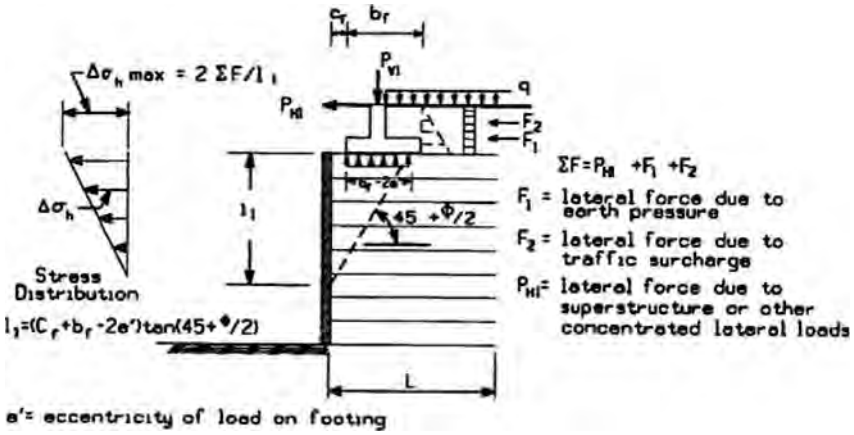

Source: AASHTO LRFD Figure 3.11.6.3-2 a (*2*)

Figure 2.14. Distribution of stress from concentrated horizontal loads.

2.3.2 Comparison between ASD and LRFD

AASHTO is in the process of changing from ASD to LRFD. The 2002 AASHTO ASD makes use of a 44.5 kN (10 kips) load for the design of the traffic barrier and for the impact load that is distributed into the MSE wall below (in the form of added load for the reinforcement). The 2004 AASHTO LRFD specifies a 240 kN (54 kips) design load (corresponding to TL-3 and TL-4) for the traffic barrier and a 44.5 kN (10 kips) load for the design of the MSE wall. Therefore, there has been a significant increase in the design load for the barrier.

The 240 kN (54 kips) load level comes from measurements made on an instrumented barrier during impact and, therefore, is a dynamic load. The increase from 44.5 kN (10 kips) to 240 kN (54 kips) for the structural design of the barrier does not increase the size of the barrier significantly because the 44.5 kN (10 kips) load is used with an elastic design analysis while the 240 kN (54 kips) load is used with an ultimate strength analysis.

However, for the moment slab design, the change from 44.5 kN (10 kips) static to 240 kN (54 kips) dynamic requires a proportional increase in the width of the moment slab if the 240 kN (54 kips) is used as a static load in the stability analysis of the barrier system. Indeed one would calculate a 1.37 m (4.5 ft) wide moment slab with AASHTO ASD and a 1.37 m (4.5 ft) × 54/10 = 7.4 m (24.3 ft) wide moment slab with AASHTO LRFD. This difference arises because that 54 kips is taken as a static load when in fact it is a dynamic load. From experience, a 7.4 m (24.3 ft) wide moment slab would be unreasonably conservative. The objective is to find out how to take into consideration the 240 kN (54 kips) for overturning and sliding of the barrier.

The design of the barrier against overturning consists of applying the load to the barrier at the prescribed height and then using moment equilibrium to find out how wide the moment slab has to be while satisfying a factor of safety against overturning equal to 2. This factor of safety of 2 is consistent with the requirement for overturning of an MSE wall but is not explicitly written in the AASHTO ASD for overturning of barriers.

The design of the barrier against sliding consists of applying the load to the barrier and then using horizontal equilibrium to find out how wide the moment slab has to be while satisfying a factor of safety of 1.5. This factor of safety of 1.5 is consistent with the requirement for sliding of an MSE wall but is not explicitly written in the AASHTO ASD for sliding of barriers.

In LRFD, the recommendations are not as detailed. The load factor γ is taken as 1.0 for the load combination of Service I and the resistance factor for sliding as 0.8 for cast-in-place concrete on soil. There are no recommendations for the resistance factor against overturning.

2.3.3 Previous Crash Test of Barrier on Edge of MSE Wall

In 1982, Terre Armée Internationale (TAI), which is closely related to the Reinforced Earth Company (RECO) in the United States, performed a crash test of a barrier on top of an MSE wall (*18*). The test vehicle was a 12,020 kg (26,500 lb) bus that impacted the barrier at a speed of 71.2 km/h (44.2 mph) and an angle of 20 degrees. The impact severity was estimated to be 30% larger than the AASHTO PL-2 (*19*) loading condition.

The barrier was an N.J. shape barrier approximately 0.81 m (32 in.) high as shown in Figure 2.15. The barrier reinforcement was minimal, consisting of two longitudinal No. 4 bars. The precast barrier units were 1.52 m (5 ft) long and tied to the moment slab through rebars. The moment slab was cast in place with a joint every 9.15 m (30 ft). The width of the moment slab was 1.25 m (4.1 ft), and its thickness was 254 mm (10 in.). The 254 mm (10 in.) of cover over the moment slab consisted of compacted soil and a layer of bituminous mix.

Source: RECO (*18*)

Figure 2.15. Precast barrier and coping with cast-in-place slab.

The MSE wall was 3.05 m (10 ft) high with two rows of 1.52 m (5 ft) tall panels. The reinforcement strips were 5 m (16.4 ft) long and the layers of strips were located at depths of 380 mm (15 in.) and 1.14 m (45 in.) below the bottom of the moment slab (best guess) and were 0.76 m (2.5 ft) apart in the horizontal direction (best guess). A horizontal gap of 19 mm (0.75 in.) was purposely left between the coping and the traffic face of the wall panels to avoid lateral contact with the wall panel during impact. Figure 2.16 shows the cracking on the front and back side of barrier after the crash test.

The test was considered successful. The bus was redirected and stayed upright. The barrier was damaged but the wall and the moment slab were not damaged. The upper part of the barrier was broken over a length of 2.2 m (7.2 ft) and a height of 508 mm (20 in.). The top panel of the wall moved 5 mm (0.19 in.) dynamically during the event and had 1.5 mm

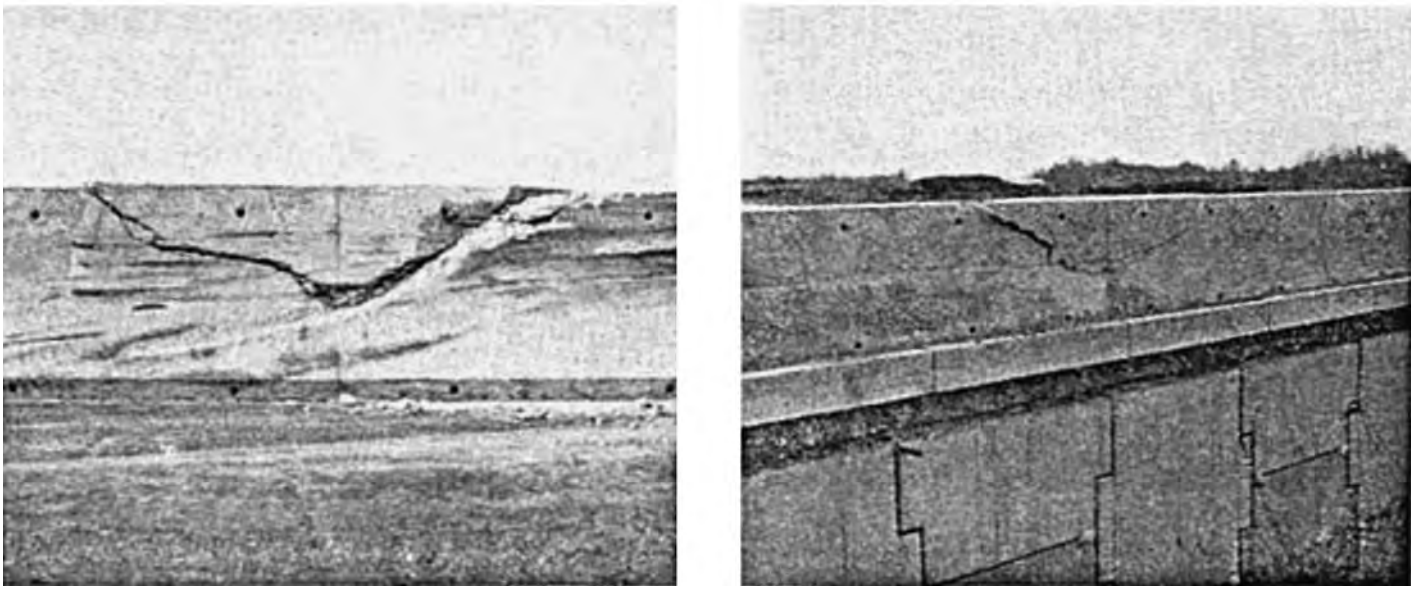

Source: RECO (*18*)

Figure 2.16. Barrier damage after RECO crash test.

(0.06 in.) of residual movement after the impact. The bottom panel did not move. No wall damage occurred. The maximum deceleration on the front and rear axles of the bus was 8g (moving average) and 14g, respectively. The maximum dynamic force recorded on the most loaded strip was 28.91 kN (6.5 kips).

The minimum reinforcement density for MSE walls gives a resistance of 42.3 kN/m (2.9 kips/ft) of wall at the top layer of strips. Pulling the strips out of the wall would require movement of the moment slab unit. For a joint spacing of the moment slab equal to 6.1 m (20 ft), the maximum load that the strips can resist at impact is 6.1 m (20 ft) × 42.3 kN/m (2.9 kips/ft) = 258 kN (58 kips; static). The 1982 TAI test leads to a load of 28.91 kN (6.5 kips) × 6.1 m (20 ft) / 0.76 m (2.5 ft) = 231.3 kN (52 kips; dynamic) if all strips within the 6.1 m (20 ft) section of barrier and moment slab were stressed at the maximum observed value. The value 258 kN (58 kips; static resistance) is much higher than the 44.48 kN (10 kips; static) value required by AASHTO. Therefore, RECO concluded that the minimum reinforcement density is adequate to resist the impact load.

2.4 Survey of State Transportation Agencies

A comprehensive survey of the nation's state transportation agencies was conducted to obtain information regarding the design, construction, and performance of barriers mounted on top of MSE walls. Major categories of the survey included MSE walls, barriers, barrier connection to wall/pavement, design, and performance. A total of 18 states responded to the survey: Alaska Department of Transportation (DOT) and Public Facilities, Arizona DOT, Arkansas State Highway and Transportation Department, Connecticut DOT, Georgia DOT, Hawaii DOT, Illinois DOT, Kansas DOT, Maryland State Highway Administration, Minnesota DOT, Mississippi DOT, Nevada DOT, New York State DOT Structures, South Carolina DOT, TxDOT, Utah DOT, Washington State DOT, and Wisconsin DOT. The blank survey instrument is shown in Appendix B, which is available from the *NCHRP Report 663* summary web page on the TRB website (www.trb.org) by searching for "NCHRP Report 663".

The data reduction of these responses is provided in two manners: (1) a weighted average based on the percentage of usage indicated by each state, which provides an indication of national usage of different alternatives within a given category (herein referred to as *Weighted Percentage of Usage from Responding States*), and (2) the number of states indicating usage in a certain category (herein referred to as *Number of States Responding Positive Usage*). For example, in the MSE wall section of the survey, the respondents were asked not only if they use a certain type of wall reinforcement in their state, but also what percentage of each type of reinforcement is used. The percentage of usage (e.g., 45% steel strips, 45% bar mats, 10% geosynthetics) is used to compute a weighted average for all respondents and is presumably indicative of average usage across the country. Additionally, the number (and corresponding percentage) of states indicating use of a given type of reinforcement is reported. Note that in the above example, the respondent indicated use of all three types of wall reinforcement and, therefore, positive usage would be indicated for each. When appropriate, the data has been presented in the form of pie charts for easier visualization of the responses. The survey question associated with each chart is provided for reference purposes. Certain data are presented in tables and/or in a written format.

2.4.1 MSE Walls

The survey section on MSE walls includes questions regarding the percentages of the type of reinforcement, the type of facing panels, and type of facing-panel connections used in MSE walls in the responding state. Figures 2.17 through 2.19 present the results for this survey section in the *Weighted Percentage of Usage from Responding States* format. Figure 2.17 indicates that approximately 57% of the MSE walls constructed within the responding states utilize steel strips as the means of reinforcement. Usage of steel strips is followed by usage of steel bar mats (24%) and geosynthetic grids (18%).

As shown in Figure 2.18, 80.7% of MSE wall construction incorporates concrete panels, while 19% are composed of

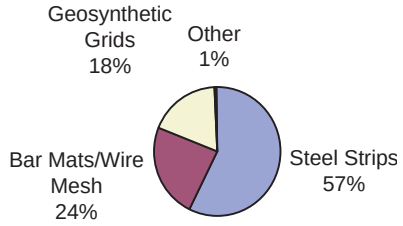

Figure 2.17. Type of reinforcement in MSE walls (Question 1).

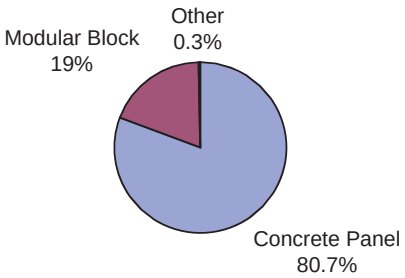

Figure 2.18. Type of facing panels in MSE walls (Question 2).

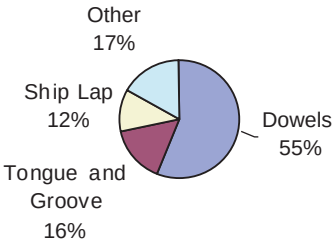

Figure 2.19. Type of facing-panel connection (Question 3).

modular blocks. Entries made by responding states in the "other" category for facing panel types noted use of wire-face walls, cast-in-place concrete walls, Gabion/exposed rock, and two-stage walls. In regard to the type of panel-to-panel connections utilized in MSE walls, Figure 2.19 indicates the majority (55%) use dowels, followed by tongue-and-groove (16%) and ship-lap (12%) connections. In the "other" category for facing panel connection type, states noted use of cast-in-place clips, friction or mesa, block lip, modular blocks, and RECO-lap. It should be noted that Georgia indicated 100% usage for both dowels and ship lap, and dowels were used in the analyses presented herein.

2.4.2 Barriers

The survey section for barriers included questions regarding the percentages of barrier categories used on MSE walls, types of guardrail and bridge rail used, and whether the barrier is precast or cast in-place. The survey also asked for the minimum segment length permissible for the precast barrier option. Figures 2.20 through 2.24 present the survey results of eighteen responses for the question on category of barriers, six responses for the question on type of guardrail, and eighteen responses for the question on type of bridge rail. Unless otherwise noted, the results are reported in the *Weighted Percentage of Usage from Responding States* format.

As shown in Figure 2.20 (which is presented in the *Number of States Responding Positive Usage* format), thirteen of the eighteen states responding to the survey (72%) use only bridge

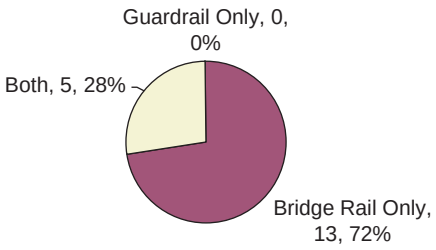

Figure 2.20. Percentage of states using different barrier categories (Question 4).

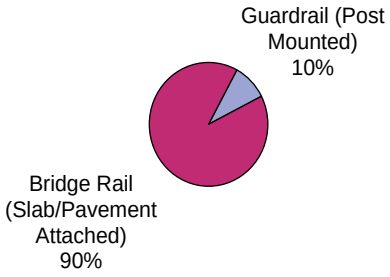

Figure 2.21. Category of barriers (Question 4).

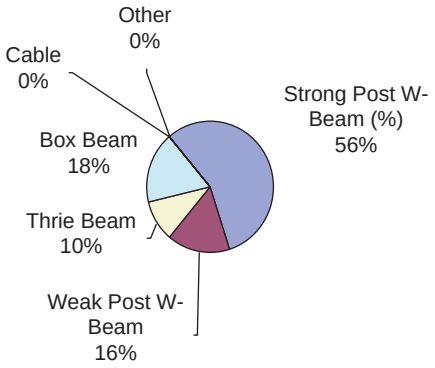

Figure 2.22. Type of guardrail (Question 5).

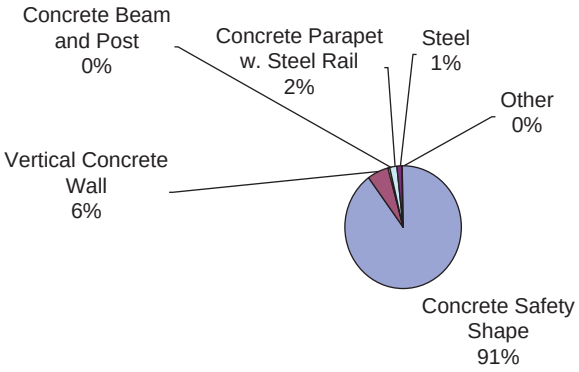

Figure 2.23. Type of bridge rail (Question 6).

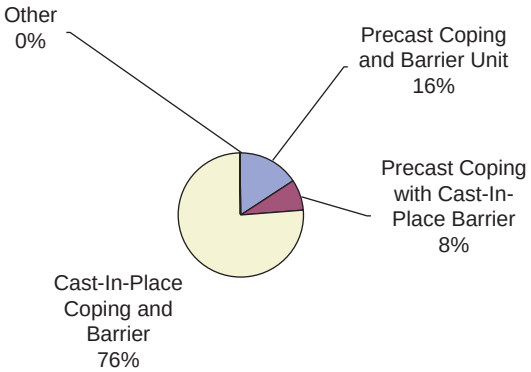

Figure 2.24. Precast barrier vs. cast-in-place barrier (Question 7).

rails atop MSE walls, while five states (28%) indicated use of both guardrail and bridge rail. There were no states that used only guardrail on MSE walls. When weighted averages of use are computed (see Figure 2.21), the results indicate that 90% of the MSE walls constructed with barriers on top utilize some type of bridge rail connected to a moment slab or pavement, while only 10% of such installations use guardrail mounted on soil-embedded posts.

Figure 2.22 shows the type of guardrail used by the six states indicating use of guardrail on MSE walls in Question 5 of the survey. Strong post W-beam is used 56% of the time, followed by box beam (18%), weak post W-beam (16%), and thrie beam (10%). The median offset from the edge of the MSE wall reported for post-mounted guardrail was 0.91 m (3 ft).

As mentioned earlier, all states responding to the survey indicated use of some percentage of bridge rail atop MSE walls. As indicated by the weighted averages shown in Figure 2.23, the vast majority (91%) of such installations incorporate some form of concrete safety shape barrier (e.g., N.J., F-shape). This type is followed by vertical concrete parapets (6%) and concrete parapets combined with a steel railing (2%).

Figure 2.24 provides information regarding precast versus cast-in-place construction practices followed by the responding states. Seventy-six percent of barrier construction on MSE walls uses cast-in-place coping and barrier. Precast coping and barrier segments are used 16% of the time, while use of a precast coping with cast-in-place barrier is limited to 8%. The median minimum segment length for the six states indicating use of precast barrier segments was 4.57 m (15 ft).

2.4.3 Barrier Connection to Wall/Pavement

The survey section dealing with the barrier connection to wall/pavement included questions regarding the percentage of the different types of pavement used on top of MSE walls, the offset of post-mounted guardrails from the edge of the wall, and asphalt concrete pavement (ACP) and reinforced concrete pavement (RCP) applications. As shown in Figure 2.25 (which is presented in the *Number of States Responding Positive Usage* format), 11 of 17 states responding to this question (64%) use both RCP and ACP on MSE walls. Four states (24%) indicated use of only RCP, while another two states (12%) use only ACP

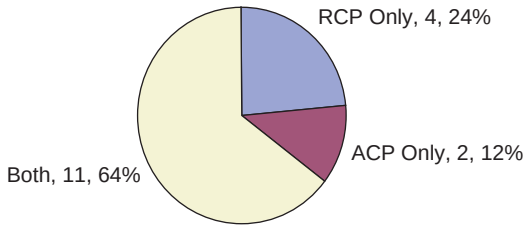

Figure 2.25. Use of different pavement types on MSE walls (Question 9).

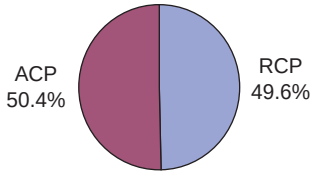

Figure 2.26. Pavement type (Question 9).

on MSE walls. When weighted averages of use are computed (see Figure 2.26), the results indicate a nearly 50-50 split between asphalt and reinforced concrete pavement applications in regard to MSE wall construction.

For slab-attached bridge rails, the barrier connection to wall/pavement section of the survey is divided into asphalt concrete pavement and reinforced concrete pavement applications. Because of the nature of these questions, the results are reported using the *Number of States Responding Positive Usage* format. The survey responses related to the use of ACP on MSE walls with barriers are presented in Figures 2.27 through 2.30. Supporting information for some of these questions and figures is presented in Table 2.1.

With reference to Table 2.1 (Question 11), the median thickness of the moment slab for MSE wall applications with ACP is 343 mm (13.5 in.). The median width of the moment slab used by the responding states is 6.5 ft (Table 2.1, Question 12). Figure 2.27 (which is based on survey Question 13) indicates that 50% of the responding states use continuous

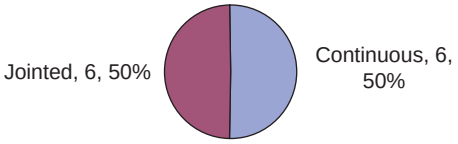

Percentages derived from number of states using the category shown divided by the total number of states responding

Figure 2.27. Continuous or jointed barrier slab/footing (ACP, Question 13).

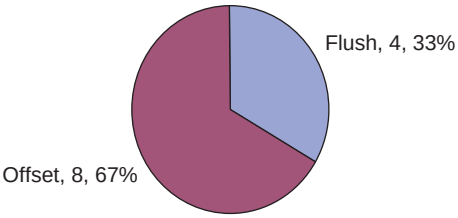

Percentages derived from number of states using the category shown divided by the total number of states responding

Figure 2.28. Barrier flush or offset from face of wall (ACP, Question 13).

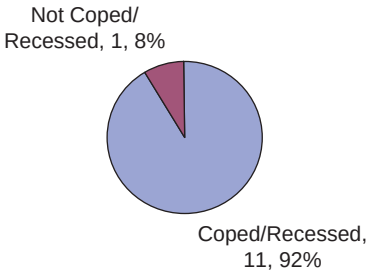

Percentages derived from number of states using the category shown divided by the total number of states responding

Figure 2.29. Wall panel coped/recessed (ACP, Question 17).

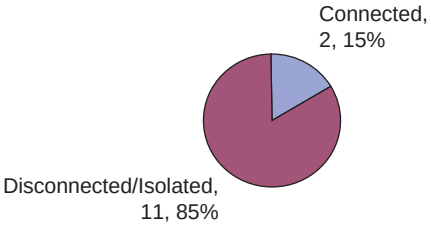

Percentages derived from number of states using the category shown divided by the total number of states responding

Figure 2.30. Lateral and vertical barrier movement connected or disconnected/isolated from wall panel (ACP, Question 19).

barrier slabs and 50% use jointed barrier slabs. Those states indicating use of jointed slabs were asked a follow-up question regarding joint spacing. The median response, shown in Table 2.1 (Question 14), was 6.1 m (20 ft). The mean, standard deviation, median, and number of responses are reported for all such questions in which length or distance was requested. Note that, if the state responded in metric units, the value was converted to U.S. customary units, and when ranges were reported, an average value was used when computing the descriptive statistics mentioned above.

Percentages derived from number of states using the category shown divided by the total number of states responding

Figure 2.31. Continuous or jointed barrier/slab footing (RCP, Question 22).

As shown in Figure 2.28, 67% of responding states report they offset their barriers from the face of the MSE wall and 33% install the barrier flush with the MSE wall. As shown in Table 2.1 (Question 16), the median barrier offset for those states that practice offsetting the barrier from the face of the MSE wall is only 140 mm (5.5 in.).

Figure 2.29 indicates that 92% of responding states recess the top wall panel into the bottom of the coping. This practice is followed to provide support for precast coping and barrier sections prior to their connection to cast-in-place slabs and as an aesthetic treatment to cover the "steps" in the panels along the top edge of the wall. The median distance that the top wall panel is recessed into the coping is 216 mm (8.5 in.) (see Table 2.1, Question 18). Additionally, 85% of states responded that lateral and vertical movement of the barrier system is isolated from the wall panels (see Figure 2.30).

Although the percentages are slightly different, the responses obtained for MSE wall applications with RCP show the same trends as the MSE wall applications in which ACP is used. The survey responses related to the use of RCP on MSE walls with barriers are presented in Figures 2.31 through 2.35. Additional information for RCP applications is presented in Table 2.2.

Table 2.1. Survey responses related to MSE walls with ACP.

Survey Question No.	Description	Mean	Standard Deviation	Median	No. of Responses
11	Thickness of barrier/slab footing (in)	15.0	4.2	13.5	12
12	Width of slab/footing (ft)	6.6	1.8	6.5	11
14	Joint spacing (ft)	32.9	28.0	20.0	6
16	Barrier offset from face of wall (in.)	7.4	9.3	5.5	8
18	Wall panel recess distance into bottom of coping (in.)	8.4	2.4	8.5	9

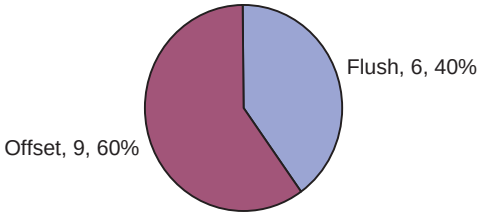

Percentages derived from number of states using the category shown divided by the total number of states responding

Figure 2.32. Flush or offset barrier from face of wall (RCP, Question 24).

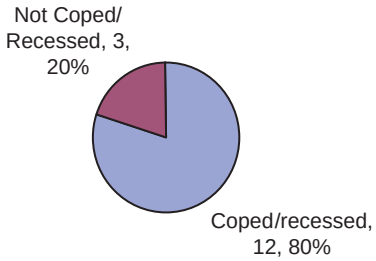

Percentages derived from number of states using the category shown divided by the total number of states responding

Figure 2.33. Wall panel coped/ recessed (RCP, Question 26).

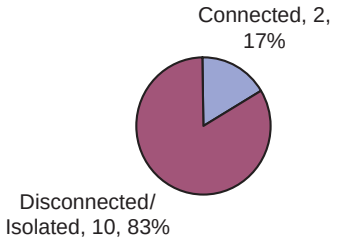

Percentages derived from number of states using the category shown divided by the total number of states responding

Figure 2.34. Lateral and vertical barrier movement connected or disconnected/isolated from wall panel (RCP, Question 28).

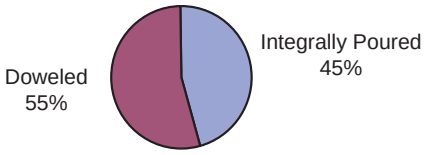

Percentages derived from number of states using the category shown divided by the total number of states responding

Figure 2.35. Integrally poured or doweled into pavement (RCP, Question 29).

Table 2.2 shows that the median barrier slab thickness (Question 20) and width (Question 21) are 305 mm (12 in.) and 2.01 m (6.6 ft), respectively. Figure 2.31 shows that 57% of the MSE walls constructed with RCP incorporate continuous barrier slabs and 43% use jointed barrier slabs. The median joint spacing for those states indicating use of jointed slabs was 6.1 m (20 ft) (see Table 2.2, Question 23).

As shown in Figure 2.32, 60% of responding states report they offset their barriers from the face of the MSE wall, while the remaining 40% install the barrier flush with the MSE wall. The median barrier offset for those states that offset their barriers from the face of the MSE wall is 140 mm (5.5 in.) (see Table 2.2, Question 25).

The practice of recessing the top wall panels into the bottom of the wall coping is followed by 80% of the responding states (see Figure 2.33). The median distance that the top wall panel is recessed into the coping is 178 mm (7 in.) (see Table 2.2, Question 27). As shown in Figure 2.34, 83% of

Table 2.2. Survey responses related to MSE walls with RCP.

Survey Question No.	Description	Mean	Standard Deviation	Median	Number of Responses
20	Thickness of barrier/slab footing (in.)	13.9	4.6	12.0	15
21	Width of slab/footing (ft)	6.7	1.2	6.6	12
23	Joint spacing (ft)	18.8	3.8	20.0	5
25	Barrier offset from face of wall (in.)	4.9	3.6	5.5	8
27	Wall panel recess distance into bottom of coping (in.)	6.9	3.8	7.0	11

states responded that lateral and vertical movement of the barrier system is isolated from the wall panels, while the remaining 17% indicated that the wall panels and barrier system are connected to one another.

A question specific to RCP applications (Question 29) is whether the barrier slab is integrally poured with the concrete pavement or doweled to it. Figure 2.35 shows that 55% of responding states use dowels to connect the barrier slab to the pavement, and 45% follow the practice of integrally casting the slab and pavement.

2.4.4 Design

For the design section of the survey, only a few of the responses can be presented in graphical format. The responses to questions referring to *NCHRP Report 350* test level (Question 31), adherence to Section 13, Railings, of *AASHTO LRFD Bridge Design Specifications* (*2*) for bridge railing design (Question 32) and whether design procedures include calculation of bending moment in the pavement slab due to impact load on barrier (Question 38) are presented below in the *Number of States Responding Positive Usage* format. Question 30 regarding the magnitude of the barrier impact load transferred to the top of the MSE wall was not included in this summary because of the high variation in the numerical value of the responses. The varying responses may have been due to confusion regarding the intent of the question.

As shown in Figure 2.36, 76% of responding states use TL-4 barriers in conjunction with MSE wall applications. TL-3 and TL-5 barriers are both used by 12% of responding states. Figure 2.37 indicates that 58% of responding states use Section 13, Railings, of the *AASHTO LRFD Bridge Design Specifications* for bridge rail design, and 42% do not. Compliance with the *AASHTO LRFD Bridge Design Specifications* is not required if a railing is successfully crash tested. The median impact load and impact location reported by the states specifying they do not follow AASHTO LRFD for bridge rail design are 44.48 kN (10 kips) and 0.84 m (2.75 ft), respectively (see Table 2.3). Only 41% of responding states reported that they calculate the bending moment in the barrier slab due to vehicular impact load (see Figure 2.38).

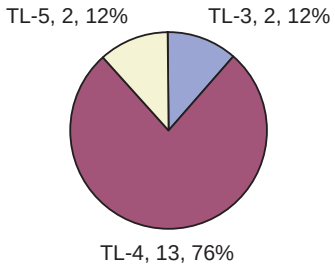

Figure 2.36. Use of NHCRP Report 350 test levels (Question 31).

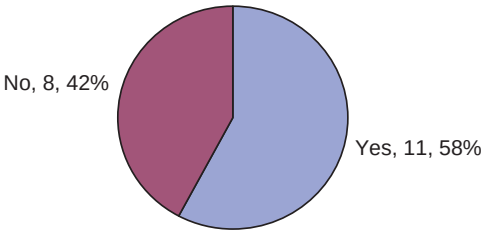

Figure 2.37. Use of AASHTO LRFD Bridge Design Specifications for rail design (Question 32).

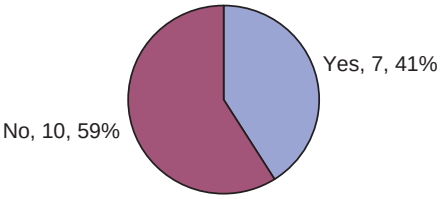

Figure 2.38. Calculation of bending moment in pavement slab due to barrier impact load (Question 38).

Table 2.3. Barrier design load and location.

Survey Question No.	Description	Mean	Standard Deviation	Median	No. of Responses
33	Magnitude of barrier design (kips)	8.4	3.6	10.0	5
34	Height of the applied design load (ft)	2.8	0.2	2.75	5

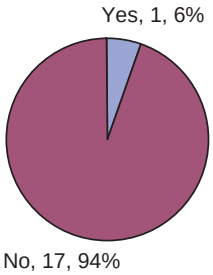

Figure 2.39. Failures of MSE walls or barriers atop MSE walls due to vehicular impact (Question 39).

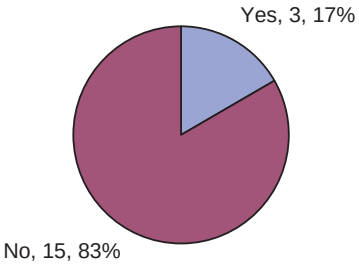

Figure 2.40. Other performance issues associated with MSE walls or barriers atop MSE walls (Question 40).

2.4.5 Performance

The last section of the survey, performance, included questions inquiring about the in-service performance and failure history of MSE walls and barriers on top of MSE walls. The survey responses for these questions are presented in Figures 2.39 and 2.40 in the *Number of States Responding Positive Usage* format based on a total of 18 responses.

The only participating agency reporting failure of an MSE wall or barrier atop an MSE wall during vehicular impact was Georgia. Georgia DOT reported that "a semi-tractor trailer knocked off a section of barrier that was lacking strap anchorages." Minnesota, New York, and Washington reported various performance issues and/or design questions associated with MSE walls or barriers atop MSE walls. Minnesota DOT reported it had seen some connection details between the barrier and the slab that are not adequate.

CHAPTER 3

Barrier Stability Study

Pavements are often built on top of MSE walls. The most common scenario is the case of an MSE wall supporting the access embankment for an overpass. Because cars and trucks travel on top of the MSE wall, traffic barriers are required. In the case of a concrete pavement, these barriers are rigidly tied to the pavement to provide the resistance needed when an impact load is generated by an errant car or truck. In the case of an asphalt pavement, that resistance is not available and the barrier must resist the impact load on its own. In this case, a barrier–moment slab system is used (Figures 3.1 and 3.2) and the resistance is generated by the inertia force required to lift the moment slab.

This chapter discusses only the barrier and moment slab design, not the MSE wall design. A barrier built on top of an MSE wall needs to be designed to satisfy three criteria during impact: (1) the barrier must have sufficient strength to contain the impacting vehicle, (2) the barrier must not overturn, and (3) the barrier must not slide away. This chapter addresses criteria 2 and 3 by defining the magnitude of the static and dynamic loads that can be resisted by a barrier attached to a moment slab. Both analytical and experimental approaches are used to better understand the behavior of the barrier–moment slab system.

3.1 Description of Barrier

The barrier used in the stability study was a TxDOT T201 barrier with a height of 0.69 m (27 in.) above grade and designed for TL-3 use. Figure 3.2 shows the dimensions of the vertical barrier and coping system as designed by RECO. The strength capacity of this vertical barrier is 325.34 kN (73.14 kips) calculated by ultimate strength analysis. The primary components of the barrier–moment slab system include a precast vertical barrier and coping section and a cast-in-place moment slab. The precast vertical barrier is 241 mm (9.5 in.) thick at the top. The cast-in-place concrete moment slab is 1.37 m (4.5 ft) wide measured from the back of the panel to the end of the moment slab. In the field, the moment slab is typically 6.1 m (20 ft) to 9.15 m (30 ft) long between joints. In this study, a smaller 3.05 m (10 ft) long moment slab and barrier section was used so that the desired movement could be imparted to the barrier without structural failure. The precast barrier unit was connected to the cast-in-place moment slab by 12 No. 6 bars. The reinforcing bars in the moment slab consist of 12 transverse No. 6 bars and 5 longitudinal No. 4 bars.

The center of gravity (CG) of the barrier system including the precast barrier, cast-in-place moment slab, and the soil above the moment slab is located as shown on Figure 3.2. The rotation point used for the overturning analysis is at the toe of the coping as shown in Figure 3.2. A concrete pad was placed under the inside leg of the coping so that the point of rotation would be well defined. The outside leg of the coping was unsupported. The moment arm l is from the CG of the barrier to the rotation point. The point of load application is located near the top of the barrier. The moment arm h is from the point of application of the load to the point of rotation A.

The moment slab was cast in place on a well-graded road base material with a significant amount of fines and particles as large as 50 mm (2 in.). This material was heavily compacted by a hydraulic plate tamper attached to the back of a backhoe. The dry density and water content of the soil in place were 18.6 kN/m^3 (118.3 pcf) and 7.17%, respectively.

3.2 Static Analyses and Static Test

The purpose of the static analyses and static test is to explain the behavior of the barrier under static loading and to determine the maximum static force that can be resisted by a barrier in a sliding failure mode and in an overturning failure mode.

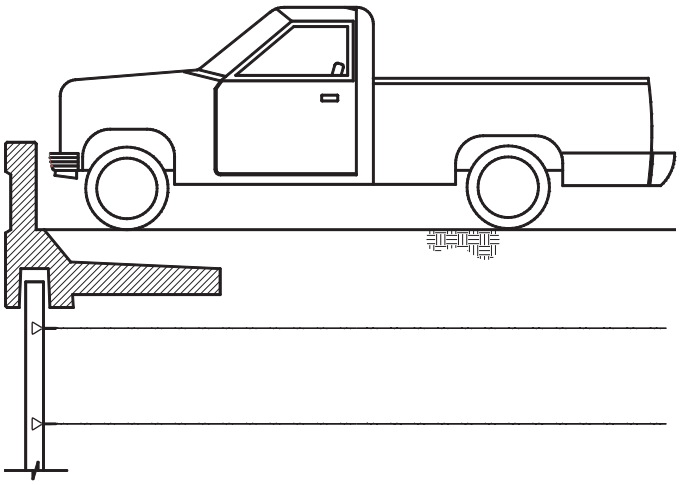

Figure 3.1. MSE retaining wall with a barrier.

3.2.1 Static Analytical Solution

The static analysis for sliding and overturning is conducted using equilibrium equations. The static force (F_s) required to generate sliding is:

$$F_s = W \tan\phi \tag{3-1}$$

where

W = weight of the barrier, moment slab, and soil system (69.6 kN or 15.7 kips)
$\tan\phi$ = moment slab–soil friction coefficient
ϕ = frictional angle of the soil

For this analysis, it is assumed that the moment slab–soil interface is rough enough that the failure plane is in the soil.

The equation for overturning equates the resisting moment and the moment causing overturning due to the applied force. The static force (F_o) required to generate overturning of the barrier–moment slab assembly is:

$$F_o = Wl/h \tag{3-2}$$

where

l = moment arm of the weight of the system (0.369 m or 1.2 ft)
h = moment arm of the force applied to the system [1.21 m (3.97 ft); see Figure 3.2].

It is assumed that the vertical barrier, moment slab, and overburden soil act as one system for the overturning analysis.

The required static forces F_s and F_o are shown on Figure 3.3 as a function of the length of the barrier–moment slab system. For the 3.05 m (10 ft) length barrier system, the required static force is 46.96 kN (10.6 kips) for sliding and 20.9 kN (4.7 kips) for overturning. Therefore, overturning controls the stability of the barrier in this case. There could be some situations where the friction between the bottom of the barriers and the soil is low enough that sliding occurs. As such both criteria should be checked.

3.2.2 Quasi-static Finite Element Analysis

To further study of the static response of the barrier–moment slab system, a finite element model of the 3.05 m (10 ft) long barrier–moment slab system was developed (Figure 3.4) for use in LS-DYNA. LS-DYNA (*20*) is a general-purpose, nonlinear, explicit finite element code used to analyze the nonlinear dynamic response of three-dimensional structures. The code was originally developed by John Hallquist at Lawrence Livermore National Laboratory and has since been enhanced by Livermore Software Technology Corporation.

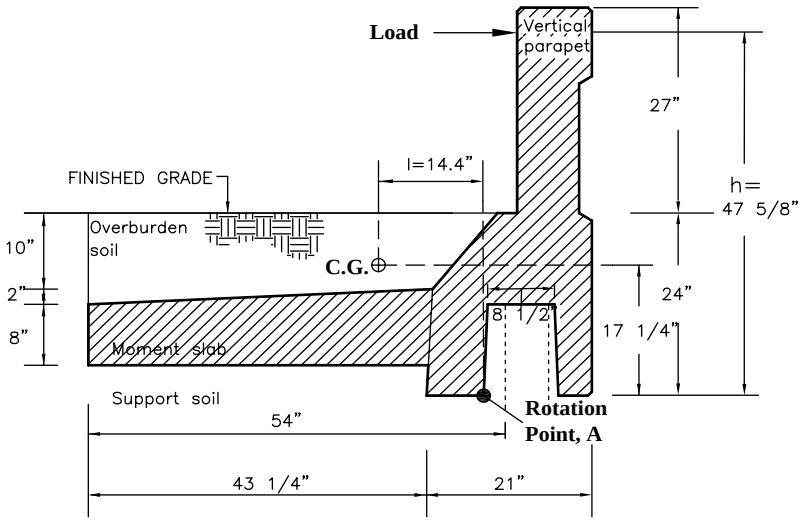

Figure 3.2. Details of the vertical barrier system.

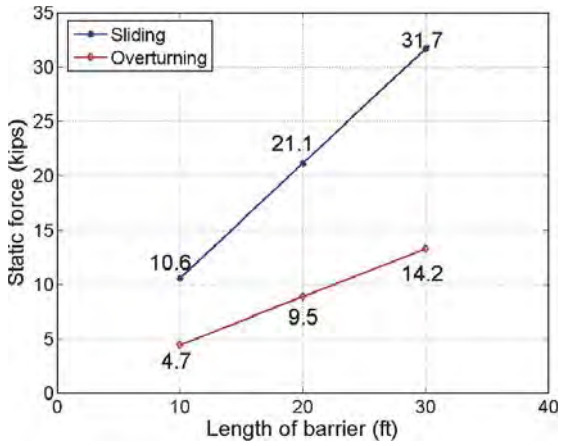

Figure 3.3. Required static force to induce sliding or overturning.

Over the past 10 years, LS-DYNA has been extensively used in the performance evaluation of roadside safety hardware.

The vertical barrier, the moment slab, and the support pad at the bottom of the coping were represented by solid elements and defined as elastic materials (designated as MAT type 1 in LS-DYNA) with concrete material properties shown in Table 3.1. The soil was also represented by solid elements and defined as an elastic-plastic material (designated as MAT type 25 in LS-DYNA) with the properties shown in Table 3.1. Details of soil material model are presented in Chapter 5. The barrier stability model had a total of 34,274 solid elements.

The interface between the soil and barrier was modeled using contacts to capture the interface force generated between the concrete structure and the soil. A wood block was used as a means of providing distribution of the applied controlled quasi-static loading definition. The size of the wood block corresponded to the block used in the static load test. The model was initialized to account for gravitational loading on the soil mass before the application of the static load.

The barrier system failed by overturning, not by sliding. The result of the simulation is presented in Figure 3.5 as a load-displacement curve. The maximum load in the simulation is 35 kN (7.9 kips) while the static hand calculations gives 21.8 kN (4.9 kips). The difference is the soil resistance at the edges of the moment slab, which is accounted for in the simulation but not in the hand calculations.

3.2.3 Full-Scale Static Test on Barrier

The purpose of the static load test was to verify the magnitude of force on the barrier required to initiate movement of the barrier–moment slab system. The setup for the static load test of the barrier system is illustrated in Figures 3.6 and 3.7. A reaction post was anchored to an existing concrete apron. The load was applied to the top edge of the vertical concrete barrier by means of a hydraulic cylinder. The load was distributed over a longitudinal barrier length of 1 m (3 ft) through the use of a steel spreader beam with a wood block applied to its face. An in-line load cell was used to measure the applied load. The load was applied in steps of 2.5 kN (500 lb), with each step lasting about 5 min. Displacement of the barrier, coping, and moment slab was recorded at the end of each load step using two dial gauges and a linear variable differential transformer (LVDT) displacement sensor (D1). The LVDT was positioned behind and along the centerline of the barrier near its top edge. A dial gauge was placed along the same centerline near the bottom edge of the coping (D2). These two displacement measurement devices were secured to a steel frame. When the lateral load applied to the top of the barrier reached 36 kN (8 kips), the

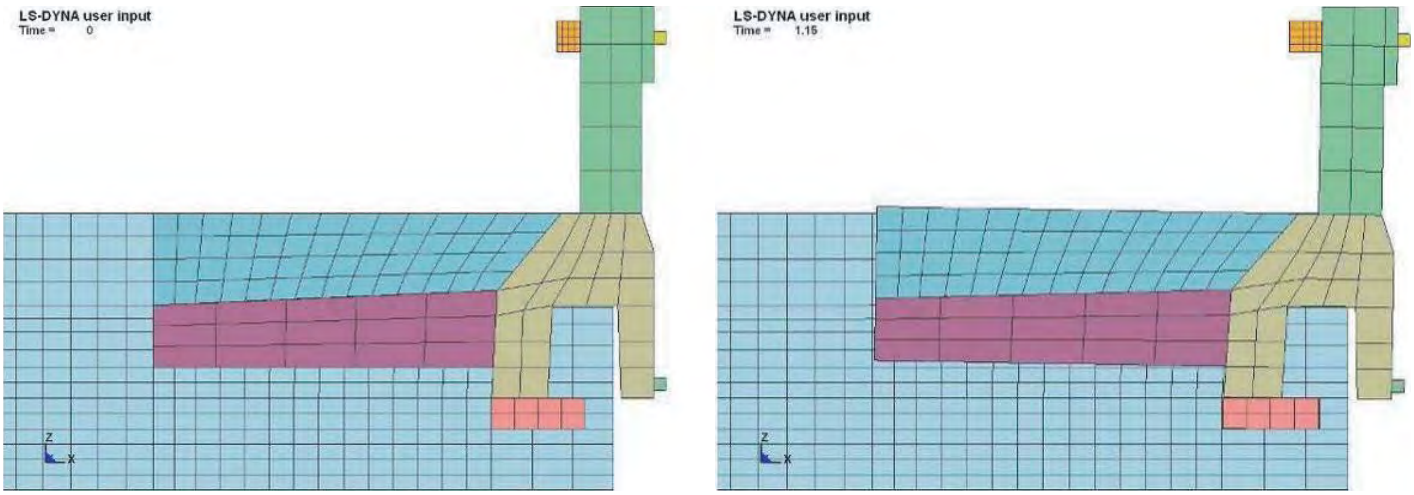

(a) (b)

Figure 3.4. Quasi-static finite element model at (a) rest and (b) end of the time.

Table 3.1. Material properties of vertical barrier, moment slab, and soil.

Material	Model	E (psi)	ν	ρ (lb/in^3)
Concrete	Vertical barrier, moment slab, and concrete pad	3.62E+6	0.17	0.084
Soil	Overburden soil and support soil	0.00288	0.35	0.076

E is Young's modulus, ν is Poisson's ratio, and ρ is the mass density.

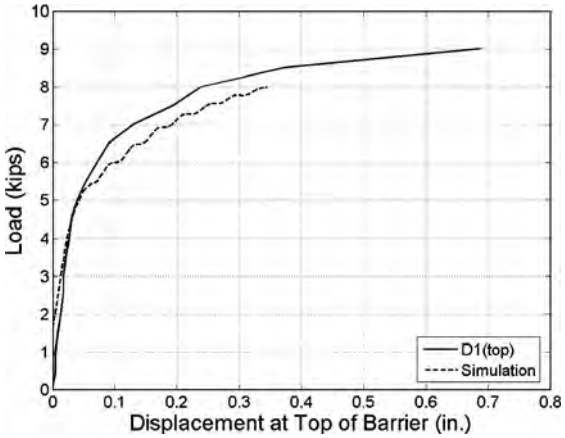

Figure 3.5. Comparison of static test and finite element static model.

soil began to crack along the edges of the moment slab. The load test was stopped at a load of 40 kN (9 kips).

The force-displacement curves generated from the test data are shown in Figure 3.8. The load-deflection response of the barrier–moment slab system was linear up to a load of 22.3 kN (5 kips). This load corresponds quite well with the load capacity of this 3 m (10 ft) barrier system based on the static equilibrium analysis shown previously (Figure 3.3). Figure 3.8 indicates that the barrier had moved 1 mm (0.04 in.) at a load of 22.3 kN (5 kips). Upon further loading beyond 22.3 kN (5 kips), the displacement of the barrier increased in a more rapid, nonlinear manner. As shown in Figure 3.8, the final horizontal displacement at the top of the barrier (D1) was 18 mm (0.69 in.), while the displacement at the bottom of the coping (D2) was only 3 mm (0.114 in.). This indicates that the barrier–moment slab system experienced

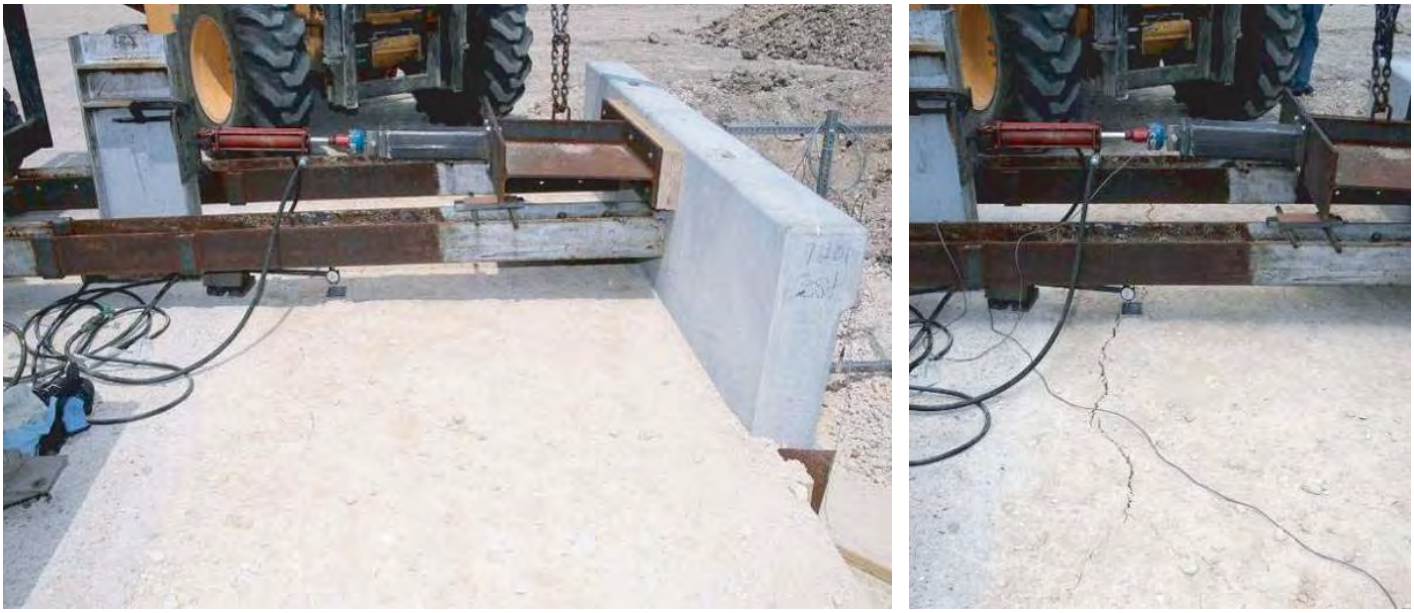

(a) **(b)**

Figure 3.6. Static test at (a) beginning of test and (b) end of test (note crack).

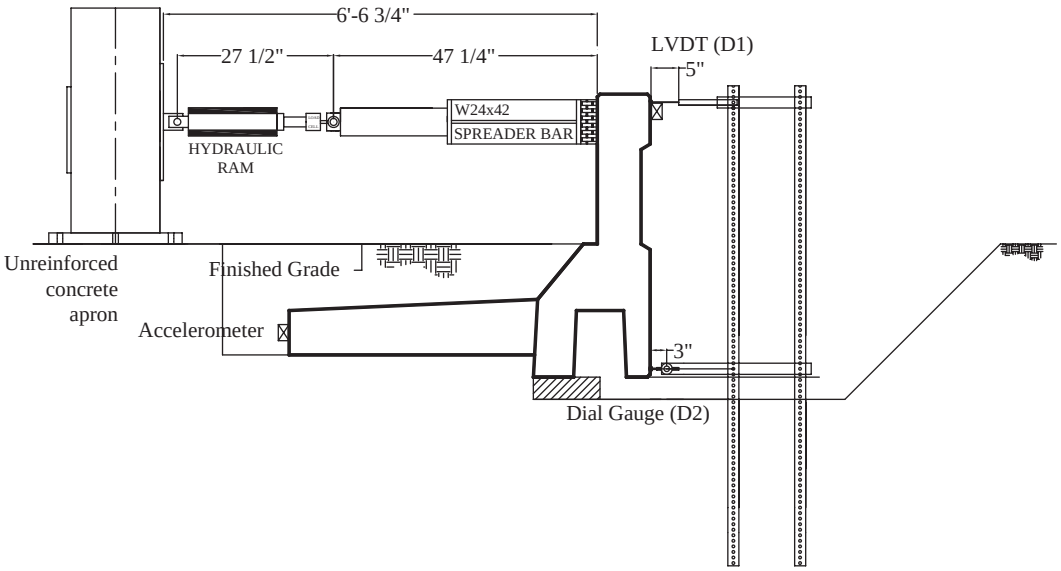

Figure 3.7. Static test installation.

mostly a rotation failure with some sliding. At the time the load test was stopped, the shear strength of the soil had been exceeded and the load-deflection curve was nearly asymptotic.

Figure 3.5 shows the load test results compared to the numerical simulation. This comparison indicates that the static resistance is made of two components: the component due to the weight of the moment slab and overburden soil, and the component due to the friction between the moment slab–overburden soil and the surrounding soil. Back-calculations indicate that the average shear strength of the concrete–soil interface at that shallow depth was 6.3 kPa or 126 psf. The results confirm that overturning is the likely mode of failure since sliding develops more resistance. This comparison also gives credibility to the numerical simulation.

3.3 Dynamic Analyses and Dynamic Test

The purpose of these dynamic analyses is to explain, theoretically, the behavior of the barrier during impact and the results of the full-scale impact test. The purpose of the full-scale impact test is to verify the theoretical results and collect data at full scale.

3.3.1 Full-Scale Dynamic Test (Bogie Test) on Barrier

Upon completion of the static load test, the soil on and around the moment slab was recompacted for a dynamic bogie impact. Two accelerometers were mounted to the bar-

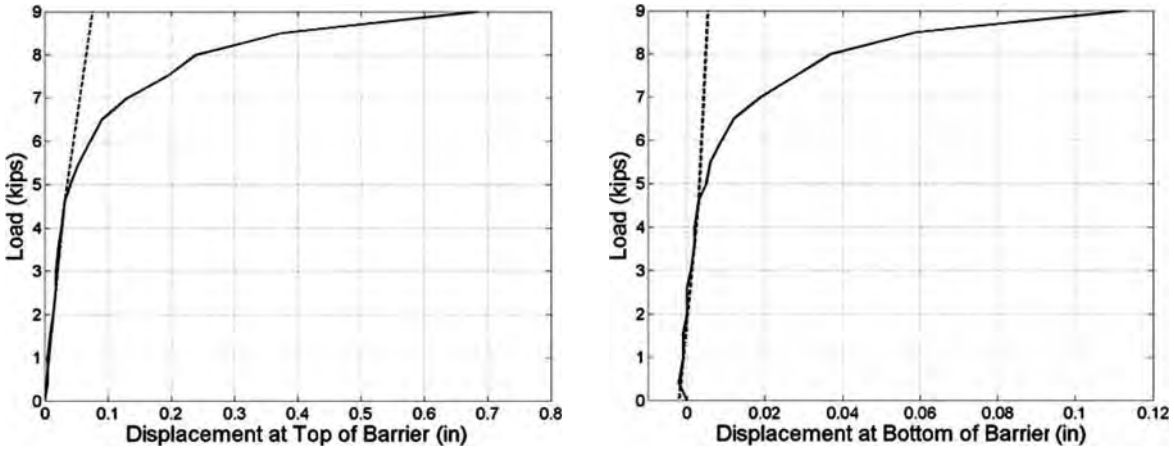

Figure 3.8. Results of static test of (a) D1 and (b) D2.

rier system to help analyze its dynamic behavior: one behind and along the centerline of the barrier at the height of impact oriented to measure longitudinal acceleration, and one on the end of the moment slab oriented to measure vertical acceleration. Additionally, the bogie vehicle was instrumented with an accelerometer.

In the first test, the 2,268 kg (5,000 lb) bogie vehicle [Figure 3.9(a)] impacted the center of the vertical barrier head-on at a speed of approximately 20.9 km/h (13 mph). The barrier system after impact is shown in Figure 3.9(b). The targets affixed to the end of the vertical barrier section were used as reference points to determine angular and translational displacement of the barrier from high-speed video. From the film analysis, the maximum dynamic displacement of the barrier was 200 mm (4.9 in.) at the top and 69 mm (2.7 in.) at the ground level [Figure 3.10(a)]. The maximum dynamic rotation angle of the barrier–coping section was 4.8 degrees. In addition to the rotation, the barrier also experienced approximately 25 mm (1 in.) of sliding. After the bogie impact, the barrier rebounded slightly and came to rest with a permanent displacement of 61 mm (2.4 in.) at the top and 36 mm (1.4 in.) at the ground level, with a rotation angle of 3.5 degrees.

Data obtained from the bogie-mounted accelerometer were analyzed and the results are presented in Figure 3.11. The acceleration history was treated using a 50-millisecond (ms) moving average (which is typically the duration selected for design) and then an SAE 60 Hz filter (which is used to reduce the noise in the data). As shown in Figure 3.11(b), the maximum deceleration was 8.5 *g*. Based on this acceleration and the mass of the bogie, the maximum impact force was calculated to be 189 kN

(a) before test

(b) after 13 mph test

(c) after 18 mph test

Figure 3.9. Bogie test photo.

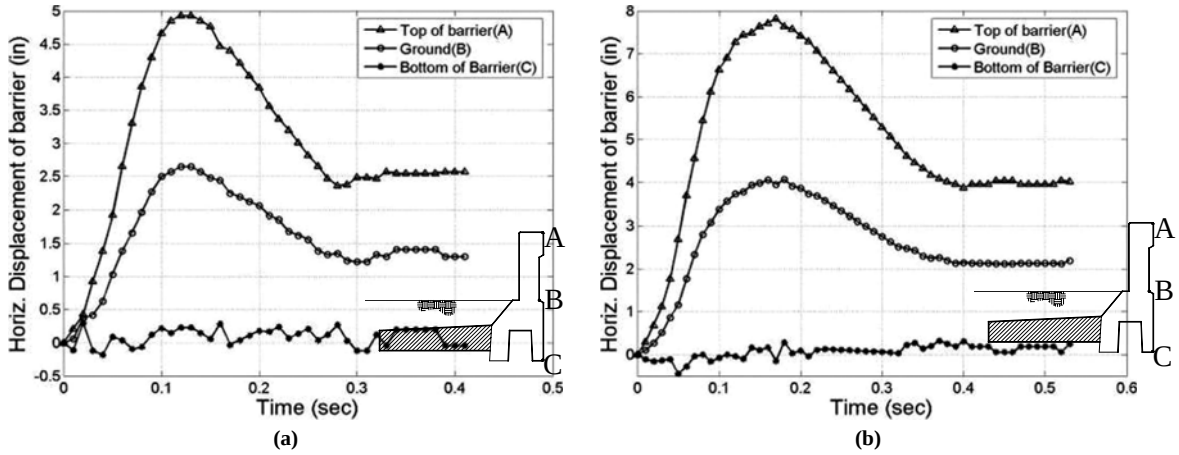

Figure 3.10. Horizontal displacement of barrier measured from the film of the (a) 13 mph and (b) 18 mph impact test.

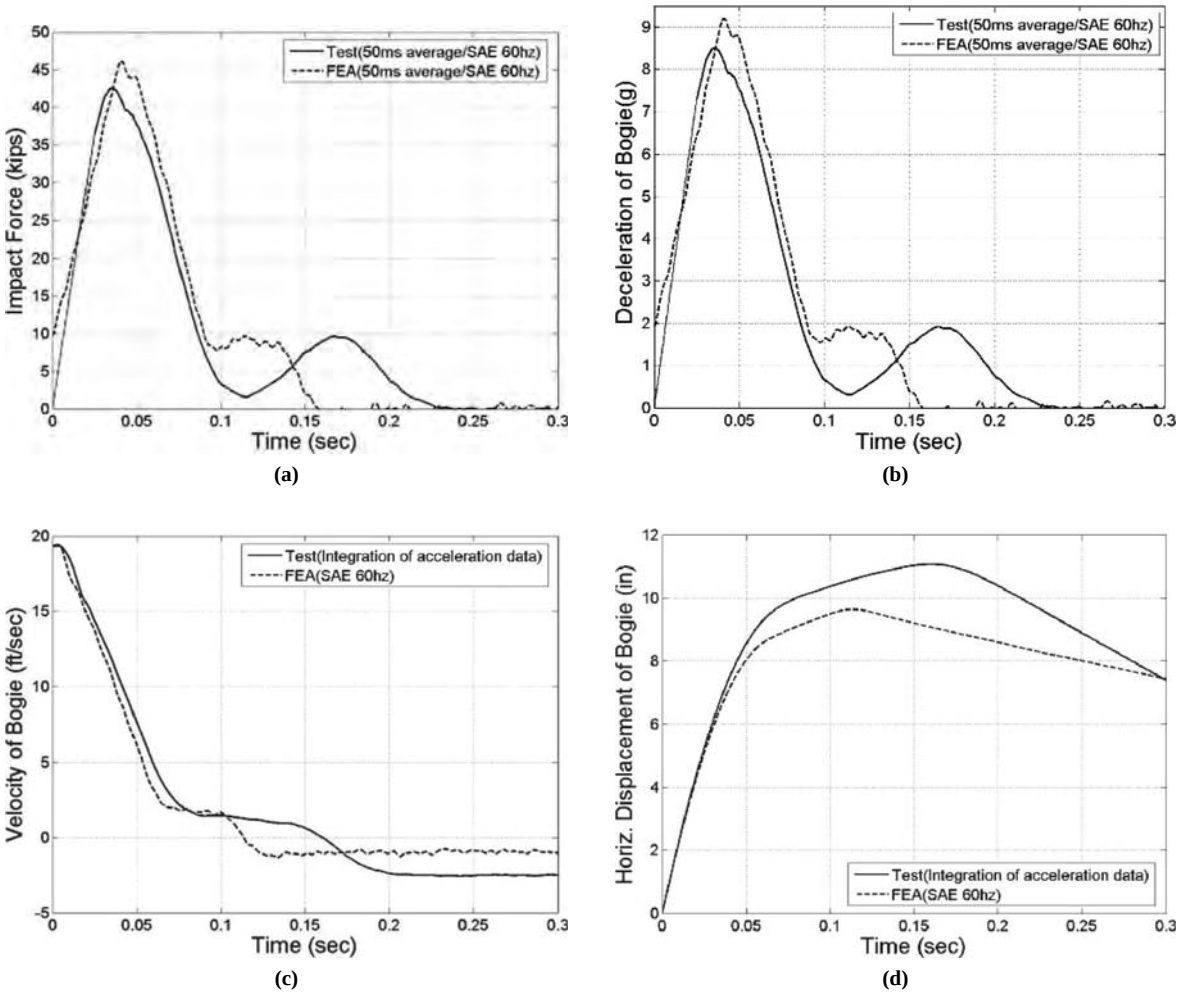

Figure 3.11. (a) Force, (b) acceleration, (c) velocity, and (d) displacement of bogie of the 13 mph dynamic test.

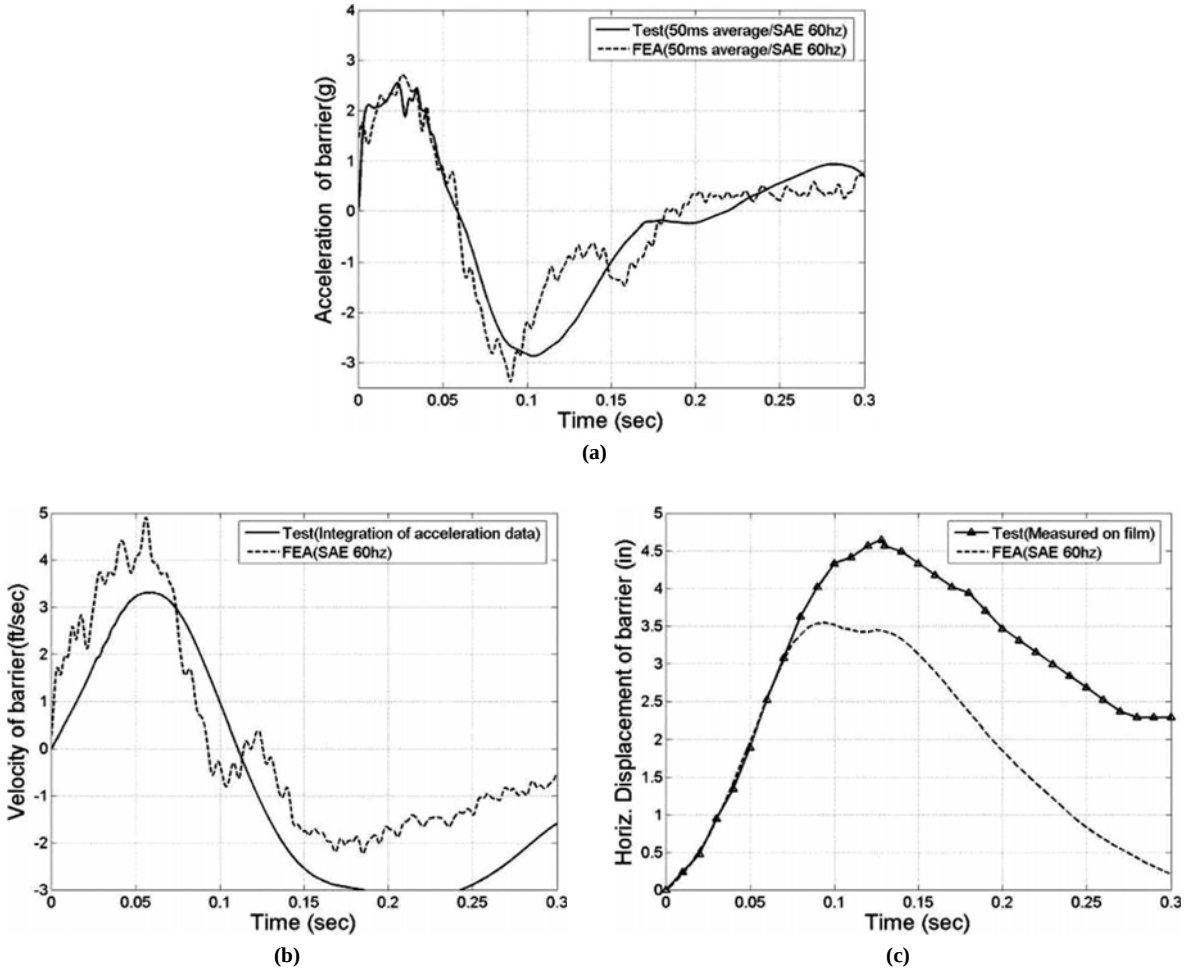

Figure 3.12. (a) Acceleration, (b) velocity, and (c) displacement of barrier of 13 mph dynamic test.

(42.5 kips) [Figure 3.11(a)]. The velocity–time and horizontal displacement–time histories of the bogie are shown in Figure 3.11(c) and (d), respectively. The maximum acceleration of the barrier, as measured by the accelerometer at the top of the barrier, was 2.8 *g* in the impact direction [Figure 3.12(a)]. The velocity–time history of the barrier, as calculated by integration of the acceleration data, is shown in Figure 3.12(b). Figure 3.12(c) presents the horizontal displacement–time history of the barrier as determined by double integration of the acceleration data and through analysis of high-speed film.

The maximum acceleration of the moment slab, as measured by the accelerometer on the end of the moment slab (Figure 3.13), was 2.2 *g* in the vertical direction [Figure 3.13(a)]. The velocity–time history and vertical displacement–time history of the end of the moment slab, as calculated by integration of the acceleration data, is shown in Figure 3.13(b) and (c), respectively. The maximum vertical displacement of the moment slab at its free edge was computed to be 91.4 mm (3.6 in.).

After recompacting the soil on and around the moment slab, a second full-scale impact test was performed at a higher velocity of 28.97 km/h (18 mph). The barrier system after impact is shown in Figure 3.9(c). From the film analysis, the maximum dynamic displacement of the barrier was 198.4 mm (7.81 in.) at the top of the barrier and 104 mm (4.09 in.) at the groundline. The maximum dynamic rotation angle of the barrier–coping section was 7.84 degrees. The displacement at the bottom of the coping was computed to be less than 7.6 mm (0.3 in.) [Figure 3.10(b)]. This displacement indicates that sliding did not occur. The acceleration history was treated using the same manner as with the 13 mph test. The maximum deceleration was 10.9 *g* as shown in Figure 3.14(b). Using the acceleration and mass of the bogie impact vehicle, the maximum impact force was calculated to be 240.65 kN (54.1 kips) (Figure 3.14).

The maximum 50 msec average acceleration of the barrier, as measured by the accelerometer at the top of the barrier, was 2.5 *g* in the direction of impact [see Figure 3.15(a)]. The

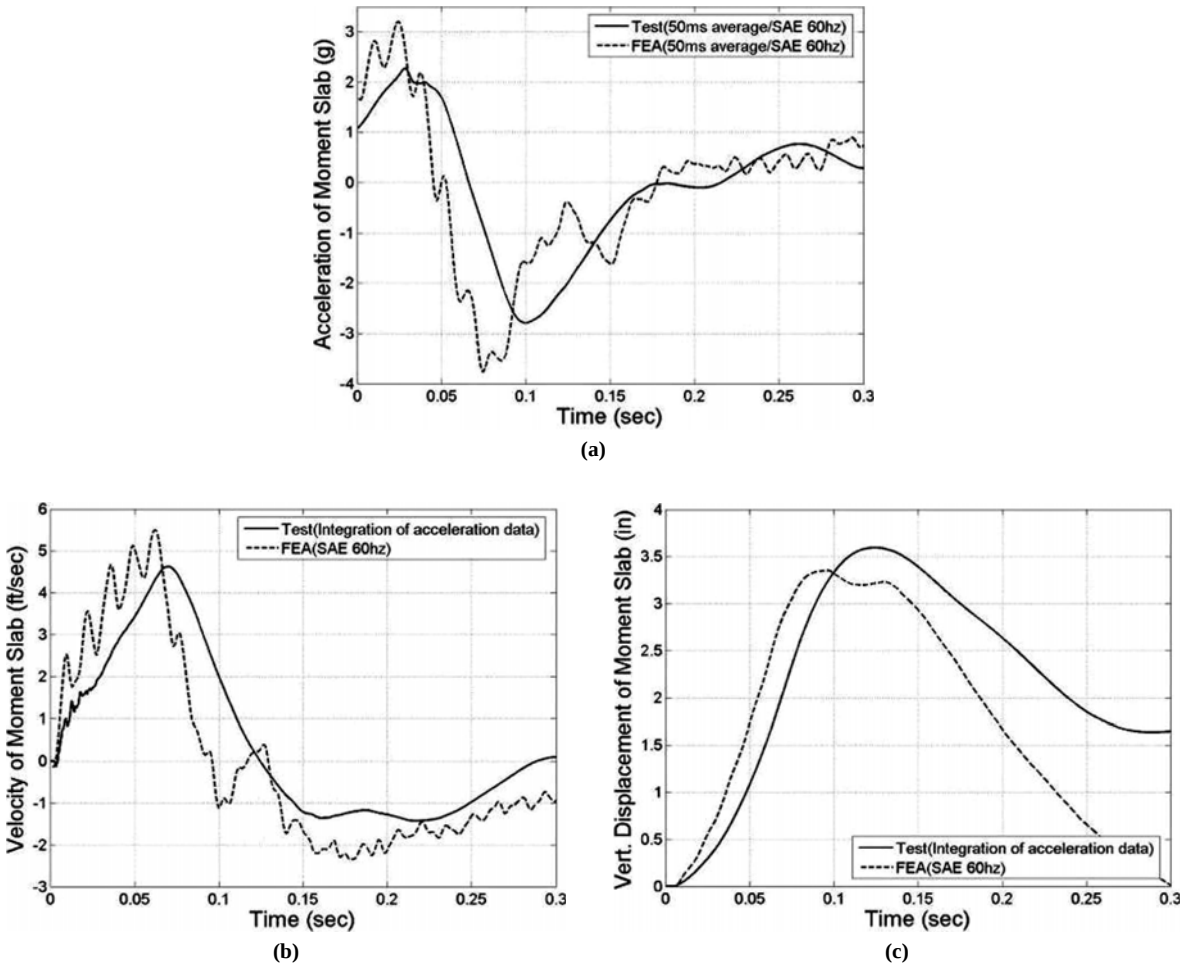

Figure 3.13. (a) Acceleration, (b) velocity, and (c) displacement of moment slab of the 13 mph dynamic test.

displacement–time history obtained from double integration of the acceleration history looked suspect and was thought to be in error. Therefore, high-speed film was used to determine the displacement–time history of the barrier shown in Figure 3.15(b).

The maximum acceleration of the moment slab, as measured by the accelerometer on the end of the moment slab (Figure 3.16), was 3.9 *g* in the vertical direction. The acceleration data was lost at some time during test; therefore, the maximum displacement of the moment slab could not be determined.

Figure 3.17 shows the comparison of the load-displacement curves for the static test and the dynamic tests. As can be seen, the ratio between peak dynamic force and the peak static force is 4.5 for the 20.9 km/h (13 mph) impact test and 5.4 for the 28.97 km/h (18 mph) impact test.

After the second dynamic bogie impact test, the overburden soil was removed to permit inspection of the moment slab and the connection between the coping and moment slab. Prior to impact [see Figure 3.18(a)], no cracking was evident in the barrier, coping, or moment slab. After impact, thin cracks were observed in the coping and moment slab on each side of the test specimen as shown in Figure 3.18. A red marker was used to highlight the cracks to assist with documentation.

Cracking observed on the top surface of the moment slab is shown in Figure 3.19. These cracks coincide with the location of reinforcing bars connecting the coping to the moment slab. The cracks in the center of the moment slab (directly beneath the point of impact on the barrier) are longer and more pronounced than those toward the ends of the moment slab. The close-up view shown in Figure 3.19(d) illustrates the transverse cracks over the reinforcing bars as well as a longitudinal crack along the cold joint between the coping and moment slab. Again, a red marker was used to highlight the cracks to assist with visualization and documentation.

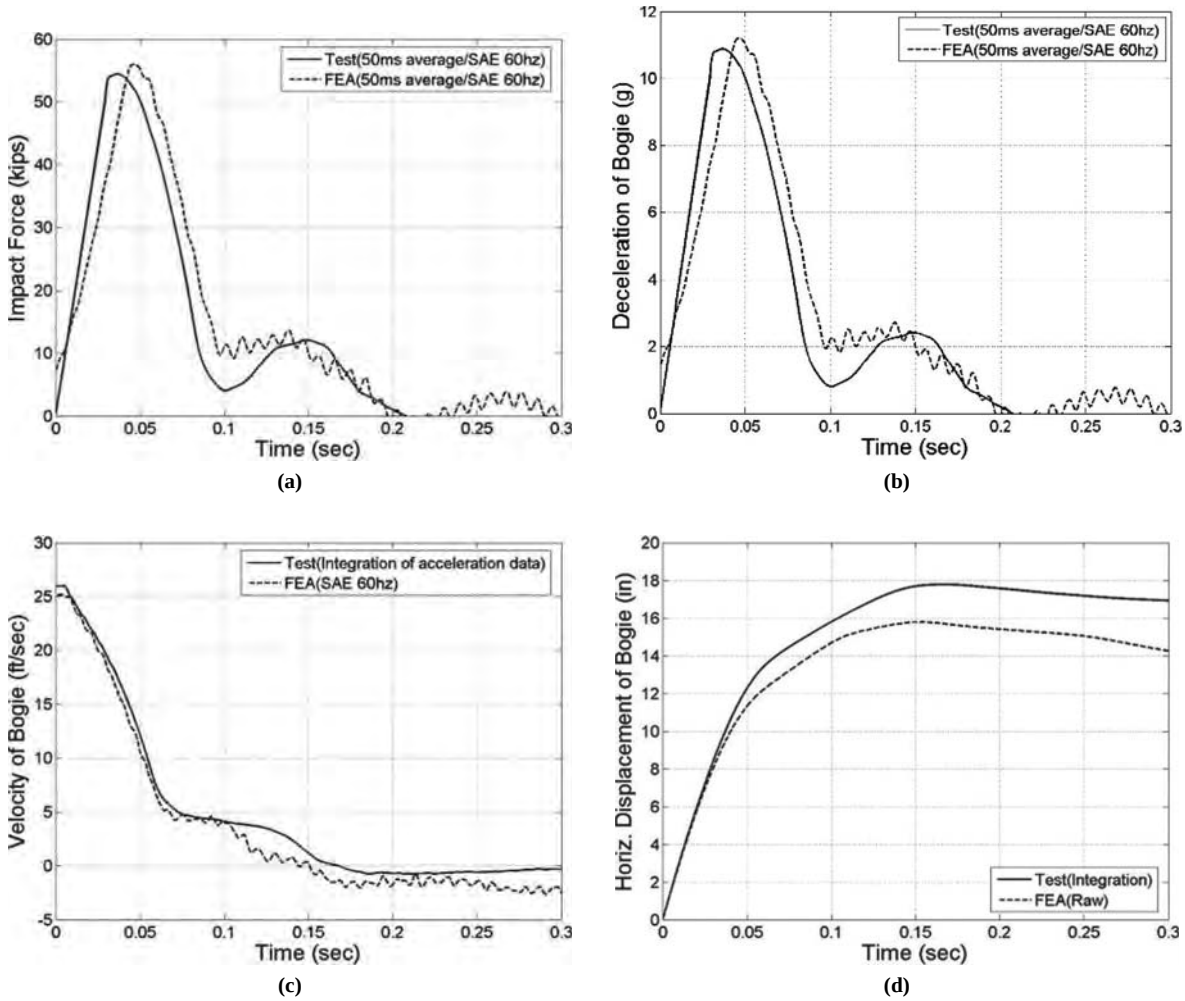

Figure 3.14. (a) Force, (b) acceleration, (c) velocity, and (d) displacement of bogie of the 18 mph dynamic test.

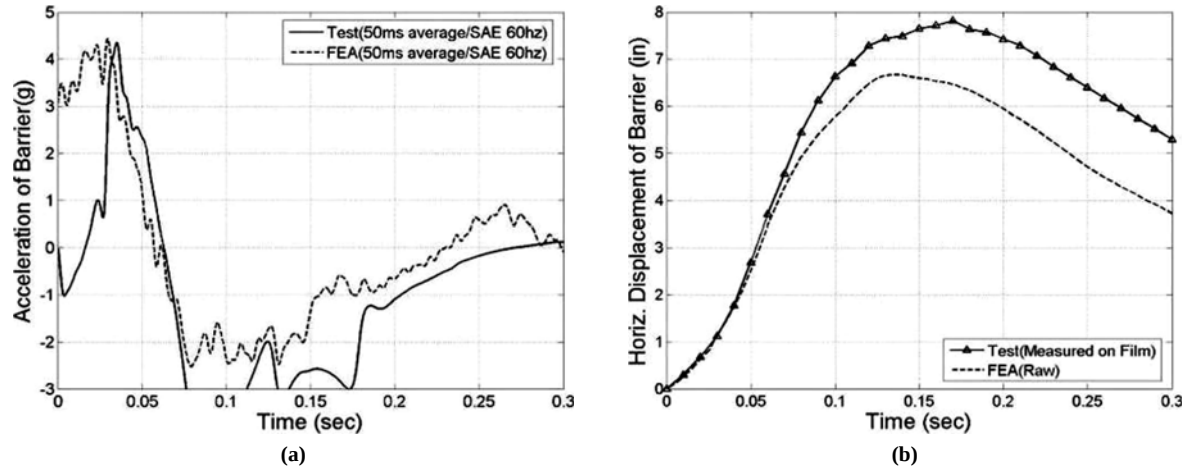

Figure 3.15. (a) Acceleration and (b) displacement of barrier of 18 mph dynamic test.

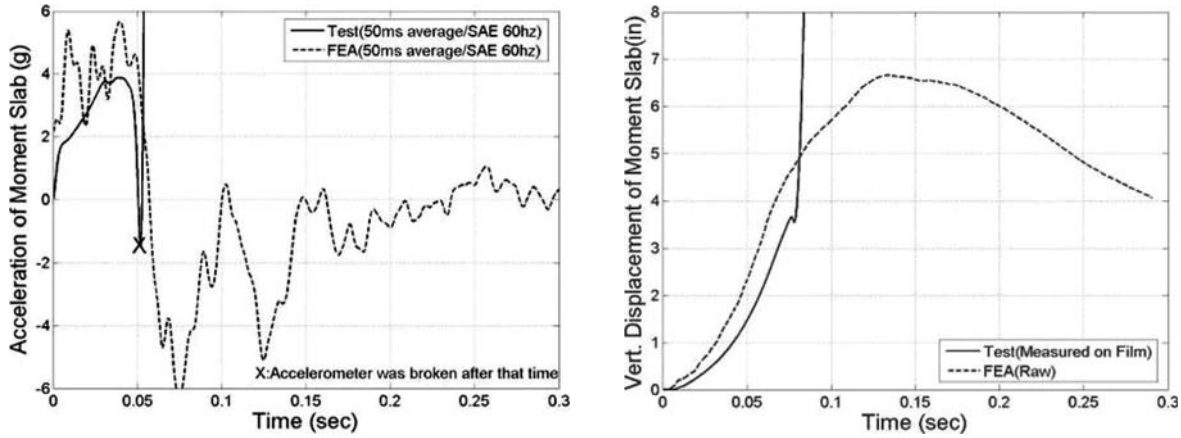

Figure 3.16. (a) Acceleration and (b) displacement of moment slab of the 18 mph dynamic test.

3.3.2 Dynamic Analytical Simple Solution

Sliding

The fundamental equation of motion is:

$$\sum F_x = m\vec{a} \tag{3-3}$$

where

ΣF_x = sum of the external forces applied to the mass (m)
a = acceleration of the mass.

In the horizontal direction, the external forces consist of the impact force at the top of the barrier (F_{impact}) and the friction force (F_{friction}) at the bottom of the barrier.

$$F_{\text{impact}} - F_{\text{friction}} = m\vec{a} \tag{3-4}$$

The impact force is obtained from the product of the mass of the bogie times the acceleration of the bogie [Figure 3.11(a)].

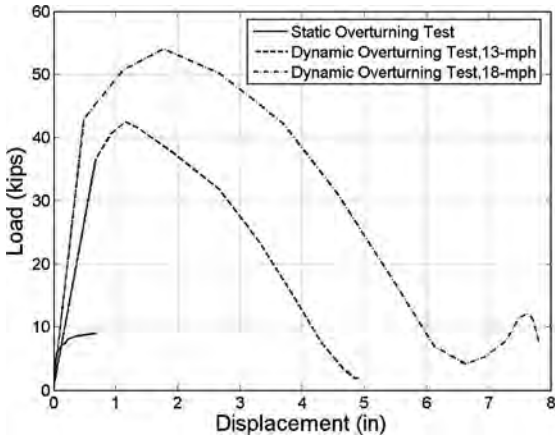

Figure 3.17. Comparison of static and dynamic overturning tests.

The trace of this force as a function of time was simplified to a triangular shape as shown in Figure 3.20(a). The friction force is equal to the coefficient of friction tan ϕ, where ϕ is the friction angle of the soil–moment slab interface, multiplied by the total weight (W) of the barrier. The weight of the barrier system as shown in Figure 3.2 is 69.6 kN (15.65 kips). The friction angle of the soil was taken as 35 degrees. The mass of the barrier system is 7,096 kg (486 slug or 15,640 lb mass). Knowing the impact force, the friction force, and the mass of the barrier system, the acceleration of the barrier can be found using Equation 3-4. The result is shown in Figure 3.20(b). The velocity history as a function of time was obtained by integration of the acceleration–time history curve [Figure 3.20(c)]. Similarly, the displacement history as a function of time was obtained by double integration of the acceleration–time history curve [Figure 3.20(d)].

Overturning

The fundamental equation for the rotation of the barrier (*21*) is:

$$\sum M_A = I_A\alpha \tag{3-5}$$

where ΣM_A is the sum of the external moments around point A applied to the barrier, which has a mass moment of inertia (I_A) around the point of rotation and an angular acceleration (α). The external moments are the moment due to the impact force and the moment due to the weight of the barrier (Figure 3.2) which gives:

$$\left(F_{\text{impact}} \times h\right) - \left(W \times l\right) = I_A\alpha \tag{3-6}$$

As mentioned before, the impact force [Figure 3.20(a)] and the weight of the barrier are known. The moment arms h

(a) before test

(b) after test

Figure 3.18. Cracking of coping and moment slab after 18 mph impact.

and l are known (Figure 3.2) and assumed to be constant in a first analysis. The mass moment of inertia around the center of gravity can be expressed as

$$I_{CG} = \frac{1}{12}\sum m_i\left(x_i^2 + y_i^2\right)$$

where the m_i values are the mass components of the barrier and the x_i and y_i values are the distances in the x and y directions from the individual centers of gravity of the mass components m_i and the CG of the entire barrier. To obtain the mass moment of inertia (I_A) with respect to an axis going through A different from the CG, one can use

$$I_A = I_{CG} + m(\bar{x}^2 + \bar{y}^2)$$

where the term $\bar{x}^2 + \bar{y}^2$ represents the square of the distance from the rotation point A to the CG. The mass moment of inertia (I_A) was found to be 4,691 kg-m^2 (3,460 slug ft^2). Knowing the impact force, the weight, the moment arms, and the

(a) Center of moment slab

(b) Right end of moment slab

(c) Left end of moment slab

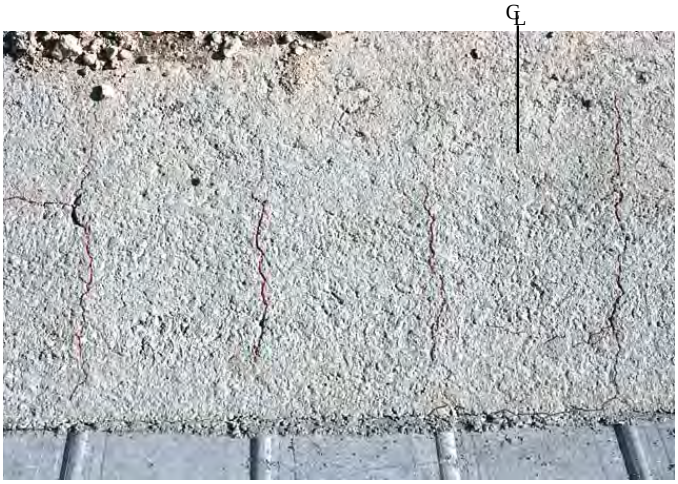

(d) Closeup near center of moment slab

Figure 3.19. Cracks observed on top of moment slab after 18 mph impact.

mass moment of inertia, one can obtain the angular acceleration (α) by using Equation 3-6. The linear acceleration at the point of impact is obtained by [Figure 3.21(b)]:

$$\vec{a}_{(t)} = \alpha_{(t)} \times h \tag{3-7}$$

Then the velocity history as a function of time at the same point [Figure 3.21(c)] was obtained by integration of the acceleration–time history curve. Similarly, the displacement history as a function of time was obtained by double integration of the acceleration–time history curve [Figure 3.21(d)].

Dynamic Analytical Advanced Solution

This solution addresses only the overturning case because it is the controlling case. Indeed the sliding requires a higher impact force to occur as shown in the previous static and dynamic analytical solutions. When the barrier rotates around A, the moment arms *h* and *l* are not constant as assumed in the first analysis. They can be expressed as:

$$h_{(t)} = h_0 \cos\left(\theta_{(t)}\right) \tag{3-8}$$

$$l_{(t)} = l_0 \cos\left(\theta_{(t)}\right) \tag{3-9}$$

where *t* is the time elapsed after impact and $\theta_{(t)}$ is the rotation angle. The moment arms vary as shown in Figure 3.22(a) and (b). Because the moment arms vary with time, it is necessary to calculate the acceleration, velocity, and displacement in time steps. The results are shown on Figure 3.21. Also shown on Figure 3.21 are the results obtained when assuming that the moment arms do not vary in time. As can be seen there is not much difference in the results.

3.3.3 Dynamic Finite Element Analysis

A finite element analysis using LS-DYNA was performed to simulate the dynamic impact behavior of the 3.05 m (10 ft) long vertical barrier–moment slab system. The results were used to further investigate the overturning behavior of the system when subjected to a dynamic impact load and to calibrate

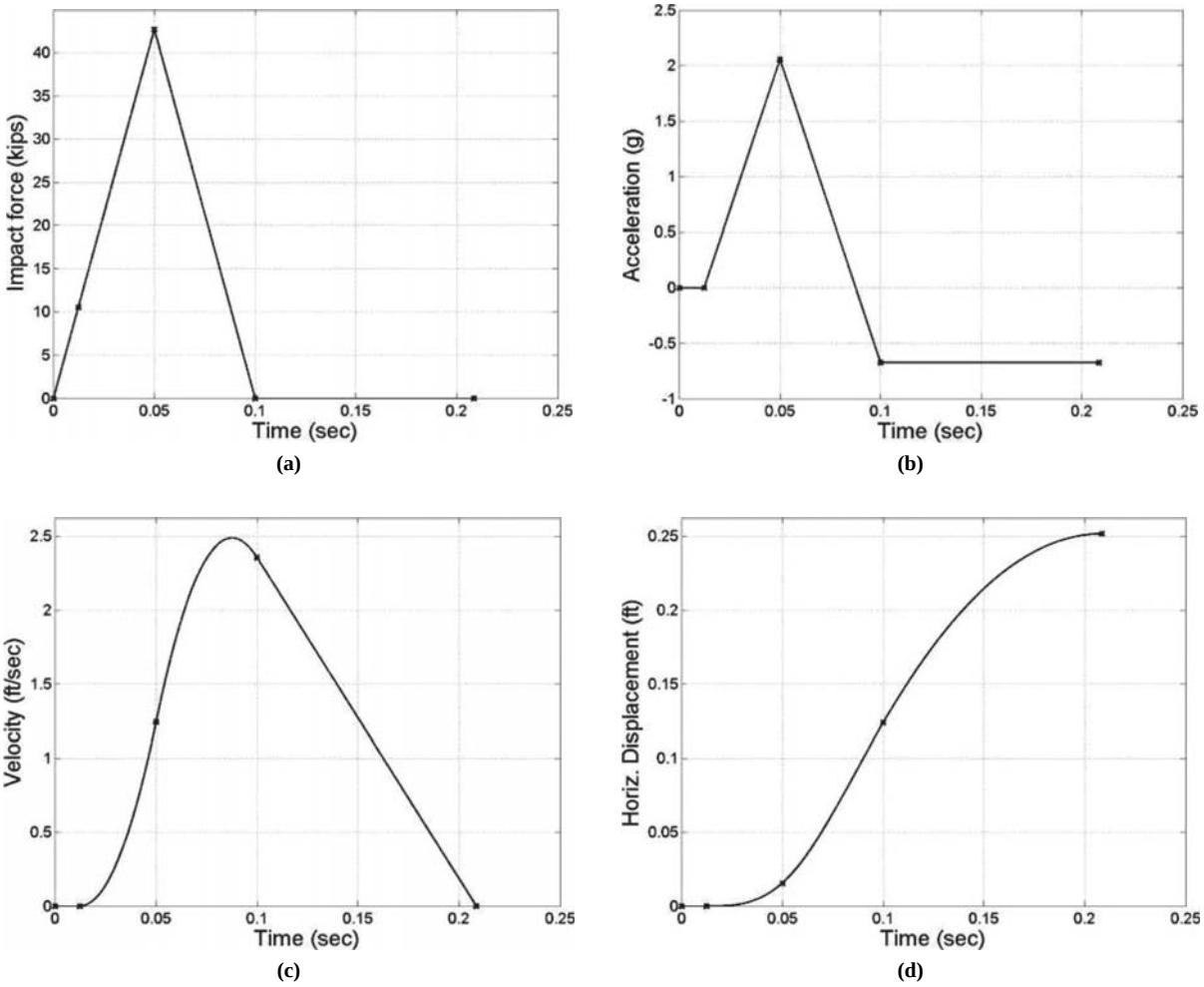

Figure 3.20. Analytical solution for sliding: (a) force, (b) acceleration, (c) velocity, and (d) displacement.

the model to improve the accuracy of subsequent predictive simulations used to design additional impact experiments. The system geometry and material properties used for the model were the same as those used in the quasi-static model. A 2,268 kg (5,000 lb) bogie was used to hit the barrier at a speed of 20.9 km/h (13 mph). Additionally, two accelerometers were incorporated into the finite element model to obtain accelerations of the barrier and moment slab for a comparison with the accelerations measured in the bogie tests (Section 3.3.1). The model was initialized to account for gravitational loading on the soil mass before the dynamic bogie impact. Figure 3.23 shows images from the 20.9 km/h (13 mph) dynamic bogie impact simulation.

The deceleration of the bogie during impact as calculated by the finite element analysis is compared to the measured deceleration of the bogie in Figure 3.11(b). The comparison is reasonably good. The acceleration of the top of the barrier during the impact as calculated by the finite element analysis is compared to the measured acceleration at the top of the barrier in Figure 3.12(a). The comparison is also reasonably good. The horizontal displacement at the top of the barrier is compared to the measured displacement of the barrier obtained by high-speed film analysis in Figure 3.12(c). The curves deviate from one another at approximately 0.07 sec. The reason is that, in the test, the soil fills the gap behind the moment slab and prevents the slab from returning to its initial position. This phenomenon is not captured in the finite element analysis. The acceleration of the end of the moment slab during the impact as calculated by the finite element analysis is compared to the measured acceleration of the moment slab in Figure 3.13(a). The comparison is also reasonably good.

3.4 Conclusions

The following conclusions are based on and limited to the content of this chapter.

1. The design impact loads for traffic barriers have evolved over the last 50 years. There are two primary values in case: 44.5 kN (10 kips) and 240 kN (54 kips). The 44.5 kN (10 kips) is an equivalent static load typically used in conjunction with an elastic analysis while the 240 kN (54 kips)

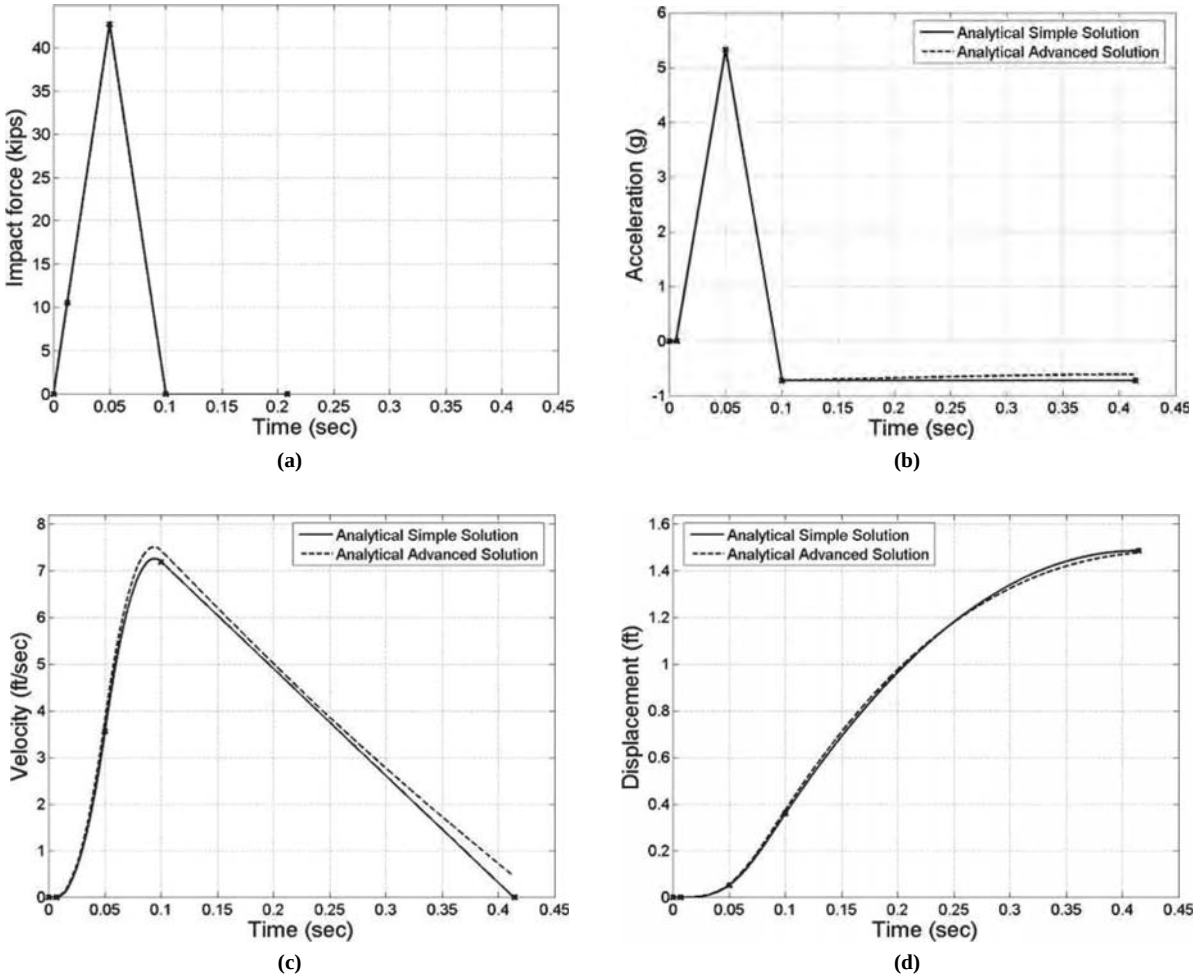

Figure 3.21. Comparison of analytical simple solution and advanced solution for overturning: (a) impact force, (b) acceleration, (c) velocity, and (d) displacement.

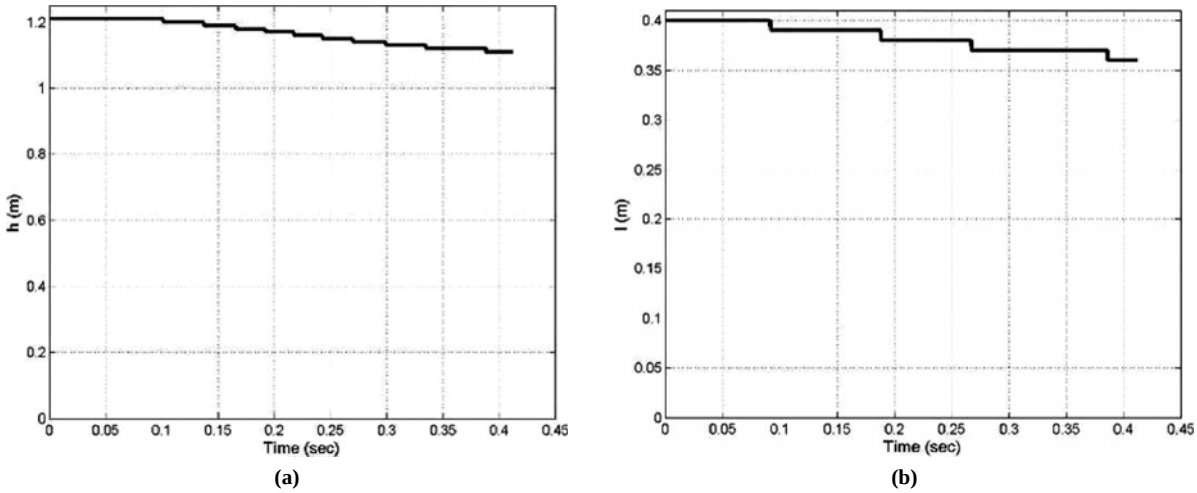

***Figure 3.22. Variations of (a)* h and *(b)* l.**

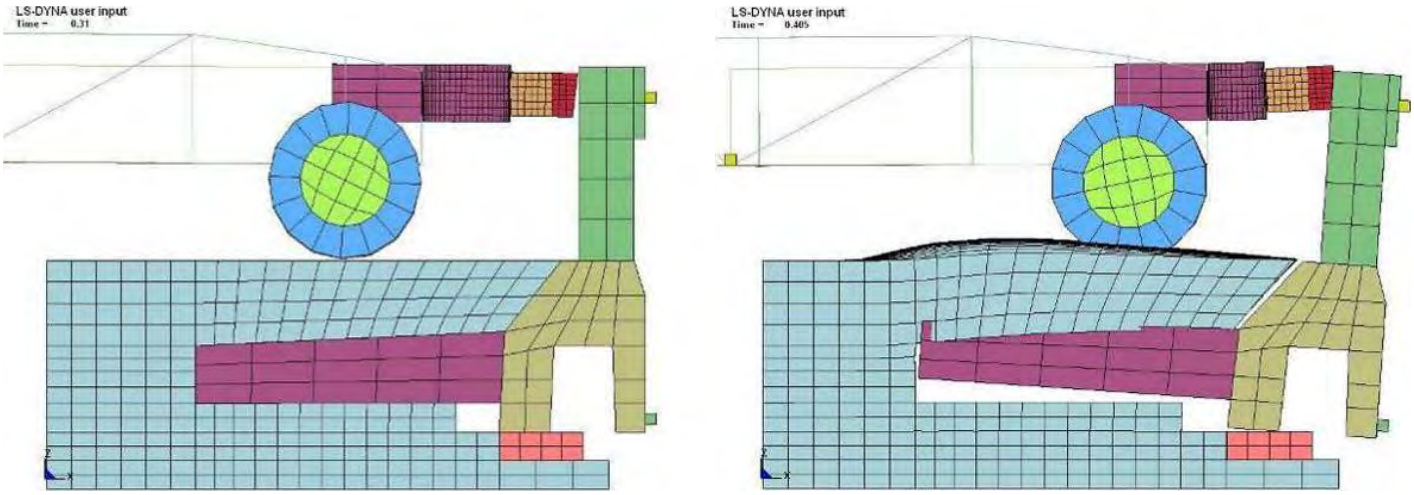

(a) (b)

Figure 3.23. Finite element model for overturning (a) at rest and (b) at impact.

is a dynamic load and is used in conjunction with an ultimate strength analysis. It is not proper to use the 240 kN (54 kips) as an equivalent static load when designing a moment slab as the results are excessively conservative.

2. Current practice uses an ASD approach. The LRFD approach is not complete yet.
3. A set of static and dynamic analytical calculations representing increasing levels of complexity are developed. One static load test and two impact tests were performed on a full-scale barrier. Comparison between the analytical results and the results of three full-scale barrier tests show good agreement.
4. In this project, overturning occurred before sliding. This was shown analytically and confirmed by the full-scale static and dynamic test results. However, both criteria should be checked.
5. There is a significant ratio between the static load and the dynamic load that the barrier can resist. For the 3.05 m (10 ft) barrier tested, the ultimate static load was 40.5 kN (9.1 kips). For the same barrier, the maximum dynamic load in a 20.9 km/h (13 mph) impact test was 189 kN (42.5 kips) for a dynamic to static ratio of 4.7. The maximum dynamic load in an 18 mph impact test was 240 kN (54 kips) for a dynamic to static ratio of 5.9. This ratio is due to the inertial resistance of the system.
6. These ratios use a static load and a dynamic load which do not correspond to the same amount of displacement. If a tolerable displacement of 25 mm (1 in.) is targeted, then the static load is still 40.5 kN (9.1 kips), but the dynamic load drops to 170 kN (38.2 kips) for the 13 mph impact test (dynamic to static ratio of 4.2) and to 210 kN (47.2 kips) for the 18 mph impact test (dynamic to static ratio of 5.2).
7. Since the static load resisted by the dead weight alone of the 3.05 m (10 ft) long barrier is 22.8 kN (5.1 kips) for a rotation point A, for a barrier to resist an equivalent static design load of 44.5 kN (10 kips) with a factor of safety of 1.5, it needs to be at least 9.15 m (30 ft) long.

CHAPTER 4

Reinforcement Pullout Tests

A series of pullout tests were performed to evaluate the influence of rate effect on the pullout capacity of the reinforcement. Ten tests were conducted: seven on steel reinforcement strips and three on steel bar mats. The group that ran the pullout tests was GeoTesting Express in Atlanta.

4.1 Rate of Loading

Three testing times to failure were used: 0.05 sec, 5 sec, and 3,600 sec. This covered five log cycles of time to failure.

4.2 Saturation

The question arose whether a fully saturated condition should be considered. The argument is that, according to theory, a saturated condition will lead to a decrease in resistance when the soil behavior goes from drained behavior to undrained behavior as the rate of loading is increased. The reason is that the pore pressures are higher in undrained conditions compared to drained conditions and, as a result, the effective stress is lower. Because the effective stress controls the strength, then undrained behavior leads to lower resistances than drained behavior. This effect was verified on pullout tests performed by Antonio Bobet (*22*) where the capacity dropped by about 30%. His study was requested by the Indiana DOT because some overpasses are in flood areas and the bottom of the wall may be submerged at times. Discussions with Antonio Bobet at Purdue, Pete Anderson at RECO, and Mark McClelland at TxDOT led to the conclusions that (1) the saturated condition is rare and (2) when it happens it usually affects only the bottom of the wall, not the top where the strips loaded by the impact on the barrier are located.

Nevertheless, it is prudent to test that condition to cover all cases. Therefore, the soil was tested under two moisture conditions: (1) at its optimum moisture content after proper compaction and (2) saturated after it was tested in the unsaturated condition.

4.3 Fines

Highway jobs have strict tolerances on the gradation of the soil used as backfill. Commercial jobs are much less stringent and allow for a much higher percent fines. The tests were limited to a soil that satisfies the DOTs' common guidelines. There are typically two types of soils used behind MSE walls: well-graded sand or crushed rock (No. 57 stones). The soil tested had the following characteristics:

- Well-graded sand
- Less than 15% passing sieve No. 200
- Less than 60% passing sieve No. 40
- Largest particle smaller than 76.2 mm (3 in.)

The grain size distribution of the sand used is given in Figure 4.1. A compaction test was also performed and is shown in Figure 4.2.

4.4 Reinforcement

Geosynthetics represent a minor component of highway wall reinforcement according to the survey. Therefore, the tests focused on inextensible reinforcement.

Two types of reinforcing materials were used in the tests. One type was reinforcing strips provided by RECO. The other type was bar mats provided by Foster Geotechnical, now merged with RECO. The dimensions of the reinforcing strips and bar mats are included in Table 4.1. Concrete sand was used in the tests as the backfill material. The concrete sand was purchased from a retail store and meets ASTM C33 requirements. Compaction and gradation tests were performed on the concrete sand. The gradation test results indicate the concrete sand meets the usual gradation requirements (less than 15% passing sieve No. 200, less than 60% passing sieve No. 40, and the largest particle smaller than 3 in.).

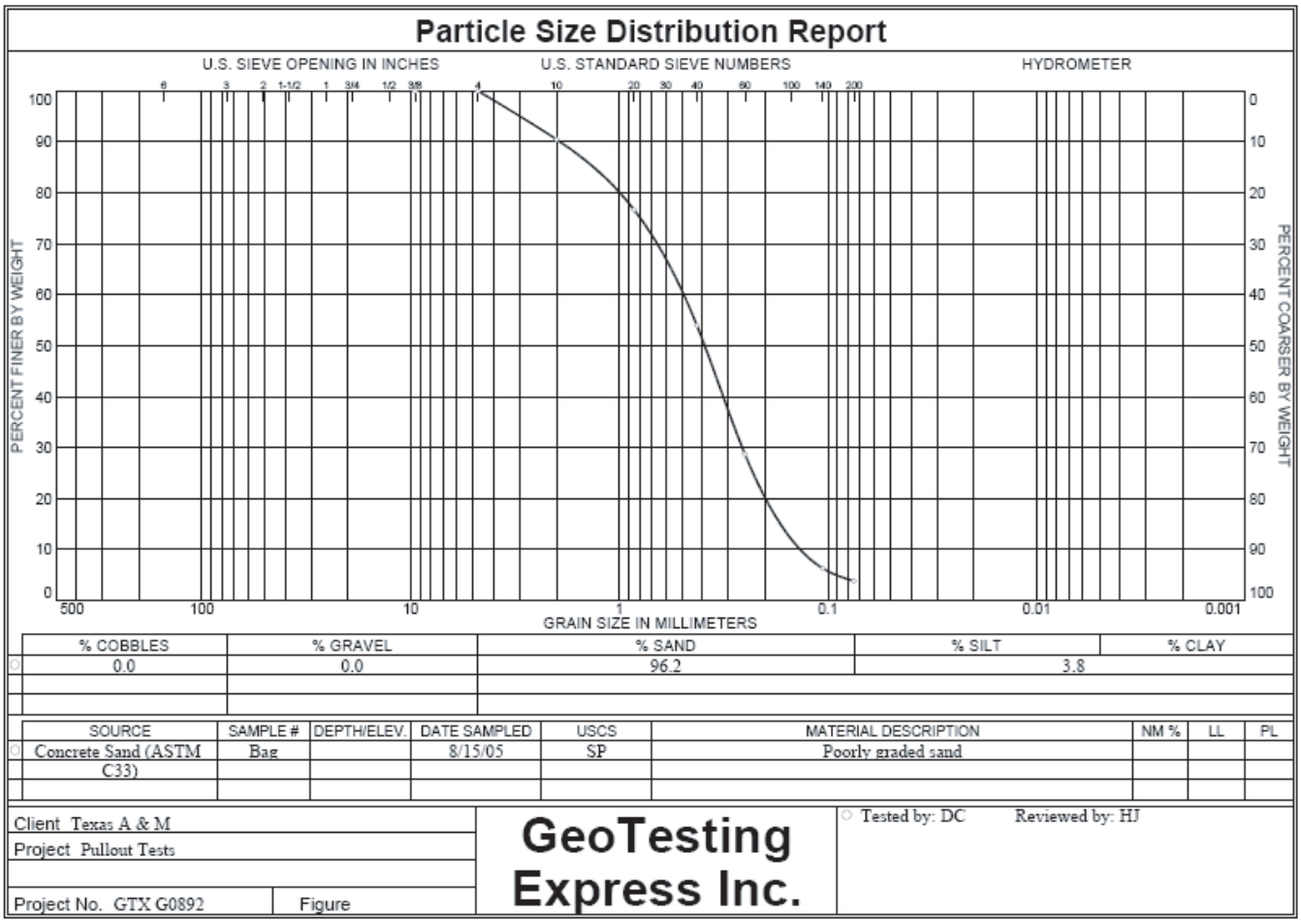

Figure 4.1. Grain size distribution of the sand used in the pullout experiments.

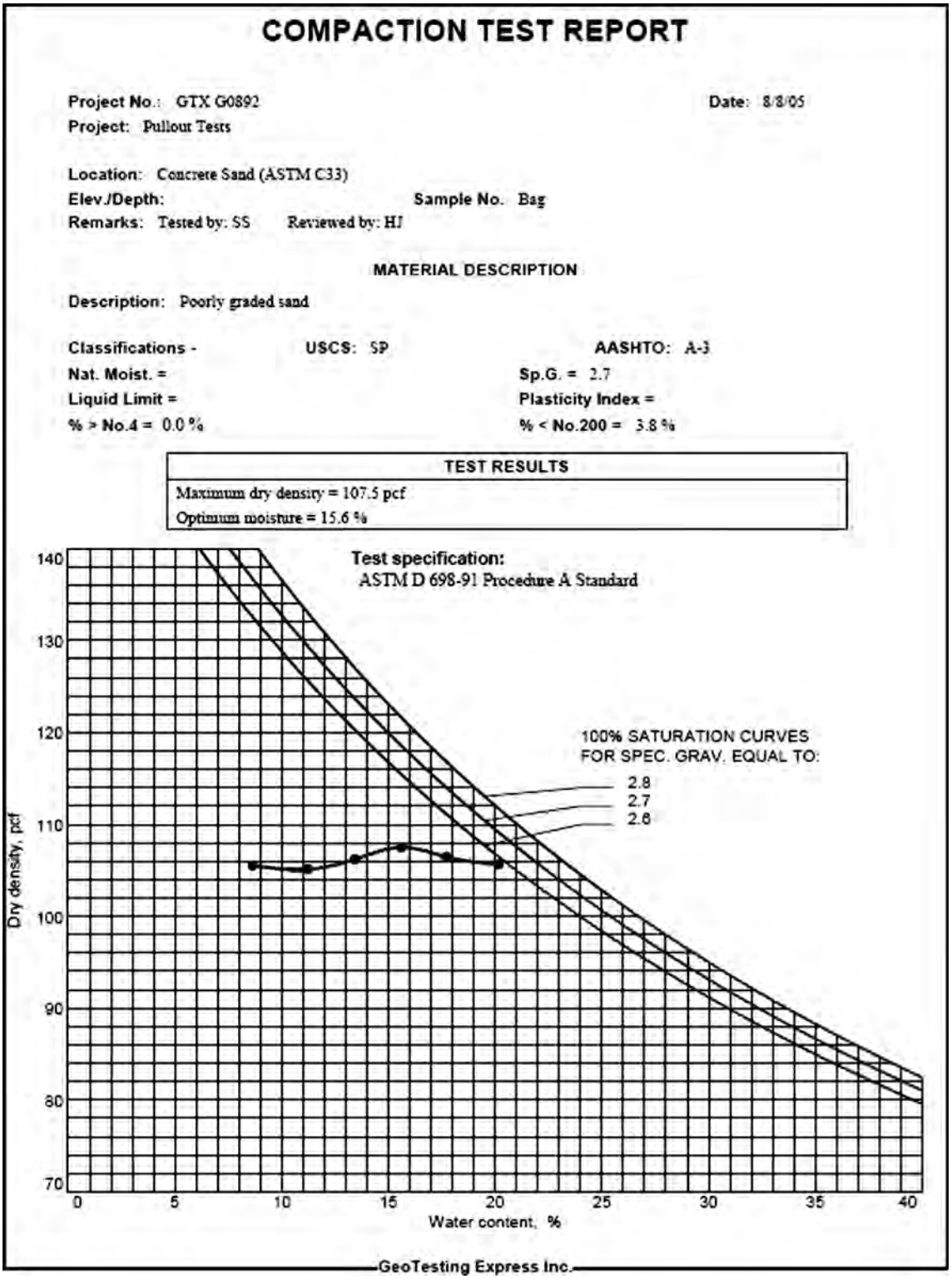

Figure 4.2. Compaction curve for the sand tested.

Table 4.1. Dimension of the reinforcing strip and bar mat.

Reinforcing Material	Length (in.)	Width (in.)	Thickness (in.)
Strip	60.0	2.0	0.2
Bar Mat	57.5	24.5	0.4

4.5 Number of Tests

A total of 10 pullout tests were performed as outlined below.

- Tests: two sets of three tests on the unsaturated backfill and one set of four tests on the saturated backfill
- Time to failure: 0.05 sec, 5 sec, and 3,600 sec for each of the two sets on the unsaturated backfill ($3 \times 2 = 6$ tests) and 0.05 sec, two for 5 sec, and 3,600 sec for the set on the saturated backfill ($4 \times 1 = 4$ tests)
- Soil: well-graded sand as described above; same soil for all 10 tests
- Reinforcement: seven tests on the steel reinforcement strips, three tests on the steel bar mats, length of reinforcement = 1.13 m (3.7 ft)
- Saturation: optimum water content and maximum dry density for six tests (three on strips and three on bar mats); saturated condition for four tests (on strips).
- Box: 701 mm × 381 mm × 1.31 m (2.3 ft × 1.25 ft × 4.3 ft).

Table 4.2 summarizes the conditions for each test.

Table 4.2. Pullout test matrix.

Test No.	Reinforcement	Target Time to Failure (s)	Soil Condition
1	Single Strip	0.05	95% MDD @ OM
2	Single Strip	5.0	95% MDD @ OM
3	Single Strip	3,600.0	95% MDD @ OM
4	Single Strip	0.05	95% MDD Saturated
5	Single Strip	5.0	95% MDD Saturated
6	Single Strip	5.0	95% MDD Saturated
7	Single Strip	3,600.0	95% MDD Saturated
8	Bar Mat	0.05	95% MDD @ OM
9	Bar Mat	5.0	95% MDD @ OM
10	Bar Mat	3,600.0	95% MDD @ OM

MDD = Maximum Dry Density; OM = Optimum Moisture

4.6 Procedure (Soil Installation, Rate of Loading, Testing)

A pullout test box was used in the tests. The box has approximate dimensions of 701 mm × 381 mm × 1.31 m (2.3 ft × 1.25 ft × 4.3 ft). Photos and sketches of the box are shown in Figure 4.3. Sand was first compacted near optimum moisture content to approximately 95% of the maximum dry density to a height 165 mm (6.5 in.) from the bottom of the box, and then the reinforcing strip or bar mat was placed. An additional 216 mm (8.5 in.) of sand was then placed and compacted to the top of the box. A steel plate was placed on the top of the sand. Dead weights were then placed on top of the steel plate to simulate 3 ft of soil overburden. A hydraulic loading system was attached to the front of the strip or bar mat to provide loading for slow- and medium-speed tests. A pneumatic loading system was used for high-speed tests. Figures 4.3 and 4.4 show the box setup and the loading systems for the strips and bar mat, respectively. Two LVDTs were mounted to the box to monitor the deflection during the tests. A ruler was also attached to the piston to measure the deflection after the LVDTs reached their limit of 38.1 mm (1.5 in.). A load cell was attached to the piston to measure the load during the tests. The LVDTs and load cell were connected to a computer data acquisition system to acquire the data during the tests.

4.7 Results and Conclusion

The soil was compacted in layers up to the location of the reinforcement. A standard size steel strip and a standard size bar mat were installed and the compaction process was completed. A surcharge was placed on top of the sand to simulate a total of 0.91 m (3 ft) of soil cover on the reinforcement. Then the reinforcement was pulled to failure.

A load displacement curve was obtained for each test. The results are shown in Figures 4.5 to 4.7. Table 4.3 shows a summary of the test results at failure. The rate effect is shown for all tests on Figure 4.8. The data indicate that there is no particular trend in the effect of the rate of loading. Indeed the pullout resistance at the fastest rate is often larger or equal to the resistance at slower rates. Therefore, these tests indicate that there is no reason to take into account any rate effect on the pullout capacity of the reinforcement during barrier impact.

The back-calculated F^* values for the steel strips ranged from 1.7 to 3.87 and averaged 3.0. This average is well within the range of values obtained in the literature (Figure 4.9) (*23*).

The present AASHTO recommendations for calculating the resistance of MSE wall reinforcement to static loading lead to a predicted reinforcement resistance smaller or equal to the actual reinforcement resistance under impact loading (safe condition). On the basis of these few tests, it is suggested that the current AASHTO recommendations be used as-is to calculate the resistance of the reinforcement to impact loads.

(a) Pullout box setup

(b) Surcharge to simulate depth

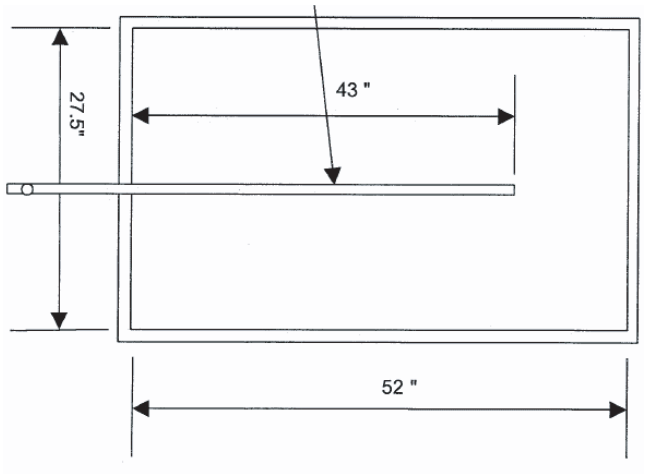

(c) Box dimensions and location of strip

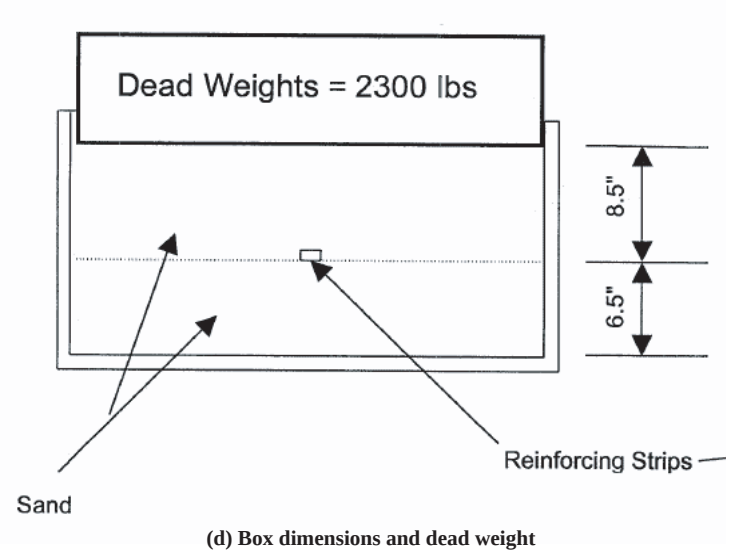

(d) Box dimensions and dead weight

(e) Placing the strip on the sand

(f) Strip coming out of the front of the box

Figure 4.3. Test setup with steel strip.

(a) Grabbing the bar mat

(b) Placing the bar mat on the sand

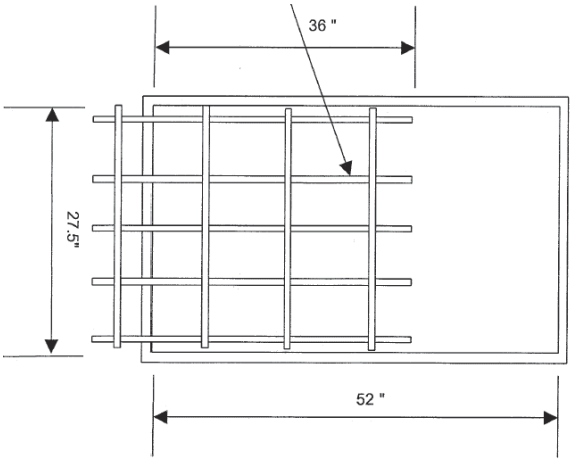

(c) Bar mat and box dimensions

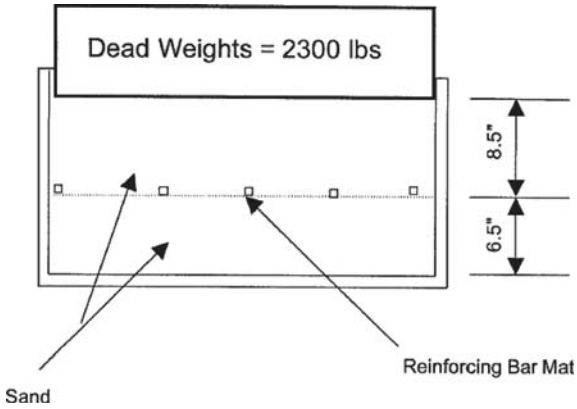

(d) Dead weight on bar mat

(e) Grabbing and loading the strip

Figure 4.4. Test setup with bar mat.

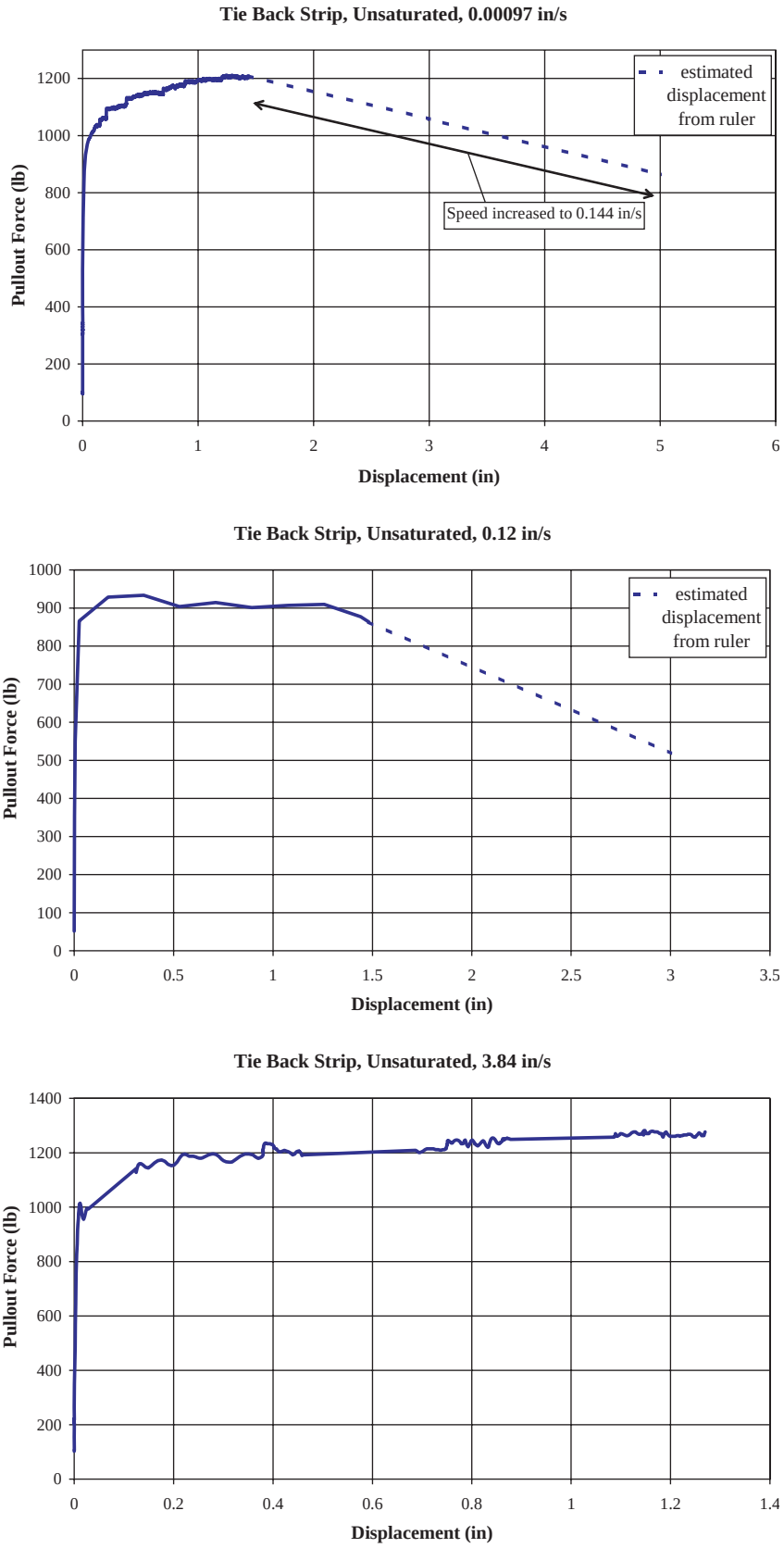

Figure 4.5. Load displacement curve obtained (tie back strip, unsaturated).

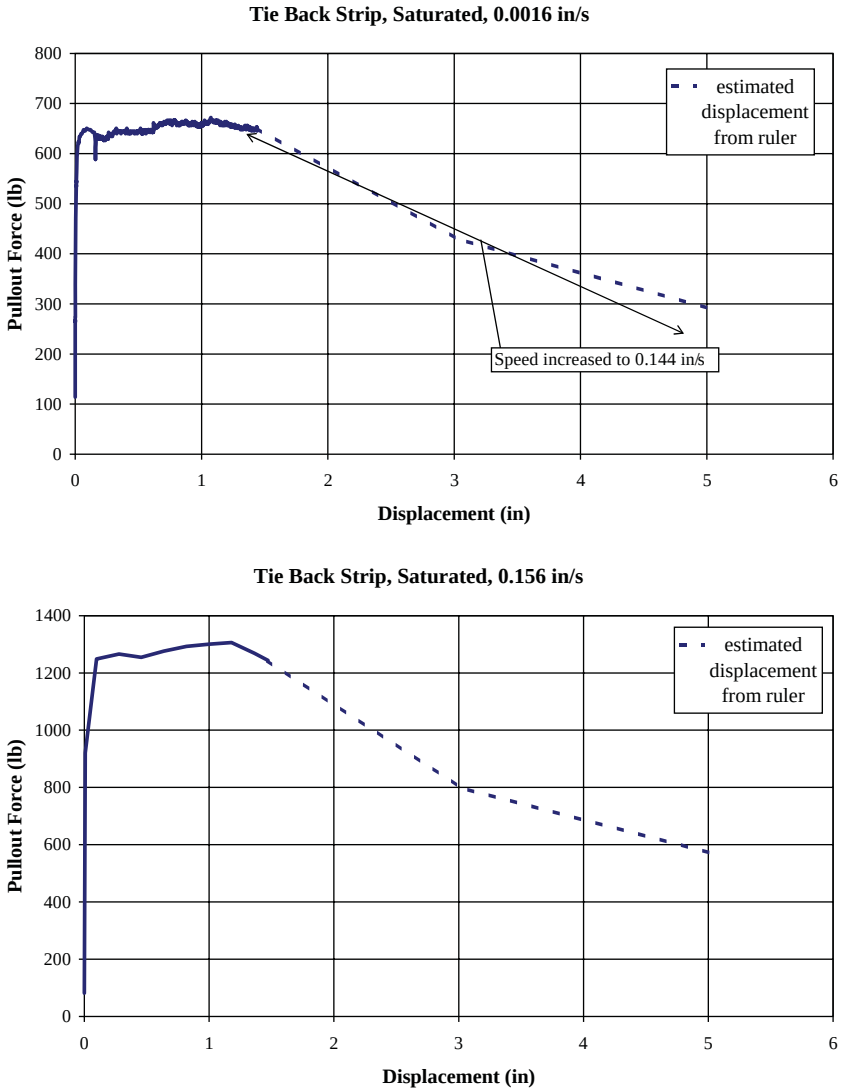

Figure 4.6. Load displacement curve obtained (tie back strip, saturated).

(continued on next page)

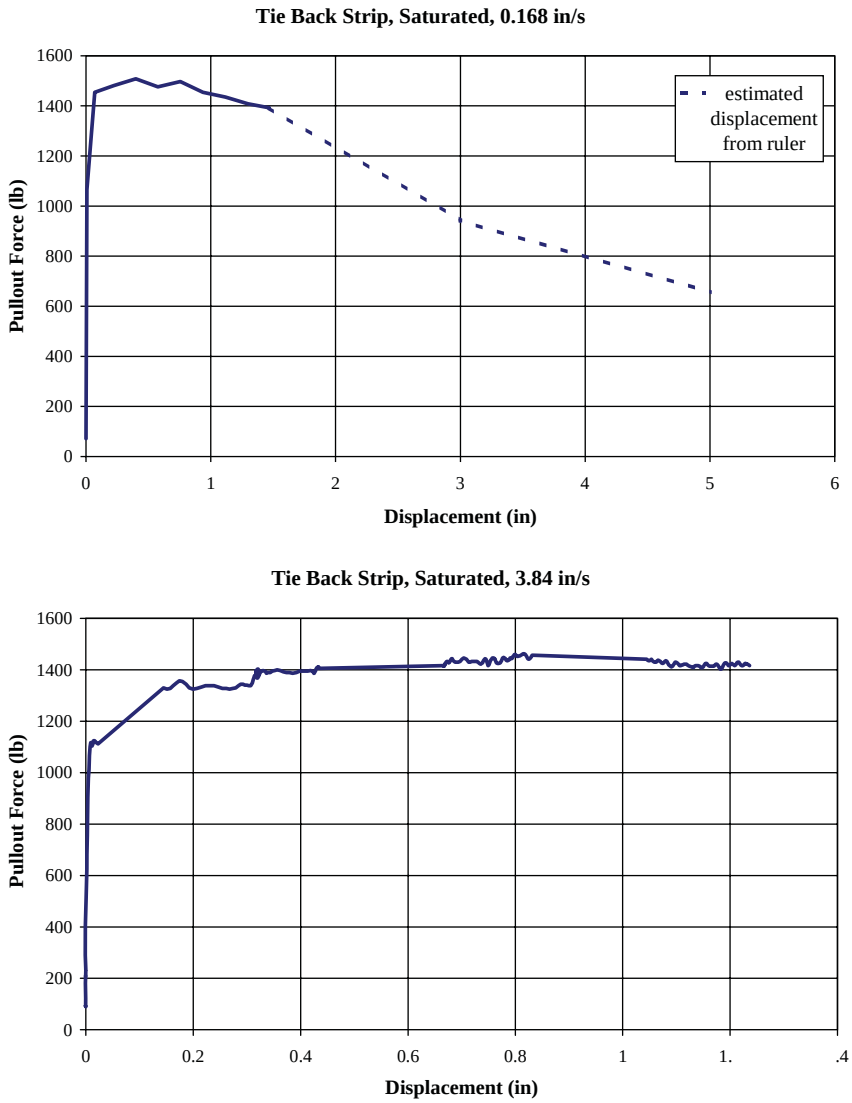

Figure 4.6. (Continued).

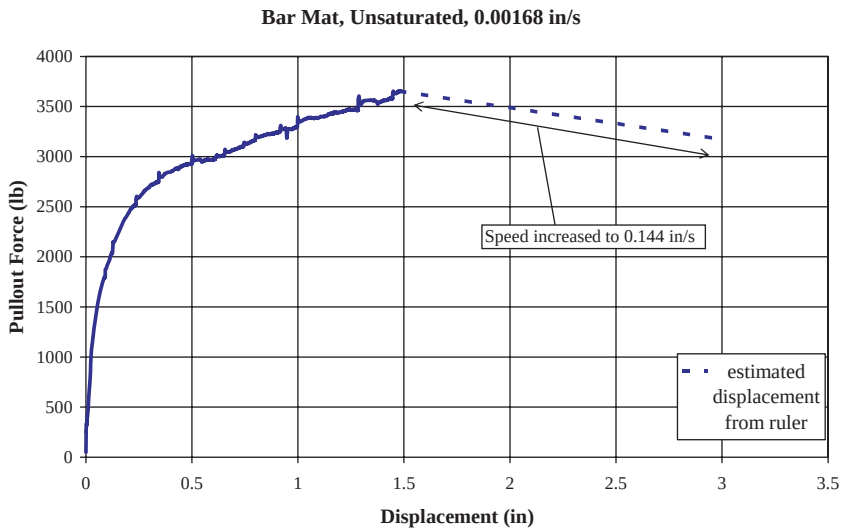

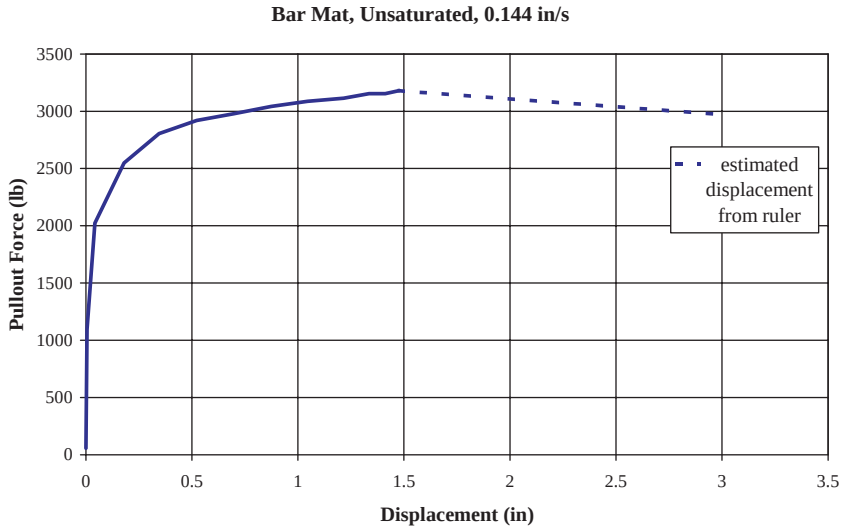

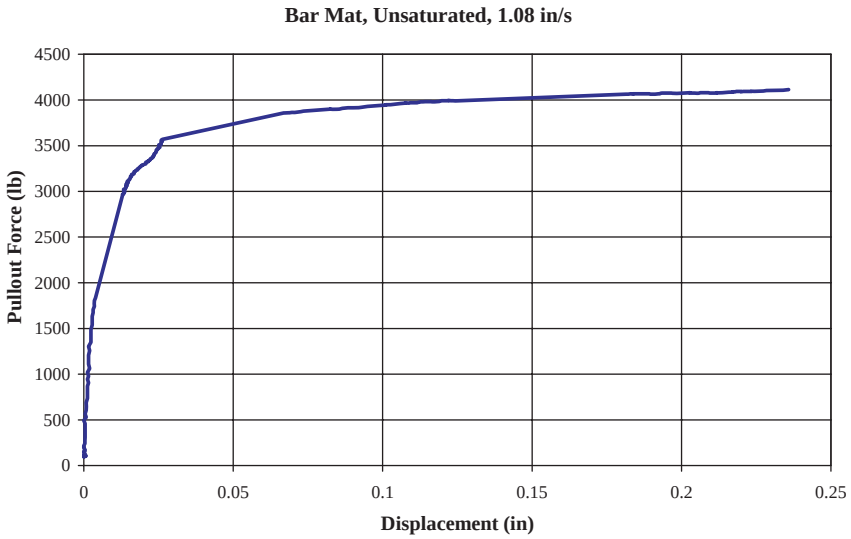

Figure 4.7. Load displacement curve obtained (bar mat).

Table 4.3. Pullout test results.

a) Tie Back Strip[a], Unsaturated

Test Condition	Pullout Speed (in./s)	Dry Density of Sand (pcf)	Normal Load (lbs)	Specimen Width (ft)	Length of Embedment (ft)	Pullout Force (lbf)	Elapsed Time at Peak (s)	Displacement at Peak (in.)	Pullout Resistance[b] (lbf/ft)
Unsaturated	0.00097	101.5	2946	0.17	3.7	1212 (1163)	1287 (862)	1.24 (0.75)	7269 (6841)
Unsaturated	0.12	101.5	2946	0.17	3.7	933	5	0.35	5602
Unsaturated	3.84	101.5	2946	0.17	3.7	1141	0.05	0.12	6848

Notes: [a] Tie Back Strip Dimension: L = 60 in., W = 2 in., Thickness = 0.2 in., Thickness at rib = 0.3 in., length of embedment = 3.7 ft
[b] Pullout resistance = Pullout Force (lbf) / width of tie back strip (ft)
For samples whose peak value occurred after 0.75 in., values in parentheses represent values at 0.75 in. displacement.

b) Tie Back Strip[a], Saturated

Test Condition	Pullout Speed (in./s)	Dry Density of Sand (pcf)	Normal Load (lbs)	Specimen Width (ft)	Length of Embedment (ft)	Pullout Force (lbf)	Elapsed Time at Peak (s)	Displacement at Peak (in.)	Pullout Resistance[b] (lbf/ft)
Saturated	0.0016	101.5	2946	0.17	3.7	650	66	0.09	3903
Saturated	0.156	101.5	2946	0.17	3.7	1306 (1286)	8 (6)	1.18 (0.75)	7835 (7720)
Saturated	0.168	101.5	2946	0.17	3.7	1508	4	0.40	9049
Saturated	3.48	101.5	2946	0.17	3.7	1357	0.06	0.17	8143

Notes: [a] Tie Back Strip Dimension: L = 60 in., W = 2 in., Thickness = 0.2 in., Thickness at rib = 0.3 in., length of embedment = 3.7 ft
[b] Pullout resistance = Pullout Force (lbf) / width of tie back strip (ft)
For samples whose peak value occurred after 0.75 in., values in parentheses represent values at 0.75 in. displacement.

c) Bar Mat[a]

Test Condition	Pullout Speed (in./s)	Dry Density of Sand (pcf)	Normal Load (lbs)	Specimen Width (ft)	Length of Embedment (ft)	Pullout Force (lbf)	Elapsed Time at Peak (s)	Displacement at Peak (in.)	Pullout Resistance[b] (lbf/ft)
Unsaturated	0.00168	101.5	2946	2	3	3655 (3129)	1811 (799)	>1.5 (0.75)	1837 (1565)
Unsaturated	0.144	101.5	2946	2	3	3180 (2996)	12 (6)	1.48 (0.75)	1590 (1499)
Unsaturated	1.08	101.5	2946	2	3	3900	0.17	0.09	1950

Notes: [a] Bar Mat Dimension: L = 57.5 in., W = 24.5 in., Bar Thickness = 0.4 in., Joint Thickness = 0.7 in., length of embedment = 3 ft, 5 bars parallel to direction of force, 4 cross-bars (3 embedded)
[b] Pullout resistance = [Pullout Force (lbf) * number of bars per unit width (2.5 bars/ft)] / number of bars parallel to direction of force (5)
For samples whose peak value occurred after 0.75 in., values in parentheses represent values at 0.75 in. displacement.

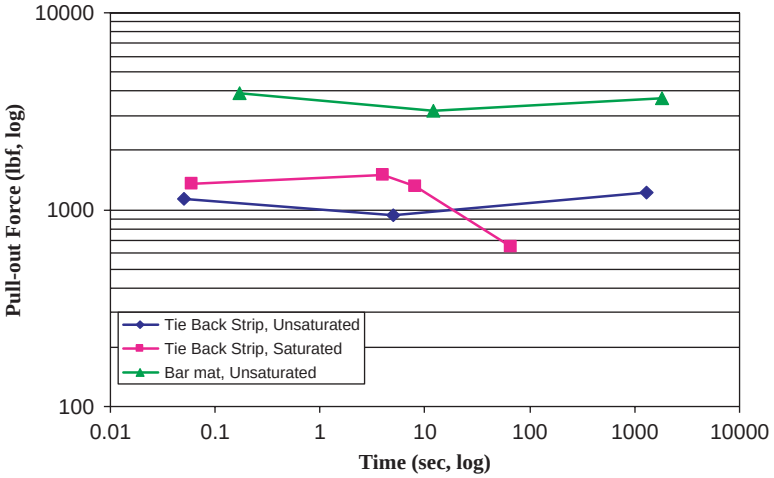

Figure 4.8. Pullout load at failure versus time to failure for all tests.

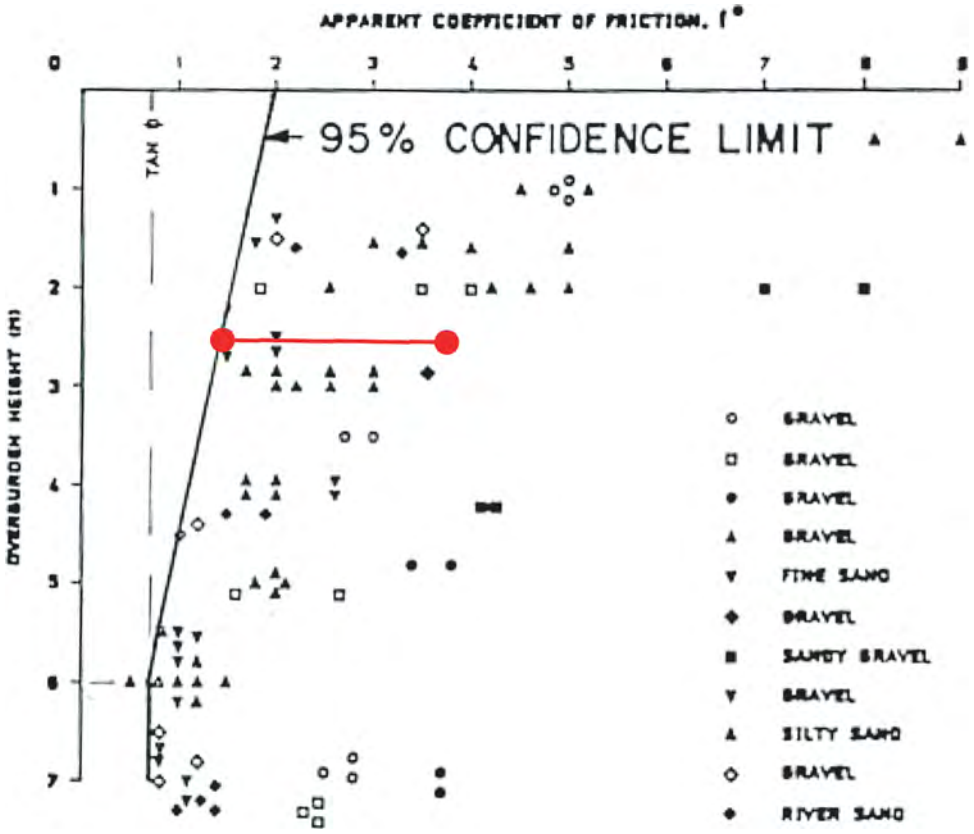

Source: The Reinforced Earth Company (*23*)

Figure 4.9. Values of apparent coefficient of friction (f) from pullout tests.*

CHAPTER 5

5 ft High MSE Wall and Barrier Study

The objectives of the bogie tests include quantification of the movement of the barrier, coping, and moment slab system and measurement of the force distributions in the reinforcement strips due to a design impact load. To help plan the bogie test, wall and finite element models were developed and impact simulations using the bogie impactor were performed using LS-DYNA. The results of bogie tests were used to develop the design guidelines for scenarios that include a traffic barrier mounted on the edge of an MSE wall.

5.1 5 ft High MSE Wall and Barrier Test Plan

Half of the test wall was constructed using 2.43 m (8 ft) long reinforcement strips, while the other half was constructed with 4.88 m (16 ft) long reinforcement strips. The 2.43 m (8 ft) long reinforcement strip represents the minimum length allowed in current practice and, therefore, constitutes the critical case for assessing wall displacement during a barrier impact. Such lengths are commonly used in short-height wall segments such as at the beginning or ending of an elevated overpass structure. At the minimum 2.43 m (8 ft) length, current design procedures typically require a density of six reinforcement strips per wall panel (three in each of two different horizontal layers of reinforcement). The other half of the wall was constructed using 4.88 m (16 ft) long reinforcement strips. This length of reinforcement is a practical maximum length used in many MSE wall installations as wall height increases. The increased length increases the pullout resistance of the reinforcement. Therefore, a wall section with 4.88 m (16 ft) strips will constitute the critical case for assessing the magnitude and distribution of impact loads in the reinforcement.

A summary of the bogie impact test plan is shown in Table 5.1. Two different barrier types were used in the test program: a N.J. safety shape (Test 1) and a vertical barrier (Tests 2, 3, and 4). Bogie Tests 1 (N.J. shape) and 4 (vertical barrier) were conducted over the portion of the wall with 4.88 m (16 ft) steel strip reinforcement. Bogie Tests 2 and 3 involved impacts into vertical concrete barriers placed over wall segments with 2.43 m (8 ft) steel strip and bar mat reinforcement, respectively.

The bogie test installation was planned on the premise that multiple impacts could be conducted on barrier segments connected to the same moment slab. This plan was accepted with the understanding that if excessive motion of the barrier–moment slab system occurred during the first test associated with a given moment slab, the ability to conduct subsequent impact tests of other barrier sections connected to the same moment slab could be compromised. Further, if the motion resulted in contact with a wall panel, the integrity of the wall might be compromised. Thus, the impact speed of the bogie had to be carefully selected to achieve the desired result of identifying the failure mechanism of the barrier–moment slab system without imparting an unnecessarily high degree of damage to the underlying wall.

5.1.1 Calculation of MSE Wall Capacity

AASHTO LRFD (*2*) was used to estimate the forces expected on the reinforcement strips due to both gravity and impact loads for the 1.52 m (5 ft) high MSE wall. This information ultimately was compared to forces estimated through simulation and measured in the bogie tests as new design procedures were developed.

In the 2.43 m (8 ft) long strip case, unfactored resistances were calculated to be 6.595 kN (1.483 kips) ($F^* = 1.837$) at the uppermost layer and 12.019 kN (2.702 kips) ($F^* = 1.674$) at the second layer. A density of three strips per layer per panel was used. The unfactored load per strip due to gravity was calculated to be 2.53 kN (0.569 kips) at the uppermost layer and 4.87 kN (1.095 kips) at the second layer. In this analysis, the traffic surcharge was not considered. The unfactored load per strip due to the impact was calculated to be 1.903 kN (0.428 kips) at the uppermost layer and 1.293 kN (0.291 kips)

Table 5.1. Bogie test plan.

Test Sequence	Barrier Type	Moment Slab Width	Barrier Length	Reinforcement Type	Reinforcement Length
Test 1	New Jersey	4.5 ft	10 ft	Steel strips	16 ft
Test 2	Vertical wall	4.5 ft	10 ft	Bar mats	8 ft
Test 3	Vertical wall	4.5 ft	10 ft	Steel strips	8 ft
Test 4	Vertical wall	4.5 ft	10 ft	Steel strips	16 ft

at the second layer. Therefore, the unfactored total load per strip was 4.433 kN (1.0 kips) at the uppermost layer and 6.163 kN (1.43 kips) at the second layer. A summary of resistance and load per strip is presented in Table 5.2.

In the 4.88 m (16 ft) long strip case, unfactored resistances were calculated to be 13.19 kN (2.965 kips) ($F^* = 1.837$) at the uppermost layer and 24.038 kN (5.404 kips) ($F^* = 1.674$) at the second layer. A density of 2 strips per layer per panel was used. The unfactored load per strip due to gravity was calculated to be 3.795 kN (0.853 kips) at the uppermost layer and 7.306 kN (1.642 kips) at the second layer. In this analysis, the traffic surcharge was not considered. The unfactored load per strip due to the impact was calculated to be 2.854 kN (0.642 kips) at the uppermost layer and 1.939 kN (0.436 kips) at the second layer. Therefore, the unfactored total load per strip was 6.65 kN (1.49 kips) at the uppermost layer and 9.245 kN (2.09 kips) at the second layer. A summary of resistance and load per strip is presented in Table 5.3.

The detailed calculations for designing the MSE test wall are provided in Appendix A.

5.1.2 Calculation of Barrier Capacity

It is important to be able to quantify the ultimate strength of the barrier sections used in the bogie test matrix to aid in analyses of the barrier–moment slab systems. For example, knowing the ultimate strength of the vertical wall section permitted the overturning test to be planned at an impact speed that will cause substantial movement (i.e., rotation) of the barrier–moment slab system without causing failure of the barrier. Also, the bogie impact speed for the planned bogie tests of the different barrier sections atop a 1.52 m (5 ft) tall MSE wall was selected such that the generated impact force would exceed the capacity of the barrier. In this way, the failure mode of the precast barrier unit can be identified and the maximum impact load will be applied to the supporting MSE wall and its reinforcement. For these reasons, the strength of the selected N.J. safety shape and vertical wall barrier sections was computed.

In regard to the analysis of the strength of a barrier, most references containing concrete barrier design information have used the yield line analysis approach (AASHTO LRFD A13.3.1). Yield line theory considers the plastic strength of all the railing system components along with barrier geometry, material strengths, applied loading, and strength of the supporting bridge structure. Steel rail systems, concrete rail systems, or a combination rail composed of a steel rail on a concrete barrier can be evaluated using these design procedures. Based on yield line theory, the limiting ultimate capacity of the railing systems used in the test program was calculated. This procedure assumes that the underlying support structure for the barrier section (e.g., deck, foundation, etc.) has sufficient strength to develop the base moment capacity of the barrier such that the failure occurs in the barrier rather than the support structure. Although this may not necessarily be the case for the precast barrier–coping sections, the yield line analysis approach was used to establish what would be considered a maximum barrier capacity. This ultimate capacity was then compared to design forces derived from simulations to determine appropriate impact speeds for the bogie vehicle tests.

The ultimate load capacity calculated following the assumed yield line failure mechanism was 515.06 kN (115.79 kips) for the 813 mm (32 in.) tall N.J. barrier. This load capacity is much

Table 5.2. Unfactored resistance and force in case of MSE wall with 8 ft long strip.

Layer	(1) T_{Static} Static Load (kips)	(2) $T_{Dynamic}$ Dynamic Load (kips)	(3)=(1)+(2) T_{Total} Total Load (kips)	R Resistance (kips)
Top	0.569	0.428	0.997	1.483 ($F^* = 1.837$)
Second	1.095	0.291	1.386	2.702 ($F^* = 1.674$)

Table 5.3. Unfactored resistance and force in case of MSE wall with 16 ft long strip.

Layer	(1) T_{Static} Static Load (kips)	(2) $T_{Dynamic}$ Dynamic Load (kips)	(3)=(1)+(2) T_{Total} Total Load (kips)	R Resistance (kips)
Top	0.853	0.642	1.495	2.965 ($F^* = 1.837$)
Second	1.642	0.436	2.078	5.404 ($F^* = 1.674$)

higher that observed in previous dynamic bogie testing. The moment capacity of the "toe" of the safety shape is large and, thus, typically restricts failure to the upper wall portion of the barrier. The ultimate load capacity of the upper wall portion of the N.J. barrier was calculated to be 329.26 kN (74.02 kips). The length of the failure mechanism calculated for the N.J. barrier section analyzed was 2.23 m (7.3 ft).

The ultimate load capacity calculated following the assumed yield line failure mechanism was 325.34 kN (73.14 kips) for the 0.69 m (27 in.) tall vertical wall barrier. Note that the height of load application assumed for calculation of the ultimate barrier load capacities was the top of the barrier. The length of the failure mechanism calculated for the vertical wall barrier section analyzed was 1.65 m (5.4 ft). This indicates that, provided the coping has sufficient capacity to develop the ultimate strength of the barrier, the 3.05 m (10 ft) section length selected for evaluation in the bogie tests should be sufficient for developing the primary failure mechanism for each barrier type.

5.2 Finite Element Analysis

The complex nonlinear interactions that occur during an impact event are difficult to capture through conventional analytical means. Therefore, an explicit nonlinear finite element methodology was used to evaluate the dynamic impact performance of the representative barrier–moment slab–MSE wall configurations considered in the test plan.

5.2.1 Modeling Methodology

The methodology followed to model the barrier on top of the MSE wall, and then simulate bogie impacts, consisted of the following steps:

1. Construct a finite element model of the barrier and MSE wall.
2. Initialize the model of MSE wall and barrier to account for gravitational loading.
3. Simulate the bogie impact against the barrier.
4. Compare results with test data and calibrate the MSE wall and barrier finite element model if needed.
5. Identify any further investigation needed.

The details of the finite element analysis are presented in the following sections.

Geometry and Meshing

The finite element representation of the MSE wall planned for use in the bogie test program consists of the following major components:

- Precast concrete barrier–coping sections
- Cast-in-place moment slab
- Steel reinforcement in the barrier, moment slab, and wall panels
- MSE wall including the backfill soil, concrete wall panels, level-up concrete, pedestal, and wall reinforcement
- Accelerometers on the barrier and moment slab.

The total length of the MSE wall model was 9.14 m (30 ft), which represented the length of one moment slab section. Three 3.05 m (10 ft) long barrier–coping sections were attached to the 9.14 m (30 ft) long moment slab. Both full and half-panels were used to construct the wall (see Figure 5.1).

The concrete barrier and moment slab were modeled using solid elements, as were various components of the MSE wall including the soil, wall panels, leveling pad, and pedestal. Three-dimensional beam elements with six degrees at each end were used to model the steel rebar inside the barriers, moment slab, and wall panels. The steel strip reinforcement for the MSE wall was modeled using shell elements with 4 mm (0.16 in.) thickness and 50.8 mm (2 in.) width.

The elements of impact barrier located in the middle of the system were meshed using an element characteristic size of about 50 mm (2 in.) to capture the barrier deformation and damage due to the impact with more accuracy. The two other barriers were meshed more coarsely to reduce computational cost of the simulations since these barriers do not interact with the bogie. The soil was modeled as three components: the reinforced backfill, the overburden soil, and the side soil for modeling continuity at the edges of the moment slab as shown in Figures 5.1 and 5.2. The soil elements located beneath the barrier and moment slab were meshed relatively fine using an element characteristic size ranging from 50 mm (2 in.) to 101.6 mm (4 in.) to improve the robustness of the contact between the coping and top edge of the soil and better capture the load transfer from the barrier to the soil during the impact. The overburden soil and side boundary soil are rather coarsely meshed, while a finer mesh is used for the reinforced backfill to capture gravity and impact loads distributed into the soil through the MSE wall and the barrier with more accuracy.

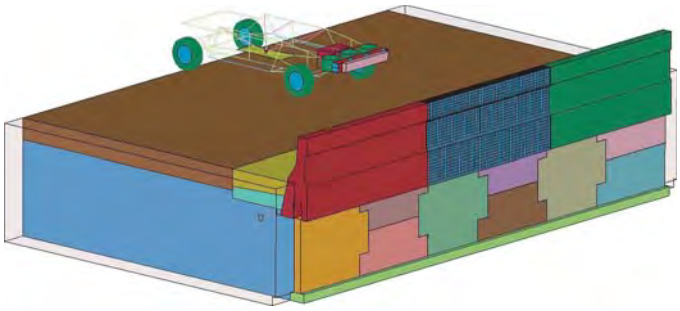

Figure 5.1. Three-dimensional view of a MSE wall and barriers model with a bogie.

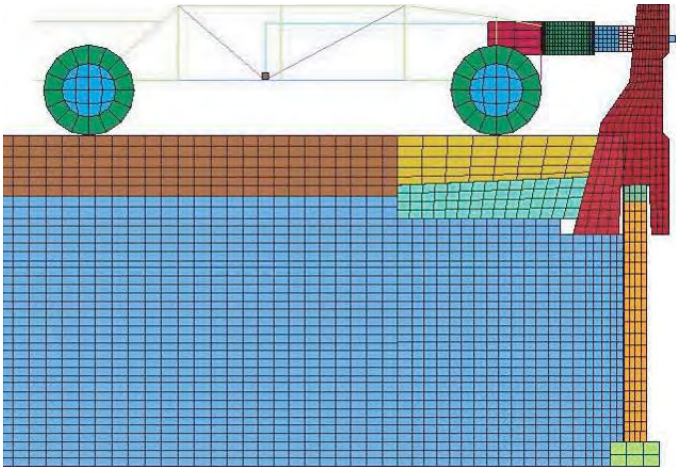

Figure 5.2. Side view of a MSE wall and barriers with a bogie.

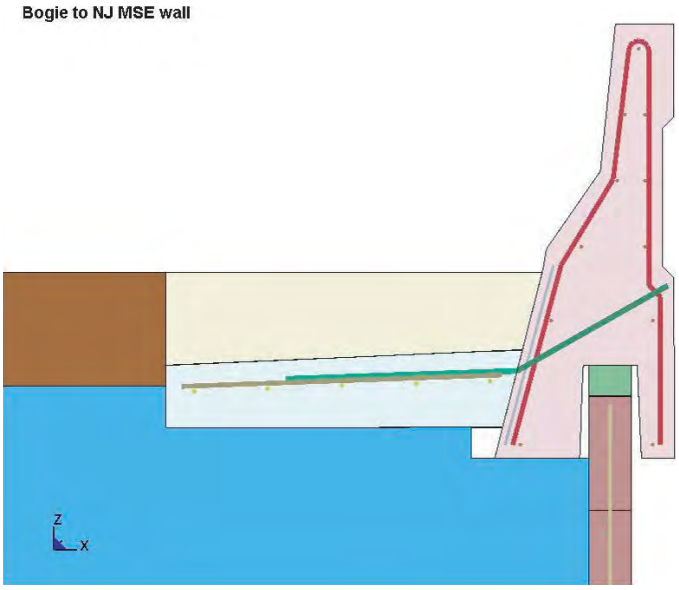

Figure 5.3. Rebars detail in N.J. barrier and moment slab.

Contact

Although LS-DYNA features some of the most advanced contact algorithms available, capturing interaction between solid and beam or shell elements is rather complex. The requirement of matching nodes to merge the reinforcing steel inside the concrete continuum would dictate the creation of elements with poor aspect ratios and the creation of unnecessarily small element sizes, which has a significant effect on time step control (*24*). To mitigate this problem, a different connection scheme was utilized between the barrier and the steel reinforcement that permits a more regular, uniform mesh of the concrete to be used throughout the barrier.

The steel reinforcements are coupled (rather than merged) to the surrounding concrete continuum to prevent the creation of poor quality elements. This coupling was achieved using the *CONSTRAINED_LAGRANGE_ IN_SOLID feature in LS-DYNA. The use of this coupling permits the concrete mesh to be constructed without consideration of the location of steel reinforcement. The steel reinforcement is treated as a slave material that is coupled with a master material composed of the moment slab and barrier concrete. The slave parts (i.e., steel reinforcing bars) can be placed anywhere inside the master continuum part without any special mesh accommodation. The soil and its reinforcement were methodologically modeled in a manner similar to the steel reinforcement in concrete to capture salient responses of the MSE wall. Reinforcing steel in the barriers sections and moment slab and steel reinforcement strips in the soil are shown in Figures 5.3 and 5.4.

Another coupling mechanism, *CONTACT_TIED_ SHELL_EDGE_TO_SURFACE, was defined to account for the connection between the panel and steel reinforcement.

The interface between the soil and concrete was modeled using contacts and/or constraints to capture interface (i.e., contact) forces generated between the concrete structure and the MSE wall. The contact friction was based on the estimated soil internal friction angle. Using a soil friction angle ϕ of 35 degrees, the contact friction was calculated to be 0.7 (tan ϕ).

Material Models and Model Parameters

Concrete and Steel Material. There are several material options to be considered for modeling the concrete structures in LS-DYNA. These material options range from the very simple elastic material to a nonlinear damage material model. The elastic material option can be useful in modeling areas that will not be subjected to significant stress in order to reduce computational costs of the simulation. If this approach is used, appropriate checks must be made to ensure the tensile stress in the concrete does not exceed its failure threshold (*24*).

The outside barrier sections were modeled using elastic material (designated as MAT type 1 in LS-DYNA) as shown in Table 5.4. However, the middle barrier that was subjected to direct impact was modeled using a nonlinear response concrete material model definition. In LS-DYNA, it is designated

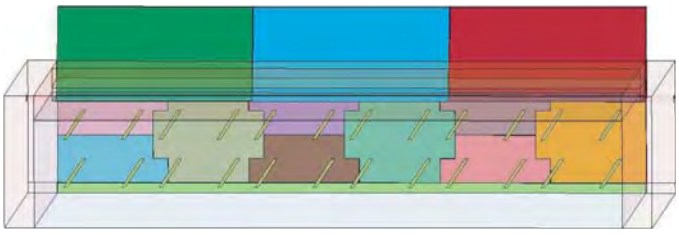

Figure 5.4. Interface between soil and strip shell element.

Table 5.4. Material properties of concrete model.

Concrete	E (psi)	ν	ρ (lb/in^3)	f'_c (psi)
Elastic (MAT type 1)	3.62E+6	0.17	0.084	–
Damage (MAT type 159)	–	–	0.084	4,000

E is Young's modulus, ν is Poisson's ratio, ρ is the mass density, and f'_c is the compressive strength.

Table 5.5. Material properties of steel model.

	E (psi)	ν	ρ (lb/in^3)	Yield Stress (psi)
Steel (MAT type 24)	30.46E+6	0.29	0.28	60,000

E is Young's modulus, ν is Poisson's ratio, and ρ is the mass density.

as material MAT type 159 developed by APTEK (*24*). This method to explicitly model concrete is more sophisticated but computationally expensive. In this model, a brittle material like concrete will lose (at a given rate) its ability to carry load when a specified damage/failure threshold is reached. This feature is very useful because it provides a more accurate representation of the failure mechanism of the concrete components, and better prediction of the impact load transfer. The parameters of MAT type 159 can be assigned using two additional concrete properties: the unconfined compressive strength of concrete (f'_c) and the maximum aggregate size, which was taken as 25.4 mm (1 in.).

The moment slab, the wall panels, the pedestal, and the level-up concrete were modeled using an elastic material model definition (MAT type 1). All steel rebars and steel strips were modeled using a piecewise linear plasticity material model (MAT type 24) that is representative of the actual stress-strain relationship of the material using the properties shown in Table 5.5. Steel rebar exhibits rate effects, and yields in a ductile manner until it breaks at an ultimate strain greater than approximately 20%. Before yielding, the material is assumed to be linearly elastic. After yielding, the steel can undergo plastic deformation and strain hardening.

Soil Material. The soil was modeled using the two-invariant geological cap material model (MAT type 25) (*20*). The advantage of the cap model over other models such as the Drucker–Prager formulation is the ability to model plastic compaction. In these models, all purely volumetric response is elastic until the stress point hits the cap surface. Therefore, plastic volumetric strain (compaction) is generated at a rate controlled by the hardening law. Thus, in addition to controlling the amount of dilatancy, the introduction of the cap surface adds another experimentally observed response characteristic of geological materials into the model (*25, 26*).

The cap model is defined in terms of the first stress invariant $I_1 = trace(\sigma) = \sigma_{11} + \sigma_{22} + \sigma_{33}$ and the second deviatoric stress invariant $J_2 = \frac{1}{2}S_{ij}S_{ij} = \frac{1}{2}(s_{11}^2 + s_{22}^2 + s_{33}^2)$, where σ is the stress tensor and $S_{ij} = \sigma_1 - \sigma_3$ is the deviatoric stress tensor. The yield surface of the cap model consists of three regions (Figure 5.5): a failure envelope $f_1(\sigma)$, an elliptical cap $f_2(\sigma, \kappa)$, and a tension cutoff region $f_3(\sigma)$, where κ is the hardening parameter. The functional forms of the three surfaces are the following:

1. Failure surface region: $f_1(\sigma) = \sqrt{J_{2D}} - F_e(I_1) = 0$,

$$\text{for } T \le I_1 < L(\kappa) \tag{5-1}$$

2. Cap surface region: $f_2(\sigma, \kappa) = \sqrt{J_{2D}} - F_c(I_1, \kappa) = 0$,

$$\text{for } L(\kappa) \le I_1 < X(\kappa) \tag{5-2}$$

3. Tension cutoff region: $f_3(\sigma) = T - I_1 = 0$, for $I_1 = T$ (5-3)

In the elastic region, $F_e(I_1)$ can be expressed as:

$$F_e(I_1) = \alpha - \gamma e^{-\beta I_1} + \theta I_1 \tag{5-4}$$

where the yield surface was determined by the parameters α, θ, γ, and β, which are usually evaluated by fitting a curve through failure data taken from a set of triaxial compression tests.

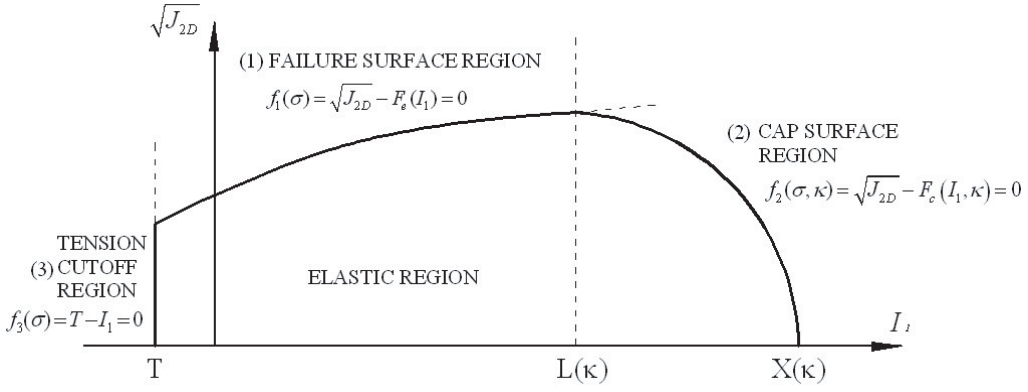

Source: Hallquist (*20*)

Figure 5.5. Yield surface of the cap model.

Table 5.6. Comparison of cap soil properties.

		Simulation	McCormick Ranch Sand	NCHRP 556
Elasticity	K (MPa)	22.219	459.676	52.19
	G (MPa)	7.407	275.792	24.087
Plasticity	α (MPa)	4.154	0.00186	0.01
	β (MPa^{-1})	0.0647	0.09718	0
	γ (MPa)	4.055	0.00117	0
	θ (radian)	0	0.02	0.2925
Hardening Law	W	0.08266	0.064	0.023
	D (MPa^{-1})	0.239	0.00725	0.87
	R	28.0	2.5	4.0
	X_0 (MPa)	–2.819	1.20658	0.01593
Tension Cut	T (MPa)	0	–2.06843	0

In Equation 5-2, $F_c(I_1, \kappa)$ can be expressed as:

$$F_c(I_1,\kappa)=\frac{1}{R}\sqrt{\left[X(\kappa)-L(\kappa)\right]^2-\left[I_1-L(\kappa)\right]^2} \quad (5\text{-}5)$$

$$X(\kappa)=\kappa+RF_e(\kappa) \quad (5\text{-}6)$$

$$L(\kappa)=\begin{cases}\kappa & \text{if } \kappa>0\\ 0 & \text{if } \kappa\le 0\end{cases} \quad (5\text{-}7)$$

where $X(\kappa)$ is the intersection of the cap surface with the I_1 axis and the hardening parameter κ is related to the plastic volume change ϵ_v^p through the hardening law

$$\epsilon_v^p=W\left\{1-\exp\left[-D\left(X(\kappa)-X_0\right)\right]\right\} \quad (5\text{-}8)$$

where the values of parameters W and D are found from hydro-static compression test data. The value of R is the ratio of major to minor axes of the quarter ellipse defining the cap surface. The parameters used in the numerical simulation are shown in Table 5.6.

To understand the failure behavior of the cap soil material, the various soil properties were collected as given in Table 5.6. Two different soil properties, McCormick Ranch Sand (*27*) and elasto-plastic soil parameters given in *NCHRP Report 556* (*28*), were compared to verify the cap property used in this study. The cap models for each case were plotted as shown in Figure 5.6. In the failure surface $[f_1(\sigma)]$ and tension cutoff region $[f_3(\sigma)]$, the three soils show good agreement, but in the elliptical cap $[f_2(\sigma, \kappa)]$, the soil material used in simulation shows a larger cap surface area than the other soils due to the large R.

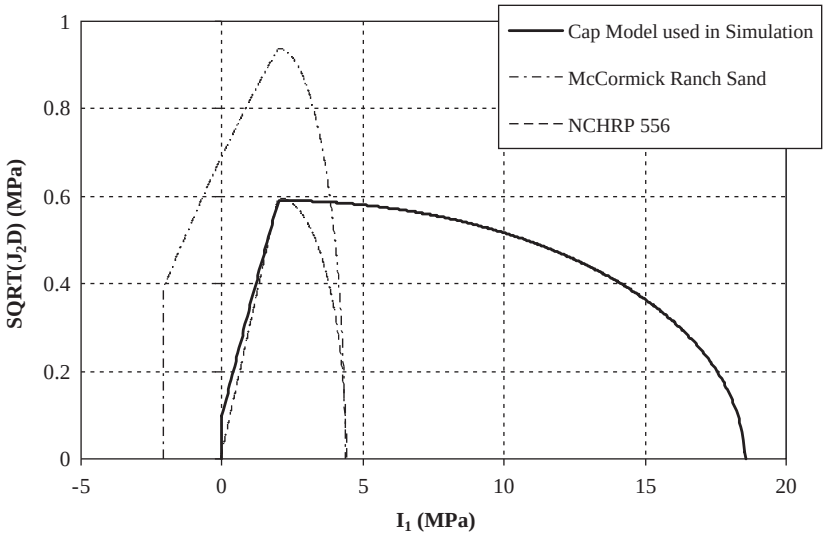

Figure 5.6. Comparison of cap models.

(a) 5,000 lb TTI test bogie.

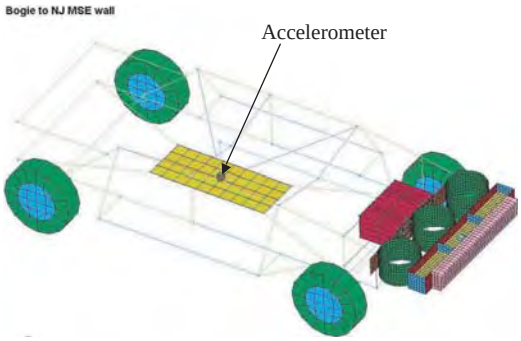

(b) 5,000 lb bogie model.

Figure 5.7. 5,000 lb bogie model.

Bogie Vehicle

The Texas Transportation Institute (TTI) test bogie is a 2,268 kg (5,000 lb) vehicle configured with three 304.8 mm (12 in.) diameter crushable steel cylinders on its nose assembly as shown in Figure 5.7. A spreader beam is attached across the three cylinders as shown in Figure 5.8. A wood block is attached to the face of the spreader beam to help dampen high-frequency noise during an impact. The bogie has an accelerometer installed at its CG.

The finite element model of the bogie consisted of a simple representation of the vehicle chassis with a more detailed representation of the crushable nose assembly. Similar to the test bogie, an accelerometer was placed at the CG of bogie model. The finite element model of the bogie consists of 3,935 elements and 4,645 nodes.

Initialization of the Model for Gravitational Loading

The MSE wall and barrier model was initialized to account for gravitational loading on the soil mass. Gravity loading effects soil pressure on the wall panels and the buildup of initial stresses in the steel strips. This step had to be done prior to vehicular impact on the barrier. It was achieved by gradually ramping up gravity on the system while imposing a diminishing mass damping on the soil mass to prevent oscillatory forces from developing. The gravity loading and damping on the soil are shown in Figure 5.9.

The weight of the system was measured and used as a convergence criterion for the steady state solution for the MSE wall model with 4.88 m (16 ft) strips as shown in Figure 5.10. For example, the total mass of the finite element model with the N.J. barrier on top of the MSE wall with 4.88 m (16 ft) long strips is 277,549 kg (19,018 slug or 611,890 lb mass). The weight of the system is calculated to be 2,721.6 kN (611.85 kips) using the mass of the finite element model and the acceleration of gravity. Therefore, after accounting for gravitational load, the weight of the model system should converge to the calculated system weight. The weight of the finite element model was 2,717.7 kN (610.96 kips) at the end of initialization step. A reasonable agreement shows that the weight of the finite ele-

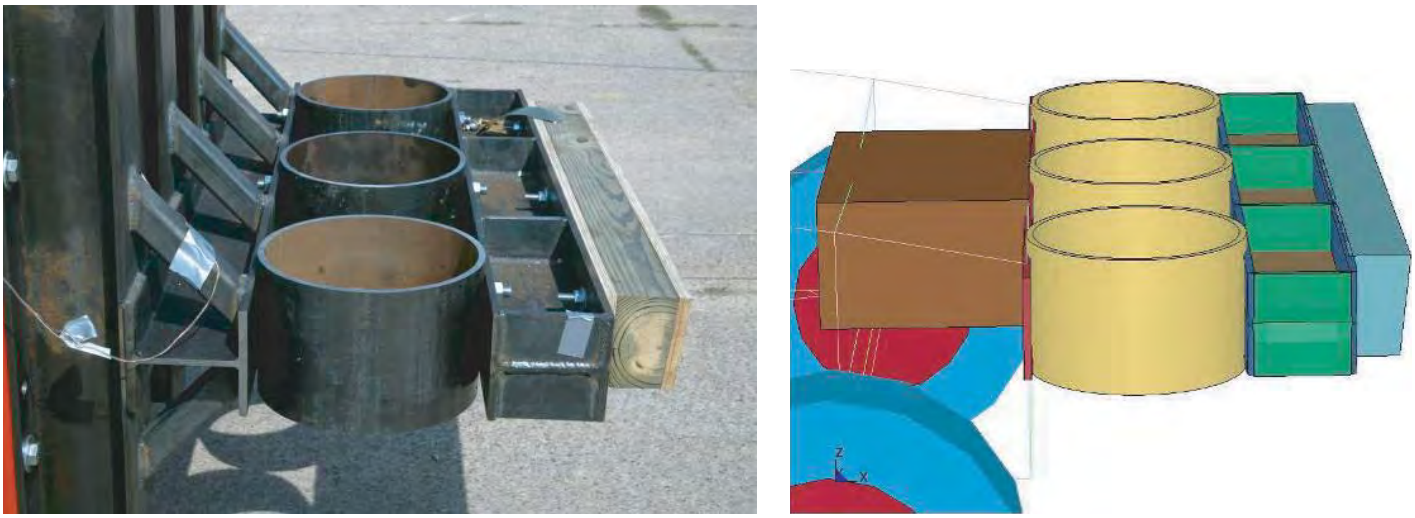

Figure 5.8. Detailed crushable cylinders of test bogie and numerical simulation.

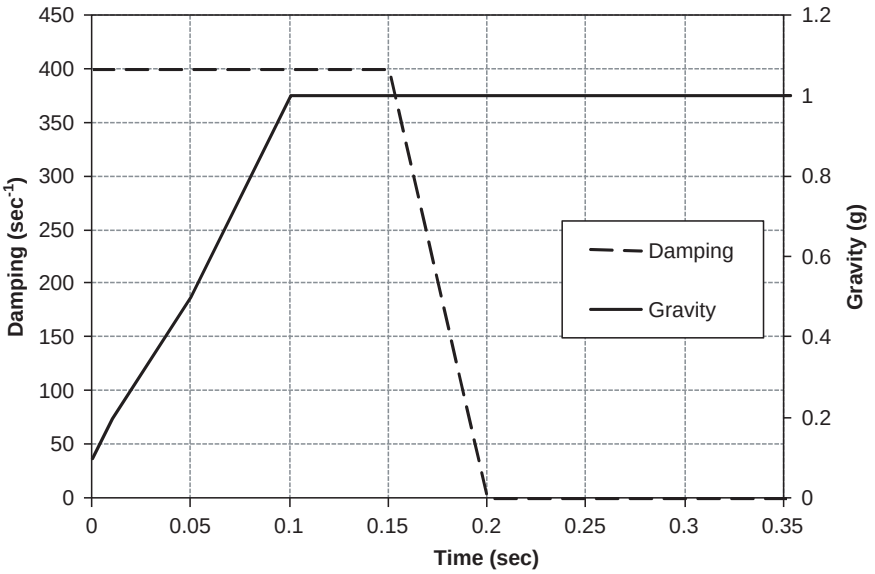

Figure 5.9. Gravity and damping of the MSE wall in steady state condition.

ment model approached the calculated weight of the model system as shown in Figure 5.10.

5.2.2 Finite Element Model: Boundary Conditions

Initially, the overburden soil on the moment slab was defined to be continuous across the front traffic edge of the moment slab. Along the sides of the moment slab, the soil was discontinuous and only constrained in the longitudinal direction (*y*-direction in Figure 5.11) to retain it in place and properly account for mass and inertial effects.

Thus, the first attempted model did not account for any friction or shear strength that might exist along the sides of the moment slab [Figure 5.12(a)]. The displacement of the barrier–moment slab system using this condition was greater than expected based on field experience with these systems. Additionally, the forces estimated in the strips were well above those computed based on current AASHTO LRFD design practice. The lateral displacement at the bottom edge of the coping was predicted to be of sufficient magnitude to contact and apply substantial force to the recessed wall panel (see the circle in Figure 5.11). This contact will undoubtedly increase the forces in the wall reinforcement and has the potential to

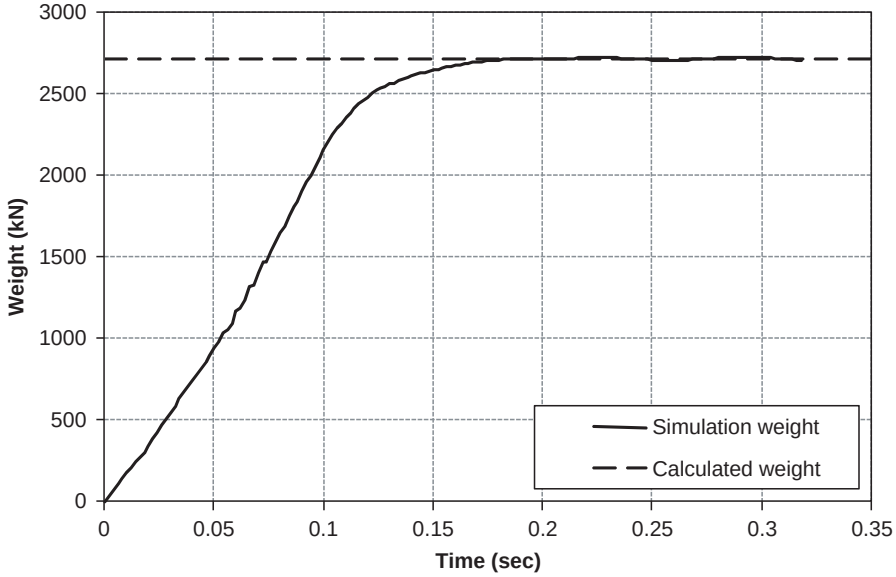

Figure 5.10. System weight of the MSE wall model.

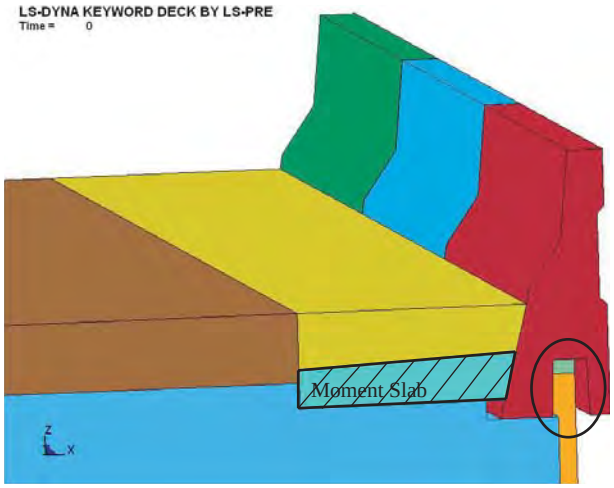

Figure 5.11. System reaction force of the MSE wall model.

fracture the wall panel and/or result in sufficient movement of the panel to cause pullout of the reinforcing strips. It was theorized that some of this "excessive movement" in the barrier–moment slab system might be attributed to the model's neglect of friction along the sides of the overburden soil and moment slab. The sensitivity of the dynamic behavior of the system to the boundary conditions along its sides was investigated through additional simulations.

In practice, the boundary conditions for a barrier–moment slab system can vary from installation to installation. In some systems, adjacent moment slabs are doweled together—a practice that greatly enhances the shear resistance at the edge of the moment slab. If dowel bars are not used, the moment slab sections act independently of one another but there will still be some shear capacity at the interface due to frictional contact. In both cases, the shear strength of the overburden

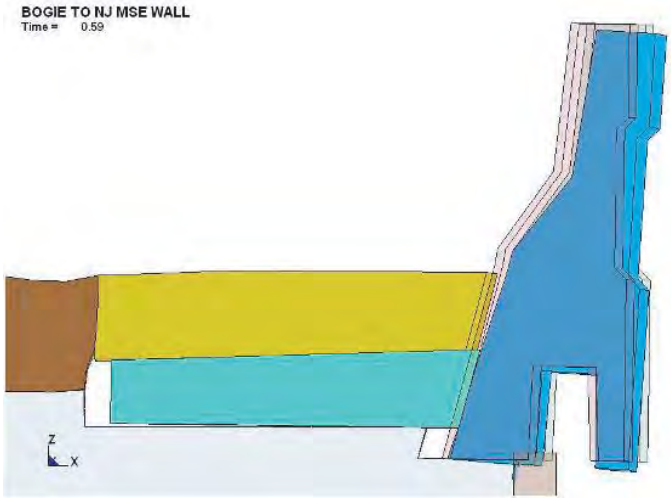

(a) No friction boundary condition

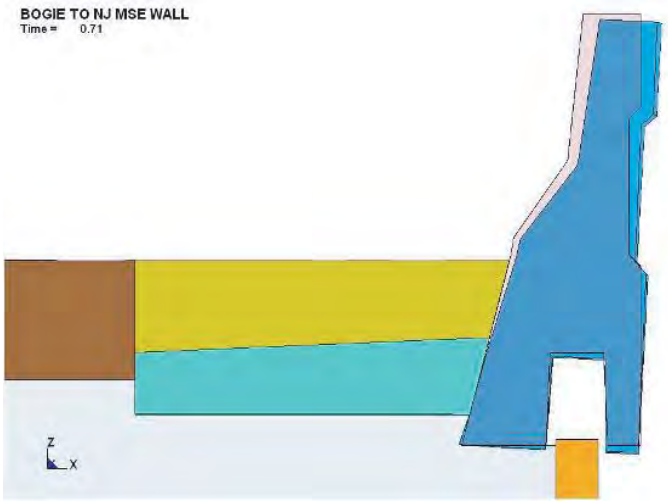

(b) Friction wall condition

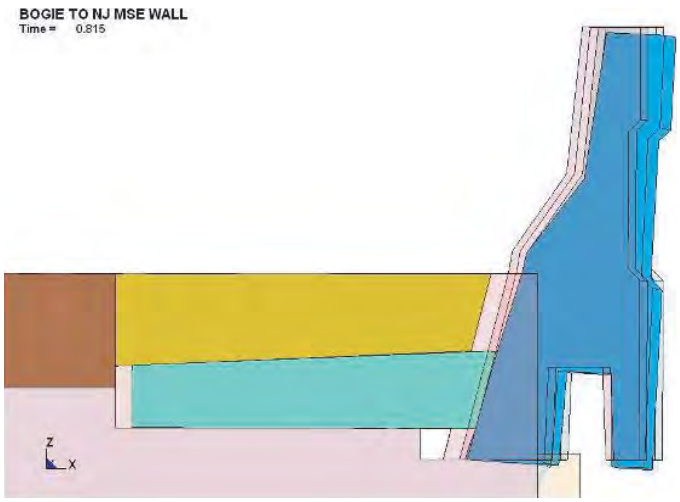

(c) Side soil condition

Figure 5.12. Comparison of simulation with different boundary condition.

soil and overlying pavement surface that is continuous across the moment slab interface will increase the overall resistance of the system to movement.

A second model was constructed with frictional contact on each side of the barrier–moment slab system and soil [Figure 5.12(b)]. The static and dynamic coefficients of friction were defined based on angles of internal friction of 35 degrees and 31 degrees, respectively.

As indicated by the results of these simulations shown in rows 1 and 2 of Table 5.7, friction at the ends of the moment slab and overburden soil can have a pronounced effect on the displacement and rotation of the barrier–moment slab system under impact load. The two simulations are thought to bracket the barrier movement likely to be observed in the bogie tests.

Given the range of movement observed at the bottom of the coping in the previous simulations, an additional simulation effort was undertaken in an attempt to more precisely define the soil and moment slab boundary conditions as shown in Figure 5.12(c). The overburden soil was extended across the edges of the moment slab, and a soil continuum was modeled adjacent to the ends of the moment slab (replacing the previously modeled side wall). The shear strength of the overburden soil was captured through the soil material model rather than through a defined frictional contact. The interface between the moment slab and adjacent soil were defined through definition of material contacts with friction coefficients assigned based on the angle of internal friction of the soil. Additionally, the row of elements directly beneath the moment slab and adjacent to the bottom edge of the coping were removed from the soil mesh [see the circle in Figure 5.12(c)]. Based on analyses of the previous simulations, it was theorized that these elements may be providing artificially high resistance to rotation of the barrier–moment slab system.

A comparison of displacements for the barrier–coping section obtained from the different simulations is shown in Table 5.7. The greatest movement was obtained for the model without side friction. The lowest displacements at the top and bottom of the barrier–coping section were obtained from the model in which the ends of the overburden soil and moment slab were in frictional contact with side walls. The model with continuous overburden soil across the ends of the moment slab fell between the other two. The fact that the simulation with continuous overburden soil is closer to the results of the model without side friction than the model with frictional side walls is at least partially due to the removal of a row of elements below the moment slab adjacent to the bottom edge of the coping.

Table 5.7. Comparison of displacements for bogie test models.

	Middle barrier at top	Middle barrier at bottom	Strip at front at impact location	Strip at end at impact location
No Side Friction	7.35 in.	4.25 in.	0.16 in. (4.0 mm)	0.13 in. (3.7 mm)
Side Wall	4.99 in.	0.03 in.	0.07 in. (2.0 mm)	0.065 in. (1.7 mm)
Continuous Soil	6.69 in.	3.30 in.	0.15 in. (4.0 mm)	0.128 in. (3.3 mm)

Table 5.7 also shows a comparison of the displacement of the reinforcement strip directly under the point of impact, which is the one that experiences the highest impact load. The displacements at the end of the strip range from 1.7 mm (0.065 in.) to 3.7 mm (0.13 in.). These displacements are due to transfer of the barrier impact load into the MSE wall (through the backfill soil) and do not include any movement that may arise because of direct contact between the coping and wall panels. While it is arguable which of the simulations most closely resembles reality, they collectively raised concern regarding the possibility of strip pullout. Movement of the strip along its entire length would limit the magnitude of the impact force. In other words, the maximum force due to impact that can be measured in the strips is limited by their pullout resistance. If pullout occurs, the maximum forces imparted to the reinforcement strips due to a barrier impact will be reduced.

Without further test data to validate the soil model and boundary conditions, it was unknown which of the modeling methodologies most closely resembles the actual system. Data derived from the bogie tests were later used to calibrate and validate the finite element model so that additional simulations can be conducted with more confidence to support the development of new design guidelines and predict the performance of the barrier–moment slab system under a full-scale vehicular impact.

5.2.3 Simulated Impact into Barrier Placed on MSE Wall with 8 ft Long Strip

The simulated bogie vehicle hit the middle vertical barrier section at a speed of 32.67 km/h (20.3 mph). The point of impact was slightly offset from the centerline of the middle barrier section to align with one of the reinforcement strips (strip D1). To enable comparison of forces and displacements, selected strip locations were assigned an alphanumeric designator that describes its horizontal position relative to the bogie impact point and its vertical reinforcement layer. The location designator used is based on a density of three strips per layer per panel. For example, strip D1 is positioned beneath the impact point in the first (i.e., upper) layer of reinforcement as shown in Figure 5.13.

Sequential images from the simulation are shown in Figure 5.14. The maximum displacement at the top of the middle barrier occurred at 0.07 sec. The maximum 50 msec average impact load was 346.38 kN (77.87 kips) at 0.04 sec as

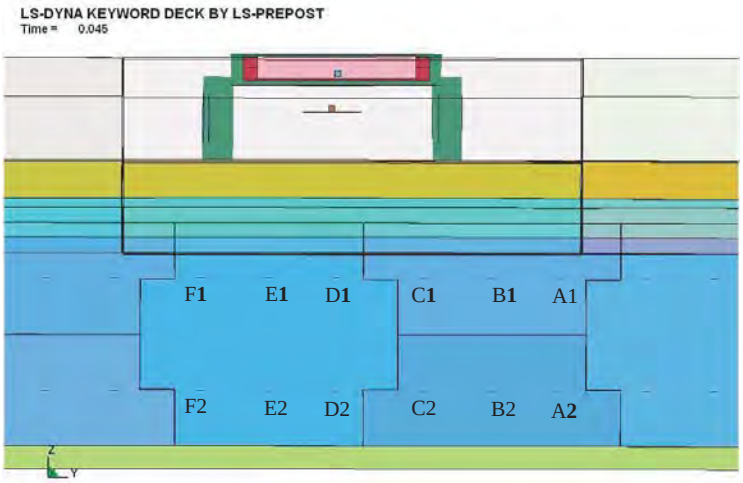

Figure 5.13. Strip location indicator.

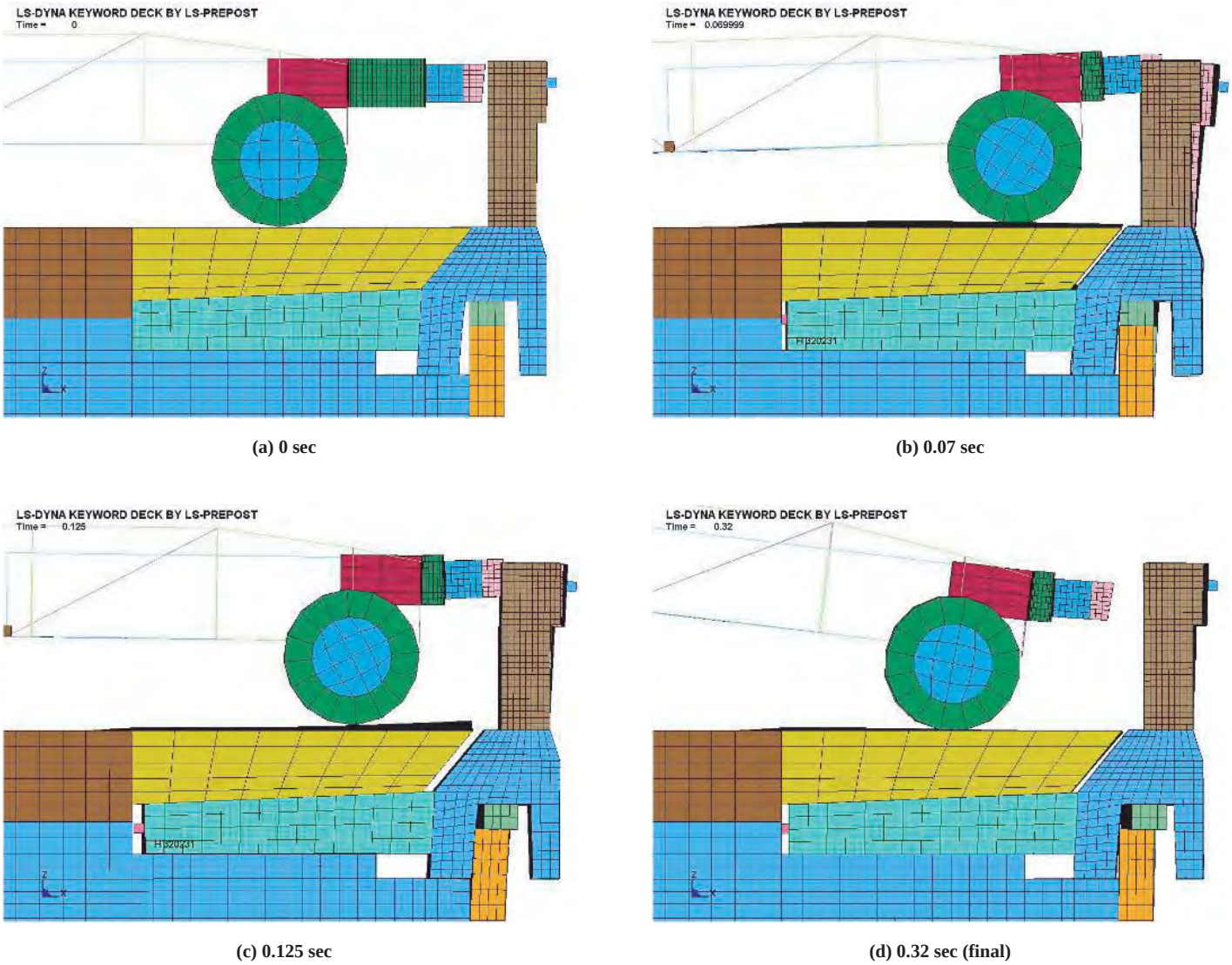

(a) 0 sec

(b) 0.07 sec

(c) 0.125 sec

(d) 0.32 sec (final)

Figure 5.14. Sequence image of model during impact.

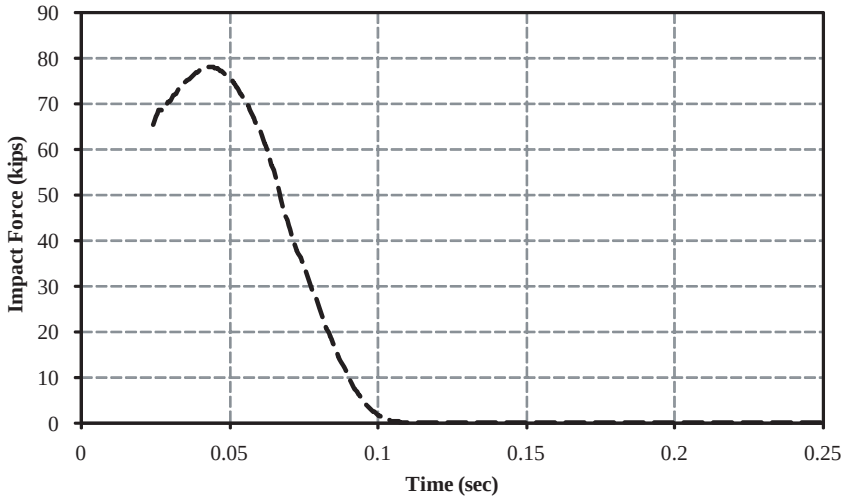

Figure 5.15. Impact load.

shown in Figure 5.15. The maximum dynamic displacement was 99 mm (3.9 in.) at the top of the barrier and 44.5 mm (1.75 in.) at the bottom of the coping. The permanent displacement was 54 mm (2.1 in.) at the top of the barrier and 33 mm (1.29 in.) at the bottom of the coping. The maximum dynamic displacement of the panel was 4.3 mm (0.17 in.) at the upper reinforcement layer and 1 mm (0.04 in.) at the second layer. The permanent displacement of the panel was 2.3 mm (0.09 in.) at the upper layer and 0.4 mm (0.02 in.) at the second layer (see Figure 5.16).

As shown in Figure 5.17, the damage profile that develops in the simulated barrier is similar to that observed in previous tests of N.J. profile barriers. It occurs above the toe of the barrier and has a parabolic shape. However, because of the short [3.05 m (10 ft)] length of the precast barrier section that was modeled, much of the damage eventually radiates out to the free ends of the section.

The strip load in the numerical simulation consists of the initialized static load and the dynamic impact load. Figure 5.18 shows the raw data of the total load in selected reinforcement strips. The maximum instantaneous load for strip D1 was 21.31 kN (4.79 kips). The total maximum 50 msec tensile load for strip D1 was 15.44 kN (3.47 kips) at a distance of 178 mm (7 in.) from the face of the panel, which corresponds to the planned location of strain gages in the test installation (Figure 5.19).

The distributions of maximum load along the reinforcement strips at the uppermost reinforcement layer (D1) are presented in Figure 5.20. As expected, the maximum load in a given strip occurs near its attachment to the wall panel and the

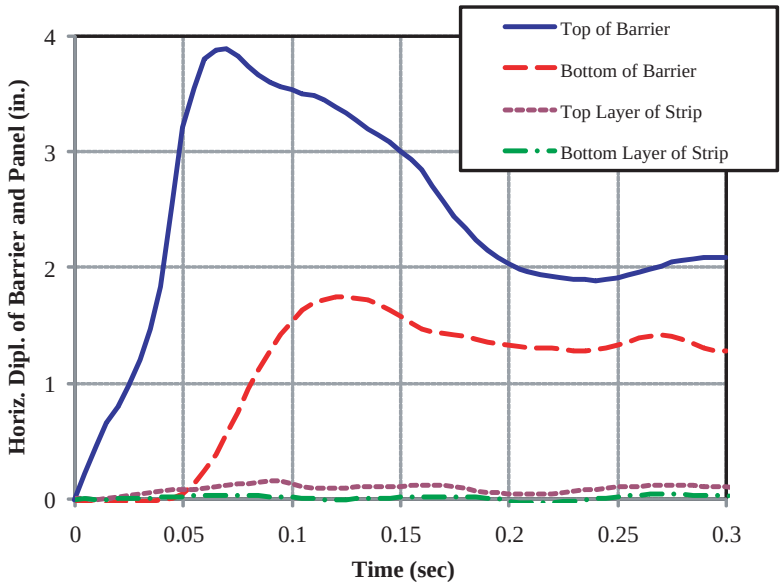

Figure 5.16. Displacement of barrier and panel.

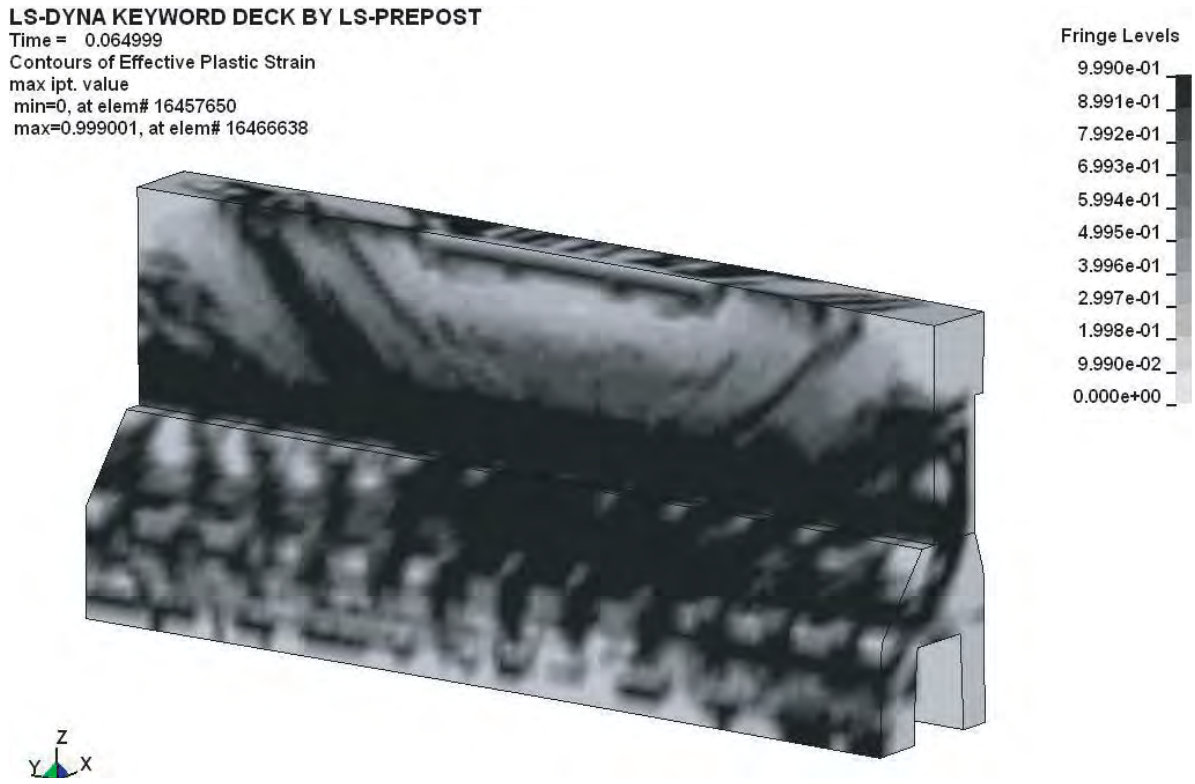

(a)

(b)

Figure 5.17. Concrete damage profile on (a) front side and (b) back side of the barrier.

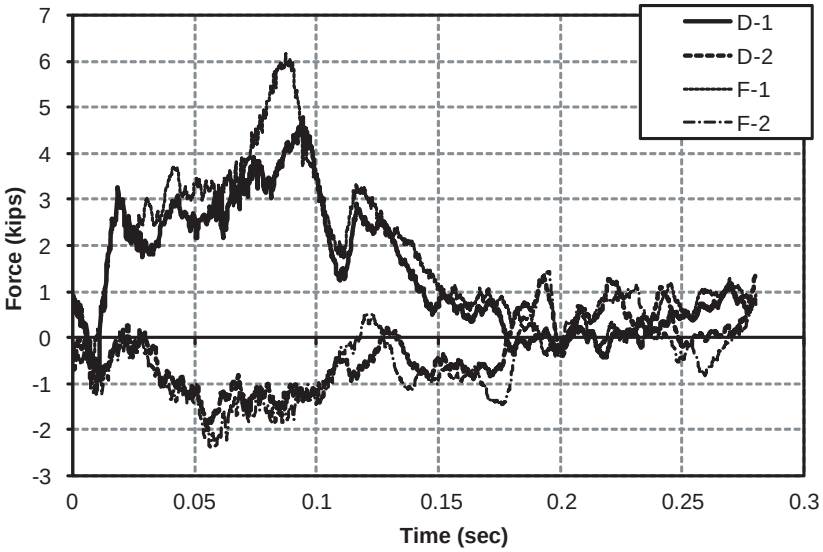

Figure 5.18. Raw data of load on the strip.

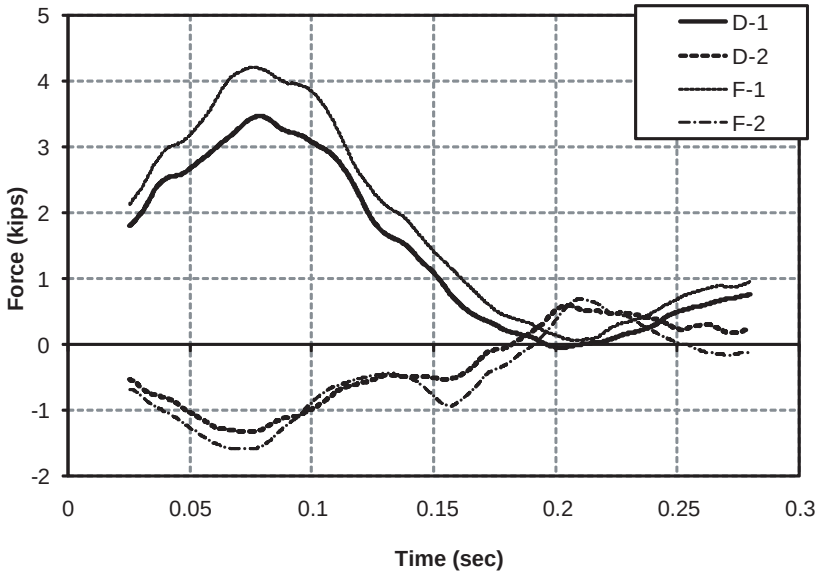

Figure 5.19. 50 msec average load on the strip.

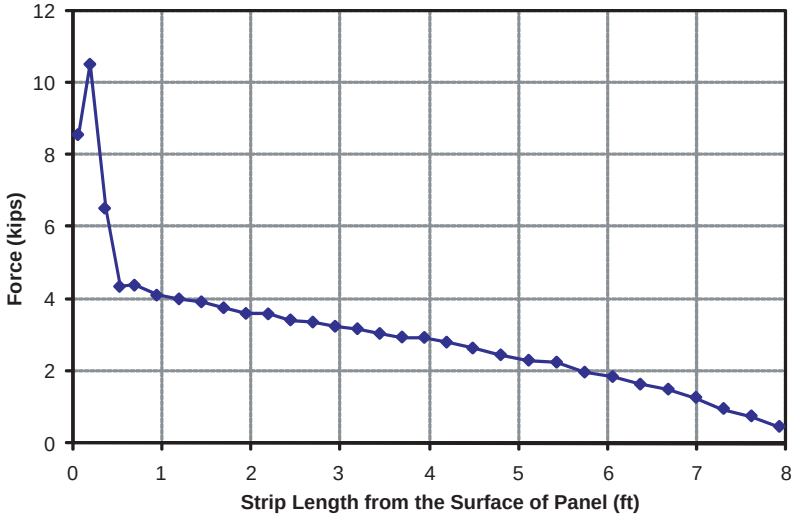

Figure 5.20. Distribution of load on the strip (D1) at 0.087 sec.

Table 5.8. Load in strips at 7 in. location from the face of the wall panel.

Load	Location on Strip			
	D1	D2	F1	F2
Total max. load (kips)	4.79	1.36	6.17	1.45
Total 50 msec average load (kips)	3.47	0.6	4.2	0.68

load decreases along its length. The loads in the strips attached to the wall panel below the point of impact in the middle of the barrier section have similar distributions. Table 5.8 shows the absolute maximum load in the strips at the location 178 mm (7 in.) from the wall end of the reinforcement.

The strain on the wall panel surface was evaluated to check the resistance of the panel-to-barrier impact loads. Figure 5.21 shows the strains predicted in the numerical simulation at strip D1. The maximum compressive strain was 0.0047 at 0.095 sec.

The maximum bending moment (M_i) per unit length of wall at the top level of reinforcement can be calculated by a simple model as shown in Figure 5.22. The moment (M_i) is generated from the horizontal shear load (H) on top of the panel times the moment arm (l) and the vertical load (V) that is transferred from the barrier to the panel during the impact times the moment arm ($t/2$) where t is the thickness of the panel. Because the simulation corresponded to a peak dynamic force of 346.38 kN (77.87 kips) when the design calls for 240 kN (54 kips), the results of the numerical simulation were decreased by the ratio of 240 kN / 346.38 kN (54 kips / 77.87 kip)

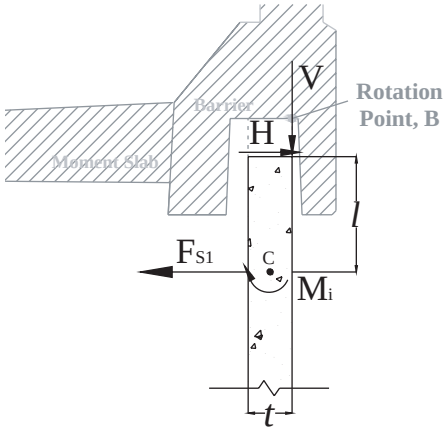

Figure 5.22. Free body diagram on the panel (rotation point B).

The distribution of shear load, vertical load, and bending moment along the panel at the time of peak force during the impact is shown in Figures 5.23, 5.24, and 5.25, respectively. In this case, the forces due to the rebars in the panel were neglected. The predicted shear load was 2.62 kN (0.59 kips) at the top of the panel during the impact due to the friction between the leveling pad and the panel. The vertical load transferred by the barrier was 9.61 kN (2.16 kips).

5.2.4 Simulated Impact into Barrier Placed on MSE Wall with 16 ft Long Strip

The simulated bogie vehicle impacted the middle N.J. barrier section at a speed of 32.19 km/h (20 mph). The point of

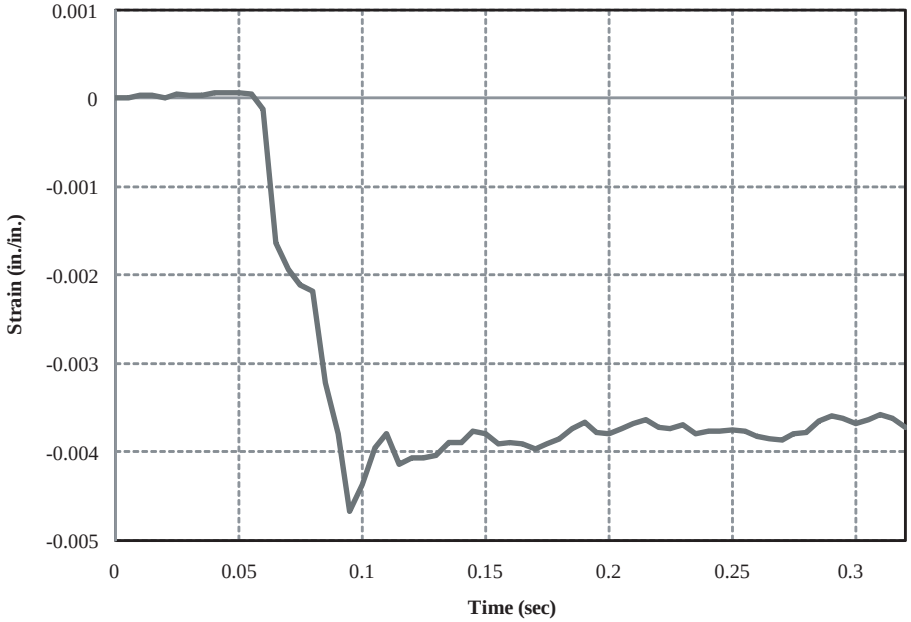

Figure 5.21. Panel strain at strip D1 in MSE wall with 8 ft long strips.

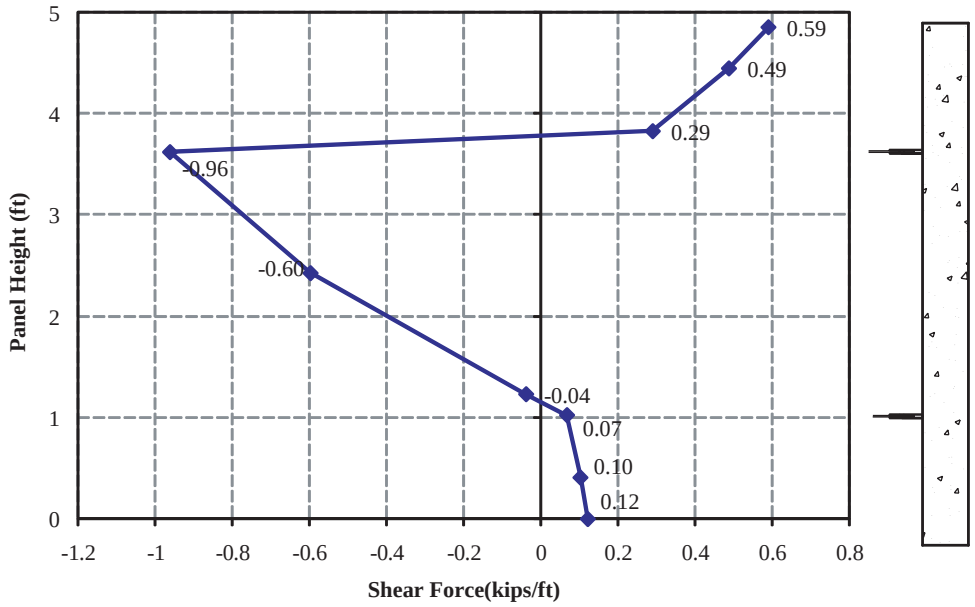

Figure 5.23. Shear load on the panel.

impact was slightly offset from the centerline of the middle barrier section to align with one of the reinforcement strips (D1). To enable comparison of forces and displacements, the same alphanumeric designators shown in Figure 5.13 were used

Sequential images from the simulation are shown in Figure 5.26. The maximum displacement at the top of the middle barrier occurred at 0.07 sec. The maximum 50 msec average impact load was 359.06 kN (80.72 kips) at 0.038 sec (Figure 5.27). The maximum dynamic displacement was 108.7 mm (4.28 in.) at the top of the barrier and 33.3 mm (1.31 in.) at the bottom of the coping. The permanent displacement was 41.1 mm (1.62 in.) at the top of the barrier and 19.6 mm (0.77 in.) at the bottom of the coping. The maximum dynamic displacement of the panel was 5.6 mm (0.22 in.) at the upper reinforcement layer and 2.5 mm (0.1 in.) at the second layer. The permanent displacement of the panel was 1.5 mm (0.06 in.) at the upper layer and 0.8 mm (0.03 in.) at the second layer (see Figure 5.28). The damage profile that developed in the barrier is shown in Figure 5.29.

Figure 5.30 shows the raw data of the total load in selected reinforcement strips. The maximum instantaneous load for strip D1 was 39.86 kN (8.96 kips) at a distance of 178 mm

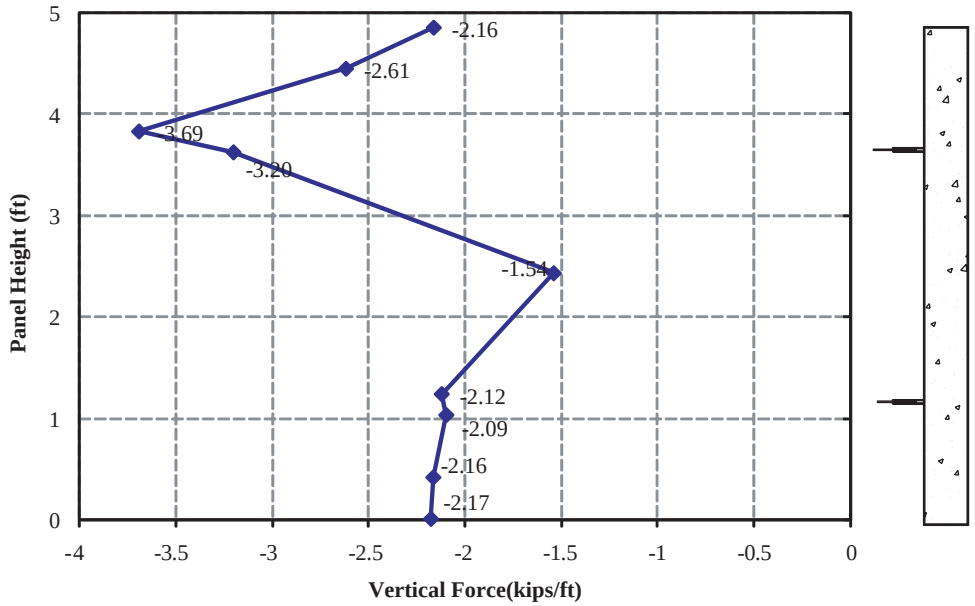

Figure 5.24. Vertical load on the panel.

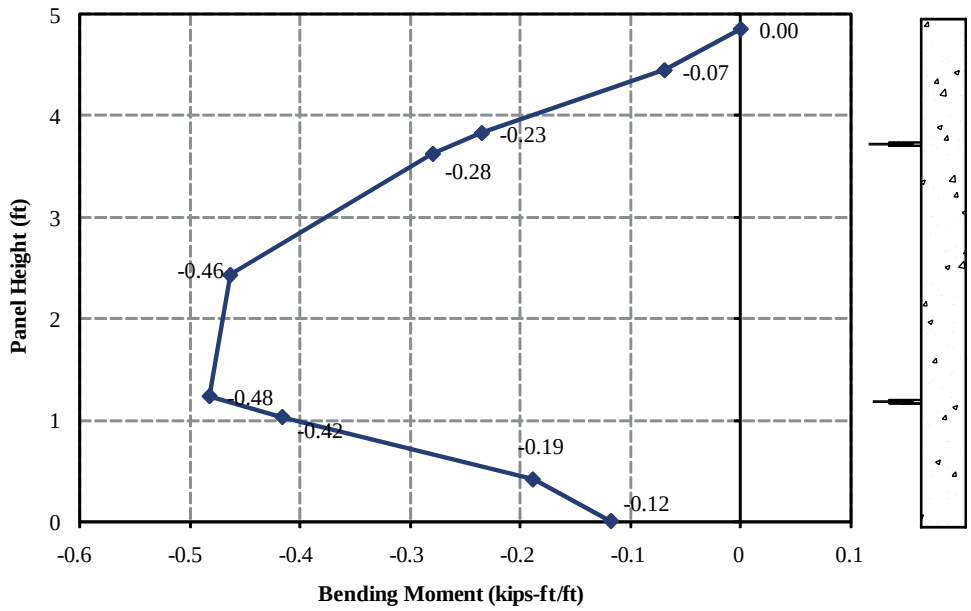

Figure 5.25. Bending moment on the panel.

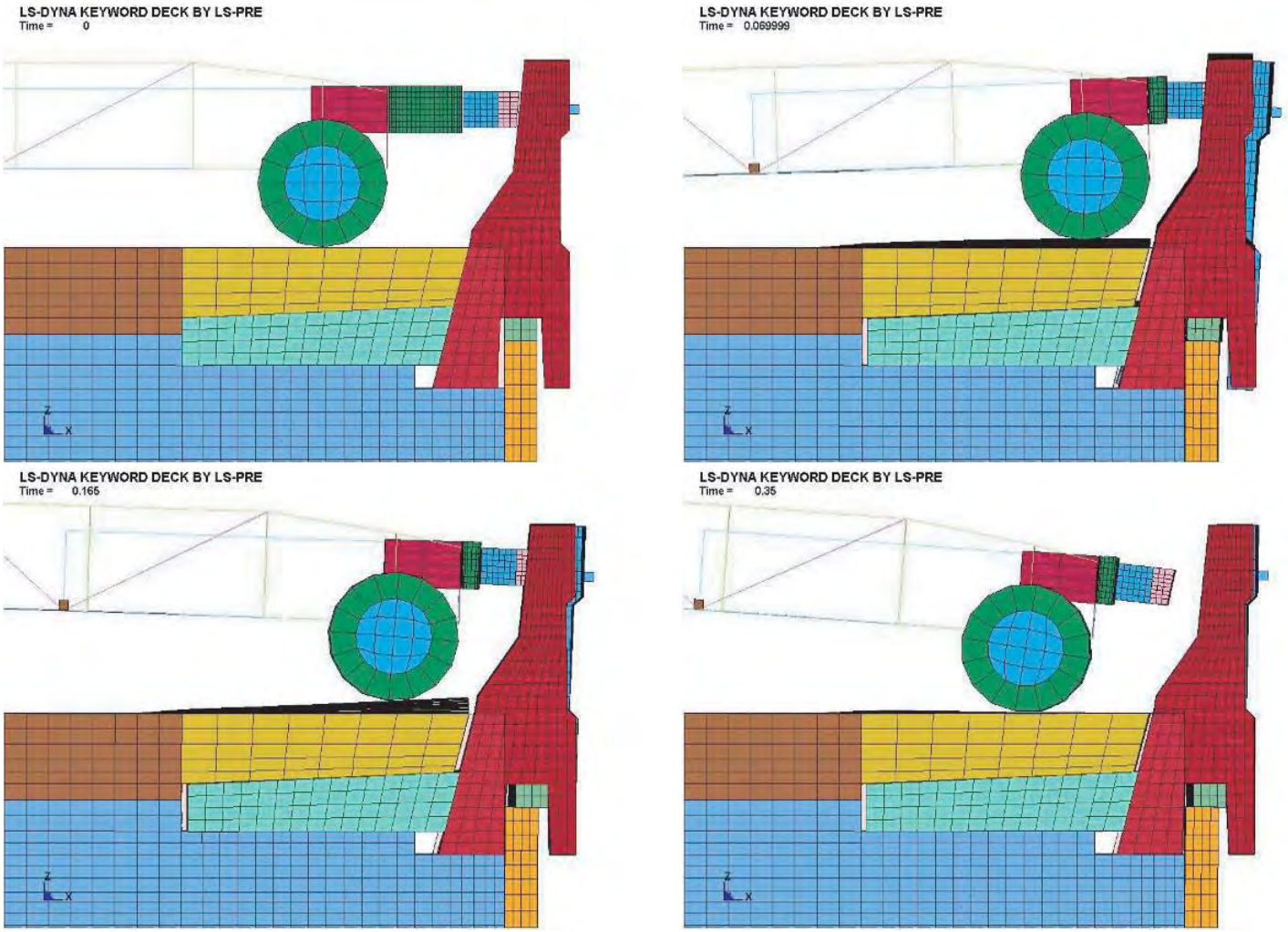

Figure 5.26. Sequence image of model during impact.

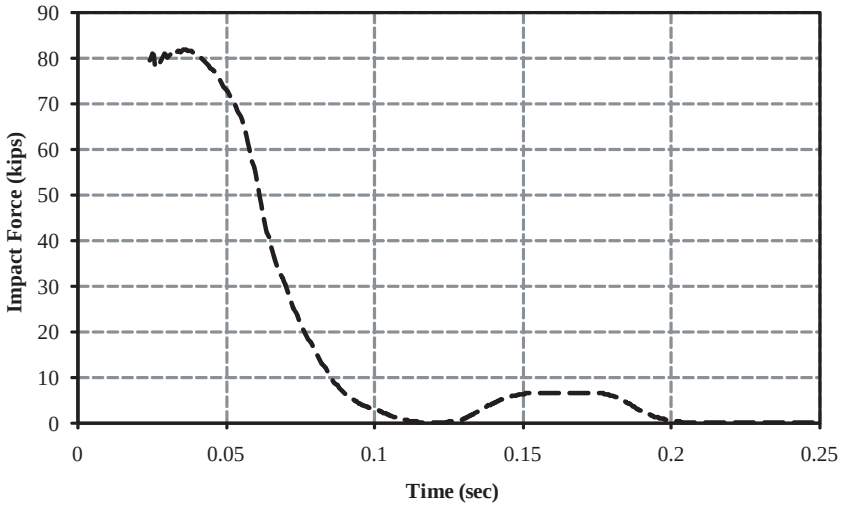

Figure 5.27. Impact load.

(7 in.) from the face of the panel which corresponds to the planned location of strain gages in the test installation. The total maximum 50 msec tensile load in the wall reinforcement was 28.96 kN (6.51 kips) (Figure 5.31).

The distribution of maximum load along strip D1 is presented in Figure 5.32. As expected, the maximum load occurs near its attachment to the wall panel and the load decreases along its length. The loads in the strips attached to the wall panel below the point of impact in the middle of the barrier section have similar distributions. Table 5.9 shows the summary of the load for the strips at a distance of 178 mm (7 in.) from the wall end of the reinforcement.

As in the previous simulation, the strain in the wall panel was evaluated to determine its ability to resist barrier impact loads. The results are shown in Figure 5.33. The maximum compressive strain was 0.0021 at 0.045 sec.

The maximum bending moment (M_i) per unit length of wall at the location of the top level of reinforcement can be calculated by the simple model shown previously in Figure 5.22. The moment (M_i) is generated from the horizontal shear load (H) on top of the panel times the moment arm (l) and the vertical load (V) which is transferred from the barrier to the panel during the impact times the moment arm (t/2) where t is the thickness of the panel. Because the simulation corresponded to a peak dynamic force of 359.06 kN (80.72 kips) when the design calls for 240 kN (54 kips), the results of the numerical simulation were decreased by the ratio of 240 kN / 359.06 kN (54 kips / 80.72 kip).

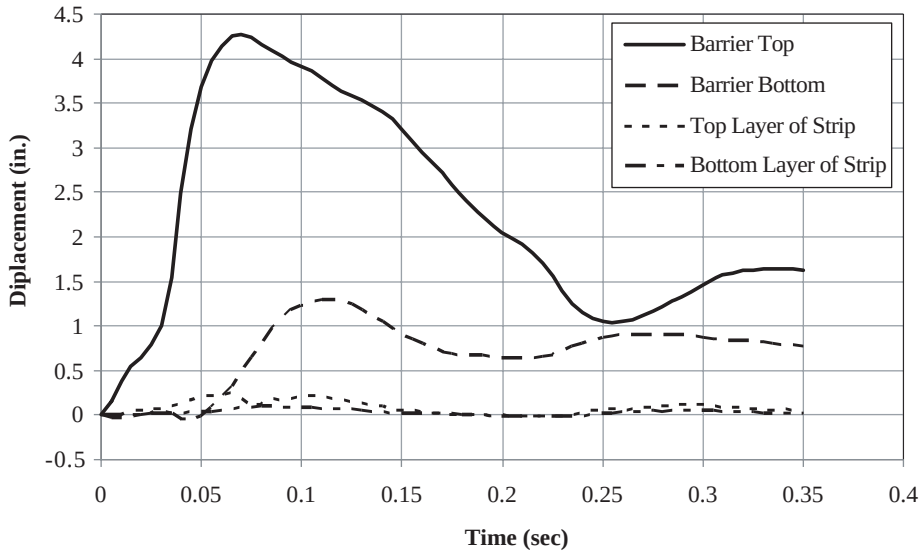

Figure 5.28. Displacement of barrier and panel.

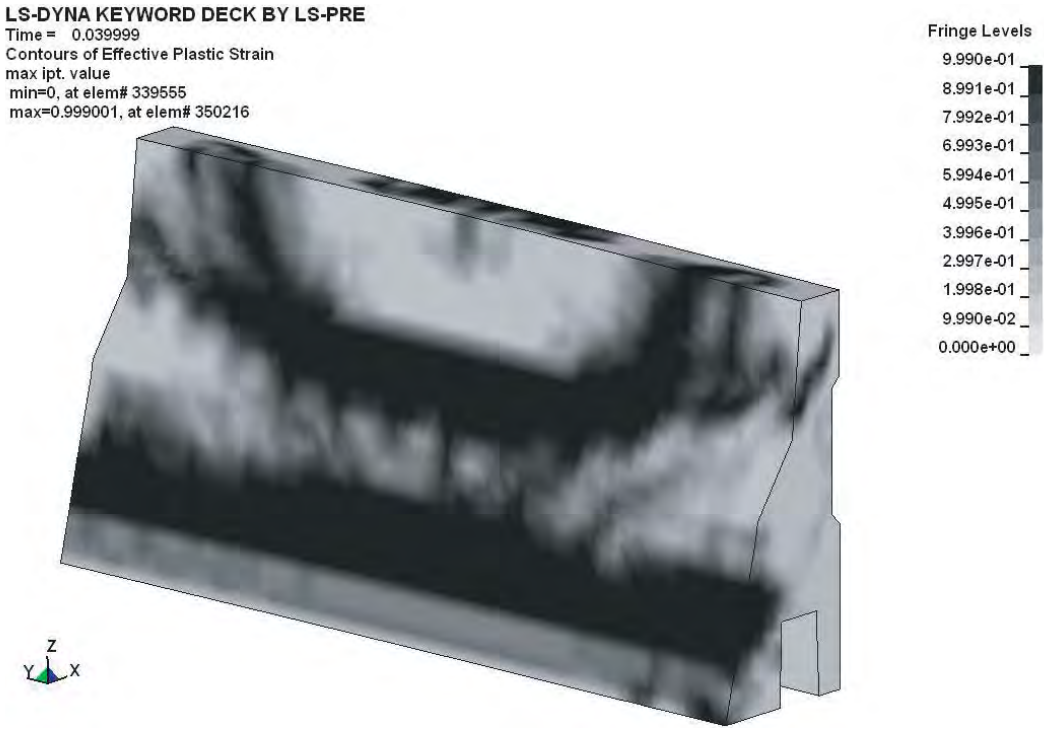

(a)

(b)

Figure 5.29. Concrete damage profile on (a) front side and (b) back side of the barrier.

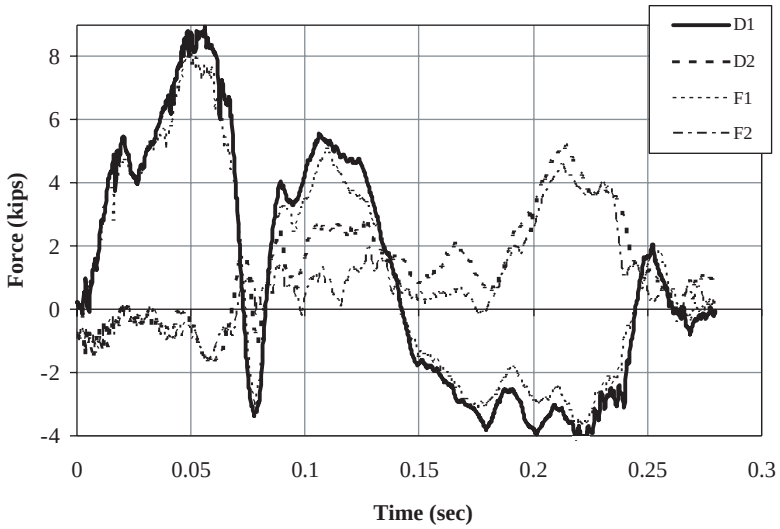

Figure 5.30. Raw data of load on the strip.

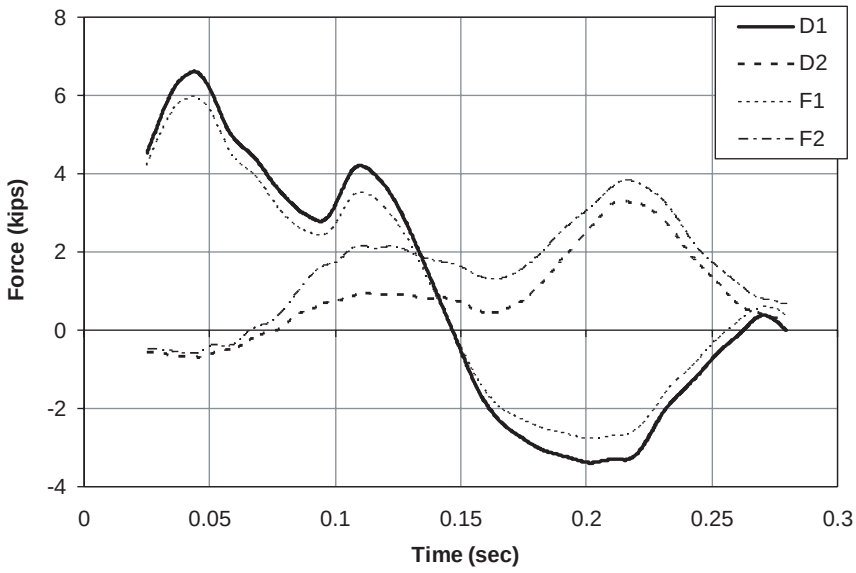

Figure 5.31. 50 msec average load on the strip.

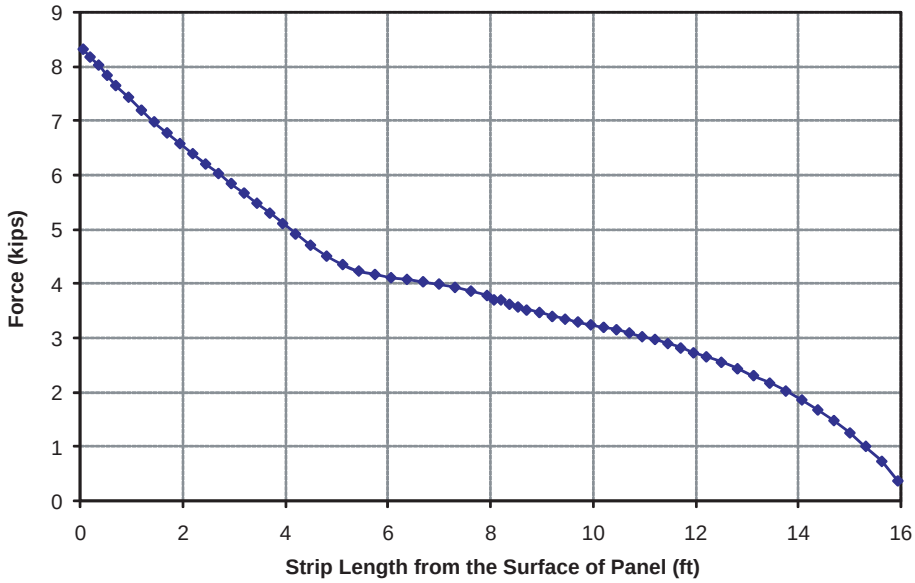

Figure 5.32. Distribution of load on the strip (D1) along the strip length.

Table 5.9. Load in strips at 7 in. location from the face of the wall panel.

Load	Location on Strip			
	D1	D2	F1	F2
Total max. load (kips)	8.96	4.59	8.35	5.22
Total 50 msec average load (kips)	6.51	3.31	5.95	3.83

The distribution of the shear load, vertical load, and bending moment along the panel at the time of peak force during the impact is shown in Figures 5.34, 5.35, and 5.36, respectively. The predicted shear load was 6.98 kN (1.57 kips) at the top of the panel during the impact due to the friction between the leveling pad and the panel. The vertical load transferred by the barrier was 76.2 kN (17.13 kips). Using the shear and vertical loads, the bending moment was calculated to be 18.15 kN-m/m (4.15 kips-ft/ft), which is higher than the calculated strength of

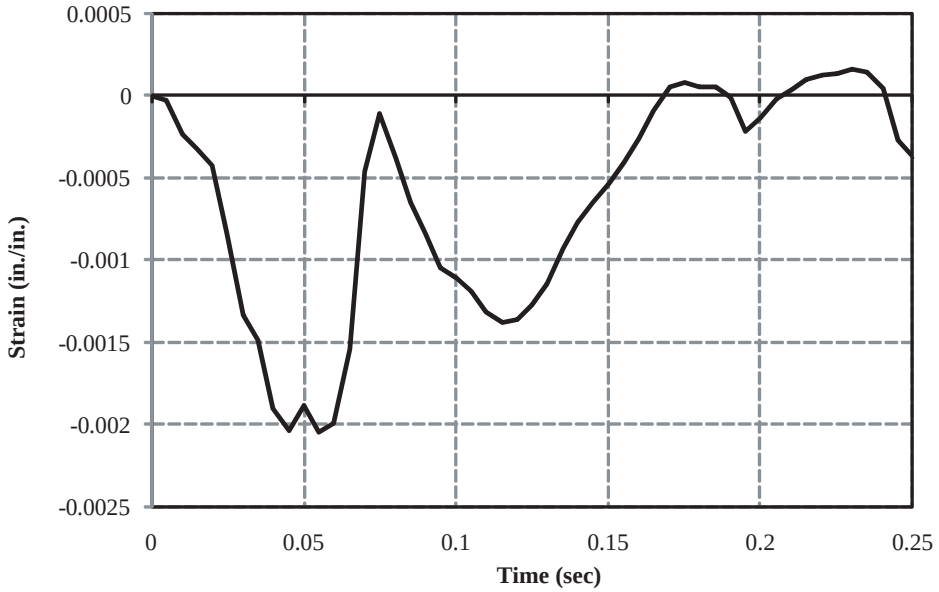

Figure 5.33. Panel strain at strip D1 in MSE wall with 16 ft long strip.

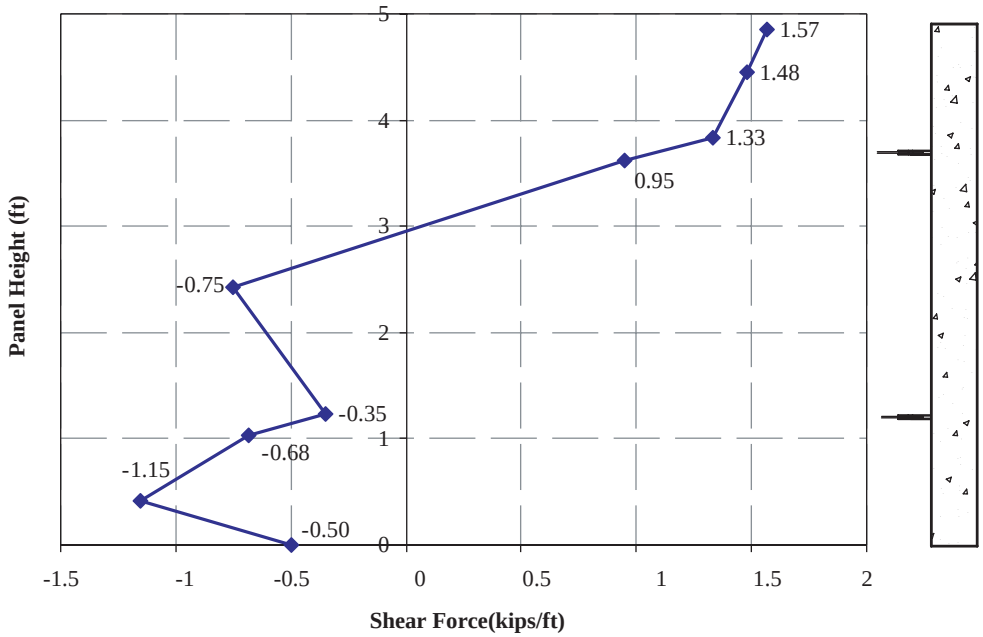

Figure 5.34. Shear load on the panel.

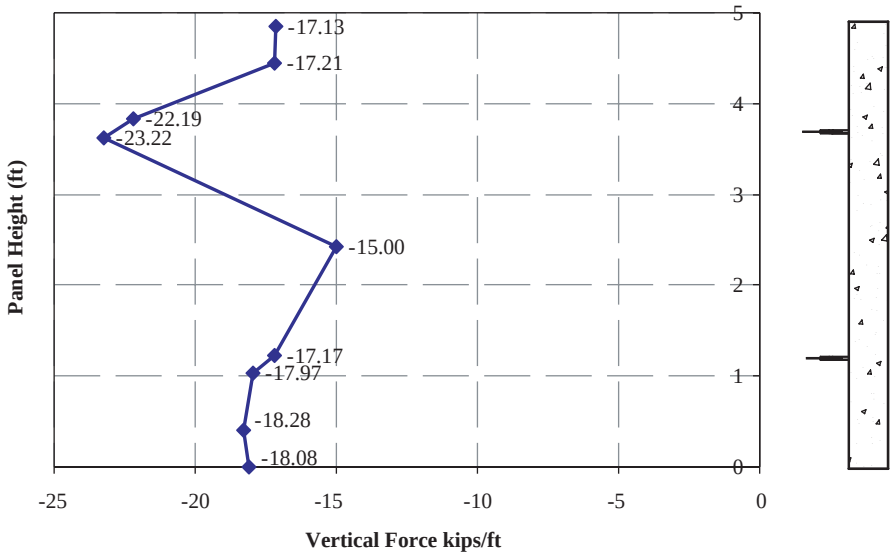

Figure 5.35. Vertical load on the panel.

the panel by ACI specifications (*29*) (12.9 kN or 2.9 kips) (details of the calculations are presented in Appendix J).

5.3 Bogie Test

5.3.1 5 ft High MSE Wall Construction and Test Installation

An elevation of the bogie test wall is shown in Figure 5.37. The total length of bogie test was approximately 18.29 m (60 ft). The MSE wall on which the six precast barrier and coping sections were placed was approximately 1.52 m (5 ft) tall and comprised full and half-panel sections that were approximately 1.52 m (5 ft) wide. The wall panels were placed on a 304.8 mm (1 ft) wide × 15.24 mm (6 in.) thick concrete leveling pad. The MSE wall had two layers of reinforcement at depths of 262 mm (0.86 ft) and 1.01 m (3.32 ft) below the bottom of the moment slab. The vertical distance between the two reinforcement layers was 0.75 m (2.46 ft). Half of the wall was constructed with 2.43 m (8 ft) reinforcement with a density of three strips per layer per panel and the other half with 4.88 m (16 ft) reinforcement with a density of two strips per layer per panel.

The wall panels were recessed inside the coping sections a distance of 203.2 mm (8 in.). The precast barrier–coping sections rested on a 101.6 mm (4 in.) thick leveling course of

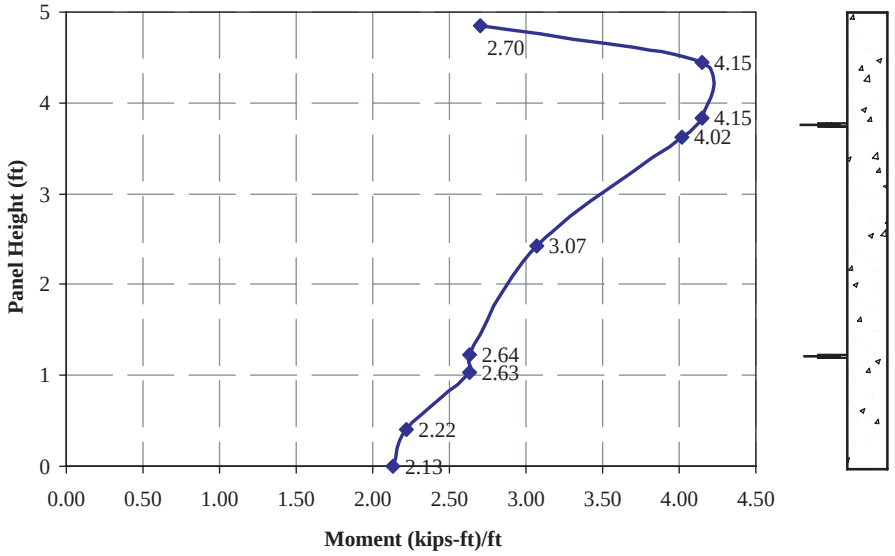

Figure 5.36. Bending moment on the panel.

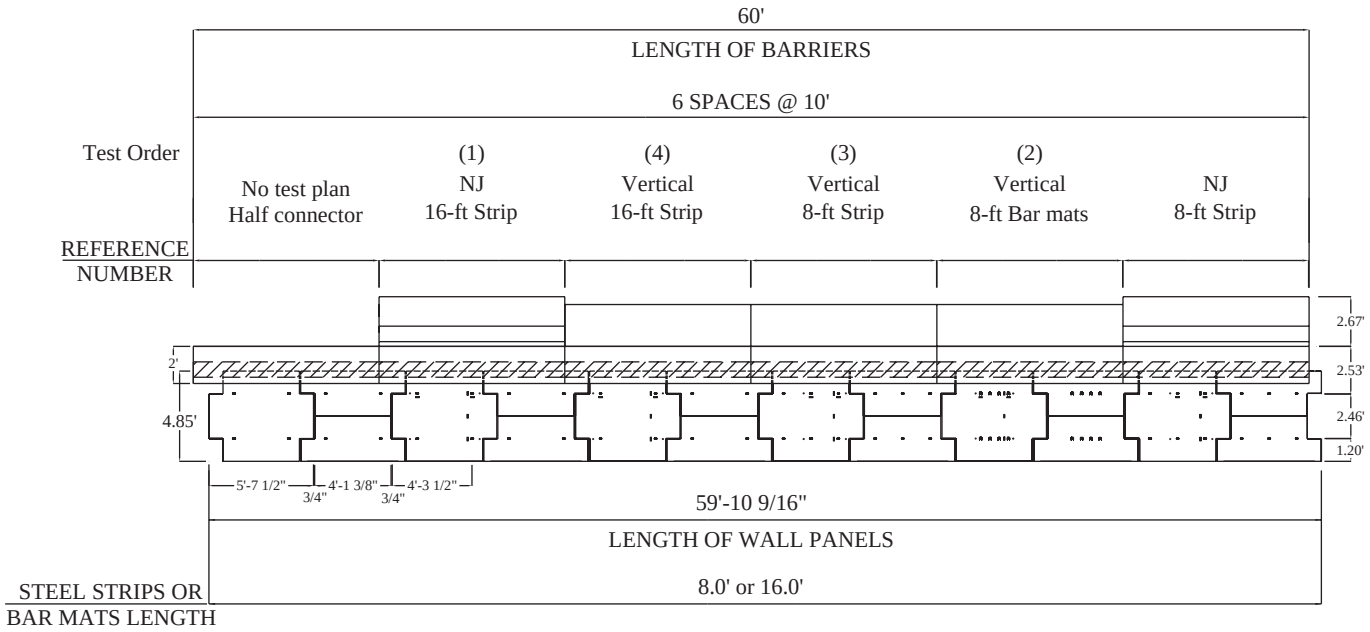

Figure 5.37. Overall elevation of installation for bogie tests.

concrete placed on top of the wall panels. The moment slab connecting the precast barrier–coping sections was cast in place in two 9.14 m (30 ft) lengths. The two 1.37 m (4.5 ft) wide, 9.14 m (30 ft) long moment slabs were connected to one another using two No. 9 shear dowels.

The backfill for the wall was crushed rock that met the specifications for TxDOT Type A backfill (*30*). The estimated friction angle for the crushed rock was 35 degrees and the unit weight was 20 kN/m^3 (0.125 kips/ft^3). The backfill was compacted in 0.15 m (6 in.) layers with 10 passes of a 1,320 kg (2,905 lb), 0.89 m (35 in.) wide drum roller. Also, the surface layer of soil was recompacted after each test. A grain size analysis was performed for the backfill material to determine the relative proportions of different grain sizes as shown in Figure 5.38. The particle diameters corresponding to 10% fines (D10) and 60% fines (D60) were 0.075 mm and 6.8 mm, respectively. The coefficient of uniformity [Cu (= D60/D10)] was determined to be 90.67, therefore, the friction factor (F*) at ground level was determined to be 2.0 in accordance with AASHTO LRFD (see Figure 2.5).

Selected reinforcement in the MSE wall was instrumented with strain gages to capture the tensile forces transmitted into the reinforcement during the dynamic bogie vehicle impacts. A total of eight strain gages were used for each reference test.

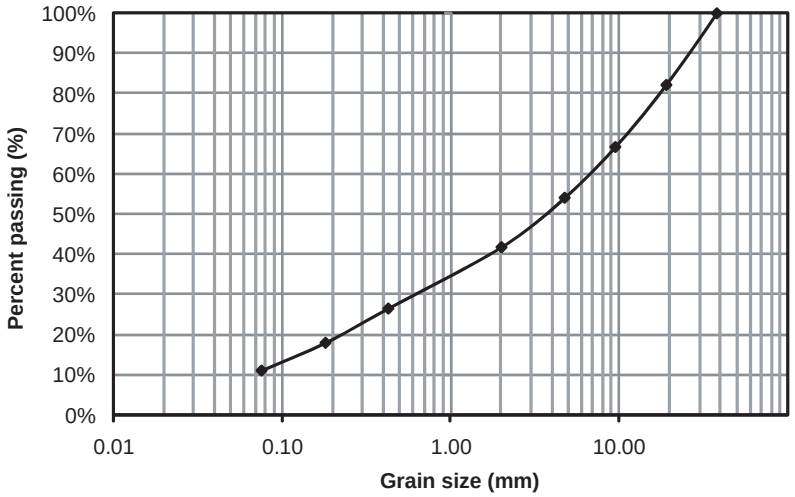

Figure 5.38. Particle size distribution curve of the backfill for bogie tests.

The placement of these strain gages was selected to measure the maximum tensile load in each layer of reinforcement as well as give an indication of the distribution of forces in the lateral, longitudinal, and vertical directions. Five strain gages were used on the upper reinforcement layer, and three strain gages were placed on the lower reinforcement layer. Two strain gages were used on both layers of reinforcement adjacent to the wall panel at the point of impact to provide some redundancy at the location expected to experience maximum tensile loading.

A contact switch was placed on the top edge of the traffic face (inside face) of the concrete leveling pad cast on top of the wall panels inside the recess of the coping. The switch indicates the time (referenced from impact) at which the barrier slides and/or rotates sufficiently for the coping to contact the wall panel/level up concrete.

The full-height wall panel below the point of impact on the barrier was instrumented with five concrete strain gages to capture normal strains in the panel induced from impact loads transmitted into the MSE wall and generated from direct contact of the barrier–coping section with the top of the wall panel. Two strain gages were placed in a horizontal position along the length of the panel just below the anchorages for the upper layer of reinforcement (region of maximum negative moment) that are below and immediately adjacent to the point of impact. These are the anchorage locations associated with the instrumented reinforcement. Three strain gages were placed in a vertical position along the height of the panel. A strain gage was placed adjacent to the anchorage locations for the upper and lower layer of reinforcement at the point of impact, and one strain gage was placed in the center of the panel between the two layers of reinforcement (region of maximum positive moment).

An accelerometer was mounted behind each barrier section at the height of impact to help analyze its dynamic response. An accelerometer also was placed on the end of each of the two 9.14 m (30 ft) long moment slabs at their midpoints to measure any acceleration or motion imparted to the moment slab during impact. Additionally, the bogie vehicle was instrumented with an accelerometer at its CG.

Angular and translational displacements and/or rotation of the barrier and wall panels were determined from high-speed video operating at 1,000 frames/s. Displacement gages were placed at the top and bottom of the precast barrier–coping section and at the upper and lower strip locations on the wall panel to assist with the displacement analysis.

String lines were placed behind the barrier and wall to measure their permanent deflection after impact. The four corner points on the barrier–coping sections and five points on each wall panel were measured. The distance from the string lines to the barrier and panel reference points were measured after each test.

A 2,268 kg (5,000 lb) bogie vehicle hit each bogie test section at a speed of approximately 35.41 km/h (22 mph) for the N.J. barrier and 32.19 km/h (20 mph) for the vertical concrete barriers. Prior numerical simulation results indicated that these velocities would provide sufficient energy to fail the barrier–coping section. By loading each barrier–coping section beyond its ultimate strength, the maximum impact loading transferred into the MSE wall would be measured.

The test sequence was selected such that the first two tests involved hitting the barrier segments in the middle of each moment slab. The other two tests were conducted on similar vertical concrete barriers located on the end of each moment slab with different strip length and density.

The precast barrier–coping sections, concrete wall panels, and steel strip wall reinforcement were provided by RECO at no cost to the project. RECO also provided supervision of the construction of the wall. The bar mat reinforcement that was used in one of the reference tests was provided by Foster Geotechnical at no cost to the project. Detailed drawings of the reference bogie test installation and construction procedure are presented in Appendix C and Appendix D, respectively, which are available from the *NCHRP Report 663* summary web page on the TRB website (www.trb.org) by searching for "NCHRP Report 663".

5.3.2 Bogie Test 1: New Jersey Barrier with 16 ft Strips

The 2,268 kg (5,000 lb) bogie vehicle, shown in Figure 5.39, hit the reference point of the N.J. profile barrier head-on at a speed of 35.08 km/h (21.8 mph). The reference impact point was 101.6 mm (4 in.) from the top of the barrier and 12.7 mm (0.5 in.) from the middle of the barrier to correspond to the location of the reinforcement in the underlying wall.

Figure 5.39. Bogie Test 1: N.J. barrier with 16 ft long strip.

Data from Accelerometers

The accelerations at the top of the barrier and end of the moment slab exceeded the range set for the accelerometers at these locations. Therefore, a portion of the signal representing the peak acceleration of the barrier and moment slab was truncated as shown in Figure 5.40(b) and (c). Consequently, the maximum 50 msec average acceleration provides lower values than expected. To prevent the reoccurrence of this problem, the range of accelerometer was increased for subsequent tests.

Data obtained from the bogie-mounted accelerometer were analyzed and the results are presented in Figure 5.41. As shown in Figure 5.41(b), the maximum 50 msec average deceleration was 14.45 *g*. Based on this acceleration and the mass of the bogie, the maximum 50 msec average impact force was calculated to be 326.5 kN (73.4 kips) [see Figure 5.41(a)]. The velocity–time and horizontal displacement–time histories of the bogie are shown in Figure 41(c) and (d), respectively. These time histories were calculated through integration of the acceleration data.

The maximum 50 msec average acceleration of the barrier, as measured by the accelerometer at the top of the barrier, was 7.35 *g* in the direction of impact [see Figure 5.42(a)]. The velocity–time history of the barrier, as calculated by integration of the raw acceleration data, is shown in Figure 5.42(b). The displacement–time history obtained from integration of the velocity history was known to have some inherent error due to the truncation of data from the barrier accelerometer. Figure 5.42(c) presents displacement–time history from both double integration of acceleration data and from analysis of the high-speed film which is considered to be more accurate.

The maximum 50 msec average acceleration of the moment slab is shown in Figure 5.43(a). The velocity–time and horizontal displacement–time histories of the moment slab are shown in Figure 5.43(b) and (c), respectively. The velocity–time his-

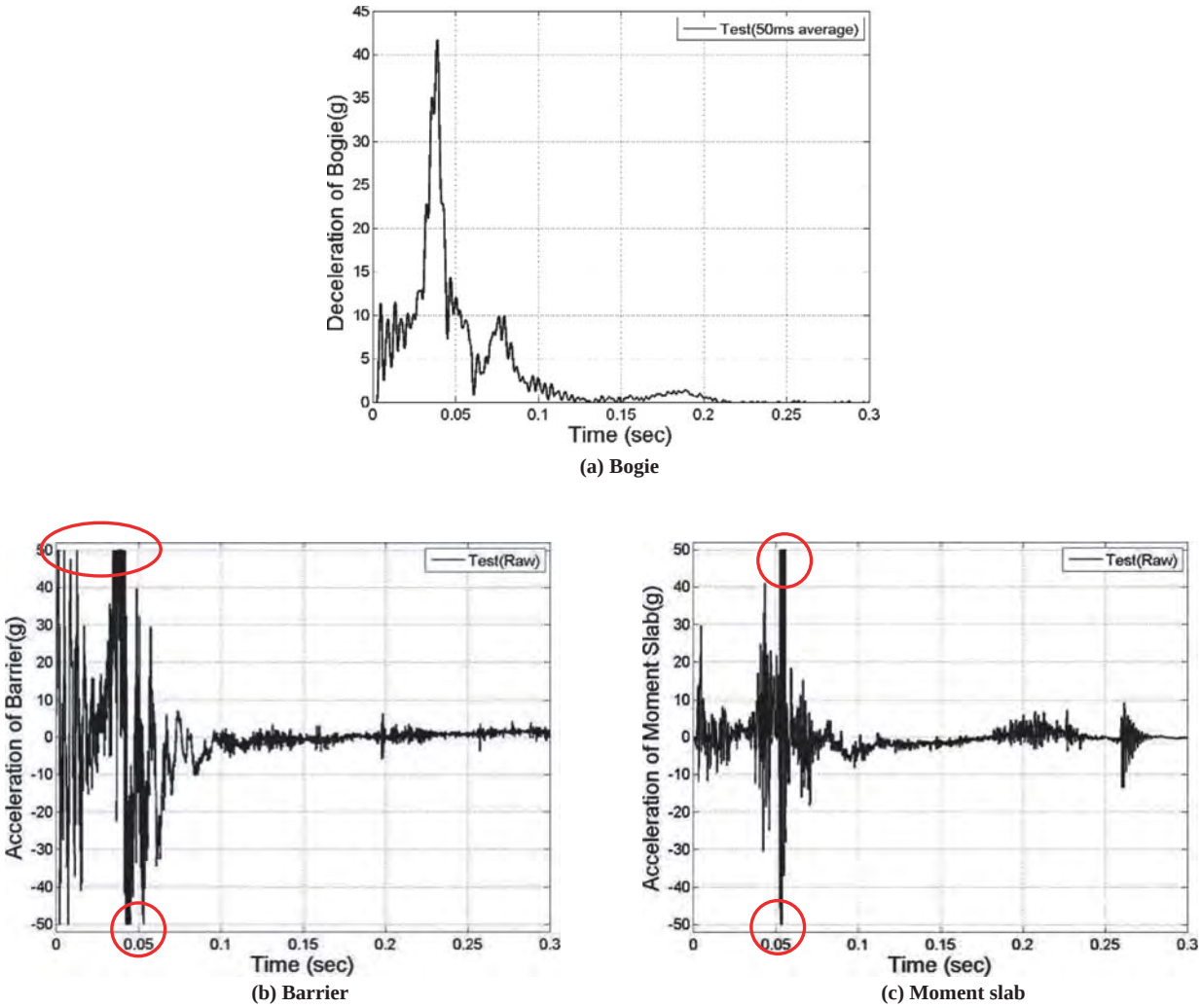

(a) Bogie

(b) Barrier

(c) Moment slab

Figure 5.40. Raw acceleration data of bogie, barrier, and moment slab (Test 1).

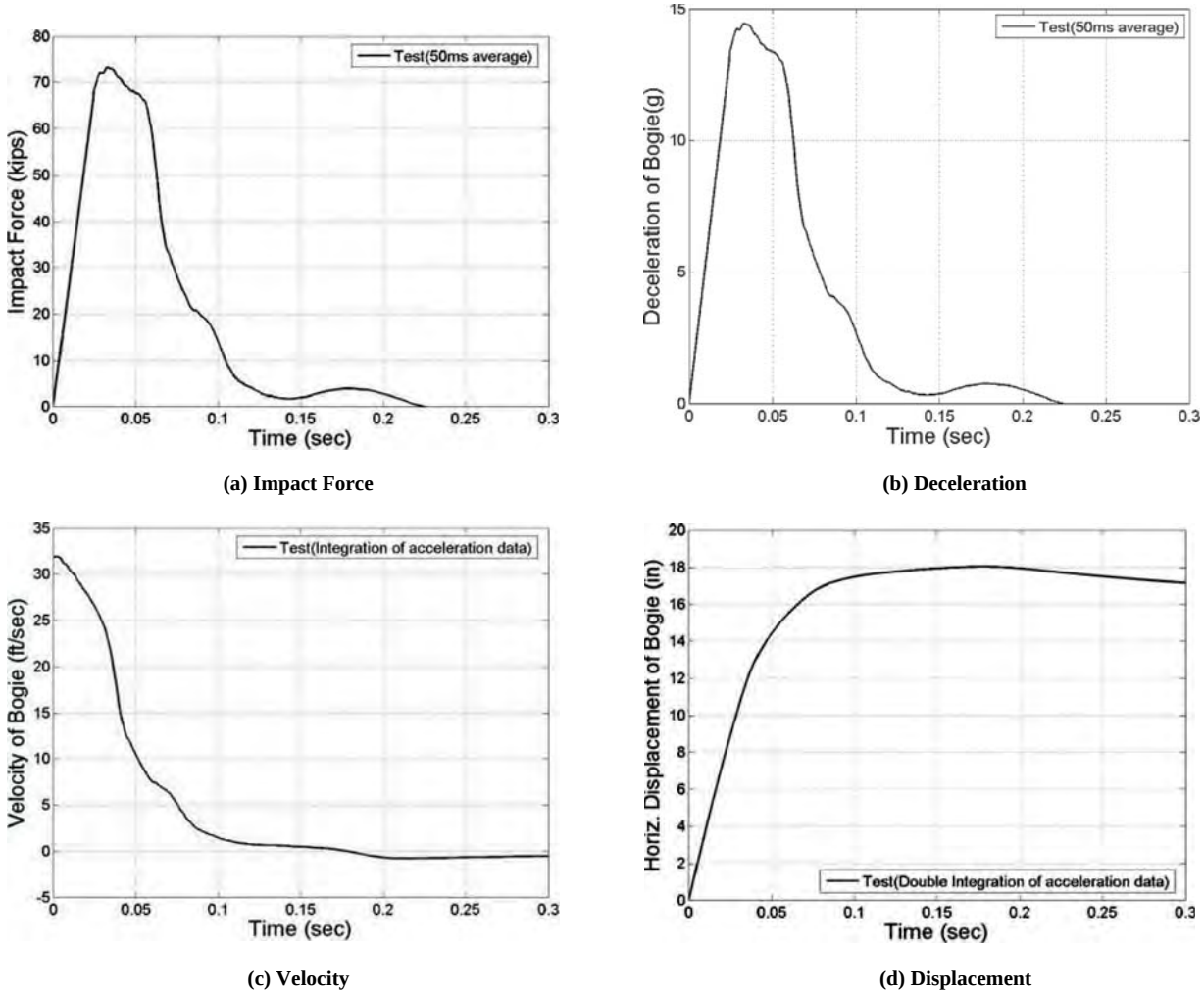

(a) Impact Force **(b) Deceleration**

(c) Velocity **(d) Displacement**

Figure 5.41. Force, acceleration, velocity, and displacement of bogie (Test 1).

tory and displacement–time histories were calculated by integration of the acceleration data.

Targets affixed to the displacement bars attached to the top and bottom of the barrier–coping section (see Figures 5.44 and 5.45) were used as reference points to determine angular and translational displacement of the barrier from analysis of high-speed film. From the film analysis, the maximum dynamic displacement of the barrier was 156 mm (6.14 in.) at the top of the barrier and 28.5 mm (1.12 in.) at the bottom of the coping. The permanent displacement of the barrier was 76.2 mm (3 in.) at the top of the barrier and 14 mm (0.55 in.) at the bottom of the coping.

Two additional targets affixed to the displacement bars attached to the wall panel at locations corresponding to the upper and lower layers of wall reinforcement were used to determine angular and translational displacement of the panel from analysis of high-speed film. From the film analysis, the maximum dynamic displacement of the panel was 16 mm (0.63 in.) at the upper reinforcement layer of the panel. The permanent displacement of the panel was 6.1 mm (0.24 in.) at the upper reinforcement layer. No movement was measured at the bottom reinforcement layer of the panel. The corresponding displacement–time histories for the barrier–coping section and wall panel are shown in Figure 5.46. Figure 5.47 shows the force–displacement curve for the top of the barrier.

Load in Reinforcement Strips

As mentioned previously, the wall reinforcement was instrumented with a total of eight strain gages as shown in Figure 5.48 to capture the tensile forces transmitted into the reinforcement during the dynamic bogie vehicle impacts. To enable comparison of loads on the reinforcement strips, the strain gage locations were assigned a unique numeric designator. The first number indicates the location of the strain gage, and the

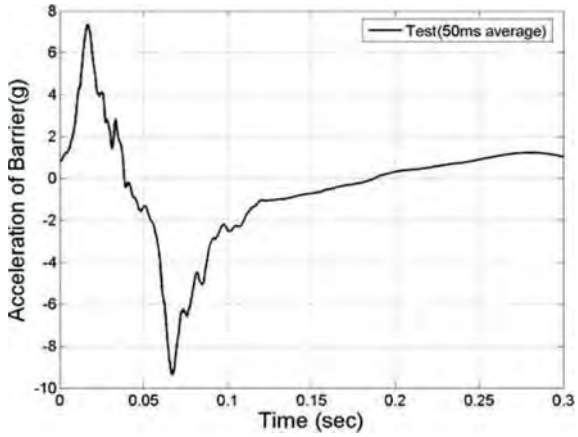

(a) Acceleration

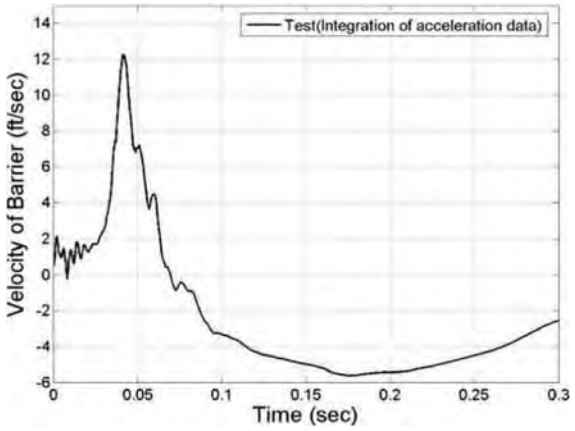

(b) Velocity

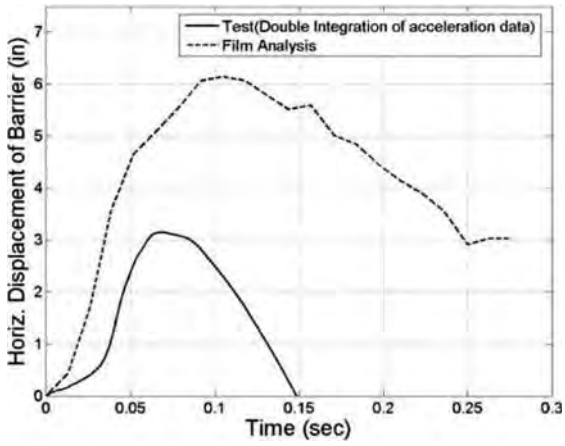

(c) Displacement

Figure 5.42. Acceleration, velocity, and displacement of barrier (Test 1).

second number indicates the reinforcement layer. For example, with reference to Figure 5.48, gage location 1-1 is positioned away from the wall on a strip beneath the impact point in the first (upper) layer of reinforcement.

Note that two strain gages were used at locations 2-1 and 2-2 adjacent to the wall panel at the point of impact to provide some measurement redundancy at the location expected to experience maximum tensile loading. One gage was placed on top of the reinforcement and one gage was placed on the bottom of the reinforcement. Measurements obtained from the strain gages during testing indicated that the reinforcement experienced some bending in addition to tensile loading. The strain gages on the top and bottom of the reinforcement enabled the bending to be canceled out and the average tensile force in the reinforcement to be calculated. Because of the bending, the average tensile loads obtained at gage locations 2-1 and 2-2 were given more credibility in the analysis of the test data and guideline development than the other locations. Note that these locations correspond to the point of impact and thus are expected to be the location of maximum loading in the reinforcement. These expectations were generally confirmed by the numerical simulations.

Raw data obtained from the strain gages on the strips were analyzed and the results are presented in Figure 5.49. The 50 msec average of the raw data was analyzed to obtain design loads for the strips, and the results are presented in Figure 5.50. The ultimate load obtained for the N.J. barrier was 326.5 kN (73.4 kips), which exceeds the barrier design load of 240 kN (54 kips) prescribed by AASHTO LRFD. To obtain the load on the strips when the barrier impact force equaled the 240 kN (54 kips) design force, the data from the bogie accelerometer [Figure 5.41(a)] were used to find the time at which the design force was reached (0.0198 sec). This time of design force as well as the time of maximum load (0.0331 sec) are shown on Figures 5.49 and 5.50. A complicating factor in the analysis is that the loads in the strips continued to increase after the maximum impact force in the barrier was reached. In other words, the time at which the maximum impact load occurred does not correspond to the time at which the maximum load in the strip occurred.

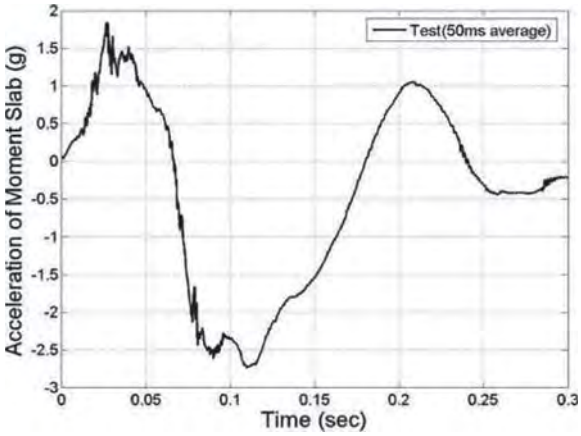

(a) Acceleration

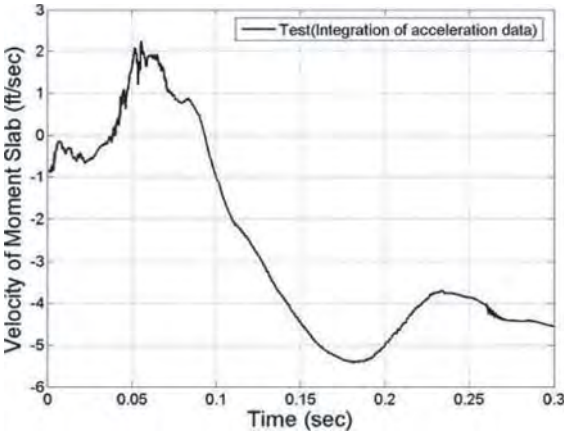

(b) Velocity

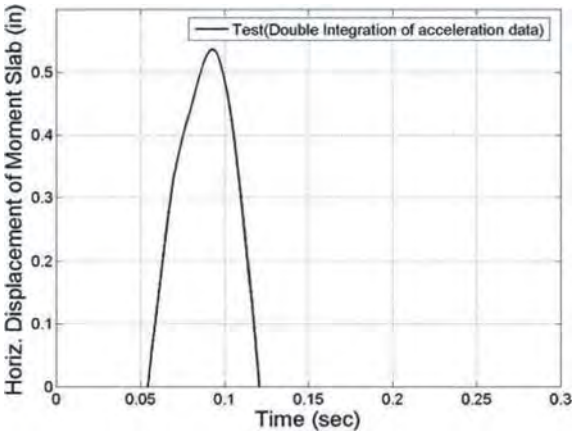

(c) Displacement

Figure 5.43. Acceleration, velocity, and displacement of moment slab (Test 1).

A contact switch placed on the top edge of the level-up concrete on top of the wall panels inside the recess of the coping indicated that the coping contacted the wall panel from 0.0784 to 0.1186 sec, which, as shown in Figure 5.50, corresponds to a period of time after maximum impact load. Thus, the barrier–coping section continued in motion under its own momentum as the impact loads were decreasing. This motion likely contributes to the increase in loads in the strips beyond the time of maximum impact load.

It is assumed that an impact of lesser severity will follow a similar pattern of behavior. For example, if an impact produces a maximum force of 240 kN (54 kips), one would expect the loads in the strips to increase beyond the values corresponding to the time of maximum impact load. Thus, it is not necessarily appropriate to use the strip load corresponding to the time at which the 240 kN (54 kips) design load was reached in the bogie impact tests as the design strip load. Assuming the increase in strip load is proportional to the barrier impact load, the design strip loads corresponding to a design impact load of 240 kN (54 kips) can be estimated as follows:

$$\text{Estimated Strip Load} = \frac{54}{73.4} \times \text{Maximum Strip Load} \qquad (5\text{-}9)$$

Table 5.10 presents a summary of the strip loads from the first bogie impact test including the maximum force, maximum 50 msec average force, and an estimate of the maximum 50 msec average force for a 240 kN (54 kips) design impact. Note that only gage locations 2-1 and 2-2 had two strain gages that could be used to account for bending. To enable comparison with other cases, the estimated design load for the strip was expressed in kips per foot of wall.

Permanent Deflection of Barrier and Panels

The string lines located 1.22 m (4 ft) from the face of the wall panels were used to measure the permanent deflection of barriers and panels at different elevations after bogie vehicle impact. After bogie vehicle impact of the N.J. barrier section, the permanent deflection was measured to be 83 mm (3.27 in.) and 70 mm (2.87 in.) at the top corners of the barrier

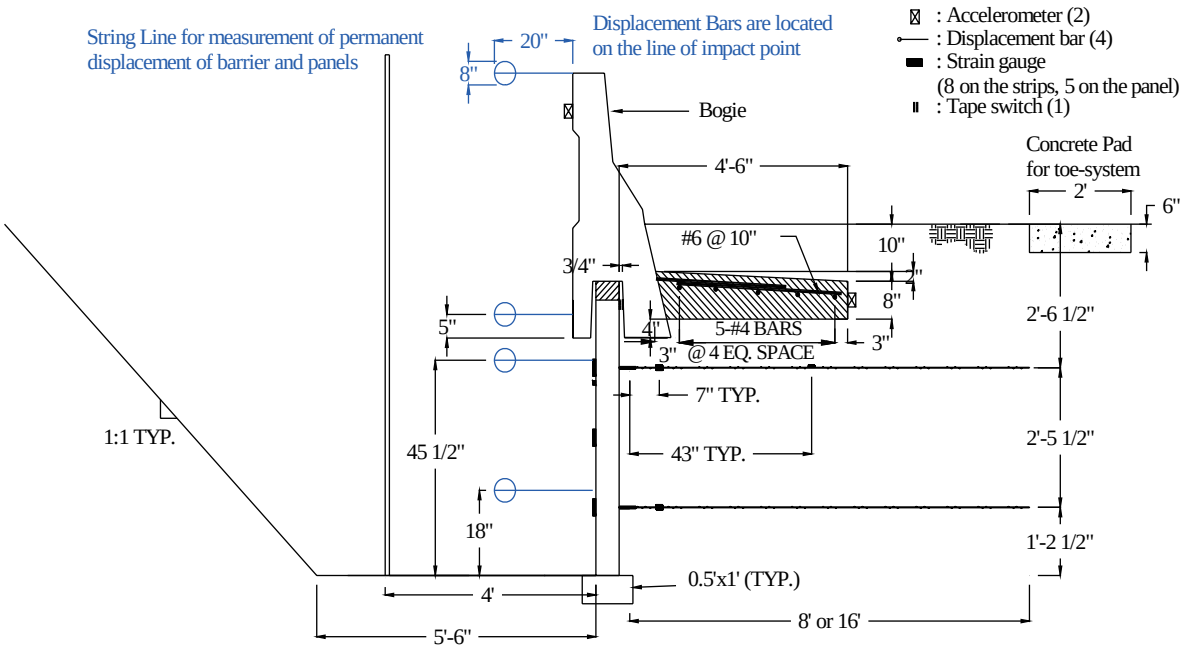

Figure 5.44. Side view of installation (Test 1).

Figure 5.45. Location of displacement bars affixed on the barrier and panels (Test 1).

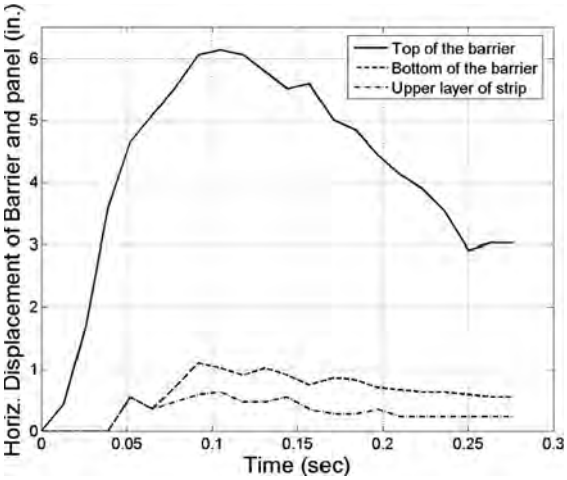

Figure 5.46. Horizontal displacement of barrier and panel measured from film (Test 1).

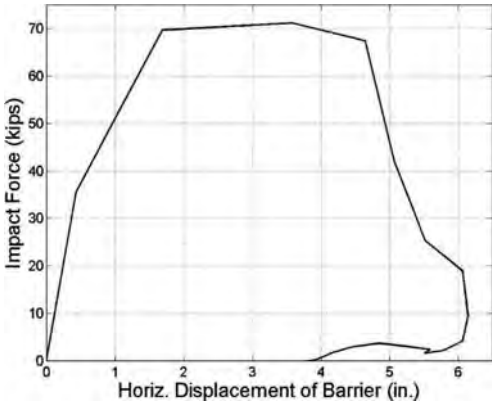

Figure 5.47. Force–displacement of the top of the barrier (Test 1).

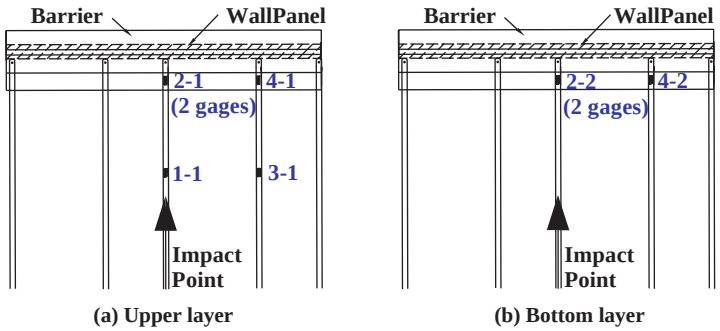

Figure 5.48. Location of strain gages and labeling (Test 1).

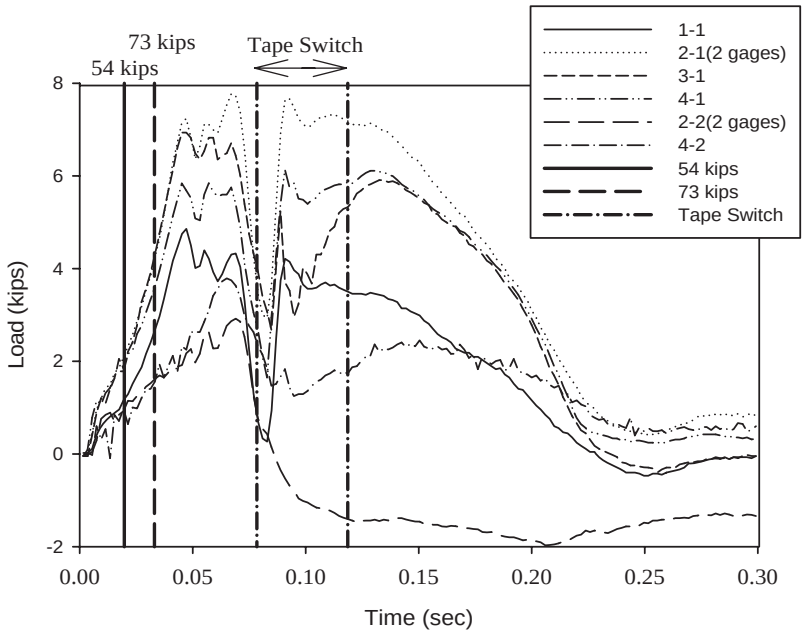

Figure 5.49. Load on the strips (Raw data, Test 1).

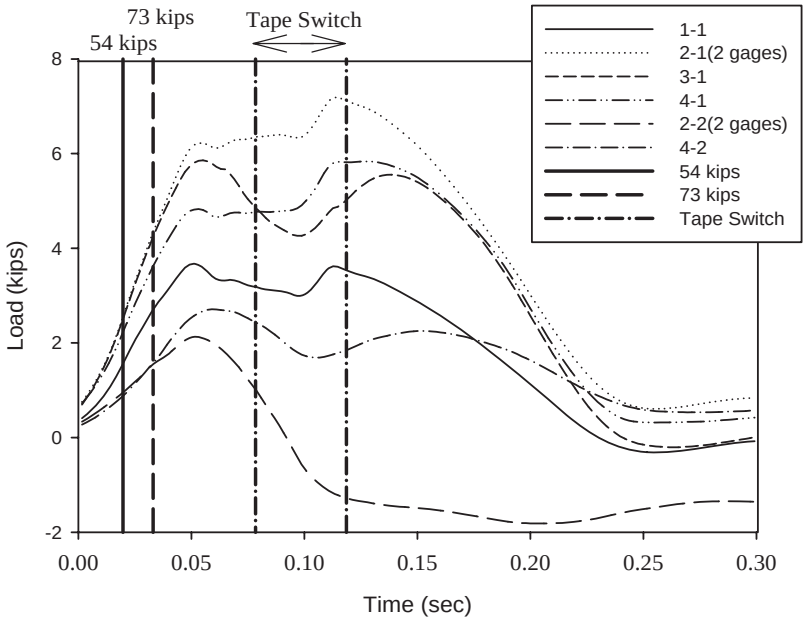

Figure 5.50. Load on the strips (50 msec avg., Test 1).

Table 5.10. Load on the wall reinforcement (Test 1).

	Upper Layer (kips)				Bottom Layer (kips)	
	Impact Point, Behind (1-1)	Impact Point, Front (2-1)	Next to Impact Point, Behind (3-1)	Next to Impact Point, Front (4-1)	Impact Point, Front (2-2)	Next to Impact Point, Front (4-2)
Maximum load from raw data (t = 0.0685 sec)	4.33	7.78	6.69	5.51	2.9	3.68
Maximum 50 msec avg. load	3.67	7.23* (7.95 top, 6.43 bot.)	5.86	5.83	–1.2* (–0.48 top, –1.92 bot.)	2.71
Estimated design load per strip	2.70	5.29	4.31	4.29	–0.88	2.00
Estimated design load per foot of wall	1.11	2.17	1.77	1.76	–0.36	0.82

* Average of top and bottom loads

and 20 mm (0.79 ins) and 13 mm (0.51 in.) at the bottom corners of the coping as shown in Figure 5.51. The permanent deflection obtained from the film analysis of the motion of the targets affixed to the barrier–coping section was 76.2 mm (3 in.) at top of the barrier and 14 mm (0.55 in.) at the bottom of the coping.

Note that the adjacent barrier–coping sections moved approximately 20 mm (0.79 in.) due to their connection to the same 9.14 m (30 ft) moment slab as the N.J. barrier section that was impacted. The permanent defection of the wall panels was measured as shown in Figure 5.51. The maximum permanent movement measured in the wall panels beneath the impact barrier section was approximately 6 mm (0.24 in.). Note that negative values indicate movement toward the traffic side of the barrier. Such movement may be the result of the panel being loaded eccentrically and rotating.

Panel Analysis

The wall reinforcement was instrumented with a total of five strain gages to capture the strains in the panel during the bogie impacts as shown in Figure 5.52. The maximum compressive strain was 0.0018 and occurred at 0.123 sec (see Figure 5.53) at the location of the uppermost layer of strip. Note that positive values for the vertical direction strain gages indicate movement toward the traffic side of the barrier. The strains at the horizontal centerline of the panel and at the second layer of strips were less than 0.0002.

Component Damage

Damage to the barrier–coping section resulting from the bogie impact is shown in Figure 5.54. Cracks were observed across the entire length of the N.J. barrier section at a height of approximately 381 mm (15 in.) above ground or above the "toe" of the barrier. The vertical reinforcing bars were exposed along some of these cracks due to fracture and spalling of the concrete. Although difficult to see in the pictures, the cracks radiated upward on either side of the barrier centerline in a U-shaped pattern observed in previous testing of safety shape barriers. This damage mechanism, which had a maximum length of 2.6 m (8.43 ft), was not as pronounced as in past test-

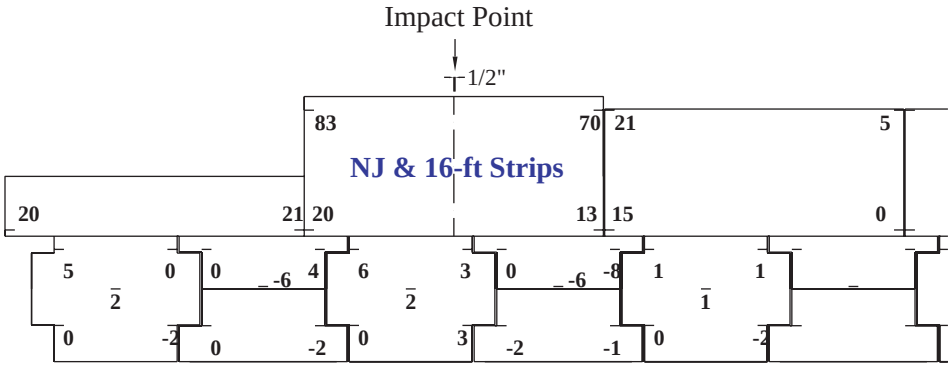

Figure 5.51. Permanent deflection of barrier and panels (Test 1, units: mm).

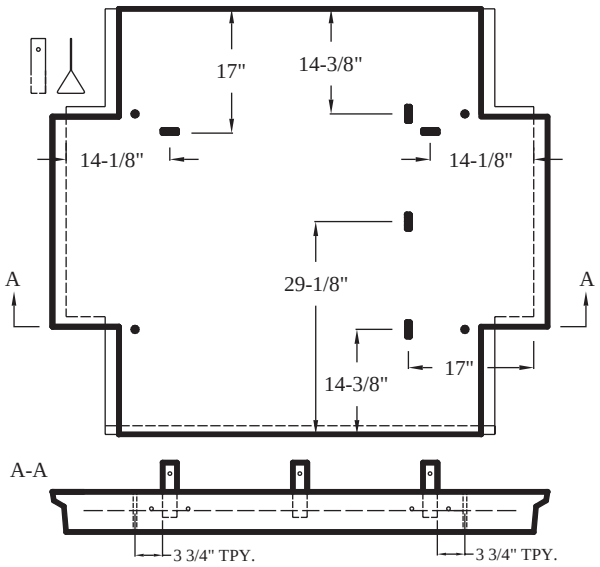

Figure 5.52. Location of concrete strain gages (Test 1).

ing because the short length of this precast barrier section caused other failure modes to occur at similar failure loads.

Cracking in the soil was observed approximately 1.22 m (48 in.) from the front face of the barrier, which corresponds with the location of the end of the moment slab. The crack, shown in Figure 5.54(c), was about 19 mm (0.75 in.) wide and extended along the entire length of the 9.14 m (30 ft) long moment slab. Although numerous cracks were observed on the back side of the barrier [see Figure 5.54(d)], they were not as wide or pronounced as those on the front of the barrier.

Damage to the panel beneath the point of impact on the barrier is shown in Figure 5.55. The leveling concrete on top of the wall panel was broken and shifted over the front edge of the panel due to contact with the inside face of the coping. The bonding of the leveling concrete to the top of the wall panel caused the top corner of the wall panel to spall as shown in Figure 5.55(b) and (c).

5.3.3 Bogie Test 2: Vertical Concrete Barrier with 8 ft Bar Mats

The second bogie test was conducted on a vertical concrete barrier connected to the mid-span of the undisturbed 9.14 m (30 ft) moment slab adjacent to the moment slab used in Test 1. This vertical barrier section was located above a wall segment that was reinforced with 2.43 m (8 ft) long bar mats. The 2,268 kg (5,000 lb) bogie vehicle, shown in Figure 5.56, impacted the reference point of the vertical barrier head-on at a speed of approximately 32.7 km/h (20.3 mph). The reference point was along the top edge of the barrier and approximately 0.37 m (14 ⅝ in.) from its centerline to coincide with the location of one of the two bar mats comprising each of the two layers of wall reinforcement below the barrier.

Data from Accelerometers

As previously discussed, the range of the accelerometers attached to the top of the barrier and end of the moment slab was increased after Test 1. However, as shown in Figure 5.57(b), some of the accelerations still exceeded the revised

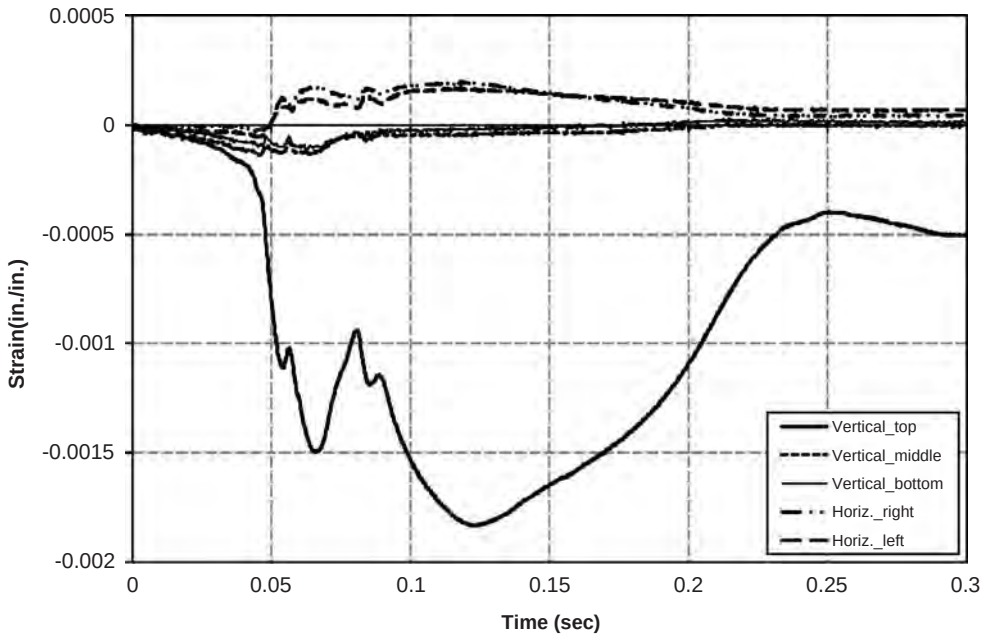

Figure 5.53. Strain on the panel (Test 1).

(a) Front side of the barrier

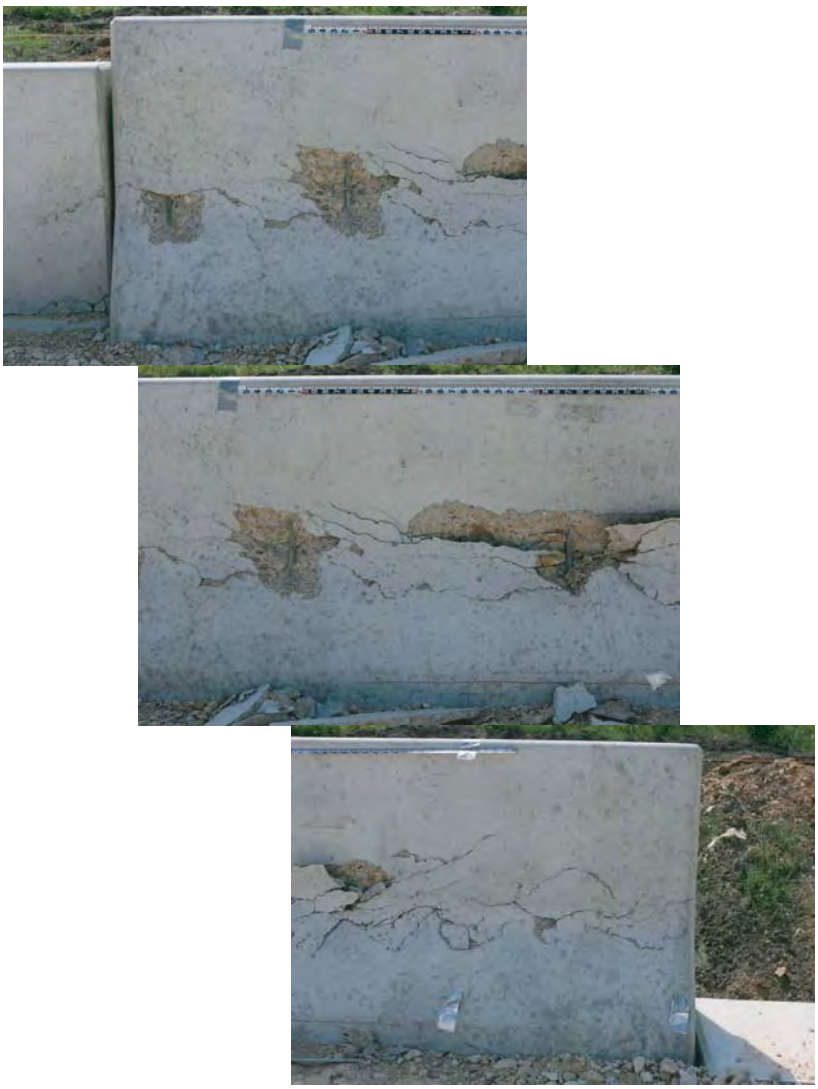

(b) Closeup of front side of the barrier

Figure 5.54. Damage to barrier after Test 1.

(c) Side view of the barrier

(d) Back view of the barrier

Figure 5.54. (Continued).

range set for the barrier accelerometer. Consequently, these data must be analyzed with appropriate caution. To prevent further occurrence of this problem, the range of the barrier accelerometer was increased substantially for subsequent tests.

Data obtained from the bogie-mounted accelerometer were analyzed and the results are presented in Figure 5.58. As shown in Figure 5.58(b), the maximum 50 msec average deceleration was 13.01 *g*. Based on this acceleration and the mass of the bogie, the maximum 50 msec average impact force was calculated to be 294.03 kN (66.1 kips) [see Figure 5.58(a)]. The velocity–time and horizontal displacement–time histories of the bogie are shown in Figure 5.58(c) and (d), respectively. These time histories were calculated through integration of the acceleration data.

The maximum 50 msec average acceleration of the barrier, as measured by the accelerometer at the top of the barrier, was 10.71 *g* in the direction of impact [see Figure 5.59(a)]. The velocity–time history of the barrier, as calculated by integration of the raw acceleration data, is shown in Figure 5.59(b). The displacement–time history obtained from integration of the velocity history is shown in Figure 5.59(c).

The raw acceleration–time history for the moment slab is shown in Figure 5.57(c). The increased range of the accelerometer was sufficient to obtain the peak acceleration of the moment slab. However, after impact, the accelerometer had a non-zero offset. The problem was traced to a connection issue that was resolved prior to the next test on this moment slab. The 50 msec average acceleration for the moment slab and the

(a) Surface of panel

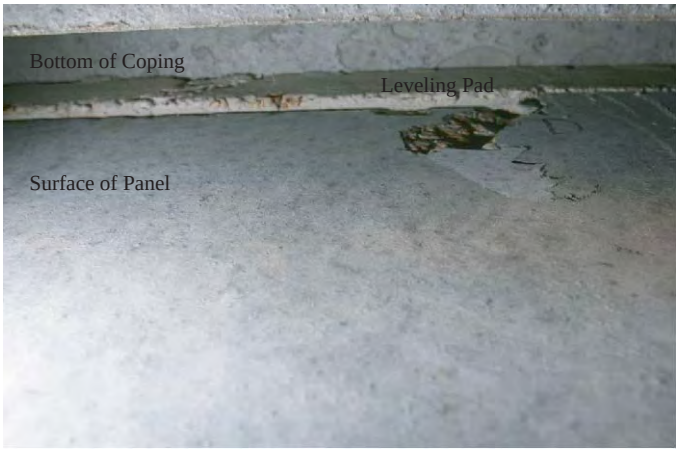

(b) Top of panel inside of recessed coping

(c) Closeup of panel inside of recessed coping

Figure 5.55. Damage to panel and leveling pad (Test 1).

Figure 5.56. Test 2: vertical concrete barrier with 8 ft bar mats.

associated velocity–time and displacement–time histories are shown in Figure 5.60.

Targets affixed to the displacement bars attached to the top and bottom of the barrier–coping section (see Figures 5.61 and 5.62) were used as reference points to determine angular and translational displacement of the barrier from analysis of high-speed film. From the film analysis, the maximum dynamic displacement of the barrier was 153.4 mm (6.04 in.) at the top of the barrier and 24 mm (0.93 in.) at the bottom of the coping. The permanent displacement of the barrier was 101.6 mm (4 in.) at the top of the barrier and 12.7 mm (0.5 in.) at the bottom of the coping.

Two additional targets affixed to the displacement bars attached to the wall panel at locations corresponding to the upper and lower layers of wall reinforcement were used to determine angular and translational displacement of the panel from analysis of high-speed film. From the film analysis, the maximum dynamic displacement of the panel was 94 mm (0.37 in.) at the upper reinforcement layer of the panel and 2.54 mm (0.1 in.) at the bottom reinforcement layer. The permanent displacement of the panel was 5.08 mm (0.2 in.) at the upper reinforcement layer and 0.51 mm (0.02 in.) at the bottom reinforcement layer.

The corresponding displacement–time histories for the barrier–coping section and wall panel are shown in Figure 5.63. Figure 5.64 shows the force–displacement curve for the top of the barrier.

Load in Reinforcement Bar Mats

A total of eight strain gages were used to instrument the bar mats to capture the tensile forces transmitted into the reinforcement during the dynamic bogie vehicle impact. The locations of strain gages were assigned a numeric designator

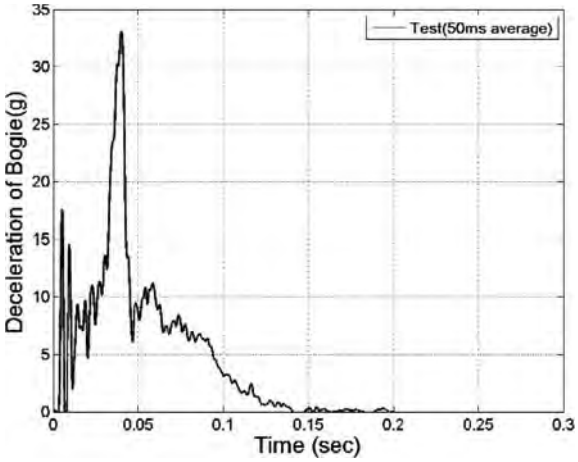

(a) Bogie

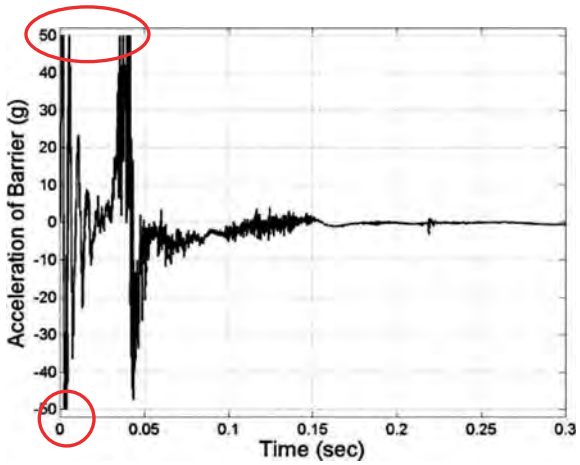

(b) Barrier

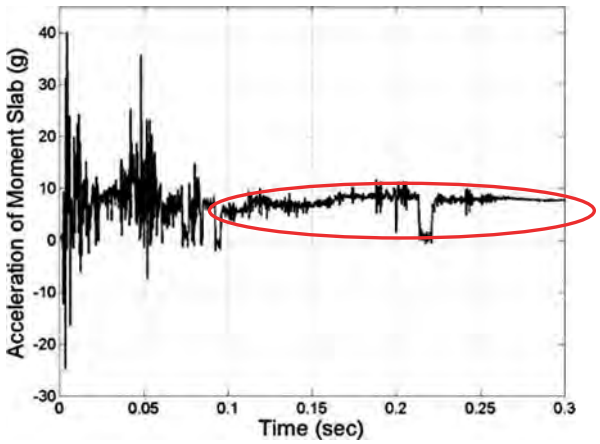

(c) Moment slab

Figure 5.57. Raw acceleration data of bogie, barrier, and moment slab (Test 2).

as shown in Figure 5.65. Note that two strain gages were used at locations 2-1 and 2-2 adjacent to the wall panel at the point of impact to provide some measurement redundancy at the location expected to experience maximum tensile loading. One gage was placed on top of the reinforcement and one gage was placed on the bottom of the reinforcement. Measurements obtained from the strain gages during testing indicated that the reinforcement experienced some bending in addition to tensile loading. The strain gages on the top and bottom of the reinforcement enabled the bending to be canceled out and the average tensile force in the reinforcement to be calculated.

Raw data obtained from the strain gages on the bar mats were analyzed and the results are presented in Figure 5.66. It can be seen in this figure that the contact switch placed on the top edge of the level-up concrete on top of the wall panels inside the recess of the coping indicated that the coping contacted the wall panel from 0.0806 to 0.1798 sec. The 50 msec average of the raw data was analyzed to obtain design loads for the strips, and the results are presented in Figure 5.67. As with the strips in Test 1, there was some increase in force in the bar mats after the time of maximum barrier impact load. The maximum 50 msec average design strip loads corresponding to a design impact load of 240 kN (54 kips) were estimated as follows:

$$\text{Estimated Strip Load} = \frac{54}{66.1} \times \text{Maximum Strip Load} \qquad (5\text{-}10)$$

where 294.03 kN (66.1 kips) is the maximum 50 msec average impact load measured for the vertical wall barrier over 2.43 m (8 ft) bar mats.

The interior wires of a bar mat are more highly stressed than exterior wires due to the soil interaction on the cross bars between the longitudinal wires. Because the strain gages were installed in the exterior wire, the interior wires may be subject to tensions that are 1.34 times the exterior wire tensions.

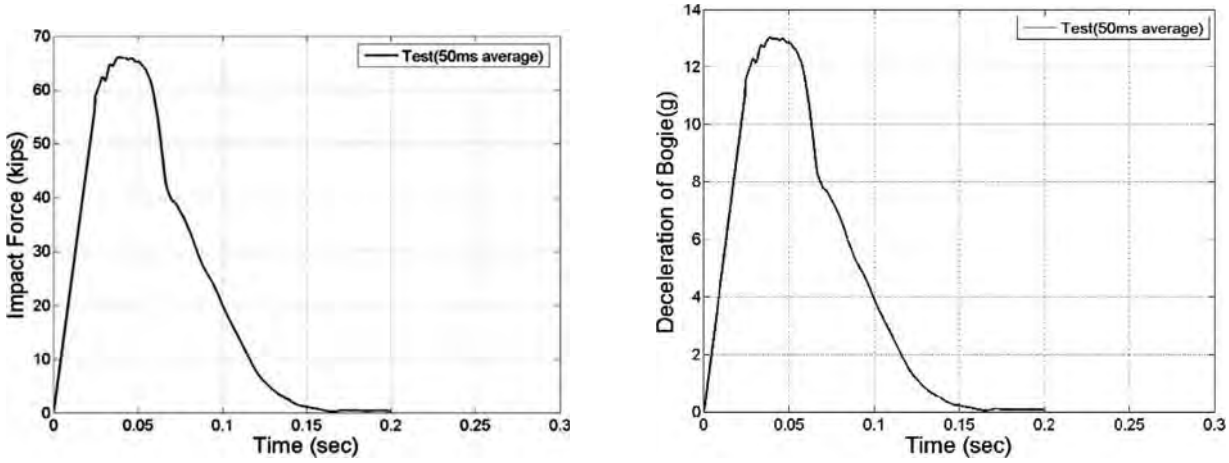

(a) Impact force **(b) Deceleration**

(c) Velocity **(d) Displacement**

Figure 5.58. Force, acceleration, velocity, and displacement of bogie (Test 2).

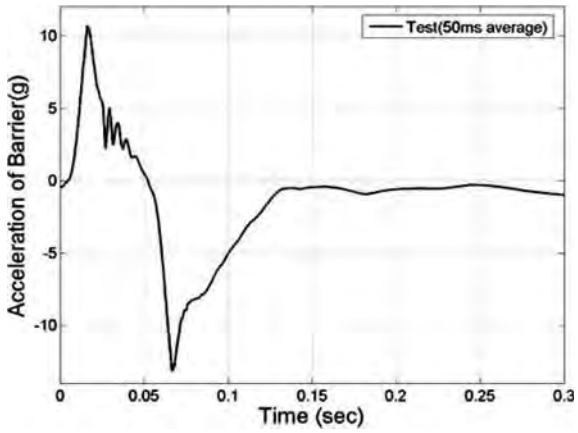

(a) Acceleration

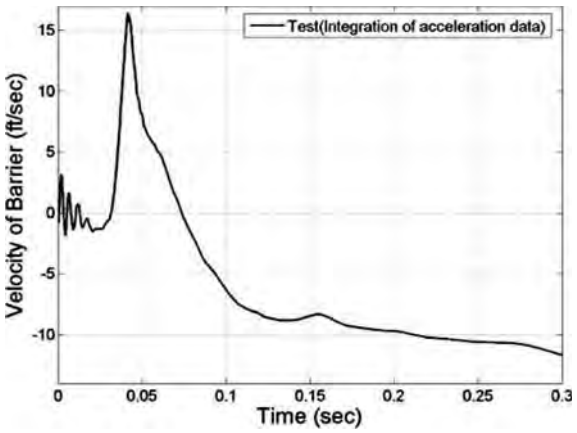

(b) Velocity

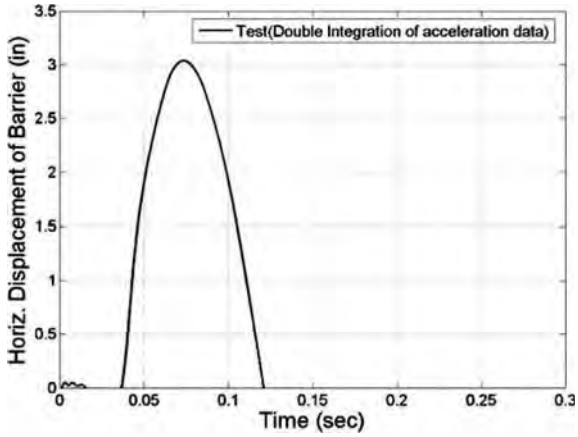

(c) Displacement

Figure 5.59. Acceleration, velocity, and displacement of barrier (Test 2).

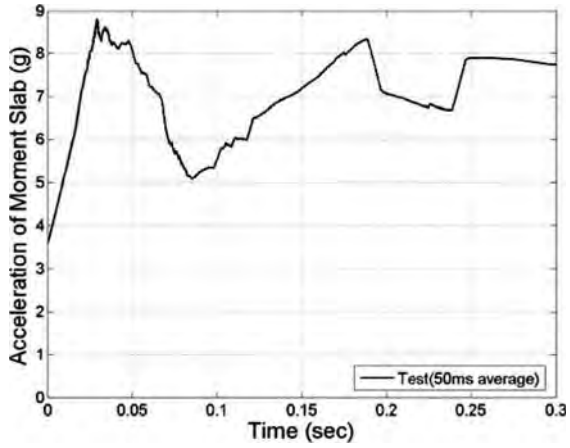

(a) Acceleration

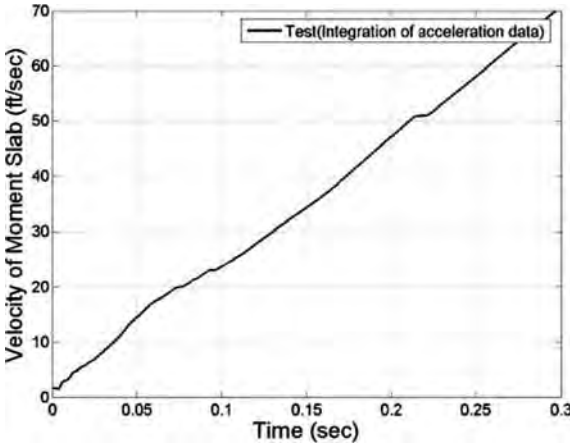

(b) Velocity

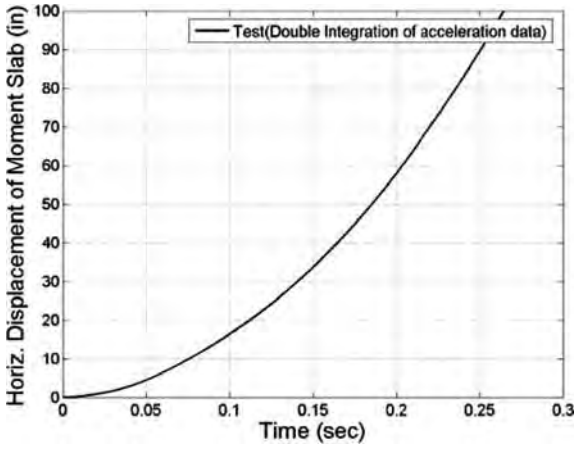

(c) Displacement

Figure 5.60. Acceleration, velocity, and displacement of moment slab (Test 2).

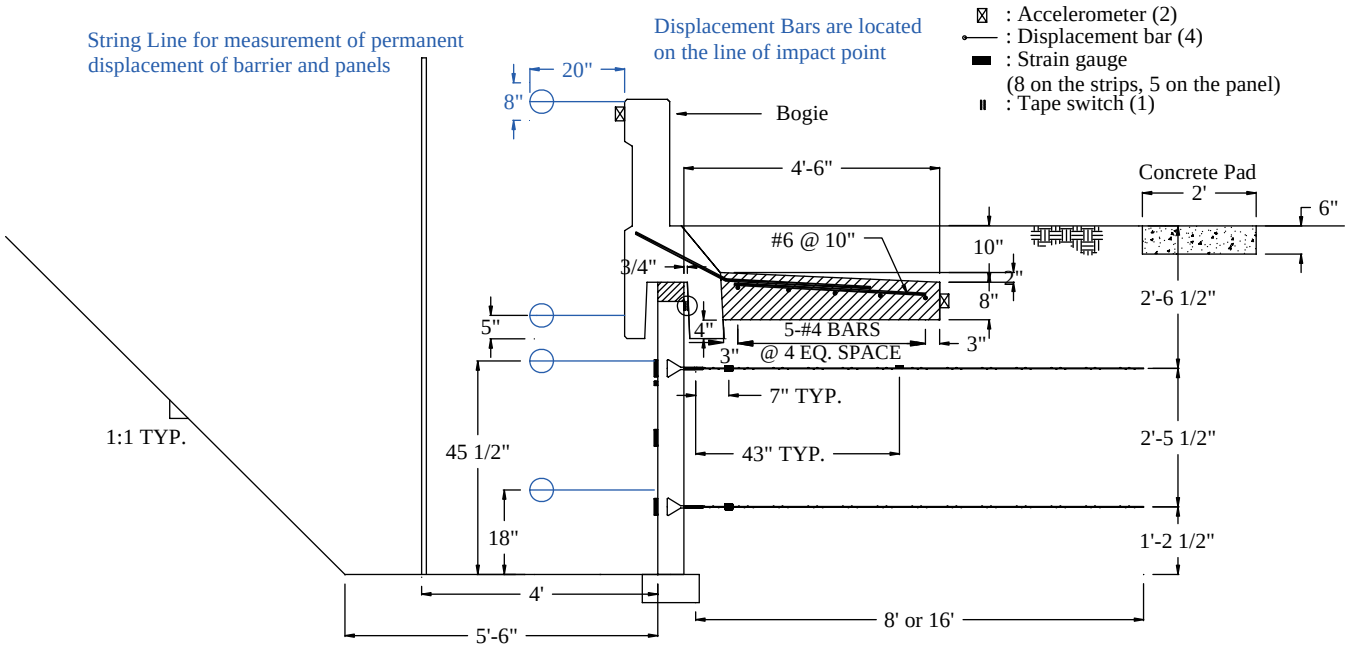

Figure 5.61. Side view of installation (Test 2, 3, and 4).

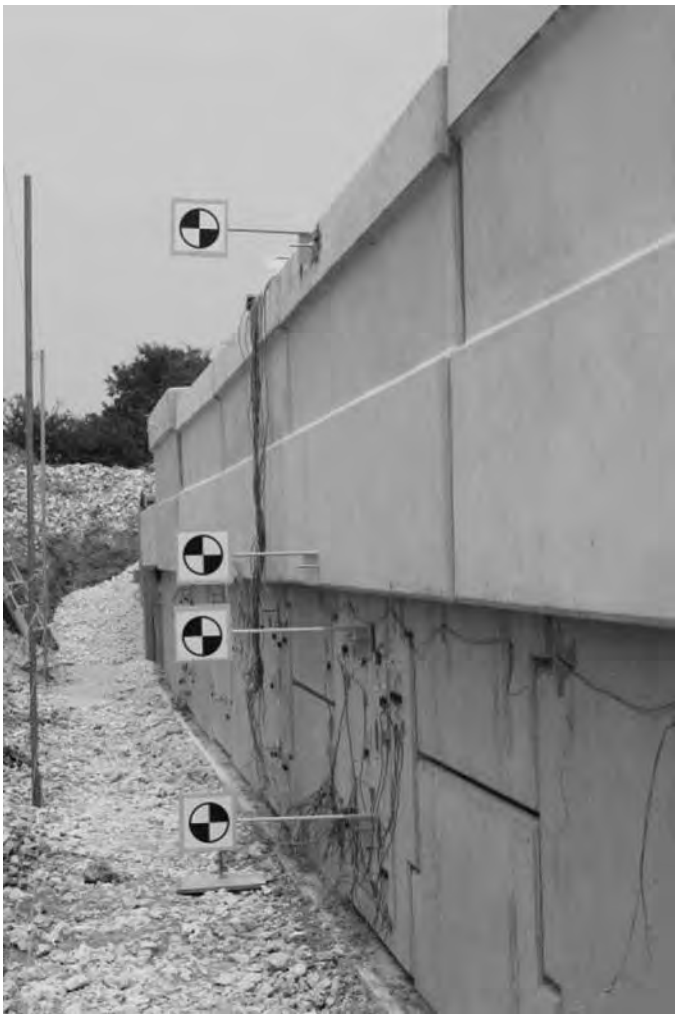

Figure 5.62. Location of displacement bars affixed on the barrier and panels (Test 2).

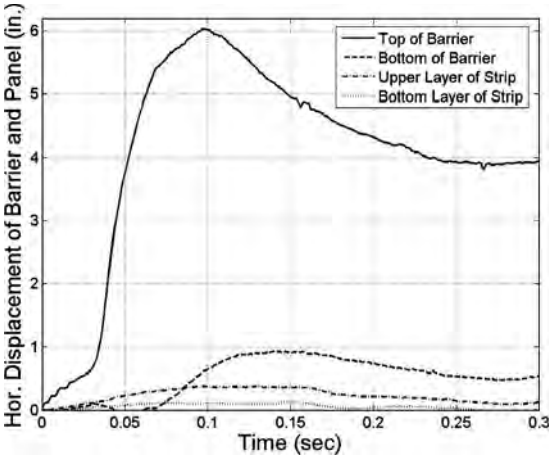

Figure 5.63. Horizontal displacement of barrier and panel measured from film (Test 2).

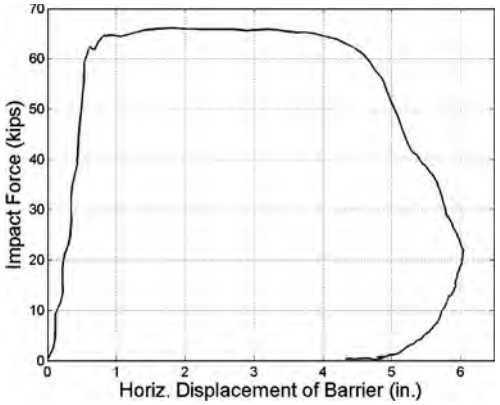

Figure 5.64. Force–displacement of the top of the barrier (Test 2).

Table 5.11 presents a summary of the forces in the bar mat obtained from the second bogie impact test including the maximum force, maximum 50 msec average force, and an estimate of the maximum 50 msec average force for a 240 kN (54 kips) design impact. To enable comparison with other cases, the estimated design load for the strips was expressed in kips per foot of wall.

Permanent Deflection of Barrier and Panels

The string lines located 1.22 m (4 ft) from the face of wall panels were used to measure the permanent deflection of barriers and panels after the bogie vehicle impact at different elevations. The permanent deflection was measured to be 99 mm (3.9 in.) and 45 mm (1.77 in.) at the top and 13 mm (0.51 in.) and 18 mm (0.71 in.) at the bottom corners of the coping as shown in Figure 5.68. Note that the reference impact point was 0.37 m (14.625 in.) left of the centerline of the barrier–coping section as shown in Figure 5.68 to align with the instrumented bar mats. This location corresponded to the side of the barrier with greater movement.

Note that the barrier–coping sections to the left and right of the section that was hit had permanent movement at the top

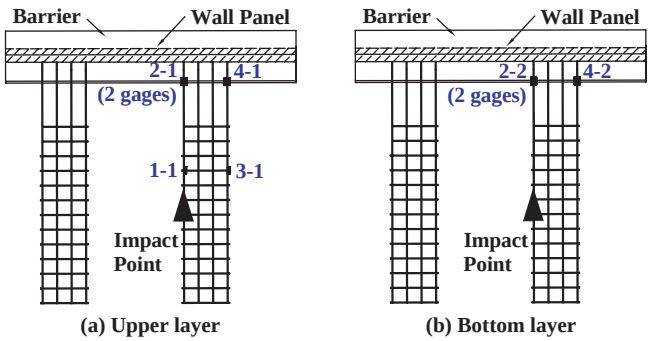

Figure 5.65. Location of strain gages and labeling (Test 2).

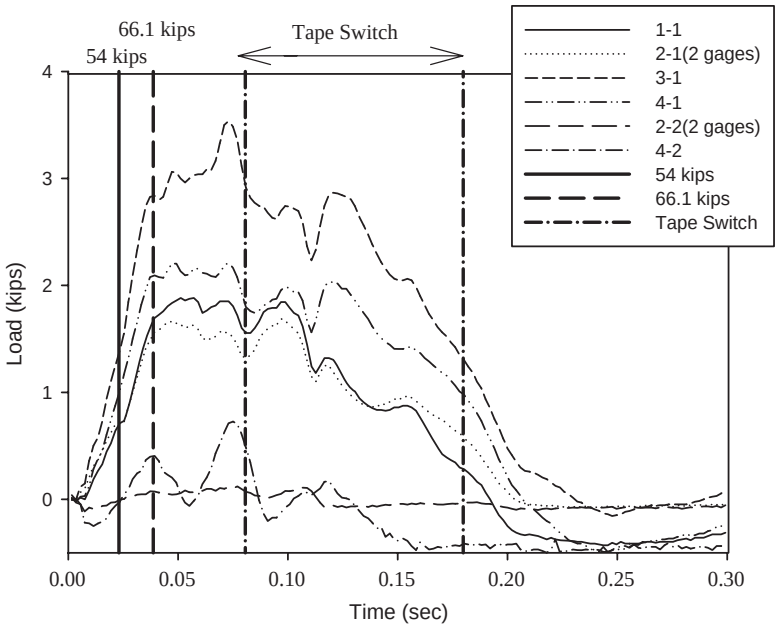

Figure 5.66. Load on the strips (Raw data, Test 2).

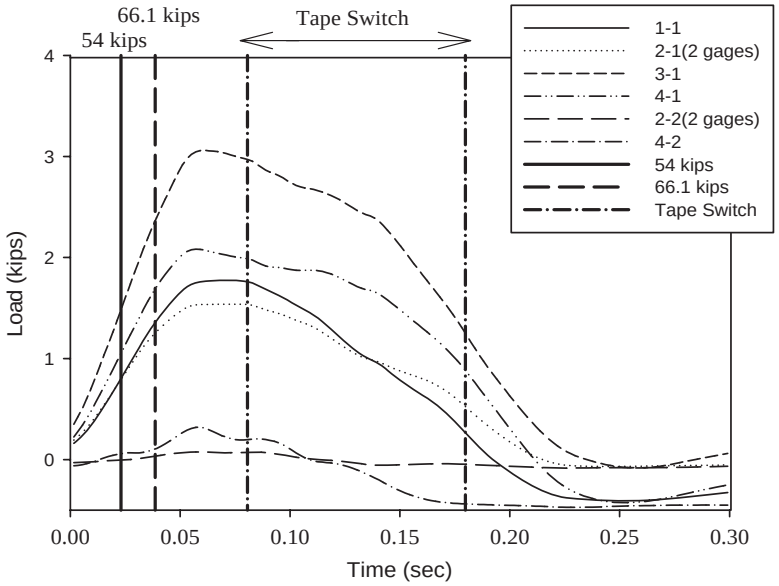

Figure 5.67. Load on the strips (50 msec avg., Test 2).

Table 5.11. Load on the wall reinforcement (Test 2).

	Upper layer (kips)				Bottom layer (kips)	
	Impact Point, Behind (1-1)	**Impact Point, Front (2-1)**	**Next to Impact Point, Behind (3-1)**	**Next to Impact Point, Front (4-1)**	**Impact Point, Front (2-2)**	**Next to Impact Point, Front (4-2)**
Maximum load from raw data (t = 0.072 sec)	1.86	1.57	3.52	2.21	0.11	0.72
Maximum 50 msec avg. load (t = 0.0607 sec)	1.76	1.54* (1.44 top 1.63 bot.)	3.06	2.07	0.076* (–0.16 top 0.31 bot.)	0.31
Estimated design load of interior wire	1.931	1.68	3.349	2.271	0.083	0.344
Estimated design load per foot of wall	2.77	2.41	4.8	3.258	0.119	0.494

* Average of top and bottom loads

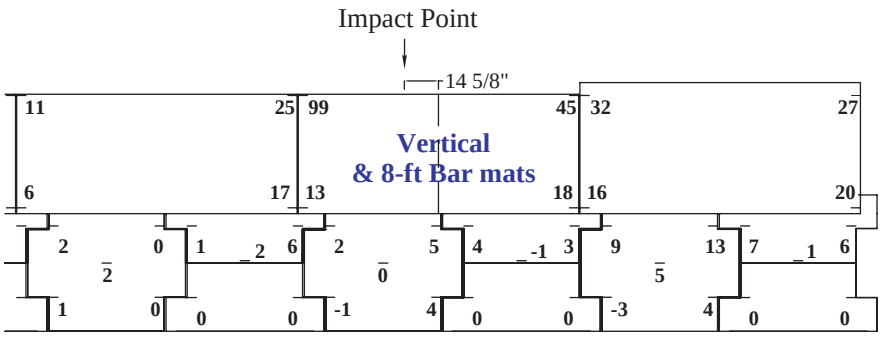

Figure 5.68. Permanent deflection of barrier and panels (Test 2, units: mm).

of the barrier of 25 mm (1 in.) and 32 mm (1.26 in.), respectively, due to their connection to the same 9.14 m (30 ft) moment slab as the vertical barrier section that was hit. The permanent defection of the wall panels was measured as shown in Figure 5.68. The maximum permanent movement measured in the wall panels beneath the impact barrier section was approximately 5 mm (0.2 in.).

Panel Analysis

The wall reinforcement was instrumented with a total of five strain gages to capture the resistance of the panel during the bogie impacts as shown in Figure 5.69. The maximum compressive strain of 0.00016 occurred at 0.056 sec (see Figure 5.70) at the location of the uppermost layer of strips. Note that positive values for the vertical direction strain gages indicate movement toward the traffic side of the barrier. The strains at the horizontal centerline of the panel and at the second layer of strips were 0.00012 and 0.00007, respectively.

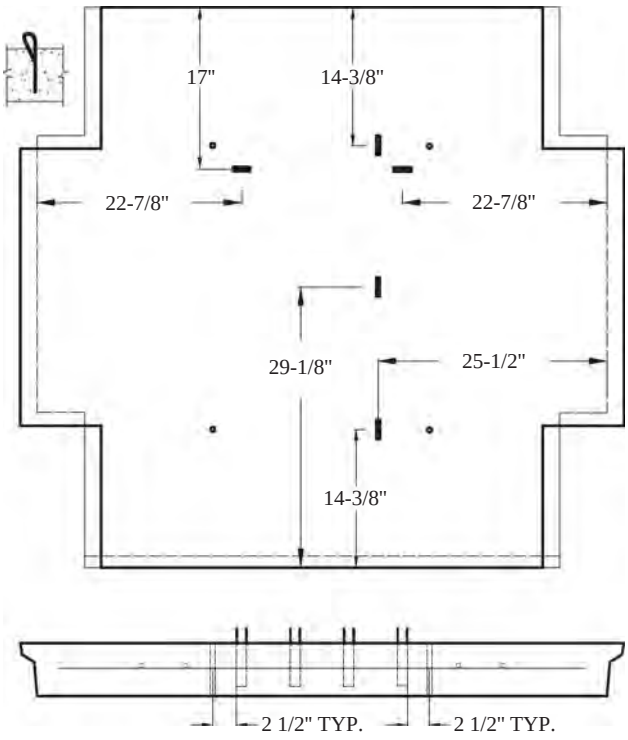

Figure 5.69. Location of concrete strain gages (Test 2).

Component Damage

Damage to the vertical wall barrier–coping section resulting from the bogie impact is shown in Figure 5.71. Left of the point of impact, the vertical barrier failed in a classical yield line pattern by developing a vertical "hinge" line at the point of impact and a diagonal hinge line radiating from the bottom to the top of the barrier. However, because the bogie impact point was offset 0.37 m (14.625 in.) from the centerline of the barrier to align with the bar mat, there was insufficient strength to develop a similar yield line failure on the right side of the barrier. Rather, a lower strength cantilever bending moment controlled failure mode on the right side of the barrier. Longitudinal cracks developing from this failure mode were observed at the groundline connection between the barrier and coping and approximately 152 mm (6 in.) above the groundline from the point of impact to the end of the vertical barrier [see Figure 5.71(b)].

Cracking in the soil was observed approximately 1.22 m (48 in.) from the front face of the barrier, which corresponds with the location of the end of the moment slab. The crack, shown in Figure 5.71(c), was about 13 mm (0.5 in.) wide and extended along the entire length of the 9.15 m (30 ft) long moment slab. Damage to the back of the vertical barrier, shown in Figure 5.71(e) and (f), mirrors that on the front face of the barrier. Most pronounced are the diagonal hinge line and the longitudinal crack at the interface between the vertical barrier and coping.

Damage to the panel beneath the point of impact on the barrier is shown in Figure 5.72. As shown in Figure 5.72(a), the surface of the panel showed little distress. The leveling concrete on top of the wall panel was broken and shifted over the

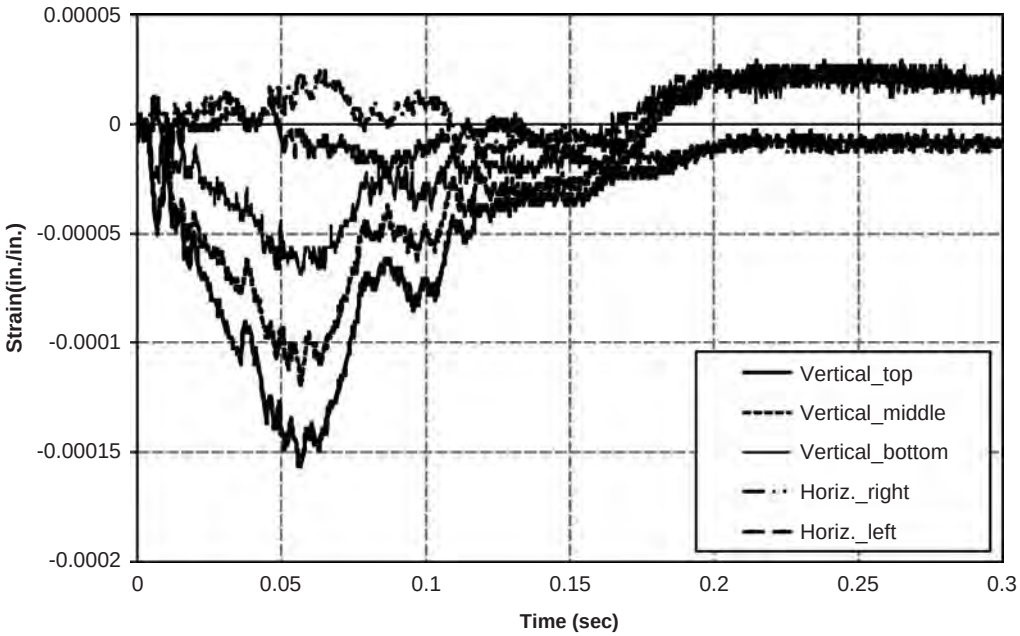

Figure 5.70. Strain on the panel (Test 2).

front edge of the panel due to contact with the inside face of the coping. The bonding of the leveling concrete to the top of the wall panel caused the top edge of the wall panel to spall as shown in Figure 5.72(b).

5.3.4 Bogie Test 3: Vertical Concrete Barrier with 8 ft Strips

Upon completion of the first two reference tests, the soil on and around the two moment slabs was recompacted for the following tests. The third bogie test was conducted on a vertical concrete barrier connected to the end of the 9.14 m (30 ft) moment slab above the wall section with 2.43 m (8 ft) long steel reinforcement strips. The 2,268 kg (5,000 lb) bogie vehicle, shown in Figure 5.73, hit the reference point of the vertical barrier head-on at a speed of approximately 32.5 km/h (20.2 mph). The reference point was along the top edge of the barrier and approximately 121 mm (4.75 in.) from its centerline to coincide with the location of a steel strip in the wall reinforcement below the barrier.

Data from Accelerometers

The increased range used for the barrier and moment slab accelerometers was sufficient to capture the accelerations arising from the bogie impact. The raw acceleration data for the bogie, barrier, and moment slab are shown in Figure 5.74.

Data obtained from the bogie-mounted accelerometer were analyzed and the results are presented in Figure 5.75. As shown in Figure 5.75(b), the maximum 50 msec average deceleration was 13.82 *g*. Based on this acceleration and the mass of the bogie, the maximum 50 msec average impact force was calculated to be 312.13 kN (70.17 kips) [see Figure 5.75(a)]. The velocity–time and horizontal displacement–time histories of the bogie are shown in Figure 5.75(c) and (d), respectively. These time histories were calculated through integration of the acceleration data.

The maximum 50 msec average acceleration of the barrier, as measured by the accelerometer at the top of the barrier, was 10.16 *g* in the direction of impact [see Figure 5.76(a)]. The velocity–time history of the barrier, as calculated by integration of the raw acceleration data, is shown in Figure 5.76(b). The displacement–time history obtained from integration of the velocity history is shown in Figure 5.76(c).

The 50 msec average acceleration for the moment slab is shown in Figure 5.77(a). The velocity–time and vertical displacement–time histories of the moment slab are shown in Figure 5.77(b) and (c), respectively. The velocity–time history and displacement–time histories were calculated by integration of the raw acceleration data.

Targets affixed to the displacement bars attached to the top and bottom of the barrier–coping section (see Figures 5.61 and 5.78) were used as reference points to determine angular and translational displacement of the barrier from analysis of high-speed film. From the film analysis, the maximum dynamic displacement of the barrier was 131 mm (5.17 in.) at the top of the barrier and 30 mm (1.16 in.) at the bottom of the coping. The permanent displacement of the barrier was 63.5 mm (2.5 in.) at the top of the barrier and 15 mm (0.6 in.) at the bottom of the coping.

(a) Front view of the barrier

(b) Close-up front side of the barrier

Figure 5.71. Cracks on the barrier after test (Test 2).

(continued on next page)

(c) Side view of the barrier

(d) Closeup side view of the barrier

(e) Back view of the barrier

Figure 5.71. (Continued).

(f) Closeup back view of the barrier

Figure 5.71. (Continued).

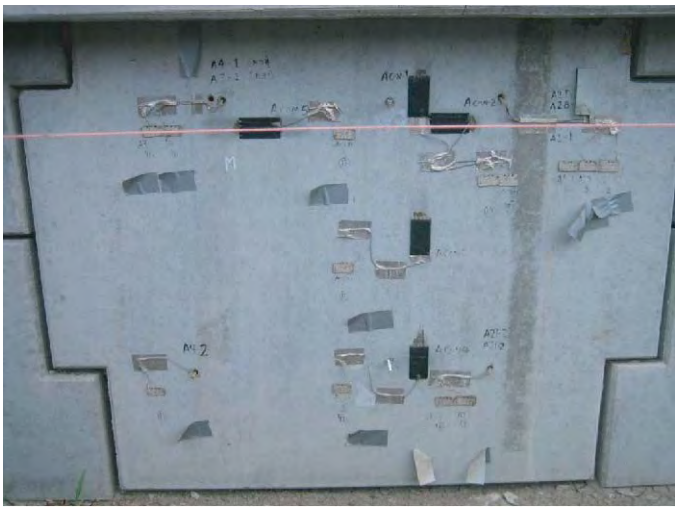

(a) Surface of panel

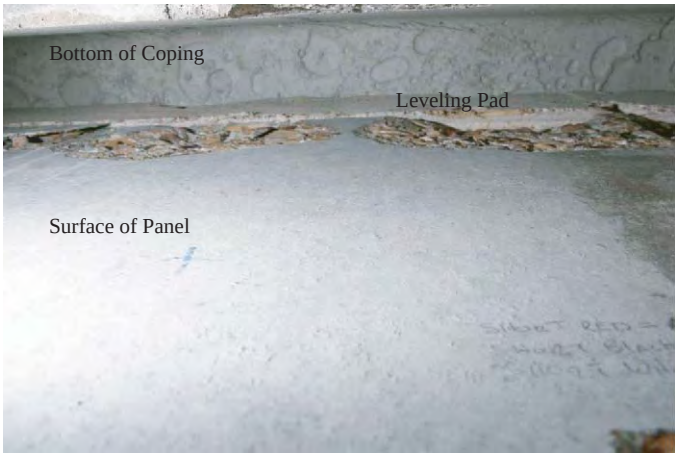

(b) Inside of panel

Figure 5.72. Cracks on the panel and leveling pad after test (Test 2).

Two additional targets affixed to the displacement bars attached to the wall panel at locations corresponding to the upper and lower layers of wall reinforcement were used to determine angular and translational displacement of the wall panel from analysis of high-speed film. From the film analysis, the maximum dynamic displacement of the panel was 23 mm (0.92 in.) at the upper reinforcement layer and 5 mm (0.19 in.) at the bottom reinforcement layer. The permanent displacement of the panel was 14 mm (0.55 in.) at the upper reinforcement layer and 5 mm (0.18 in.) at the bottom reinforcement layer.

The corresponding displacement–time histories for the barrier–coping section and wall panel obtained from film analysis are shown in Figure 5.79. Figure 5.80 shows the impact force–displacement curve for the top of the barrier.

Figure 5.73. Test 3: Vertical wall barrier with 8 ft long strip.

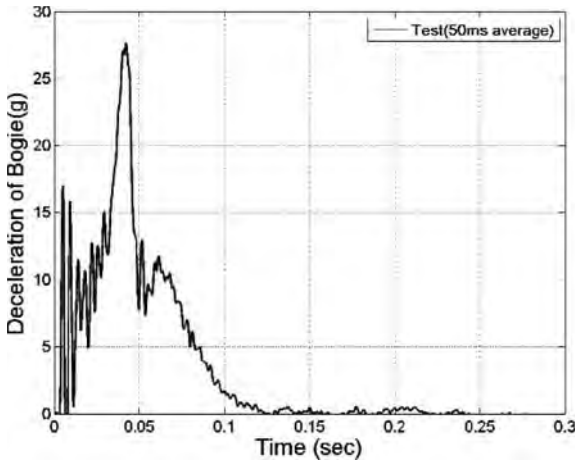

(a) Bogie

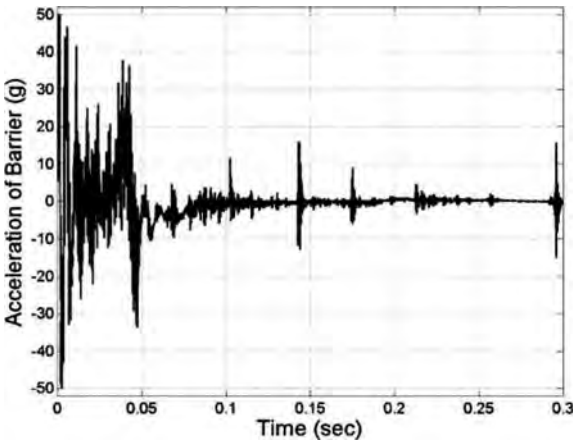

(b) Barrier

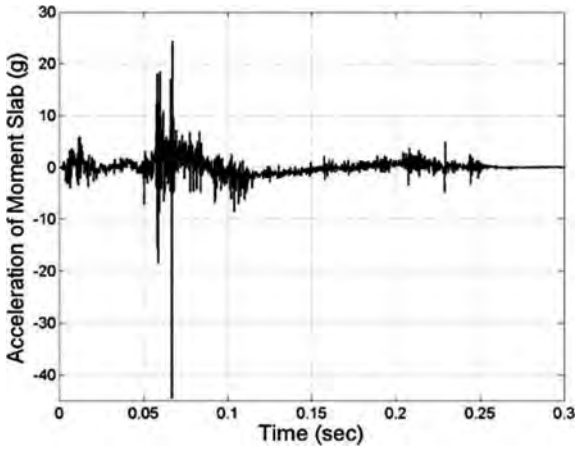

(c) Moment slab

Figure 5.74. Raw acceleration data of bogie, barrier, and moment slab (Test 3).

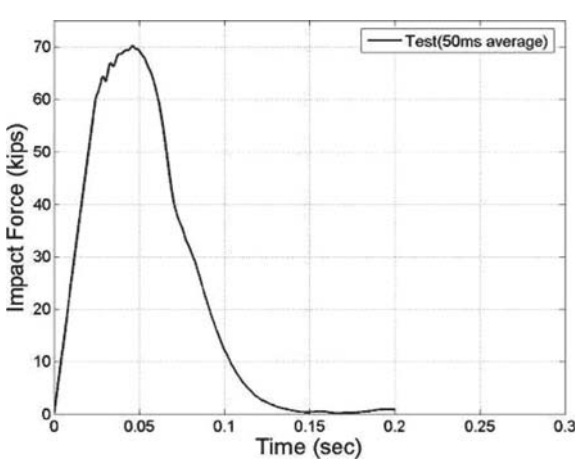

(a) Impact force

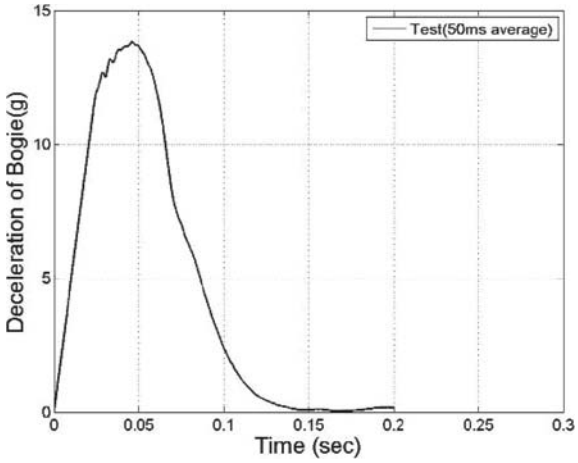

(b) Deceleration

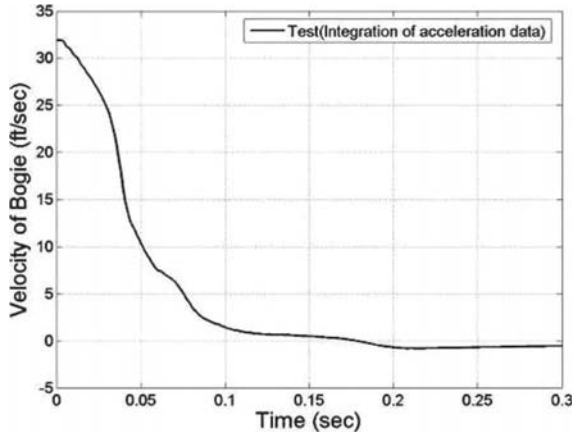

(c) Velocity

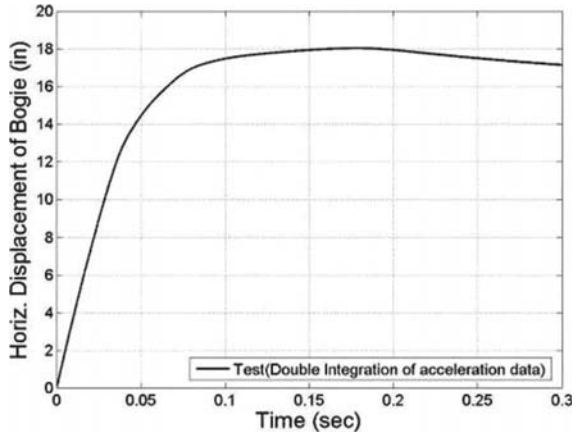

(d) Displacement

Figure 5.75. Force, acceleration, velocity, and displacement of bogie (Test 3).

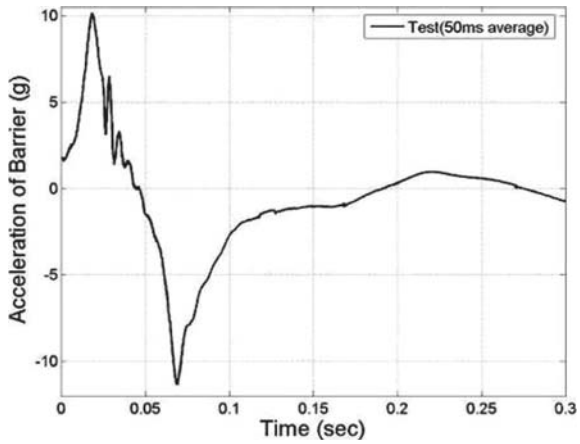

(a) Acceleration

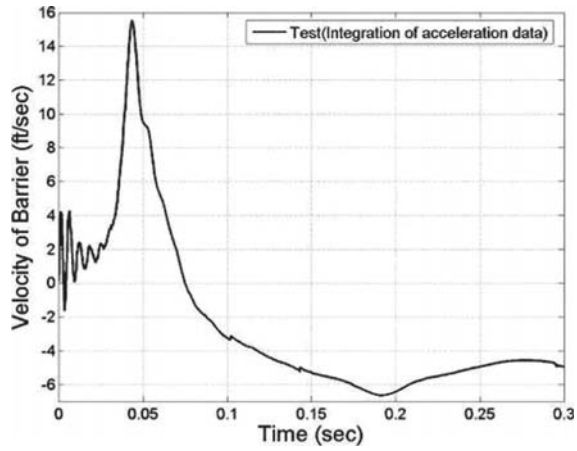

(b) Velocity

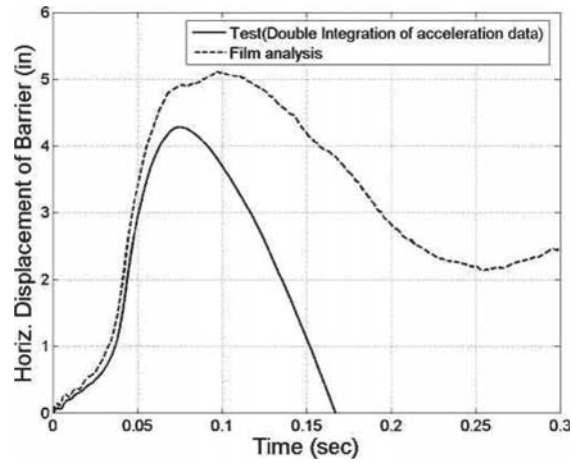

(c) Displacement

Figure 5.76. Acceleration, velocity, and displacement of barrier (Test 3).

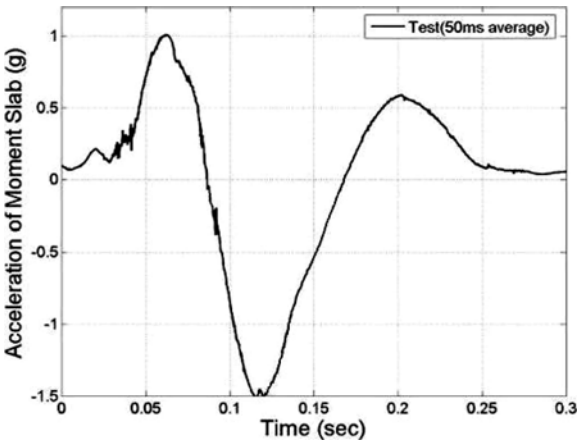

(a) Acceleration

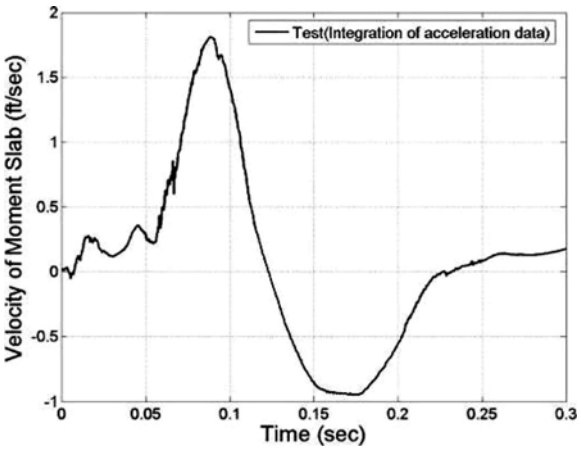

(b) Velocity

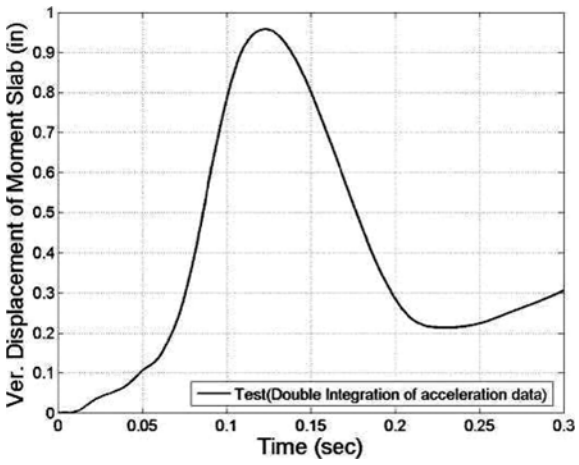

(c) Displacement

Figure 5.77. Acceleration, velocity, and displacement of moment slab (Test 3).

Figure 5.78. Location of displacement bars affixed on the barrier and panels (Test 3).

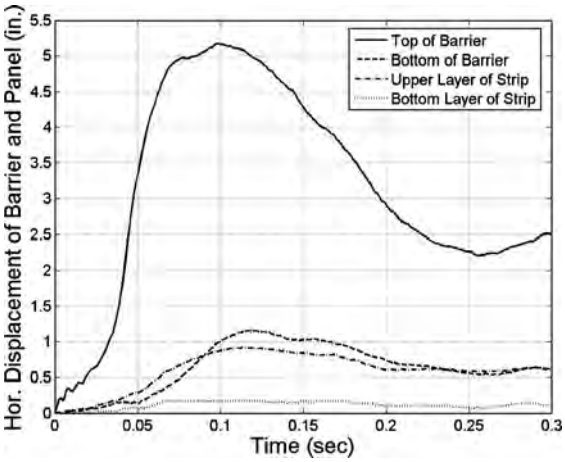

Figure 5.79. Horizontal displacement of barrier and panel measured from film (Test 3).

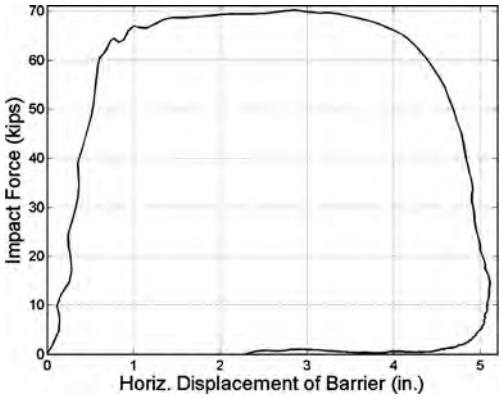

Figure 5.80. Force–displacement of the top of the barrier (Test 3).

Load in the Reinforcement Strips

A total of eight strain gages were used to instrument the strips to capture the tensile forces transmitted into the reinforcement during the dynamic bogie vehicle impact. To enable comparison of loads on the strips, the locations of strain gages were assigned a numeric designator as shown in Figure 5.81. Note that two strain gages were used at locations 2-1 and 2-2 adjacent to the wall panel at the point of impact to provide some measurement redundancy at the location expected to experience maximum tensile loading. One gage was placed on top of the reinforcement and one gage was placed on the bottom of the reinforcement. Measurements obtained from the strain gages during testing indicated that the reinforcement experienced some bending in addition to tensile loading. The strain gages on the top and bottom of the reinforcement enabled the bending to be canceled out and the average tensile force in the reinforcement to be calculated.

Raw data obtained from the strain gages on the bar mats were analyzed and the results are presented in Figure 5.82. A contact switch placed on the top edge of the level-up concrete on

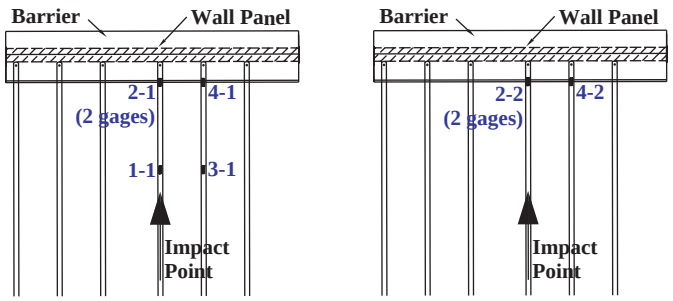

Figure 5.81. Location of strain gages and labeling (Test 3).

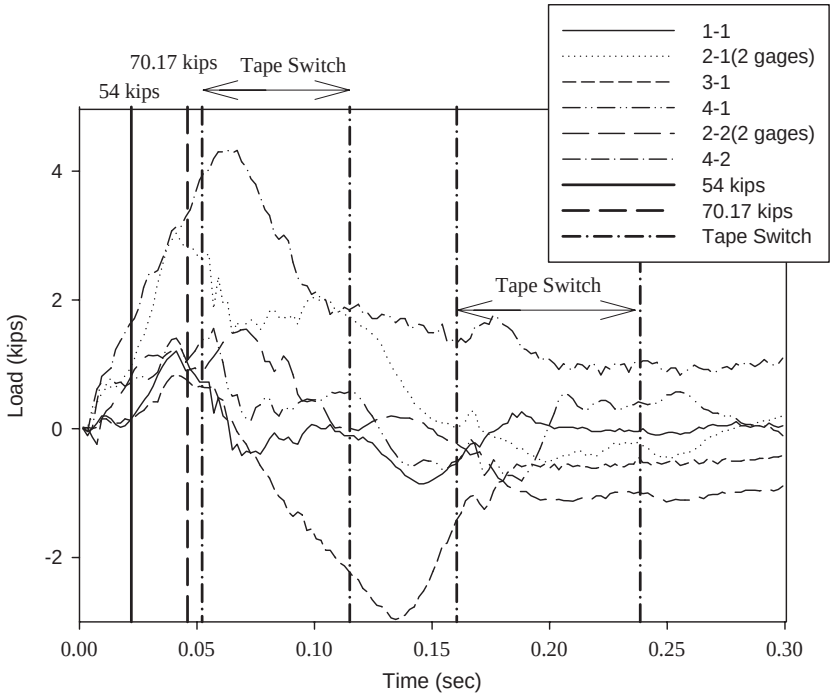

Figure 5.82. Load on the strips (Raw data, Test 3).

top of the wall panels inside the recess of the coping activated twice from 0.0522 to 0.115 sec and from 0.1605 to 0.2385 sec, which indicates that the coping was in contact with the wall panel and/or leveling concrete during these times. The 50 msec average of the raw data was analyzed to obtain design loads for the strips, and the results are presented in Figure 5.83. As shown in this figure, there was some increase in force in the strips observed after the time of maximum barrier impact load, but the increase was not as significant as that seen in Test 1. The maximum 50 msec average design strip loads corresponding to a design impact load of 240 kN (54 kips) were estimated as follows:

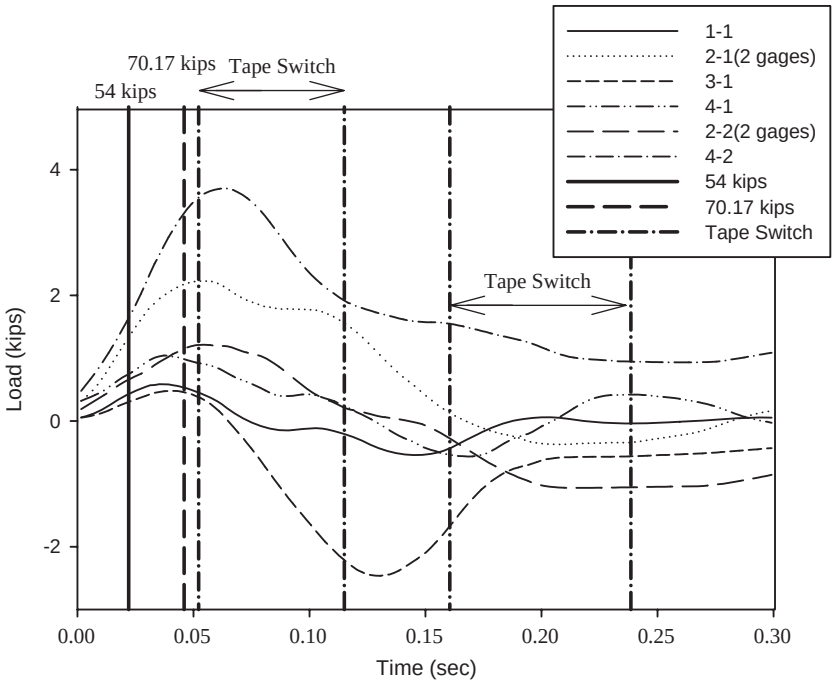

Figure 5.83. Load on the strips (50 msec avg., Test 3).

Table 5.12. Load on the wall reinforcement (Test 3).

	Upper layer (kips)				Bottom layer (kips)	
	Impact Point, Behind (1-1)	Impact Point, Front (2-1)	Next to Impact Point, Behind (3-1)	Next to Impact Point, Front (4-1)	Impact Point, Front (2-2)	Next to Impact Point, Front (4-2)
Maximum load from raw data (t = 0.0643 sec)	–0.11	1.76	0.37	0.53	1.38	4.46
Maximum 50 msec avg. load (t = 0.0635 sec)	0.24	2.13* (–0.3 top 4.56 bot.)	0.06	0.79	1.19* (0.98 top 1.4 bot.)	3.71
Estimated design load	0.18	1.64	0.05	0.60	0.92	2.85
Estimated design load per foot of wall	0.11	1.01	0.03	0.37	0.57	1.76

* Average of top and bottom loads

$$\text{Estimated Strip Load} = \frac{54}{70.17} \times \text{Maximum Strip Load} \qquad (5\text{-}11)$$

where 312.13 kN (70.17 kips) is the maximum 50 msec average impact load measured for the vertical wall barrier over 2.43 m (8 ft) strips.

Table 5.12 presents a summary of the forces in the steel strips obtained from the third bogie impact test including the maximum force, maximum 50 msec average force, and an estimate of the maximum 50 msec average force for a 240 kN (54 kips) design impact. To enable comparison with other cases, the estimated design load for the strips was expressed in kips per foot of wall.

Permanent Deflection of Barrier and Panels

The string lines located 1.22 m (4 ft) from the face of the wall panels were used to measure the permanent deflection of barriers and panels after bogie vehicle impact. After the bogie vehicle impact of the vertical barrier, the permanent deflection was measured to be 63 mm (2.48 in.) and 53 mm (2.09 in.) at the top corners of the barrier and 17 mm (0.7 in.) and 15 mm (0.59 in.) at the bottom corners of the coping as shown in Figure 5.84. Note that the reference impact point was offset 95 mm (3.75 in.) left from the centerline of the barrier–coping section as shown in Figure 5.84 to align with the steel strip reinforcement. The left side of the barrier on Figure 5.84 was therefore slightly closer to the reference impact point.

The barrier–coping sections to the left of the section that was impacted had permanent movement at the top of the barrier of 24 mm (0.95 in.). This indicates that the shear dowels are effective in transferring load to the adjacent moment slab. The permanent defection of the wall panels was measured as shown in Figure 5.84. The maximum permanent movement measured in the wall panels beneath the impact barrier section was approximately 16 mm (0.63 in.), which was about three times the movement observed in the previous tests with the 4.88 m (16 ft) strips and 2.43 m (8 ft) bar mats. The magnitude of movement appears to indicate that the strips reached their pullout capacity. This conclusion is supported by the lower loads measured in the strips for this test compared to the previous tests.

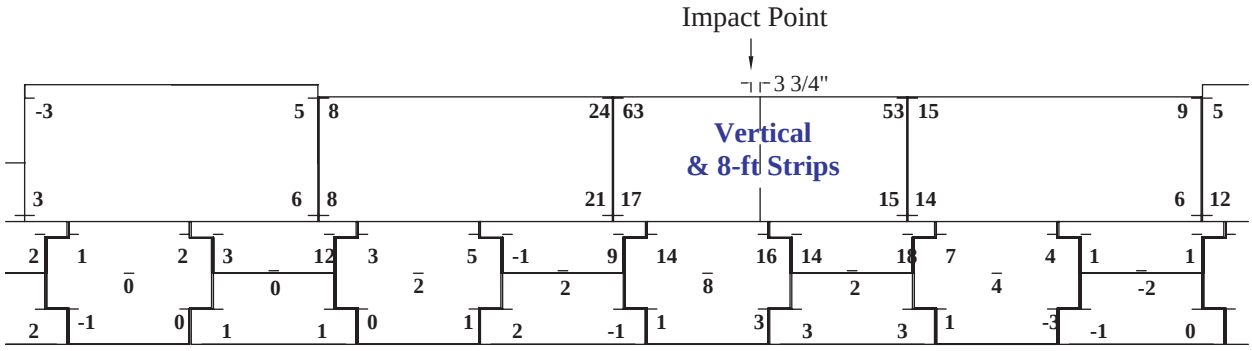

Figure 5.84. Permanent deflection of barrier and panels (Test 3, units: mm).

Panel Analysis

The wall reinforcement was instrumented with a total of five strain gages to capture the resistance of the panel during the bogie impacts as shown in Figure 5.85. The maximum compressive strain of 0.00022 occurred at 0.056 sec (see Figure 5.86) at the location of the uppermost layer of strips. Note that positive values for the vertical direction strain gages indicate movement toward the traffic side of the barrier. The strains at the horizontal centerline of the panel and at the second layer of strips were 0.00018 and 0.00014, respectively.

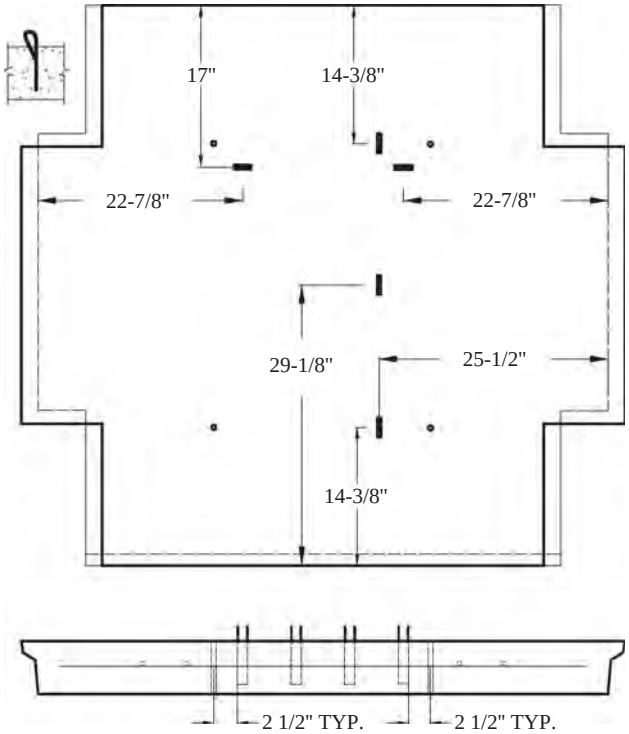

Figure 5.85. Location of concrete strain gages (Test 3).

Component Damage

Damage to the vertical wall barrier–coping section resulting from the bogie impact is shown in Figure 5.87. Although difficult to discern from the photos because the cracks are not large, the vertical barrier failed in a classical yield line pattern by developing a vertical "hinge" line at the point of impact and two diagonal hinge lines radiating from the bottom to the top of the barrier on either side of impact. As shown in Figure 5.87(b), three cracks were observed along the diagonal hinge lines. The length between the two inside most cracks on either side of the impact point was 1.98 m (6.51 ft). The lengths between the middle and outer sets of cracks were 2.19 m (7.17 ft) and 2.52 m (8.28 ft), respectively.

Cracking in the soil was observed approximately 1.22 m (48 in.) from the front face of the barrier, which corresponds with the location of the end of the moment slab. The cracking,

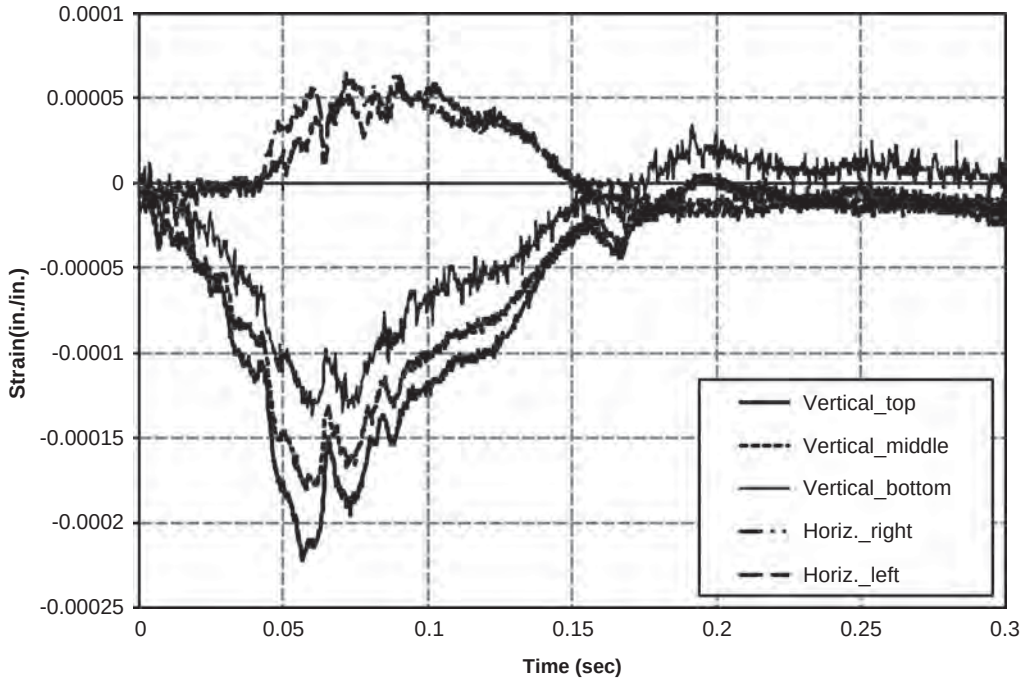

Figure 5.86. Strain on the panel (Test 3).

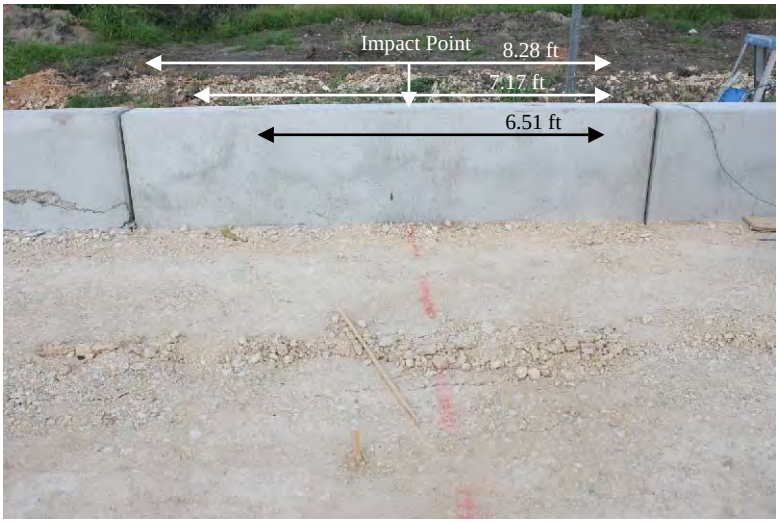

(a) Front view of the barrier

(b) Closeup front view of the barrier

Figure 5.87. Cracks on the barrier after test (Test 3).

(continued on next page)

(c) Side view of the barrier

(d) Top view of the barrier

(e) Back view of the barrier

Figure 5.87. (Continued).

shown in Figure 5.87(c), extended 18.29 m (60 ft) along the entire length of both moment slabs. This indicates that the two No. 9 shear dowels placed between the moment slabs were able to transfer substantial load to the adjacent moment slab. Damage to the back of the vertical barrier is shown in Figure 5.87(e). Damage to the panel beneath the point of impact on the barrier is shown in Figure 5.88. As shown in this figure, the surface of the panel showed little distress.

5.3.5 Bogie Test 4: Vertical Concrete Barrier with 16 ft Strips

Test 4 was similar to Test 3 with the exception that the vertical barrier was installed over a segment of wall having 4.88 m (16 ft) long reinforcement strips. As in Test 3, the vertical barrier was connected to the end of a 9.14 m (30 ft) moment slab doweled to the adjacent moment slab using two No. 9 bars. The 2,268 kg (5,000 lb) bogie vehicle as shown in Figure 5.89 hit the center of the vertical barrier head-on at a speed of approximately 32.5 km/h (20.2 mph), which was the same as reference Test 3. The reference point was along the top edge of the barrier and approximately 41.3 mm (1.625 in.) from its centerline to coincide with the location of a steel strip in the wall reinforcement below the barrier.

Data from Accelerometers

The raw acceleration data for the bogie, barrier, and moment slab are shown in Figure 5.90. Data obtained from the bogie-mounted accelerometer were analyzed and the results are presented in Figure 5.91. As shown in Figure 5.91(b), the maximum 50 msec average deceleration was 12.69 *g*. Based on this acceleration and the mass of the bogie, the maximum 50 msec average impact force was calculated to be 286.55 kN (64.42 kips) [see Figure 5.91(a)]. The velocity–time and horizontal displacement–time histories of the bogie are shown in Figure 5.91(c) and (d), respectively. These time histories were calculated through integration of the acceleration data.

The maximum 50 msec average acceleration of the barrier, as measured by the accelerometer at the top of the barrier, was 13.04 *g* in the direction of impact [see Figure 5.92(a)]. The velocity–time history of the barrier, as calculated by integration of the raw acceleration data, is shown in Figure 5.92(b). The displacement–time history obtained from integration of the velocity history is shown in Figure 5.92(c).

The 50 msec average acceleration for the moment slab is shown in Figure 5.93(a). The velocity–time history of the moment slab is shown in Figure 5.93(b). The velocity–time history was calculated by integration of the raw acceleration data.

Targets affixed to the displacement bars attached to the top and bottom of the barrier–coping section (see Figures 5.61 and 5.94) were used as reference points to determine angular and translational displacement of the barrier from analysis of high-speed film. From the film analysis, the maximum dynamic displacement of the barrier was 153 mm (6.02 in.) at the top of the barrier and 17.5 mm (0.69 in.) at the bottom of the coping. The permanent displacement of the barrier was 76.2 mm (3 in.) at the top of the barrier and 5.6 mm (0.22 in.) at the bottom of the coping.

Two additional targets affixed to the displacement bars attached to the wall panel at locations corresponding to the upper and lower layers of wall reinforcement were used to

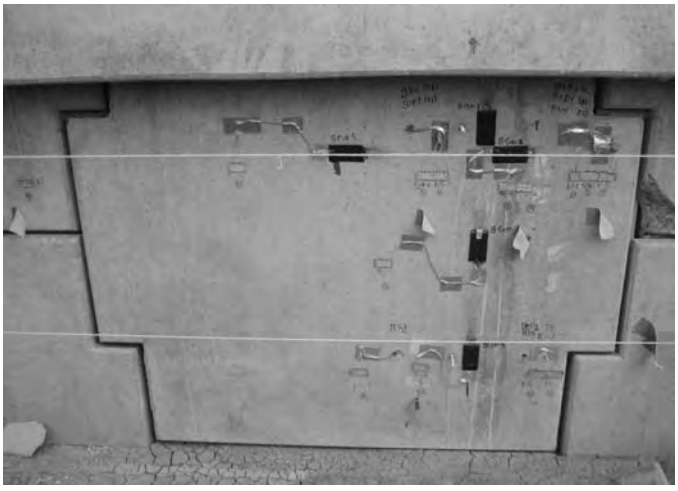

Figure 5.88. Panel surface after test (Test 3).

Figure 5.89. Test 4: Vertical wall barrier with 16 ft long strips.

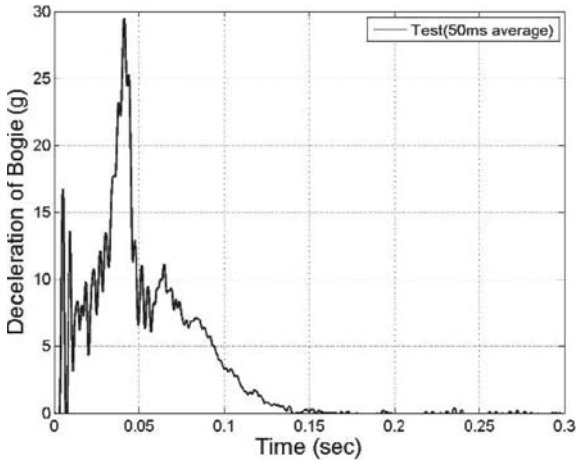

(a) Bogie

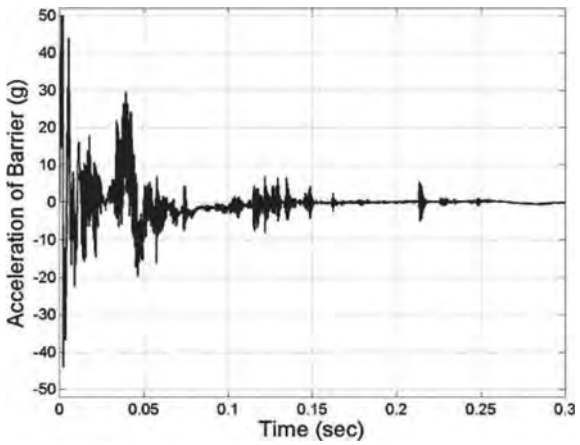

(b) Barrier

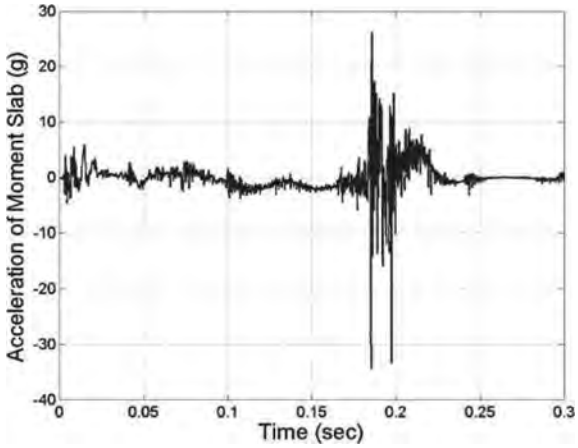

(c) Moment slab

Figure 5.90. Raw acceleration data of bogie, barrier, and moment slab (Test 4).

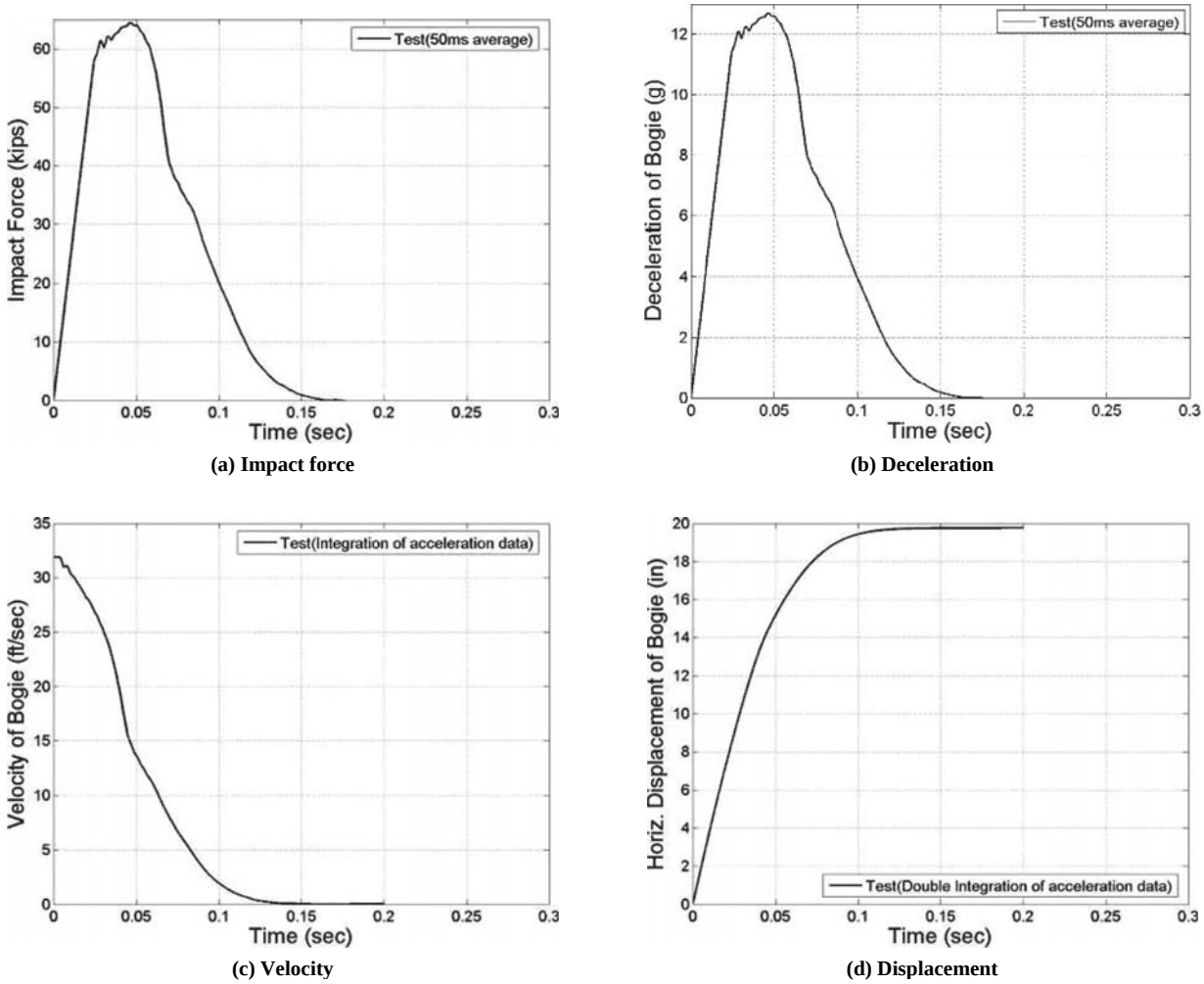

(a) Impact force **(b) Deceleration**

(c) Velocity **(d) Displacement**

Figure 5.91. Force, acceleration, velocity, and displacement of bogie (Test 4).

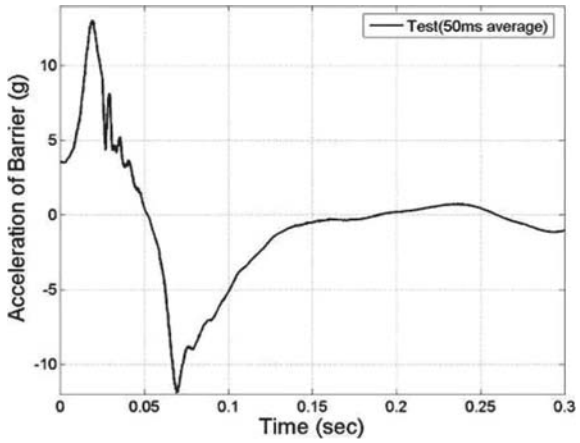

(a) Acceleration

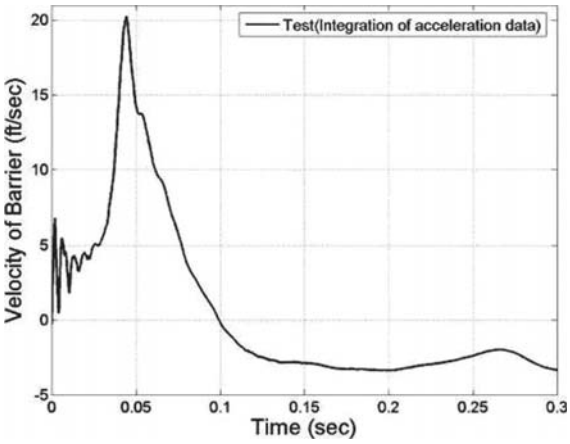

(b) Velocity

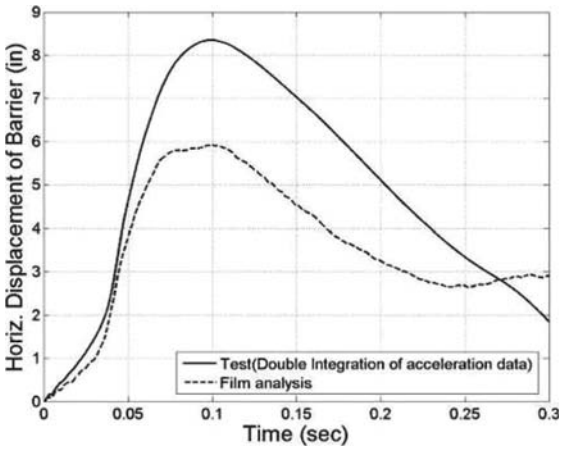

(c) Displacement

Figure 5.92. Acceleration, velocity, and displacement of barrier (Test 4).

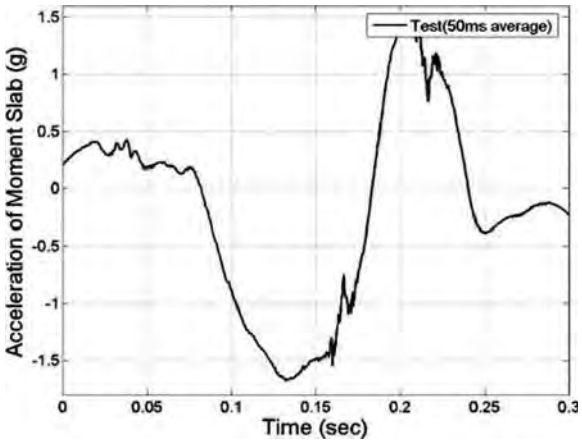

(a) Acceleration

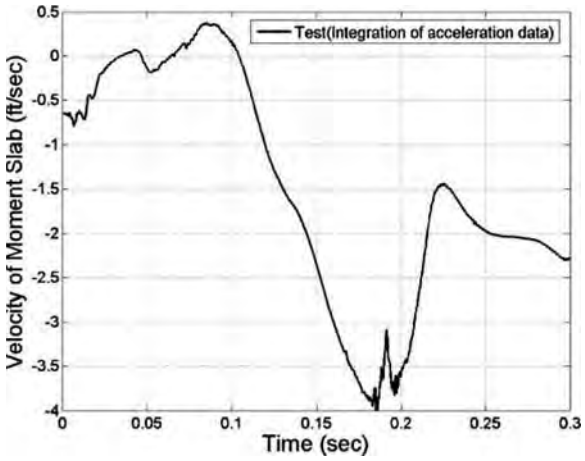

(b) Velocity

Figure 5.93. Acceleration and velocity of moment slab (Test 4).

Figure 5.94. Location of displacement bars affixed on the barrier and panels (Test 4).

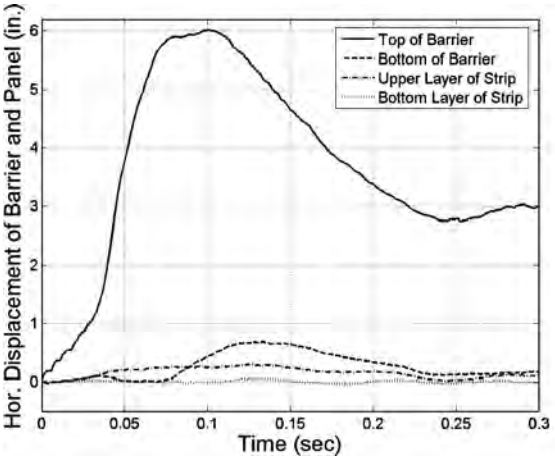

Figure 5.95. Horizontal displacement of barrier and panel measured from film (Test 4).

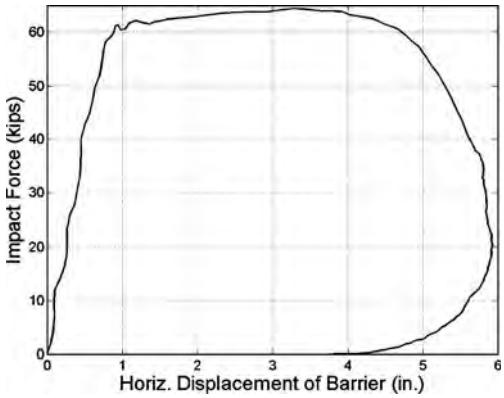

Figure 5.96. Force–displacement of the top of the barrier (Test 4).

determine angular and translational displacement of the wall panel from analysis of high-speed film. From the film analysis, the maximum dynamic displacement of the panel was 7.6 mm (0.3 in.) at the upper reinforcement layer of the panel and 1.8 mm (0.07 in.) at the bottom reinforcement layer. The permanent displacement of the panel was 1.8 mm (0.07 in.). There was little discernable movement of the panel at the bottom reinforcement layer.

The corresponding displacement–time histories for the barrier–coping section and wall panel obtained from film analysis are shown in Figure 5.95. Figure 5.96 shows the impact force–displacement curve for the top of the barrier.

Load in the Reinforcement Strips

A total of eight strain gages were used to instrument the strips to capture the tensile forces transmitted into the reinforcement during the dynamic bogie vehicle impact. To enable comparison of loads on the strips, the locations of strain gages were assigned a numeric designator as shown in Figure 5.97. Note that two strain gages were used at locations 2-1 and 2-2

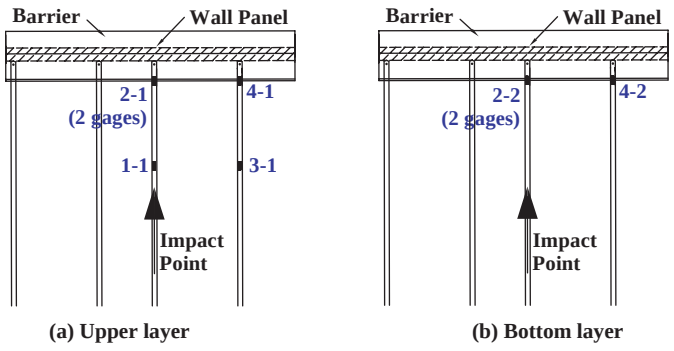

Figure 5.97. Location of strain gages and labeling (Test 4).

adjacent to the wall panel at the point of impact to provide some measurement redundancy at the location expected to experience maximum tensile loading. One gage was placed on top of the reinforcement and one gage was placed on the bottom of the reinforcement. Measurements obtained from the strain gages during testing indicated that the reinforcement experienced some bending in addition to tensile loading. The strain gages on the top and bottom of the reinforcement enabled the bending to be canceled out and the average tensile force in the reinforcement to be calculated.

Raw data obtained from the strain gages on the bar mats were analyzed and the results are presented in Figure 5.98. A contact switch placed on the top edge of the level-up concrete on top of the wall panels inside the recess of the coping activated twice from 0.0655 to 0.1183 sec and from 0.173 to 0.1802 sec, which indicates that the coping was in contact with the wall panel and/or leveling concrete during these times. The 50 msec average of the raw data was analyzed to obtain design loads for the strips, and the results are presented in Figure 5.99. As shown in this figure, there was some increase in force in the strips observed after the time of maximum barrier impact load, but the increase was not as significant as that seen in Test 1. The maximum 50 msec average design strip loads corresponding to a design impact load of 240 kN (54 kips) were estimated as follows:

$$\text{Estimated Strip Load} = \frac{54}{64.42} \times \text{Maximum Strip Load} \qquad (5\text{-}12)$$

where 286.55 kN (64.42 kips) is the maximum 50 msec average impact load measured for the vertical wall barrier over 4.88 m (16 ft) strips.

Table 5.13 presents a summary of the forces in the steel strips obtained from the fourth bogie impact test including the maximum force, maximum 50 msec average force, and an estimate of the maximum 50 msec average force for a 240 kN (54 kips) design impact. To enable comparison with other cases, the estimated design load for the strips was expressed in kips per foot of wall.

Permanent Deflection of Barrier and Panels

The string lines located 4 ft from the face of wall panels were used to measure the permanent deflection of barriers and panels after bogie vehicle impact at different elevations. After bogie vehicle impact of the vertical barrier, the permanent deflection was measured to be 67 mm (2.64 in.) and 68 mm (2.68 in.) at the top corners of the barrier and 2 mm (0.08 in.) and 8 mm (0.31 in.) at the bottom corners of the coping as shown in Figure 5.100. Note that the reference impact point was offset 41.3 mm (1.625 in.) left of the centerline of the barrier–coping section as shown in Figure 5.100 to align with the steel strip reinforcement.

The permanent defection of the wall panels was measured as shown in Figure 5.100. The maximum permanent movement measured in the wall panels beneath the impact barrier section was only about 4 mm (0.16 in.), which is considerably

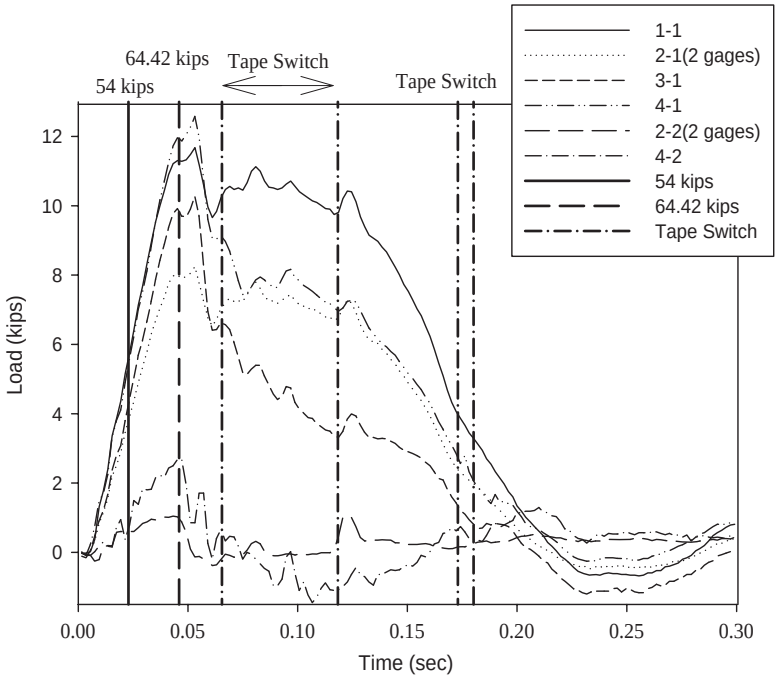

Figure 5.98. Load on the strips (Raw data, Test 4).

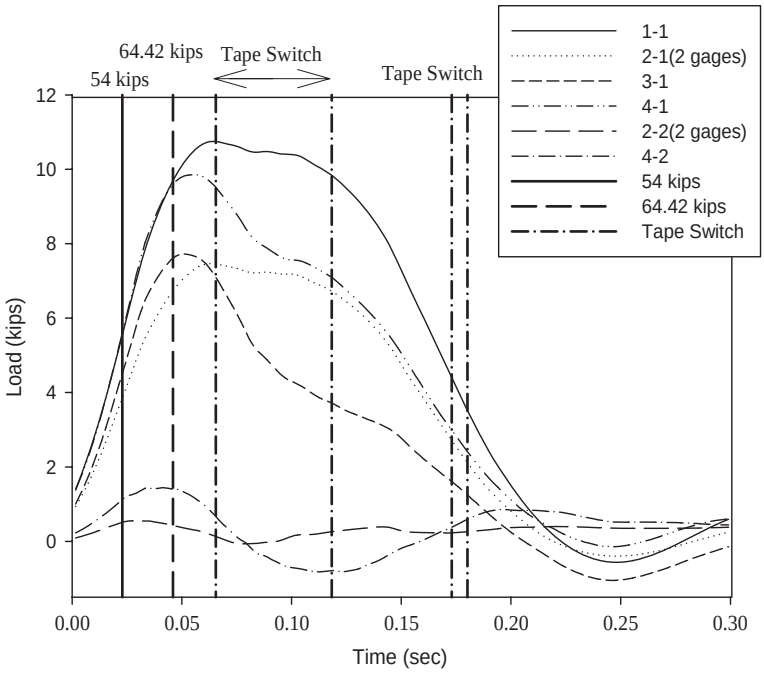

Figure 5.99. Load on the strips (50 msec avg., Test 4).

Table 5.13. Load on the wall reinforcement (Test 4).

	Upper layer (kips)				Bottom layer (kips)	
	Impact Point, Behind (1-1)	Impact Point, Front (2-1)	Next to Impact Point, Behind (3-1)	Next to Impact Point, Front (4-1)	Impact Point, Front (2-2)	Next to Impact Point, Front (4-2)
Maximum load from raw data (t = 0.054 sec)	11.59	8.08	10.25	12.51	–0.16	1.25
Maximum 50 msec avg. load (t = 0.0645 sec)	10.75	7.46* (7.53 top 7.40 bot.)	7.20	9.58	0.15* (–2.44 top 2.74 bot.)	0.73
Estimated design load	9.01	6.25	6.03	8.03	0.13	0.62
Estimated design load per foot of wall	3.70	2.57	2.48	3.30	0.05	0.25

* Average of top and bottom loads

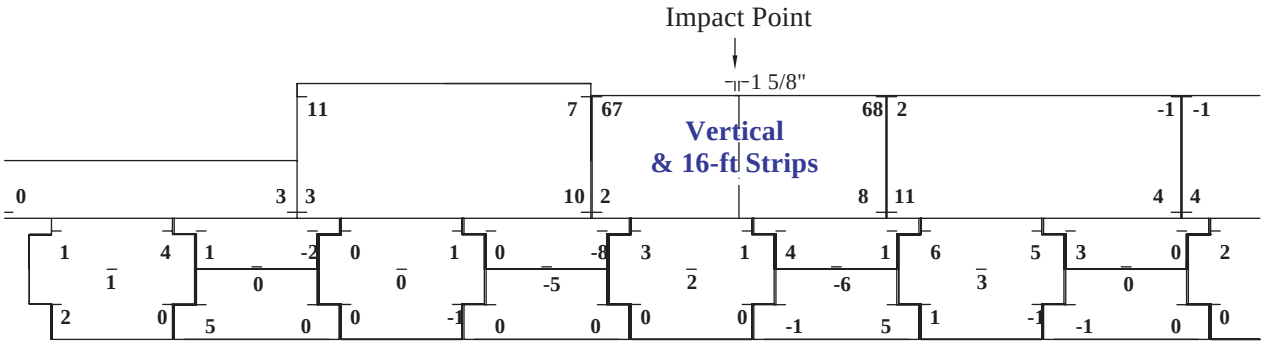

Figure 5.100. Permanent deflection of barrier and panels (Test 4, units: mm).

less than the movement observed in the previous test of the vertical barrier with the 8 ft strips.

Panel Analysis

The wall reinforcement was instrumented with a total of five strain gages to capture the resistance of the panel during the bogie impacts as shown in Figure 5.101. The maximum compressive strain of 0.0024 occurred at 0.11 sec (see Figure 5.102) at the location of uppermost layer of strips. Note that positive values for the vertical direction strain gages indicate movement toward the traffic side of the barrier. As shown in Figure 5.102, the strain dropped suddenly after 0.05 sec. The strains at the horizontal centerline of the panel and at the second layer of strips were 0.00014 and 0.00008, respectively.

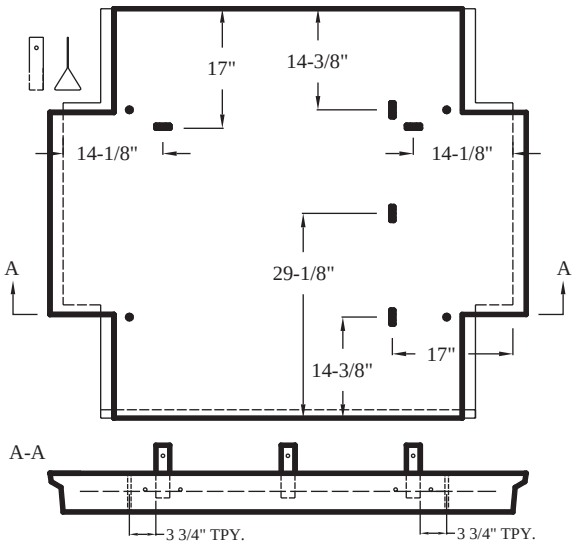

Figure 5.101. Location of concrete strain gages (Test 4).

Component Damage

Damage to the vertical wall barrier–coping section resulting from the bogie impact is shown in Figure 5.103. Although difficult to discern from the photos because some of the crack widths are not large, the vertical barrier has characteristics of a classical yield line pattern by developing a vertical "hinge" line at the point of impact and two diagonal hinge lines radiating from the bottom to the top of the barrier on either side of impact. As shown in Figure 5.103(b), several cracks were observed along the diagonal hinge lines. The length between the two inside most cracks on either side of the impact point was 1.76 m (5.77 ft). There were also signs of a flexural-type failure mode with the entire length of the barrier cracked near the groundline at the connection between the barrier and coping and also 0.51 m (20 in.) above ground.

Cracking in the soil was observed approximately 1.22 m (48 in.) from the front face of the barrier, which corresponds with the location of the end of the moment slab. The cracking,

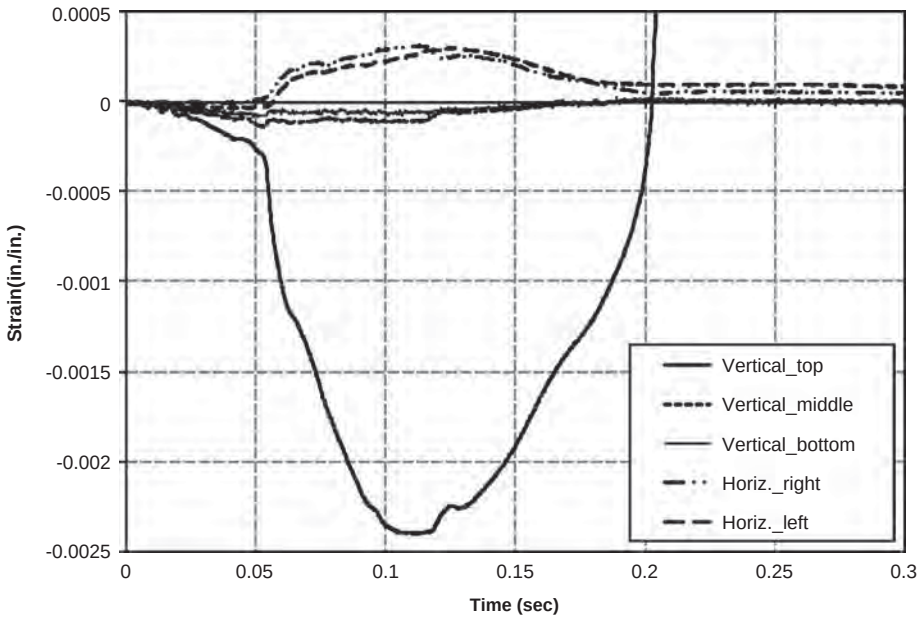

Figure 5.102. Strain on the Panel (Test 4).

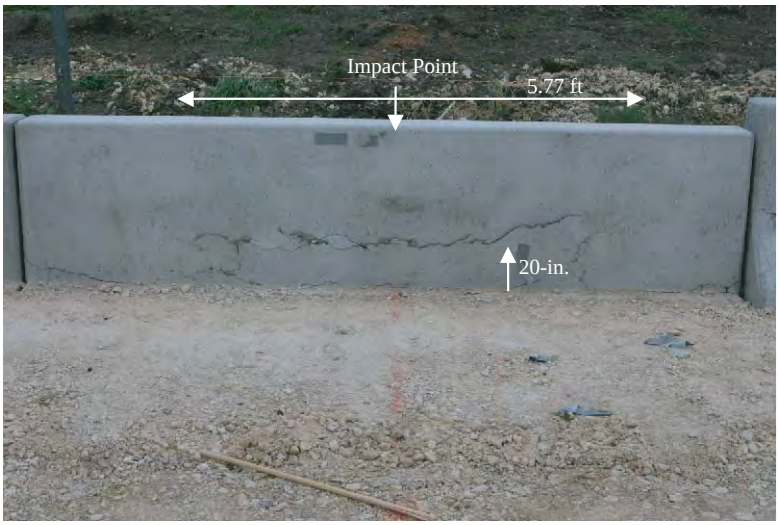

(a) Front view of the barrier

(b) Closeup front view of the barrier

Figure 5.103. Cracks on the barrier after test (Test 4).

(continued on next page)

(c) Side view of the barrier

(d) Top view of the barrier

(e) Back view of the barrier

Figure 5.103. (Continued).

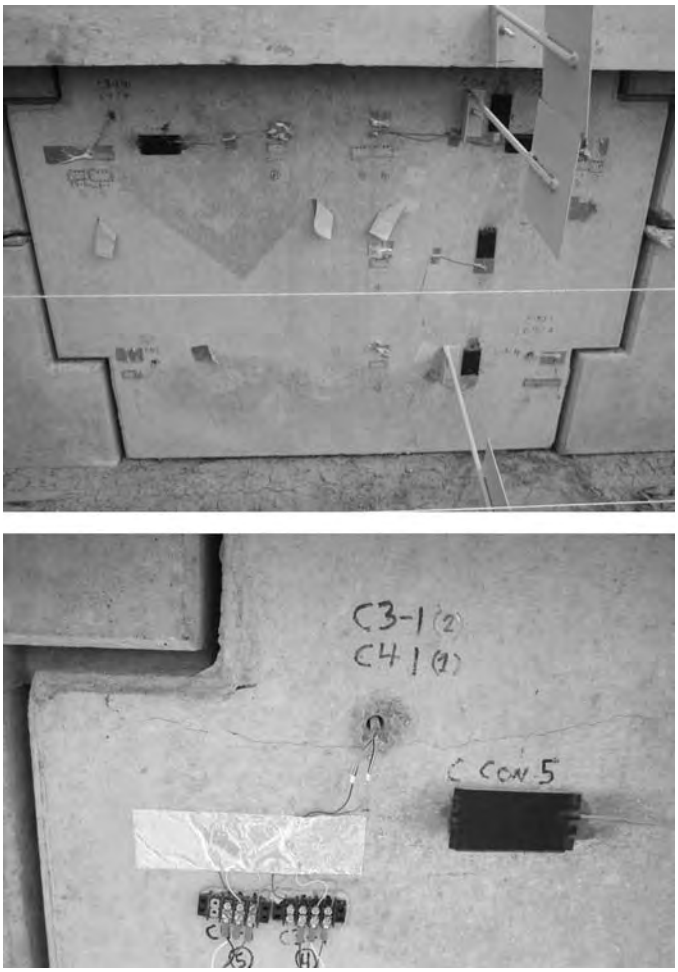

Figure 5.104. Cracks on the panel after test (Test 4).

shown in Figure 5.103(c), extended 18.29 m (60 ft) along the entire length of both moment slabs. This indicates that the two No. 9 shear dowels placed between the moment slabs were able to transfer substantial load to the adjacent moment slab. Damage to the back of the vertical barrier is shown in Figure 5.103(e). Damage to the panel beneath the point of impact on the barrier is shown in Figure 5.104. Note that the panel is cracked along its length at an elevation corresponding to the upper layer of reinforcement. It appears the additional resistance provided by the 4.88 m (16 ft) strips enabled more load to be transferred to the wall panel.

5.3.6 Damage of Moment Slab after Test

After the bogie impact test, the overburden soil was removed to permit inspection of the moment slab and the connection between the coping and moment slab. After impact, cracks were observed in the top of the moment slab close to its connection to the coping as shown in Figure 5.105. Transverse cracks were found in the moment slab at locations corresponding to the joints as shown in Figure 5.106.

(a) Bogie Test 1

(b) Bogie Test 2

(c) Bogie Test 3

(d) Bogie Test 4

Figure 5.105. Cracks in the moment slab below barrier.

5.4 Summary of Bogie Tests

Four reference tests were conducted as summarized in Table 5.14. The impact speeds of bogie vehicle varied from 32.5 km/h (20.2 mph) to 35.08 km/h (21.8 mph). The barrier types used were a 0.81 m (32 in.) tall N.J. shape barrier (Test 1) and a 0.69 m (27 in.) tall vertical wall barrier (Test 2 through Test 4). Wall reinforcement types included 4.88 m (16 ft) steel strips at a density of four per panel (Test 1 and 4), a 2.43 m (8 ft) bar mat (Test 2), and 2.43 m (8 ft) steel strips at a density of six per panel (Test 3).

The maximum 50 msec average impact load on the barriers varied from 286.55 kN (64.42 kips) to 326.5 kN (73.4 kips) and

(a) Test 1 and Test 4

(b) Test 2 and Test 3

(c) Test 3 and Test 4

Figure 5.106. Cracks in the moment slab near joint between barriers.

are all higher than the 240 kN (54 kips) dynamic force associated with the design of barriers for AASHTO TL-3 and TL-4.

Table 5.14 also presents the dynamic and permanent deflection at the top and bottom of the barrier and at the upper and lower layer of reinforcement. The maximum dynamic horizontal displacement at the top of the barrier varied from 131 mm (5.17 in.) to 156 mm (6.14 in.). The maximum dynamic horizontal displacement at the bottom of the barrier varied from 18 mm (0.69 in.) to 30 mm (1.16 in.). The maximum dynamic horizontal displacement of the panel at the top layer of reinforcement varied from 8 mm (0.3 in.) to 23 mm (0.92 in.). The maximum dynamic horizontal displacement of the panel at the bottom layer of reinforcement varied from 0 mm to 5 mm (0.19 in.).

The permanent movements of the target locations were obtained in two ways: high-speed film analysis and distances from the reference string line stretched in front of the wall. The string line permanent measurements consisted of measuring the distance with a tape measure from the target to the string before and after each test. The permanent horizontal displacement at the top of the barrier varied from 6.3 mm (0.25 in.) to 99 mm (3.9 in.). The permanent horizontal displacement at the bottom of the barrier varied from 8 mm (0.31 in.) to 20 mm (0.79 in.). The permanent horizontal displacement of the panel at the level of the top row of reinforcement varied from 1 mm (0.04 in.) to 16 mm (0.63 in.). The permanent horizontal displacement of the panel at the level of the bottom row of reinforcement varied from 0 mm to 4.1 mm (0.16 in.).

Even though the wall systems were subjected to loads higher than design conditions, all movements were considered acceptable from a performance point of view. The wall system composed of the 2.44 m (8 ft) strip reinforcement (Test 3) had the highest panel movements, while the lowest movements were recorded for the configuration that incorporated 4.88 m (16 ft) strips and the vertical wall barrier (Test 4). In Test 4, the top panel exhibited a horizontal hairline fracture crack along a line corresponding to the location of the top layer of reinforcement. It is possible that this damage occurred as a result of accumulated and repeated movement of the coping, thereby decreasing the clearance between the coping and the panel. As a result, the coping engaged the panel earlier in the dynamic event and may have lead to higher load.

5.5 Comparison of Test and Numerical Simulation

A comparison between the results of Test 1 [N.J. barrier with 4.88 m (16 ft) long strip] and the numerical simulations was performed to determine if further calibration of the numerical model was needed. The calibrated model was used in the subsequent study of the 3.05 m (10 ft) high MSE wall and barrier described in Chapter 6. To enable comparison of forces and displacements, selected strip locations have been assigned an alphanumeric designator that describes their horizontal position relative to the bogie impact point and the corresponding vertical reinforcement layer (see Figure 5.107).

As shown in Figures 5.108 and 5.109, the damage profile that develops in the simulated barrier is similar to that observed in the test in that it occurs above the toe of the barrier and has a parabolic shape. However, due to the short [3.05 m (10 ft)] length of the precast barrier section that was modeled, much

Table 5.14. Bogie test results.

	Test 1	Test 2	Test 3	Test 4*
Test Installation				
Barrier Type	New Jersey	Vertical Wall	Vertical Wall	Vertical Wall
Reinforcement	16 ft long strip (4 per panel)	8 ft long bar mat	8 ft long strip (6 per panel)	16 ft long strip (4 per panel)
Speed of Bogie	21.8 mph	20.3 mph	20.19 mph	20.19 mph
Test Results				
Peak Acceleration				
Bogie	14.45 *g*	13.00 *g*	13.82 *g*	12.69 *g*
Barrier	7.36 *g*	10.71 *g*	10.16 *g*	13.04 *g*
Moment Slab	1.84 *g*	N/A	1.00 *g*	N/A
Impact Force	73.4 kips	66.1 kips	70.17 kips	64.42 kips
Displacement				
Top of Barrier				
Dynamic	6.14 in.	6.04 in.	5.17 in.	6.02 in.
Permanent	3.00 in.	4.00 in.	2.50 in.	3.00 in.
Bottom of Coping				
Dynamic	1.12 in.	0.93 in.	1.16 in.	0.69 in.
Permanent	0.55 in.	0.50 in.	0.60 in.	0.22 in.
Panel (Upper Layer)				
Dynamic	0.63 in.	0.37 in.	0.92 in.	0.30 in.
Permanent	0.24 in.	0.20 in.	0.55 in.	0.07 in.
Panel (Second Layer)				
Dynamic	0.00 in.	0.10 in.	0.19 in.	0.07 in.
Permanent	0.00 in.	0.02 in.	0.18 in.	0.00 in.
Loads in Strips				
Upper Layer				
Max. 50 msec**	7.23 kips	1.54 kips	2.13 kips	7.46 kips
Design Load	5.29 kips (2.17 kips/ft)	1.68 kips (2.14 kips/ft)	1.64 kips (1.01 kips/ft)	6.25 kips (2.57 kips/ft)
Second Layer				
Max. 50 msec**	–1.20 kips	0.08 kips	1.19 kips	0.15 kips
Design Load	–0.88 kips (–0.36 kips/ft)	0.08 kips (0.12 kips/ft)	0.92 kips (0.57 kips/ft)	0.13 kips (0.05 kips/ft)
Total Design Load***	1.81 kips/ft	2.26 kips/ft	1.58 kips/ft	2.62 kips/ft

* Test Section 4 was between Test Sections 1 and 3 and Test 4 was carried out after Tests 1 and 3. Residual deformations from Tests 1 and 3 may have influenced the results of Test 4.
** Average of top and bottom loads.
*** Average of loads in the strips at upper and second layers.

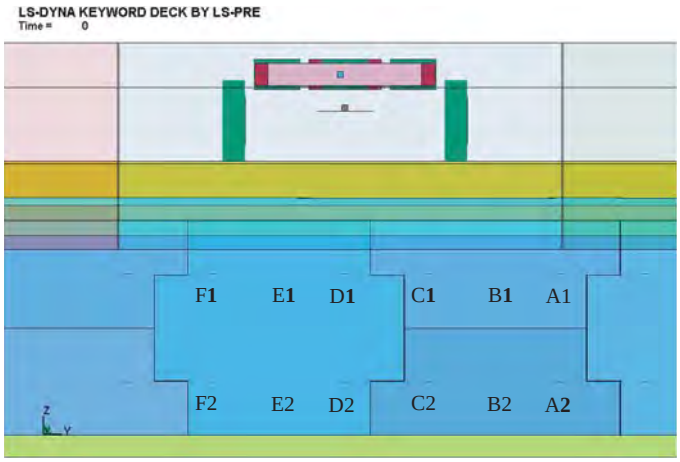

Figure 5.107. Strip location indicator.

(a)

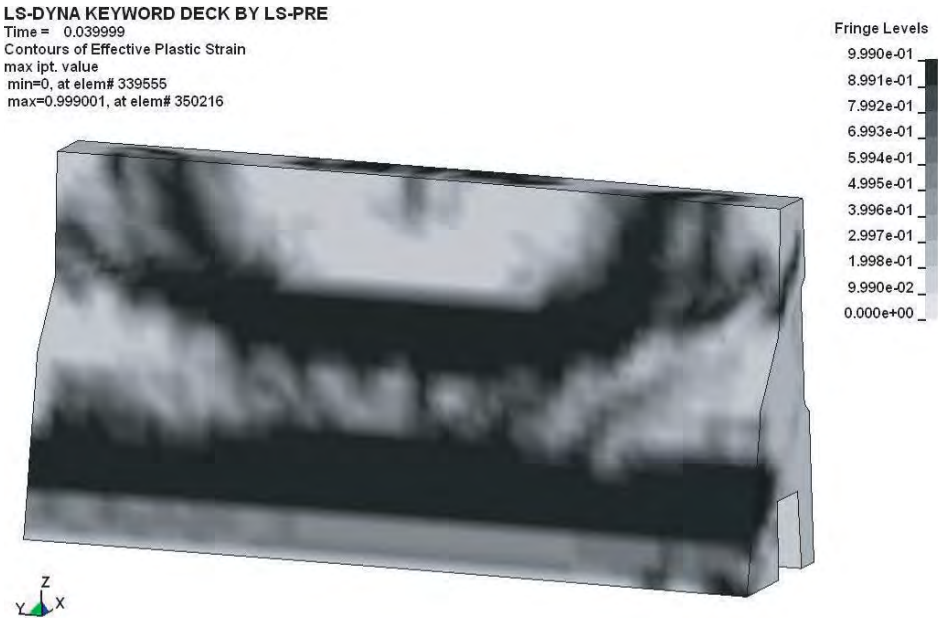

(b)

Figure 5.108. Concrete damage profile on front side of (a) Test 1 and (b) simulation.

of the damage eventually radiates out to the free ends of the section.

The maximum 50 msec average impact loads on the barrier were 326.5 kN (73.4 kips) from Test 1 and 365.1 kN (81.85 kips) from the simulation as shown in Figure 5.110. The comparison of the horizontal displacement of the barrier and the wall panel is shown in Figure 5.111.

The strip loads in the simulation include the static load due to the earth pressure and the dynamic load due to the barrier impact. To compare the simulation results to the test, the static load in the strips was calculated based on AASHTO LRFD and subtracted from the simulation result. The static loads in the upper and lower layers of reinforcement were computed to be 3.69 kN (0.83 kips) and 7.07 kN (1.59 kips), respectively (Table 5.15). Figure 5.112 shows the comparison of the raw data of load on the strip. In the simulation, the maximum dynamic load in the strip was calculated to be 33.23 kN (7.47 kips) [total load 36.92 kN (8.3 kips)—strip load 3.69 kN (0.83 kips)]. The maximum dynamic load measured in the strip in Test 1 was 34.7 kN (7.8 kips) at 0.0675 sec. The load was shown to drop down at this time in both cases and then rebound. The 50 msec average of the forces in the strip with maximum load

(a)

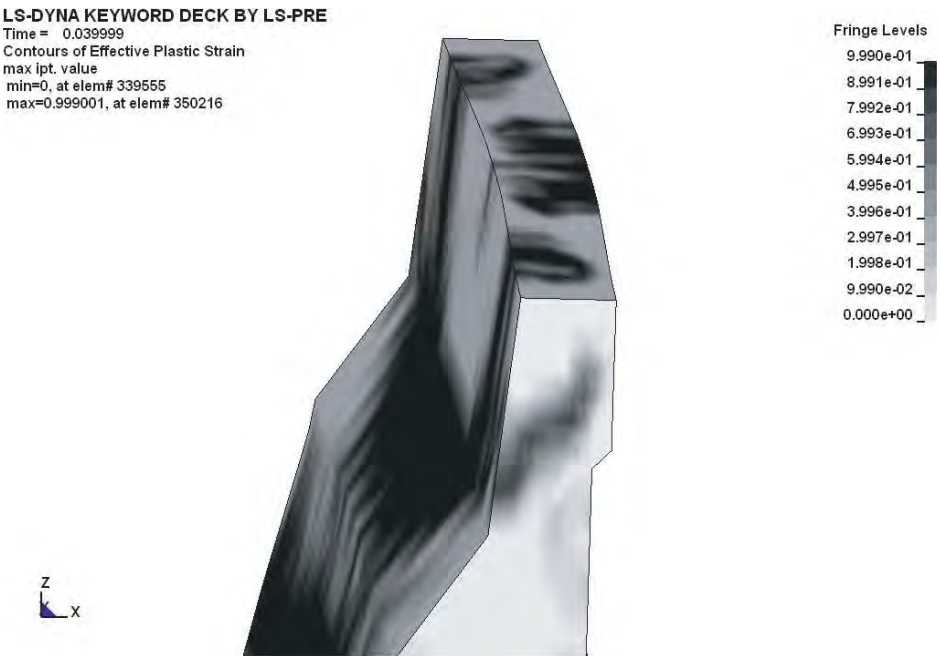

(b)

Figure 5.109. Concrete damage profile on side view of (a) Test 1 and (b) simulation.

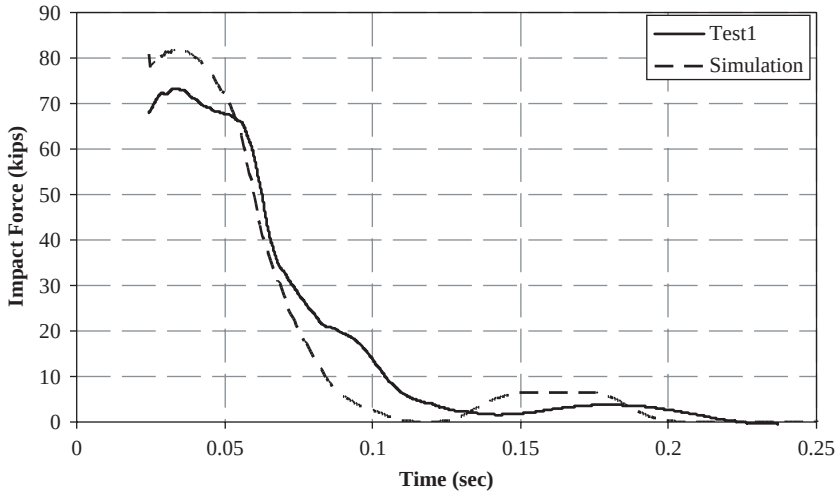

Figure 5.110. Impact load.

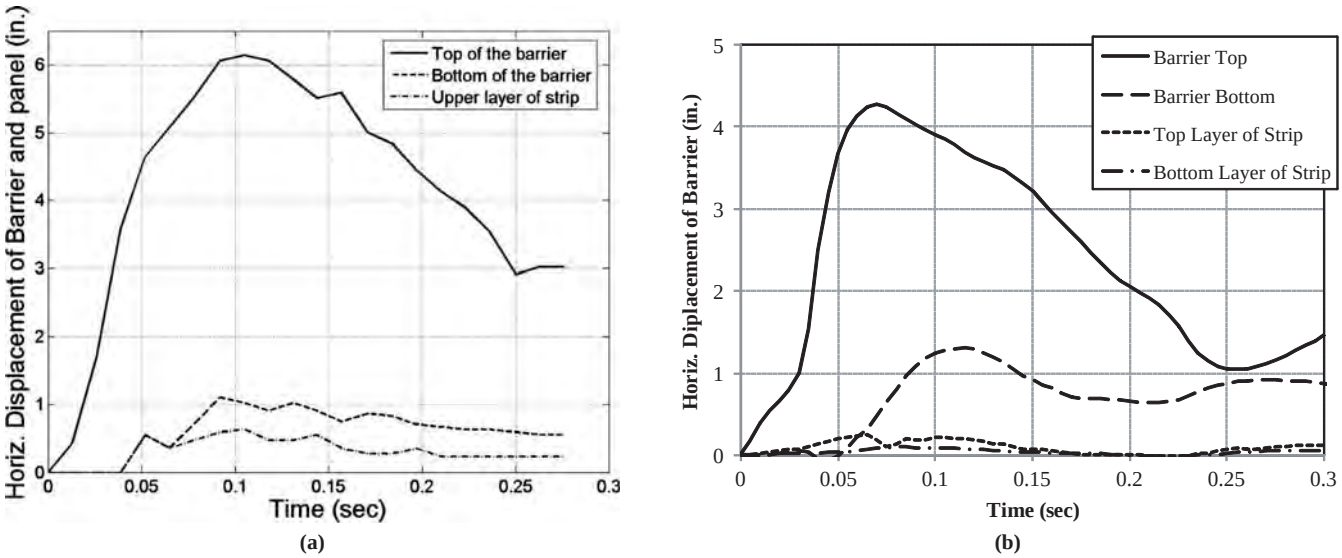

Figure 5.111. Displacement of barrier and panel of (a) Test 1 and (b) simulation.

Table 5.15. Total loads on the wall reinforcement.

Layer	Static Load by AASHTO LRFD (kips)	Dynamic Load Measured (kips)	Total Load Measured (kips)	Total Load by Simulation (kips)
Top	0.83	7.19 (raw) 5.29 (50 msec avg.)	8.02 (raw) 6.12 (50 msec avg.)	8.30 (raw) 5.22 (50 msec avg.)
Second	1.59	–1.20 (raw) –0.88 (50 msec avg.)	–	8.30 (raw) 3.83 (50 msec avg.)

is shown in Figure 5.113. The maximum loads were shown to be 27.58 kN (6.2 kips) at 0.05 sec in Bogie Test 1 and 25.22 kN (5.67 kips) [total load 28.91 kN (6.5 kips)—strip load 3.69 kN (0.83 kips)] at 0.045 sec in the simulation.

The strain on the wall panel was evaluated as shown in Figure 5.114. The maximum compressive strain in the simulation wall panel was 0.0021 at 0.045 sec. The simulation reasonably captured the rate of strain increase and maximum strain in the panel, but did not capture a delay in the response of the panel that occurred during the first 0.05 sec of the tests with 4.88 m (16 ft) long reinforcement strips (Tests 1 and 4).

These bogie impact simulations and tests were used to support the development of design guidelines and predict the performance of the barrier–moment slab system and MSE wall in the full-scale crash test. These efforts are described in the following chapters of the report.

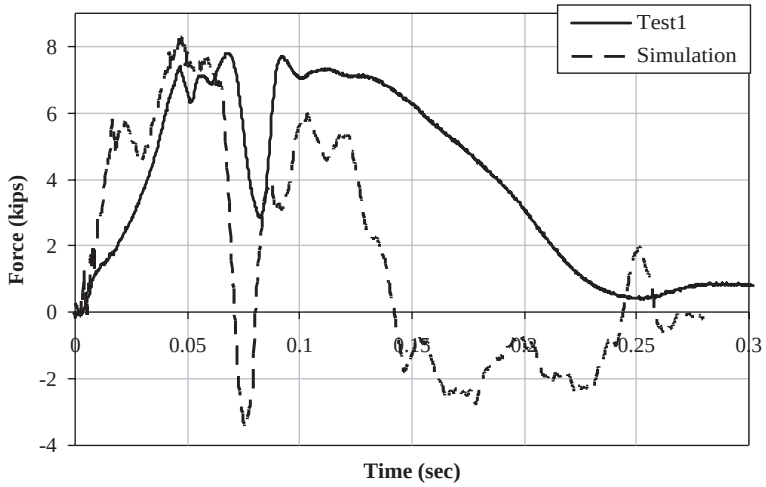

Figure 5.112. Comparison of raw data of load on the strip.

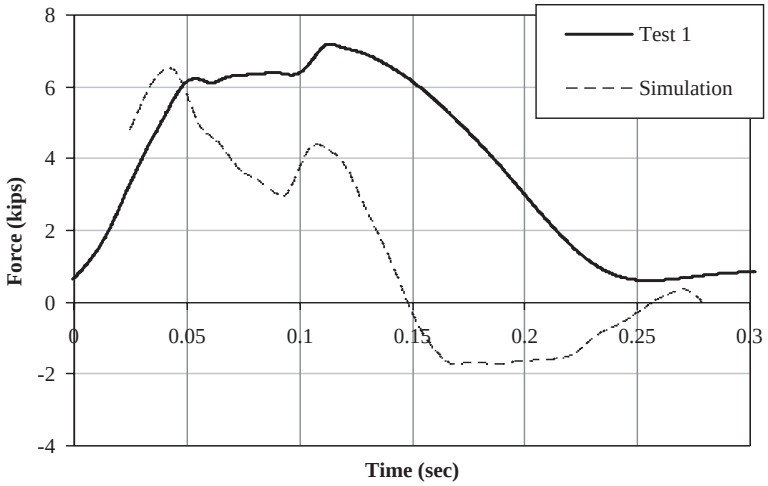

Figure 5.113. Comparison of 50 msec average data of load on the strip.

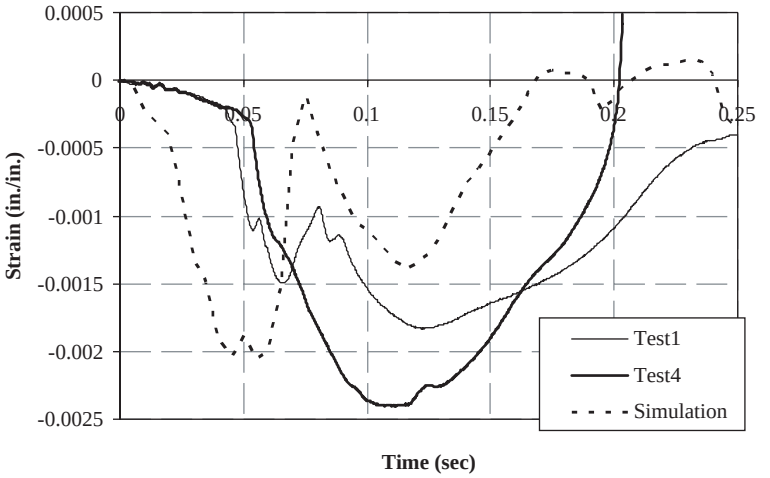

Figure 5.114. Panel strain at D1.

CHAPTER 6

10 ft High MSE Wall and Barrier Study

A full-scale crash test was performed to validate the preliminary design guidelines and/or modify them as necessary. The finite element analysis using LS-DYNA was performed to help plan and predict the outcome of the TL-3 crash test.

6.1 10 ft High MSE Wall and Barrier Study Description

The total length of the installation was about 27.43 m (90 ft). The MSE wall on which the nine 3.05 m (10 ft) long precast barrier–coping sections were placed was approximately 2.74 m (9 ft) tall and comprised full and half-panel sections that were approximately 1.52 m (5 ft) wide. The bottom wall panels were placed on a 304.8 mm (1 ft) wide × 152.4 mm (6 in.) thick concrete leveling pedestal. The MSE wall had three layers of reinforcement. The steel reinforcement strips were 3.05 m (10 ft) long. The wall panels were recessed inside the coping of the precast barrier–coping sections a distance of 19 mm (0.75 in.). The moment slabs connecting the 3.05 m (10 ft) long precast barrier–coping sections were cast in place in three 9.14 m (30 ft) lengths. The three 1.37 m (4.5 ft) wide × 9.14 m (30 ft) long moment slabs were connected to one another using two No. 9 shear dowels across each joint.

The barrier portion of the precast barrier–coping sections consisted of a vertical concrete barrier conforming to the Texas Type T221 traffic barrier. The barrier portion was 0.81 m (2.67 ft) in height (measured from the roadway to the top of the barrier) and 304.8 mm (12 in.) wide at the top.

At the direction of the NCHRP Project 22-20 panel, the draft AASHTO Manual for Assessing Safety Hardware (MASH) was used for the full-scale crash test. MASH test designation 3-11 involves a 2,270 kg (5,000 lb), 0.5-ton, four-door pickup truck (denoted 2270P) impacting the barrier at a speed of 100 km/h (62 mph) and an angle of 25 degrees. At the time the finite element analysis was performed, a model of the 2270P design vehicle was not available. Therefore, the impact simulation was performed with a model of a Chevrolet C2500 pickup that conforms to the design test vehicle of *NCHRP Report 350* (*3*).

6.1.1 Calculation of MSE Wall Capacity

AASHTO LFRD (*2*) was used to estimate the forces expected in the reinforcement strips due to both gravity and impact loads for the planned MSE wall with 3.05 m (10 ft) long strips. This information ultimately was compared to forces estimated through numerical simulation and measured in the TL-3 crash test.

The unfactored pullout resistance of the reinforcement was calculated to be 9.129 kN (2.052 kips) ($F^* = 1.668$) at the uppermost layer, 15.183 kN (3.413 kips) ($F^* = 1.524$) at the second layer, and 19.946 kN (4.484 kips) ($F^* = 1.381$) at the third layer. The unfactored static load per strip due to gravity was calculated to be 3.06 kN (0.688 kips) at the uppermost layer, 5.359 kN (1.205 kips) at the second layer, and 7.467 kN (1.679 kips) at the third layer. In this analysis, the traffic surcharge was not considered. The unfactored dynamic load per strip due to barrier impact was calculated to be 1.762 kN (0.396 kips) at the uppermost layer, 1.151 kN (0.259 kips) at the second layer, and 0.541 kN (0.122 kips) at the third layer. Therefore, the unfactored total load per strip was calculated to be 4.822 kN (1.084 kips) at the uppermost layer, 6.51 kN (1.464 kips) at the second layer, and 8.01 kN (1.8 kips) at the third layer. A summary of resistance and load per strip is presented in Table 6.1. The detailed design calculations for designing the MSE test wall are provided in Appendix A.

6.1.2 Calculation of Barrier Capacity

The ultimate load capacity for the 0.81 m (32 in.) tall vertical barrier was computed to be 440.95 kN (99.13 kips) using the yield line failure mechanism in AASHTO LRFD. The length of the failure mechanism calculated for the barrier section analyzed was 1.75 m (5.73 ft) for the 0.81 m (32 in.) tall verti-

Table 6.1. Unfactored resistance and force in case of MSE wall with 10 ft long strip.

Layer	(1) T_{Static} Static Load (kips)	(2) $T_{Dynamic}$ Dynamic Load (kips)	(3)=(1)+(2) T_{Total} Total Load (kips)	P Resistance of Pullout (kips)
Top	0.688	0.396	1.084	2.052 (F*=1.668)
Second	1.205	0.259	1.464	3.413 (F* = 1.524)
Third	1.679	0.122	1.800	4.484 (F* = 1.381)

cal wall barrier. This indicates that, provided the coping has sufficient capacity to develop the ultimate strength of the barrier, the 3.05 m (10 ft) section length selected for evaluation in the TL-3 crash test should be sufficient for developing the primary failure mechanism for the barrier.

6.2 Finite Element Analysis

The MSE wall model used in the bogie impact simulation was modified to model the proposed full-scale test installation. The modifications to the model included:

- Extending the model length from 9.14 m (30 ft) to 18.28 m (60 ft) by incorporating two moment slab components each of which was 9.14 m (30 ft) long
- Incorporating two 22.6 mm (⅞ in.) diameter, 0.91 m (36 in.) long dowel connectors between the moment slabs
- Modeling the 0.81 m (32 in.) high vertical barrier with explicit reinforcement details as shown in Figure 6.1
- Raising the wall height to reflect an MSE wall configuration composed of two rows of 1.52 m (5 ft) tall panels using a total of four layers of reinforcement
- Incorporating 3.05 m (10 ft) long soil reinforcement strips
- Using a density of three strips per panel for the top layer of reinforcement and a density of two strips per panel for the other layer of reinforcement
- Incorporating the model of the Chevrolet C2500 pickup truck (reflective of the 2000P test vehicle in *NCHRP Report 350*).

Figures 6.2 and 6.3 show the model setup of the 3.49 m (11.46 ft) high MSE wall with the Chevrolet C2500 vehicle model. The vehicle model was given an initial velocity of 100 km/h (62 mph) and hit the barrier at an angle of 25 degrees per Test Level 3-11 impact conditions. To enable comparison of forces and displacements, barriers and selected strip locations were assigned an alphanumeric designator that describes their horizontal position and vertical reinforcement layer. For example, strip B3-A-1st is positioned beneath the third barrier at vertical position A in the first (i.e., upper) layer of reinforcement. Figure 6.4 shows the rebar details of vertical concrete barrier and moment slab, which was modeled based on the drawings provided by RECO. Figure 6.5 shows the relative position of the vehicle with respect to the middle barrier joint. This barrier joint is aligned with the joint between the two moment slab sections that were modeled.

The first phase of the simulation process was to account for the steady-state conditions of the system due to the gravitational

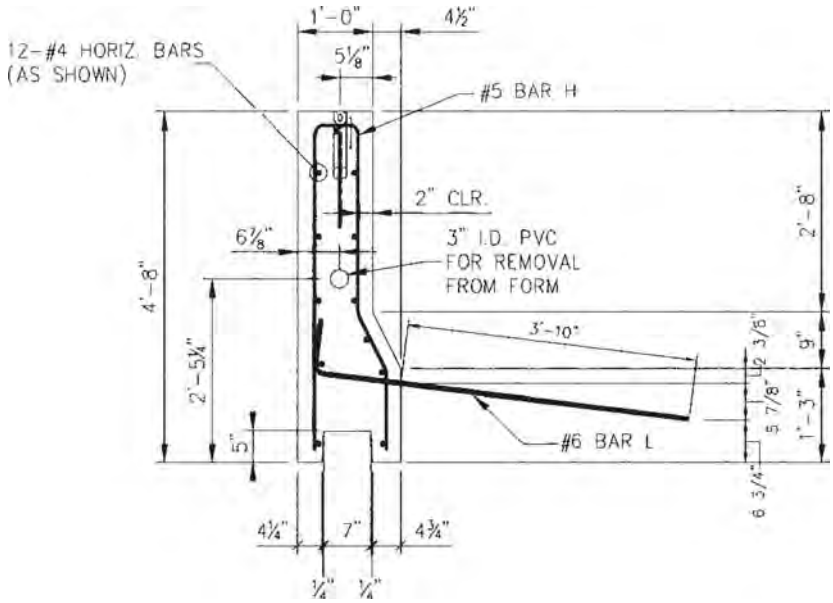

Figure 6.1. RECO vertical concrete barrier detail.

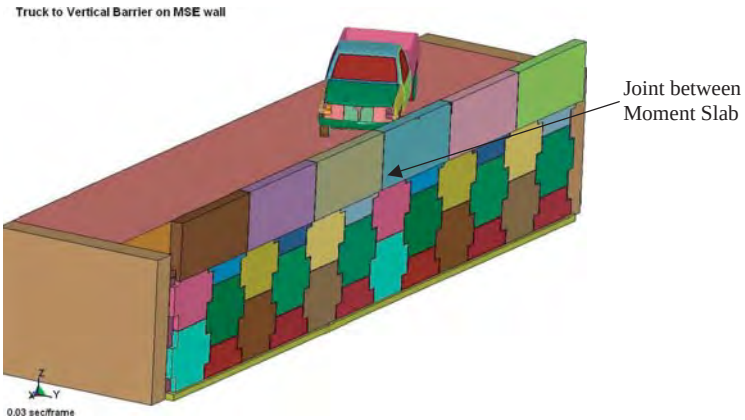

(a) Three-dimensional view

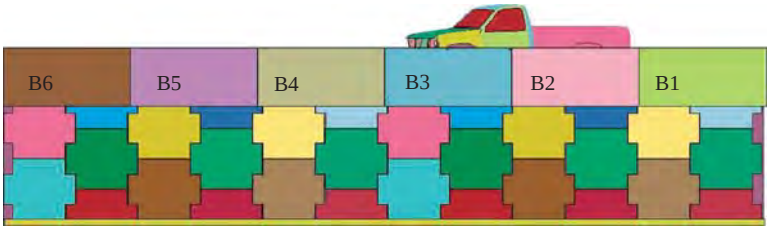

(b) Elevation view

Figure 6.2. MSE wall, barrier, and C2500 model.

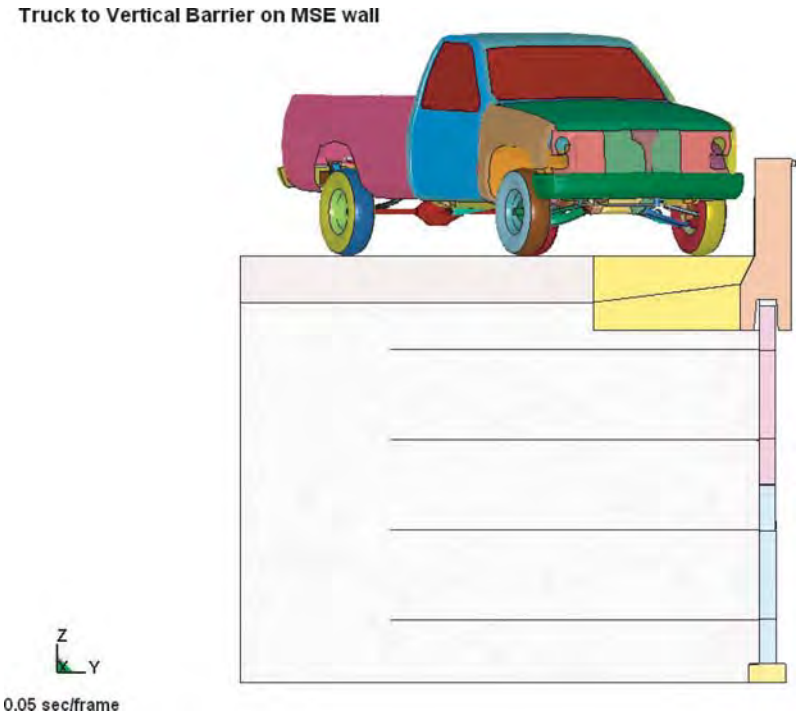

Figure 6.3. Downstream view of model showing profile of barrier and embedded soil strips.

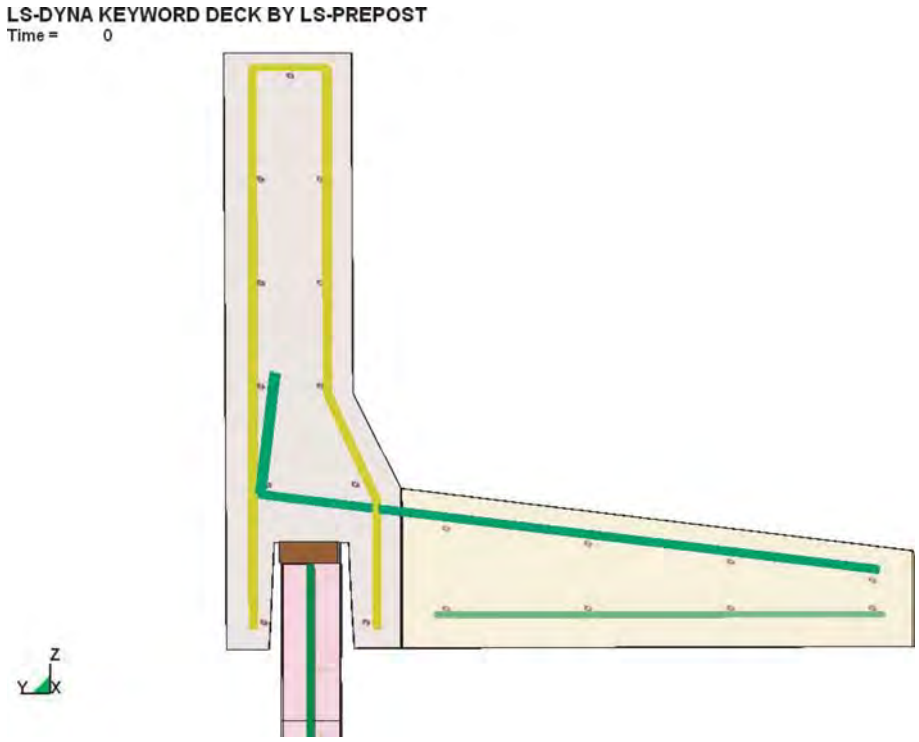

Figure 6.4. Rebar detail in the barriers and panels of model.

load. The weight of the system was measured and used as a convergence criterion for the steady-state solution. The total mass of the model for the vertical wall barrier on top of the MSE wall with 3.05 m (10 ft) long strips is 664,630 kg (45,542 slug or 1,465,258 lb mass). The weight of the system is calculated to be 6,517 kN (1,465 kips) using the mass of the finite element model and the acceleration of gravity. Therefore, after accounting for gravitational load, the weight of the model system should converge to the calculated system weight. The weight of the finite element model was 6,531 kN (1,468 kips) at the end of the initialization step. A reasonable agreement shows that the weight of the finite element model approached the calculated weight of the model system as shown in Figure 6.6.

The initialized model was then set up with the C2500 vehicle model, and the impact simulation was conducted. The vehicle was successfully contained and redirected by the barrier. Figure 6.7 shows sequential images of the impact that correspond to the following events:

0.06 sec:	Maximum force on the barrier
0.1 sec:	Maximum load in the strips
0.195 sec:	Back slap impacts the barrier
0.345 sec:	Back bumper impacts the barrier
0.5 sec:	Vehicle exits the barrier

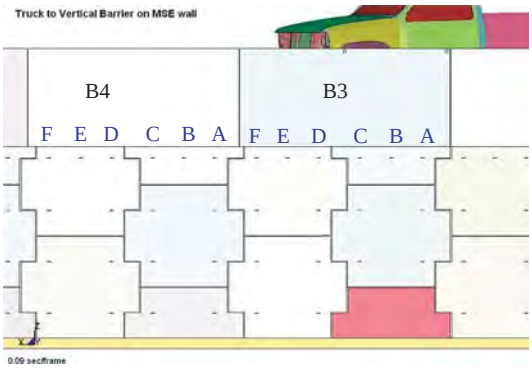

Figure 6.5. Side view of the model showing the distribution of the strips.

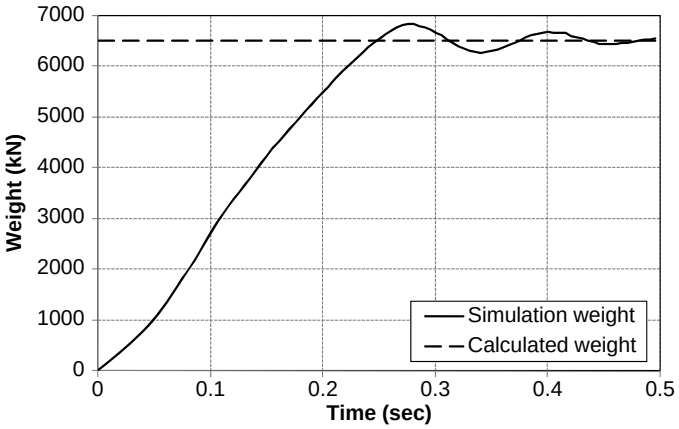

Figure 6.6. System reaction force of the MSE wall model.

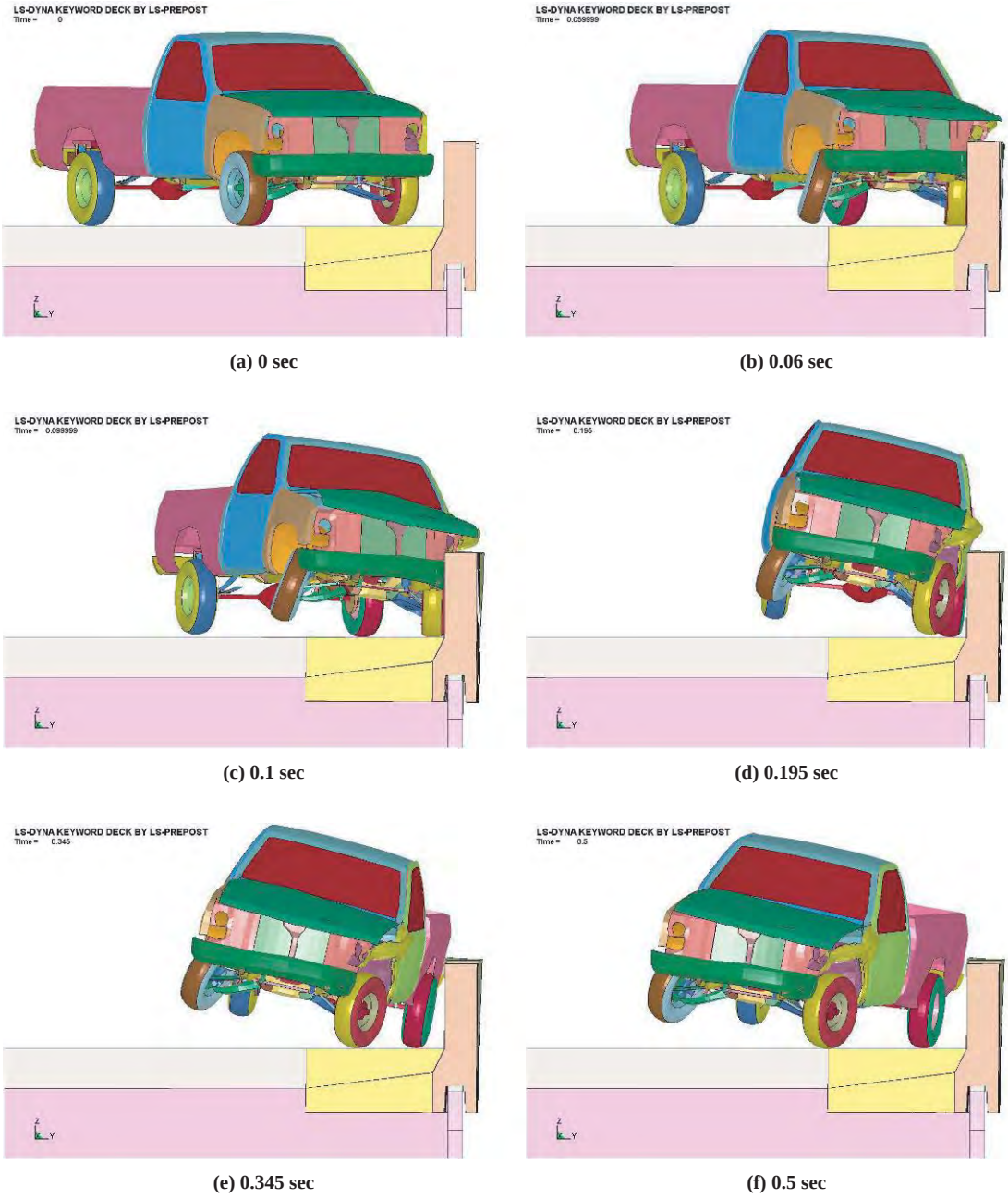

(a) 0 sec **(b) 0.06 sec**

(c) 0.1 sec **(d) 0.195 sec**

(e) 0.345 sec **(f) 0.5 sec**

Figure 6.7. Vehicle position at each significant moment.

6.2.1 Barrier Damage and Displacement

The calculated impact force on the barrier was 248.21 kN (55.8 kips) at 0.0575 sec as shown in Figure 6.8. At 0.198 sec, the second peak impact force occurred due to the back slap impact.

The damage to the concrete barrier is shown in Figures 6.9 and 6.10. The concrete barrier exhibited a damage profile typically observed in impacts on barrier joints. The damage profiles shown in Figures 6.9 and 6.10 are limited to the surface elements and did not indicate failure of the barrier.

The maximum displacement at the top of the barrier occurred in barrier section B4. The displacement–time history for this barrier section is shown in Figure 6.11. The initial impact induced a displacement of 41.4 mm (1.63 in.) at the top of the barrier. The barrier was rebounding back when the back slap impact occurred, which resulted in a maximum displacement of 48.5 mm (1.91 in.). As the barrier was rebounding from the back slap, the rear bumper of the pickup contacted the barrier and the barrier displacement momentarily increased to 37.3mm (1.47 in.).

Figure 6.12 shows the displacement distribution on barrier segments B3 and B4 at 0.1 sec.

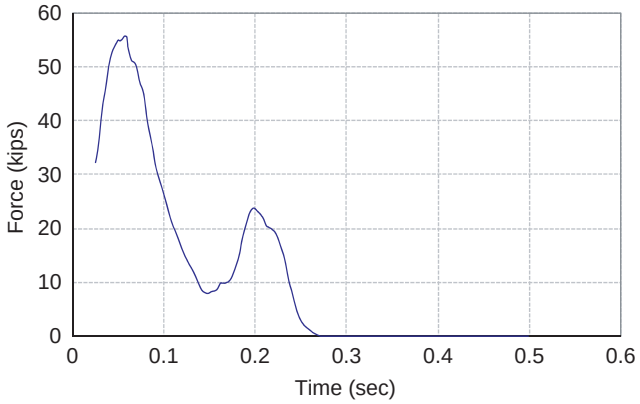

Figure 6.8. Time history of impact force on barrier (50 msec average).

6.2.2 Loads and Displacements in Reinforcement Strips

The load–time histories for selected strips in the upper layer of reinforcement are presented in Figure 6.13(a). The 50 msec moving average is shown in Figure 6.13(b). Figures 6.14 through 6.16 show 50 msec average load–time histories for strips in the second through fourth layers of reinforcement, respectively. The maximum 50 msec average load in the strips is 18.7 kN (4.2 kips) in strip B4-A-1st [Figure 6.13(b)]. The strip loads in each layer show similar load histories, therefore, one strip was chosen to represent the load at each layer in Figure 6.17.

Maximum displacement of the strips was 2.8 mm (0.11 in.) at 0.085 sec at strip B4-A-1st as shown in Figure 6.18. Because the strips and panels were tied together, the maximum displacement of the panel also corresponds to this value. Figure 6.19 shows the displacement distribution of the strips at 0.085 sec.

6.2.3 Panel Analysis

The strain on the wall panel was evaluated as shown in Figure 6.20. The maximum compressive strain was 18 micro strains at 0.065 sec. The distribution of bending moment along the panel at the time of peak force during the impact is shown in Figure 6.21.

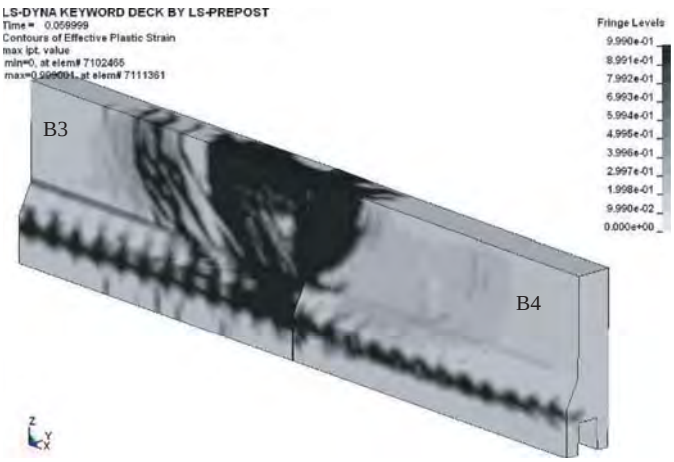

(a) 0.06 sec. (at Max. Impact Load)

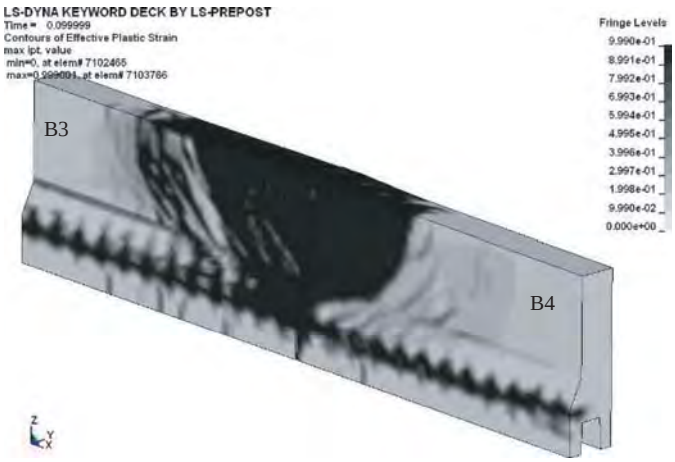

(b) 0.1 sec (at Max. Strip Load)

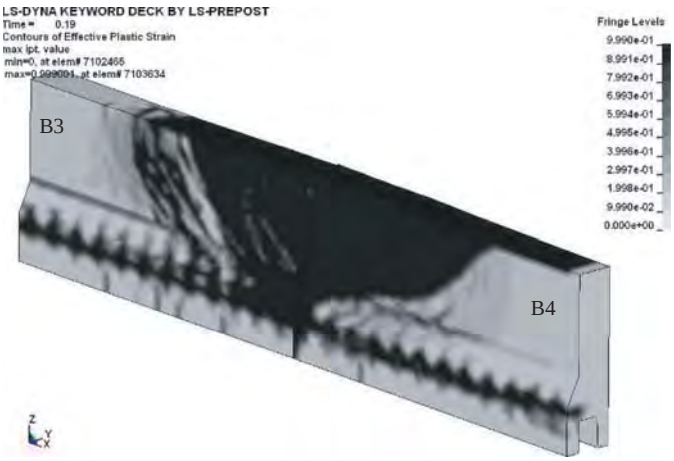

(c) 0.19 sec. (at Rear Tire Hit)

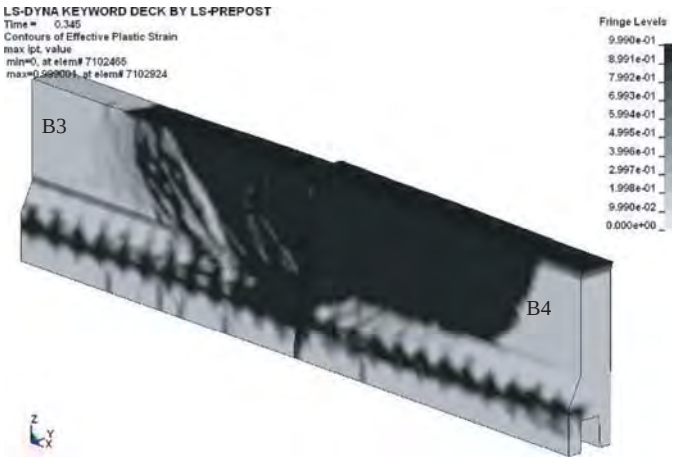

(d) 0.345 sec. (at Back Bumper Hit)

Figure 6.9. Damage to the concrete barrier at the front of the joint.

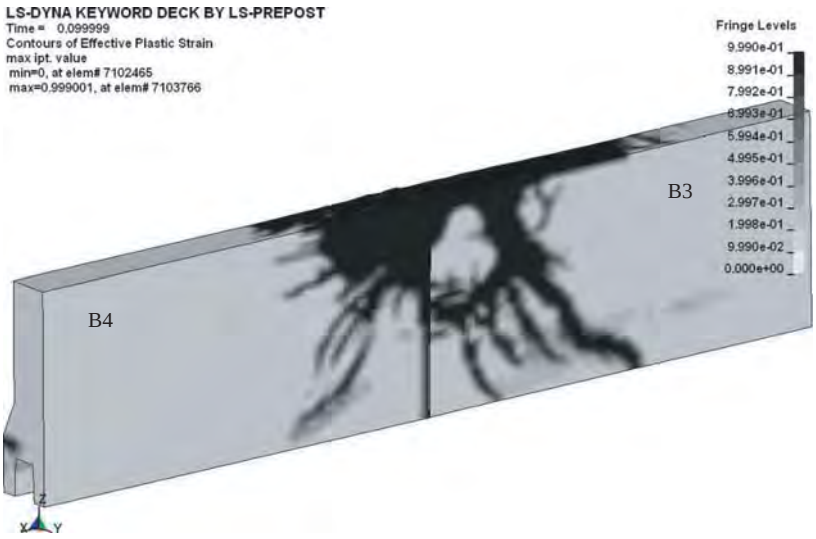

Figure 6.10. Damage to the back of the concrete barrier (0.1 sec).

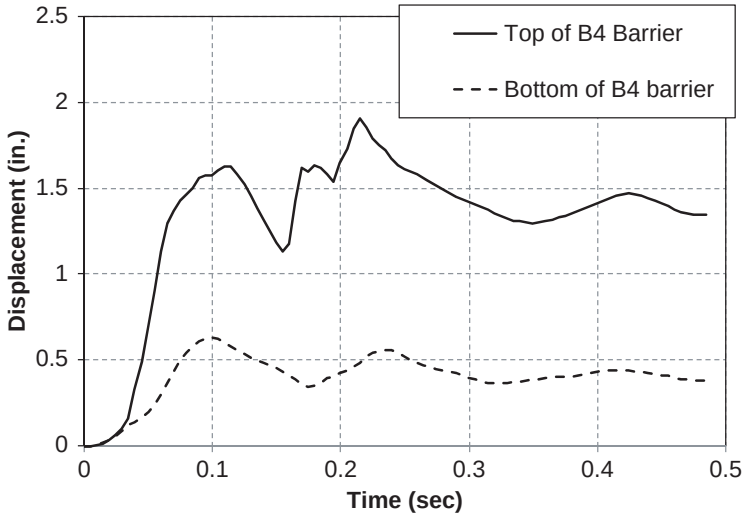

Figure 6.11. Barrier displacement–time history (Barrier B4).

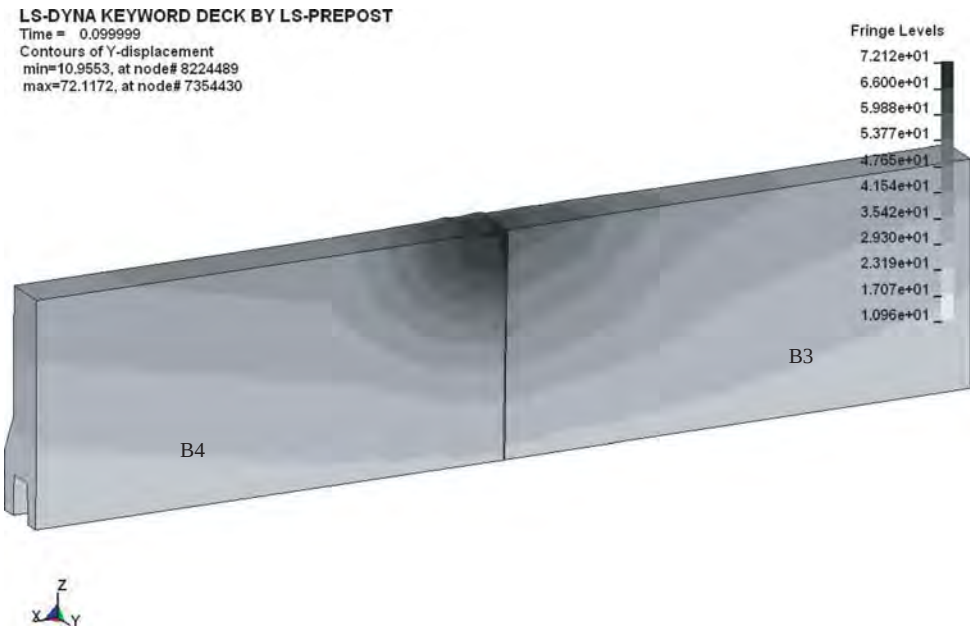

Figure 6.12. Distribution of barrier displacement (Barrier B3 and B4).

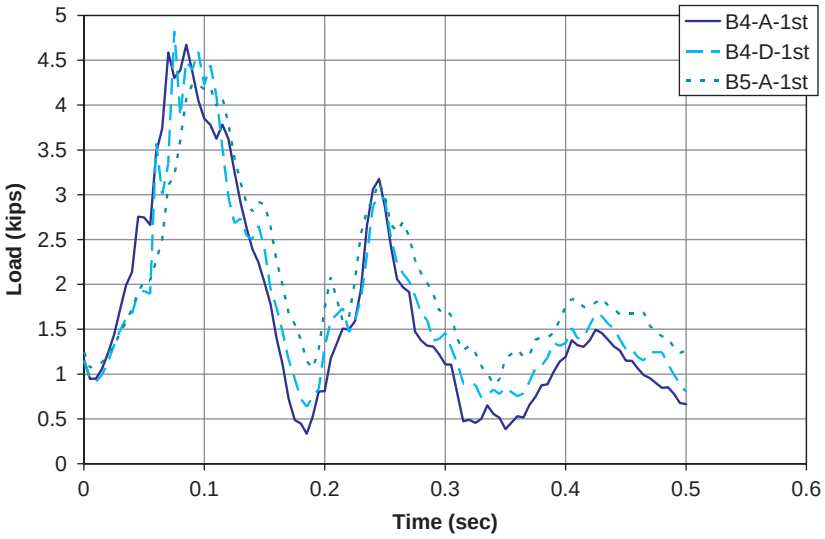

(a) Raw data

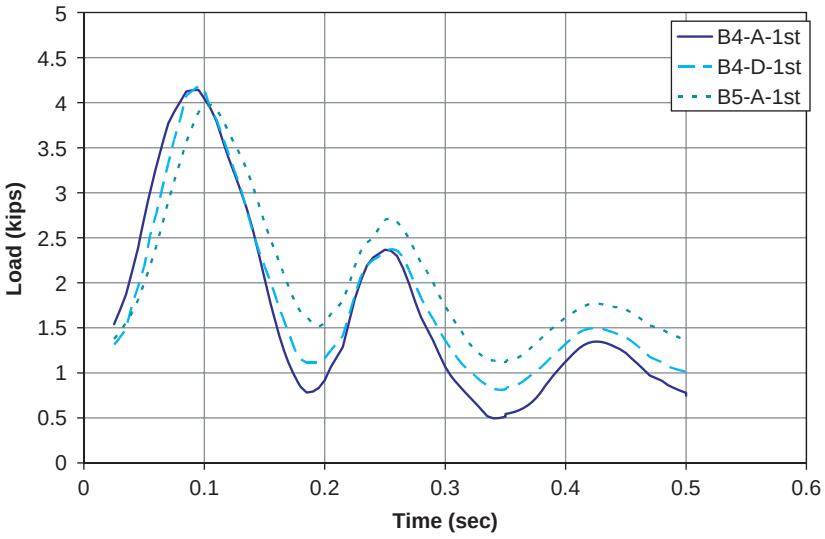

(b) 50 msec average

Figure 6.13. Total load on the strip at uppermost layer.

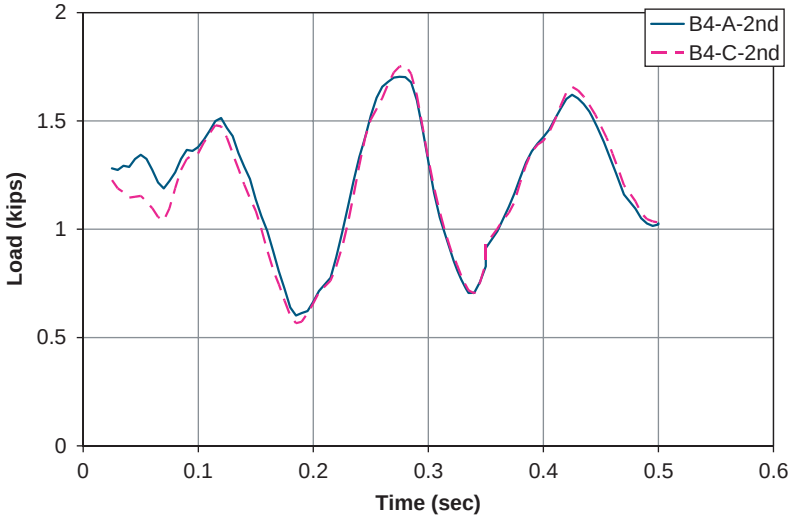

Figure 6.14. Total load on the strip at second layer.

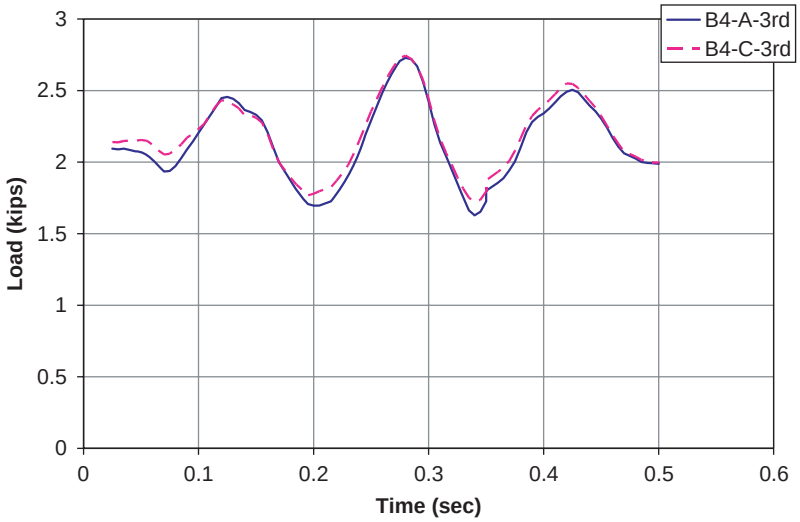

Figure 6.15. Total load on the strip at third layer.

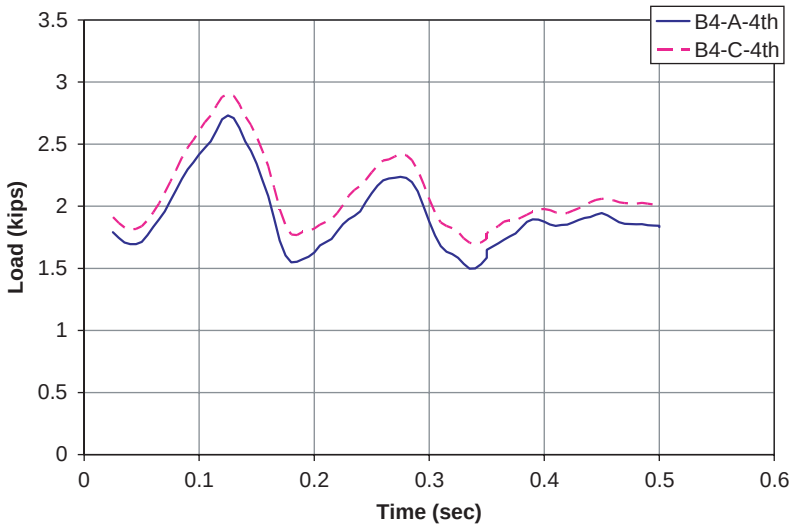

Figure 6.16. Total load on the strips at fourth layer.

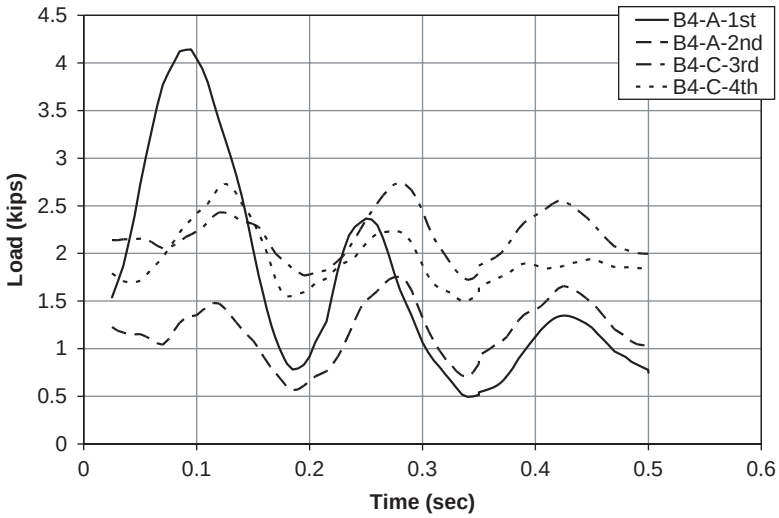

Figure 6.17. Load on the strips for all layers.

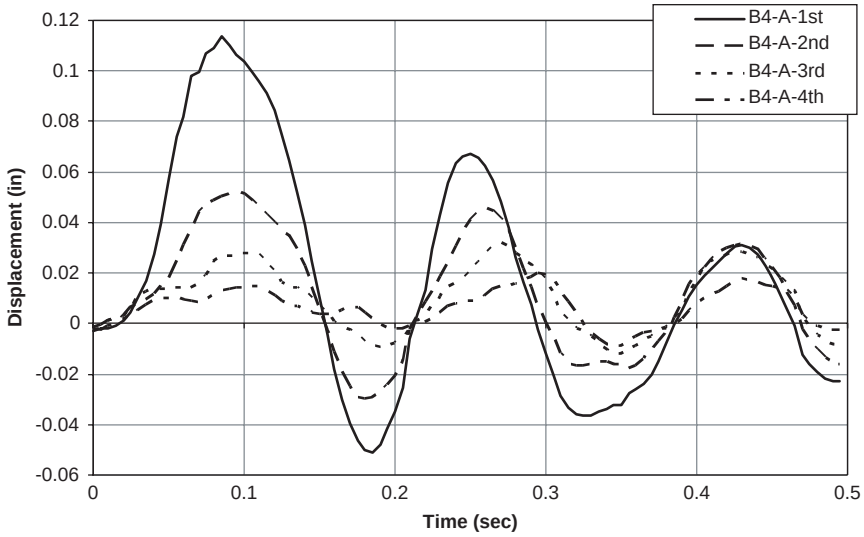

Figure 6.18. Displacement in the strips at B4-A.

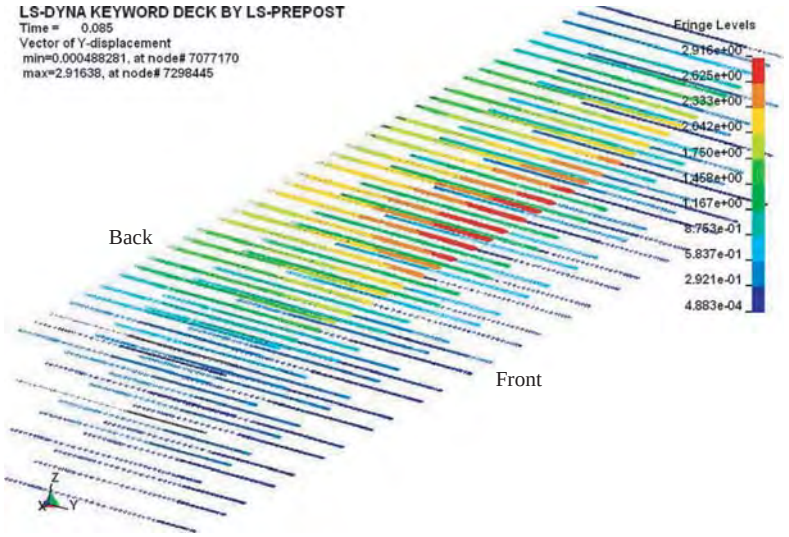

Figure 6.19. Distribution of displacement in the strips at 0.085 sec (unit: mm).

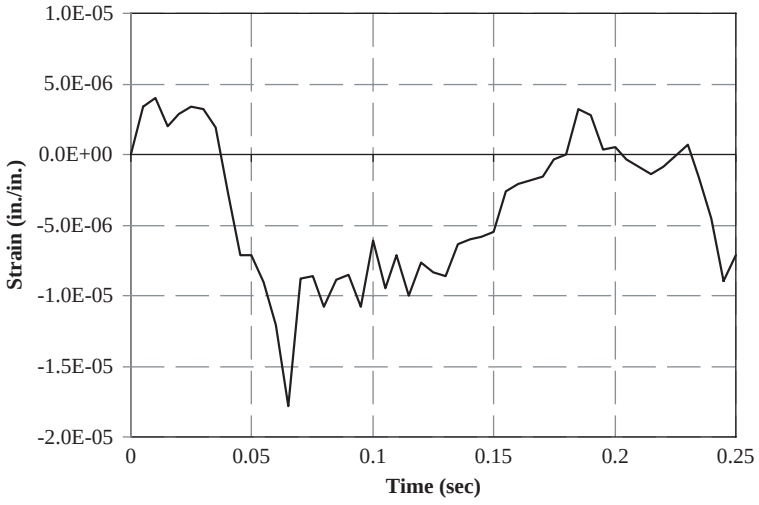

Figure 6.20. Panel strain at D1.

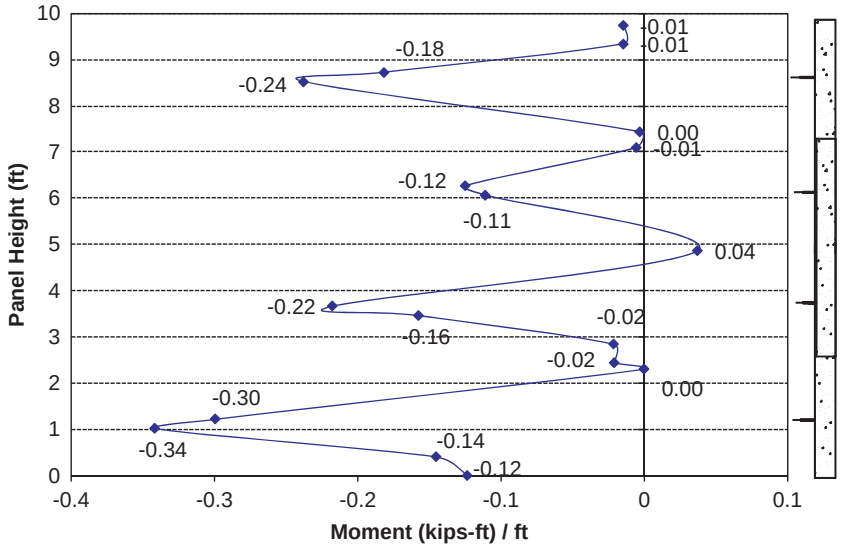

Figure 6.21. Bending moment on the panel (B4-A).

6.3 TL-3 Crash Test

6.3.1 10 ft High MSE Wall Construction and Test Installation

An overall layout of the 3.05 m (10 ft) high MSE wall test installation is shown in Figure 6.22. The instrumented MSE wall was about 27.43 m (90 ft) long and approximately 2.74 m (9 ft) tall and comprised full and half-panel sections that were approximately 1.52 m (5 ft) wide. The bottom wall panels were placed on a 304.8 mm (1 ft) wide × 152.4 mm (6 in.) thick concrete leveling pedestal. The MSE wall had three layers of reinforcement. The uppermost layer was at a depth of 0.91 m (3 ft) below the ground surface. The vertical spacing of the successive reinforcement layers was approximately 0.76 m (2.5 ft). The steel reinforcement strips were 3.05 m (10 ft) long. The reinforcement had a density of three strips per layer per panel. The wall panels were recessed inside the coping of the precast barrier–coping sections. The barrier–coping sections rested on a 66.7 mm (2.625 in.) layer of a level-up concrete placed on top of the wall panels. The moment slabs connecting the

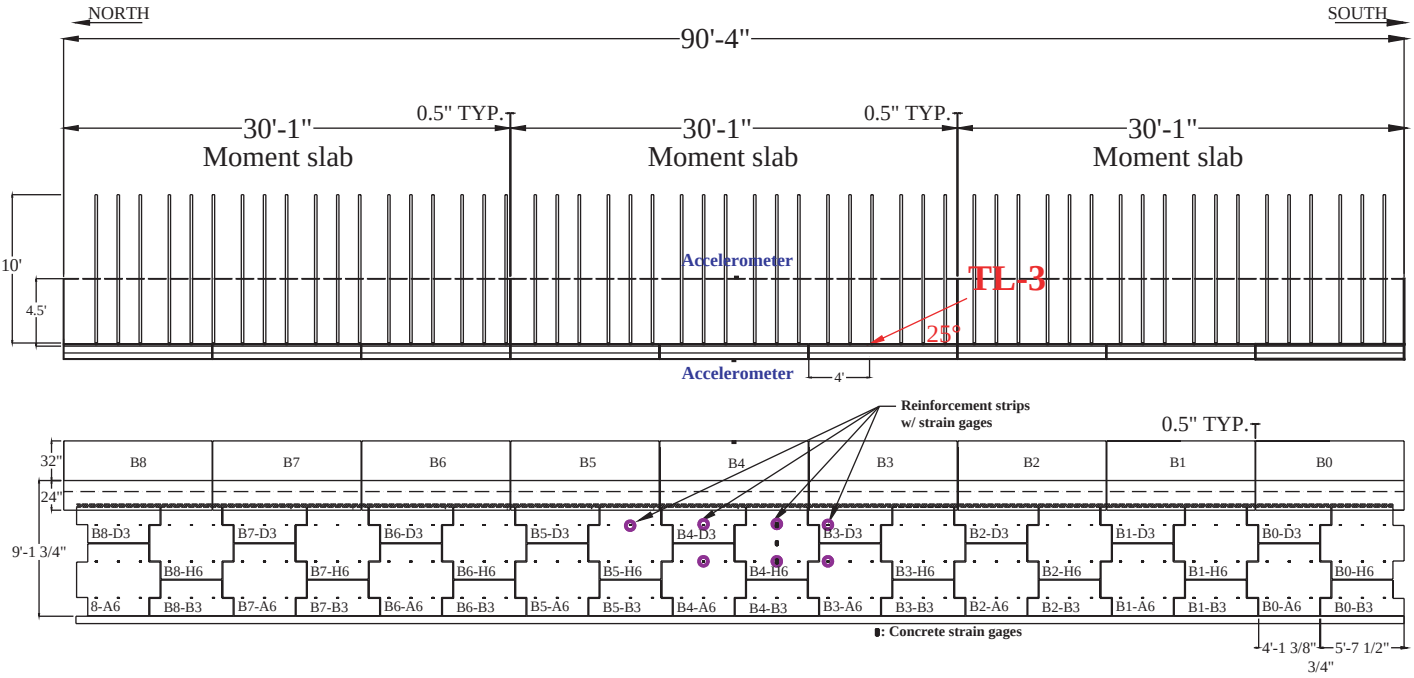

Figure 6.22. Layout of the barrier on MSE wall.

3.05 m (10 ft) long precast barrier–coping sections were cast in place in three 9.14 m (30 ft) lengths. The three 1.37 m (4.5 ft) wide × 9.14 m (30 ft) long moment slabs were connected to one another using two No. 9 shear dowels across each joint.

The barrier portion of the precast barrier–coping sections consisted of a vertical concrete barrier that conforms to the Texas Type T221 traffic rail. The barrier portion was 0.81 m (2.67 ft) in height (measured from the roadway to the top of barrier) and 304.8 mm (12 in.) wide at the top. The coping was 0.61 m (2 ft) in height (measured from the bottom of the coping to the roadway). Longitudinal reinforcement in the barrier–coping section consisted of ten No. 4 bars. Transverse reinforcement consisted of alternating No. 5 bars spaced 254 mm (10 in.) apart. The barrier–coping sections are attached to the moment slab using No. 6 bars spaced at 254 mm (10 in.) Figure 6.23 shows a cross section of the barrier–coping section and MSE wall. Figure 6.24 shows photos of the instrumented MSE wall before the TL-3 crash test. The barriers and panels were assigned alphanumeric designators as described earlier. The precast barrier–coping sections, concrete wall panels, and steel strip wall reinforcement were provided by RECO at no cost to the project.

The MSE wall backfill was made of two layers: a poorly graded clean sand from the bottom of the wall to the bottom of the moment slab [2.18 m (7.15 ft)] and a limestone rock fill usually used as road base from the bottom of the moment slab to the riding surface [0.61 m (2 ft)]. The sand backfill and the road base satisfied the gradation limits of TxDOT Type B (Table 6.2) and Type A backfill material respectively. For the sand, the particle diameters corresponding to 10% fines (D_{10}) and 60% fines (D_{60}) were 0.25 mm and 1.1 mm, respectively, and the percent passing a #200 sieve was 0% as shown in Figure 6.25. For the road base, the particle diameters corresponding to 10% fines (D_{10}) and 60% fines (D_{60}) were 0.18 mm and 14 mm, respectively, and the percent passing a #200 sieve was 7%. Both the sand and the road base layers were compacted in 0.15 m (6 in.) layers with 10 passes of a 12.9 kN (2,905 lb), 0.89 m (35 in.) wide drum roller. The in situ dry density and the water content as compacted were 17.3 kN/m^3 and 6% for the sand and 23.1 kN/m^3 and 3.9% for the road base. These dry densities represented 93% and 105% of the maximum dry densities obtained in the modified Proctor test for the sand and the road base, respectively. The friction angle of the sand was measured in the direct shear test by recompacting the sand at its in situ dry density; a value of 40 degrees was obtained together with an apparent cohesion of 9 kPa (1.31 psi). The friction angle of the road base was measured in a large triaxial cell by recompacting the road base to its in situ dry density; a value of 45 degrees was obtained with a cohesion intercept of 80 kPa (11.6 psi). The modulus of the sand and the road base were measured with the Briaud Compaction Device (*31*); the values obtained were 15.1 MPa and 67.2 MPa respectively. The friction factor (F*) used in the calculation of the strip resistance to pullout in the sand was calculated to be 1.84 at the ground level according to AASHTO LRFD. The particle diameters corresponding to 10% fines (D_{10}) and 60% fines (D_{60}) were 0.25 mm and 1.1 mm, respectively. The coefficient of uniformity [Cu (= D_{60} / D_{10})] was determined to be 4.4. The friction factor (F*) was calculated to be 1.84 at the ground level.

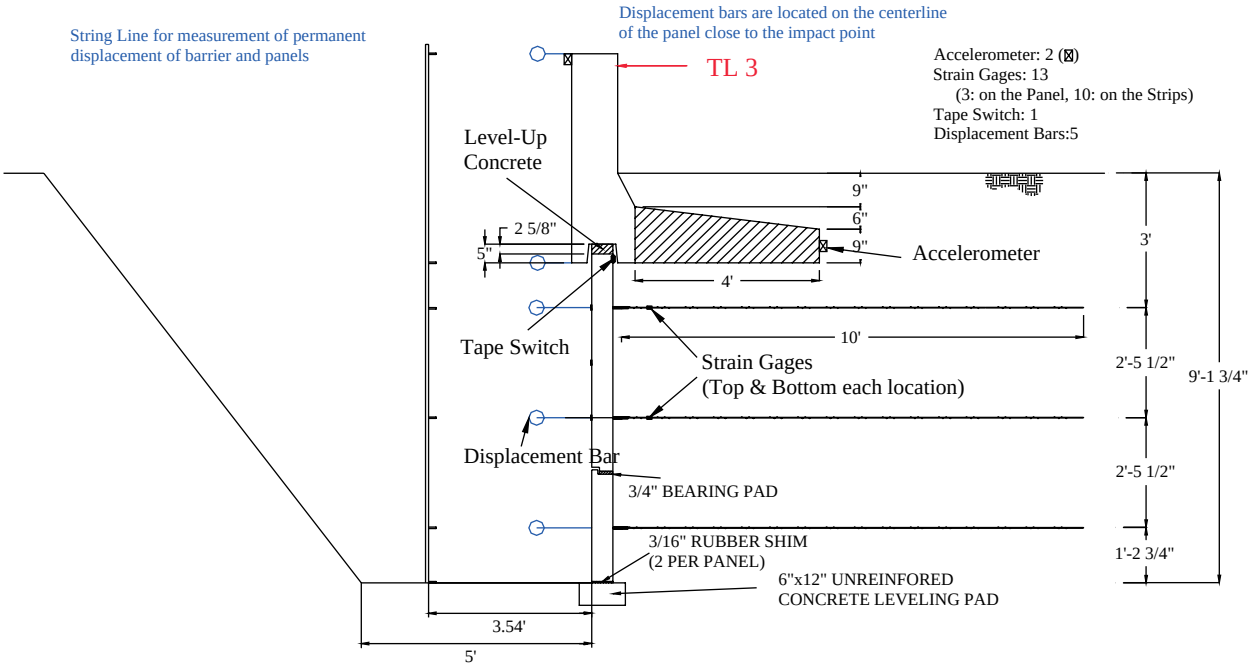

Figure 6.23. Side view of TL-3 crash test with 32 in. tall vertical wall barrier.

Figure 6.24. Barrier on MSE wall prior to testing.

Selected reinforcement strips in the MSE wall were instrumented with strain gages to capture the tensile forces transmitted into the reinforcement during the full-scale crash test. A total of 14 strain gages were used. The four strips in the upper layer and the three strips in the middle layer of reinforcement on the wall panel immediately downstream from the impact location were instrumented. The simulation results indicate that these strips develop the maximum tensile loads during impact. Two strain gages were used at each selected location (one on the top of the strip and one on the bottom of the strip) to compensate for any bending in the strip.

A contact switch was placed on the top edge of the traffic face (inside face) of the wall panels inside the coping recess. The switch indicates the time (referenced from impact) at which the barrier slides and/or rotates sufficiently for the coping to contact the wall panel.

The wall panel attached to the instrumented strips was instrumented with three concrete strain gages to capture normal strains in the panel induced from impact loads transmitted into the MSE wall through the soil and generated from direct contact of the barrier–coping section with the top of the wall panel. The strain gages were placed in a vertical position along the height of the panel. A strain gage was placed adjacent to the anchorage locations for the upper and lower layer

Table 6.2. Gradation limits for TxDOT Type B select backfill.

Sieve Size	Percentage Retained
3 in.	0
No. 4	See Note
No. 40	40–100
No. 200	85–100

Note: If 85% or more material is retained on the No. 4 sieve, the backfill will be considered rock backfill.
Source: *Standard Specifications for Construction and Maintenance of Highways, Streets, and Bridges* (*30*)

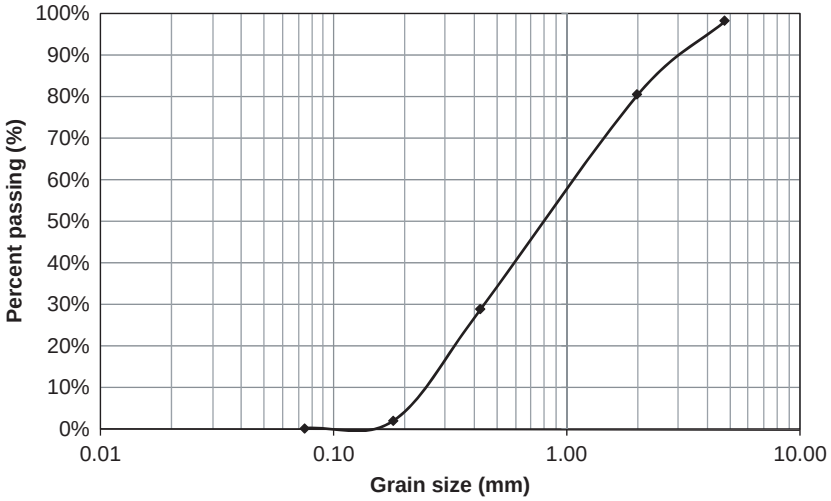

Figure 6.25. Particle size distribution curve of the backfill for TL-3 crash test.

of reinforcement, and one strain gage was placed in the center of the panel between the two layers of reinforcement.

An accelerometer was mounted behind and at the top of the barrier section immediately downstream of impact (which was shown in the simulation to experience the maximum load and displacement). An accelerometer also was placed on the end of the 9.14 m (30 ft) long moment slab to which this barrier section was attached at its midpoint to measure any acceleration or motion imparted to the moment slab during impact.

Displacement and/or rotation of the barrier and wall panels were determined from high-speed film operating at 1,000 frames/second. Displacement gages were placed at the top and bottom of the precast barrier–coping section and on the wall panels at heights corresponding to the three layers of soil reinforcement. The location of the strain gages and other instrumentation are shown in side view in Figure 6.22. The location of the strain gages on the steel reinforcement strips is shown in plan view in Figure 6.23. Detailed drawings of the test installation and photographs of the construction procedure are presented in Appendix E and F, respectively, which are available from the *NCHRP Report 663* summary web page on the TRB website (www.trb.org) by searching for "NCHRP Report 663".

6.3.2 Impact Conditions

The MASH (*10*) test guidelines were applied for the TL-3 crash test. MASH test designation 3-11 (*10*) involves a 2270P vehicle weighing 2,270 kg ± 50 kg (5,000 lb ± 100 lb) and hitting the bridge rail at an impact speed of 100 km/h ± 4 km/h (62.2 mph ± 2 mph) and an angle of 25 degrees ± 1.5 degrees. The target impact point was 1.2 m (4 ft) upstream of the fourth barrier joint. The 2004 Dodge Ram 1500 quad-cab pickup truck used in the test weighed 2,246 kg (4,951 lb), and the actual impact speed and angle were 101.7 km/h (63.2 mph) and 25.6 degrees, respectively. The actual impact point was 1.3 m (4.3 ft) upstream of the fourth barrier joint.

6.3.3 Test Vehicle

A 2004 Dodge Ram 1500 quad-cab pickup truck, shown in Figures 6.26 and 6.27, was used for the crash test. Test inertia weight of the vehicle was 2,246 kg (4,951 lb). The height to the lower edge of the vehicle front bumper was 349 mm (13.75 in.), and the height to the upper edge of the front bumper was 660 mm (26.0 in.). The vehicle was directed into the installation using the cable reverse tow and guidance system and was released to be free-wheeling and unrestrained just prior to impact. Detailed test vehicle properties and information are presented in Appendix G, which is available from the *NCHRP Report 663* summary web page on the TRB website (www.trb.org) by searching for "NCHRP Report 663".

6.3.4 Test Description

The 2270P vehicle, traveling at an impact speed of 101.7 km/h (63.2 mph), hit the MSE wall 1.31 m (4.3 ft) upstream of the fourth barrier joint at an impact angle of 25.6 degrees. At approximately 0.027 sec after impact, the vehicle began to redirect, and at 0.092 sec, the right front tire began to ride up the barrier face. The right rear tire lost contact with the ground surface at 0.129 sec, and the right rear of the vehicle began to rise at 0.147 sec. At 0.166 sec, the vehicle was traveling parallel with the barrier at a speed of 92.4 km/h (57.4 mph). The rear of the vehicle contacted the barrier at 0.186 sec, and the vehicle began to roll counterclockwise at 0.237 sec. At 0.338 sec, the vehicle lost contact with the barrier and was traveling at an exit speed and angle of 88.8 km/h (54.9 mph) and 7.9 degrees, respectively. As the vehicle continued forward, the vehicle

Figure 6.26. Vehicle/installation geometrics.

Figure 6.27. Vehicle before test.

yawed clockwise and came to rest 53.34 m (175 ft) downstream of impact and 1.83 m (6 ft) forward of the traffic face of the barrier. Sequential photographs of the test period are shown in Appendix H, which is available from the *NCHRP Report 663* summary web page on the TRB website (www.trb.org) by searching for "NCHRP Report 663".

6.3.5 Test Article and Vehicle Damage

Damage to the barrier was mostly cosmetic, as shown in Figures 6.28 and 6.29. In the soil forward of the face of the barrier, there were two cracks. The first was a 4 mm (0.16 in.) crack 1,321 mm (52 in.) forward of the traffic face of the barrier that started at the joint between barrier B2 and B3 and ended at the joint between barrier B5 and B6. The second was a 2 mm (0.08 in.) crack 1,372 to 1,727 mm (54 to 68 in.) forward of the traffic face of the barrier, starting 6 m (2 ft) upstream of the joint between barrier B0 and B1 and ending 0.6 m (2 ft) downstream of the joint between barrier B2 and B3. Length of contact of the vehicle with the barrier was 4.1 m (13.6 ft). No measurable deflection of the barrier occurred.

The 2270P vehicle sustained damage to the front left and left side, as shown in Figure 6.30. The left upper A-arm, left outer tie rod end, left frame rail, and rear axle were deformed and the left upper ball joint broke. Also damaged were the

Figure 6.29. Installation after test.

Figure 6.28. Vehicle trajectory path after test.

Figure 6.30. Vehicle after test.

front bumper, hood, grill, radiator and support, fan, left front fender, left front and rear doors, left and right exterior bed, rear bumper, and tailgate. The windshield sustained stress cracks at the left lower corner, which radiated upward toward the roof and center. Maximum exterior crush to the vehicle was 0.4 m (15.75 in.) in the left side plane at the left front corner at bumper height. Maximum occupant compartment deformation was 54 mm (2.1 in.) laterally across the cab at hip height in the instrument panel area. Photographs of the interior of the vehicle are shown in Figure 6.31.

6.3.6 Occupant Risk

Data from the accelerometer, located at the vehicle center of gravity, were digitized for evaluation of occupant risk and were computed as follows. In the longitudinal direction, the occupant impact velocity was 12.8 ft/s (3.9 m/s) at 0.088 sec, the highest 10 msec occupant ridedown acceleration was −4.4 *g* from 0.088 to 0.098 sec, and the maximum 50 msec average acceleration was −6.5 *g* between 0.009 and 0.059 sec. In the lateral direction, the occupant impact velocity was 29.2 ft/s (8.9 m/s) at 0.088 sec, the highest 10 msec occupant ridedown acceleration was 9.2 *g* from 0.199 to 0.209 sec, and the maximum 50 msec average was 15.7 *g* between 0.037 and 0.087 sec. Theoretical head impact velocity (THIV) was 34.6 km/h or 9.6 m/s at 0.087 sec, and post-impact head deceleration (PHD) was 9.3 *g* between 0.199 and 0.209 sec. These data and other pertinent information from the test are summarized in Figure 6.32.

6.3.7 Data from Accelerometers

To estimate the impact force from the vehicle accelerometer data, Equation 6-1 was used.

Figure 6.31. Interior of vehicle for test.

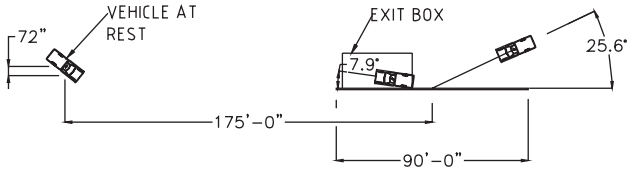

General Information
Test Agency..... Texas Transportation Institute
Test No. 475350-1
Date..... 2008-09-25
Test Article
Type..... 32 in. Vertical Barrier (T-221)
Name..... MSE Wall
Installation Length..... 90 ft
Material or Key Elements.....

Soil Type and Condition..... TxDOT Type B Backfill, Dry
Test Vehicle
Type/Designation..... 2270P
Make and Model..... 2004 Dodge Ram 1500 Quad-Cab
Curb..... 4794 lb
Test Inertial..... 4951 lb
Dummy..... No. Dummy
Gross Static..... 4951 lb

Impact Conditions
Speed.....63.2 mi/h
Angle.....25.6 degrees
Location/Orientation.....4.3 ft upstream of 4th joint
Exit Conditions
Speed.....54.9 mi/h
Angle.....7.9 degrees
Occupant Risk Values
Impact Velocity
Longitudinal.....12.8 ft/s
Lateral.....29.2 ft/s
Ridedown Accelerations
Longitudinal.....–4.4*g*
Lateral..... 9.2 *g*
THIV.....34.6 km/h
PHD.....9.3*g*
Max. 0.050 s Average
Longitudinal..... –6.5 *g*
Lateral.....15.7*g*
Vertical..... –3.7 *g*

Post-Impact Trajectory
Stopping Distance.....175 ft downstream
6 ft toward traffic
Vehicle Stability
Maximum Yaw Angle..... 42 degrees @ 1.04 sec
Maximum Pitch Angle.....–10 degrees @ 1.64 sec
Maximum Roll Angle.....-39 degrees @ 0.58 sec
Vehicle Snagging.....No
Vehicle Pocketing.....No
Test Article Deflections
Dynamic.....0.84 in. (top of barrier)
Permanent.....0.37 in. (bot. of barrier)
Working Width.....0
Vehicle Damage
VDS.....11LFQ5
CDC.....11FLEW4
Max. Exterior Deformation.....15.75 inches
Max. Occupant Compartment Deformation.....2.1 inches
CDI.....LF0000100

Figure 6.32. Summary of results for MASH test 3-11 on the MSE wall.

$$F_i(t) = F_x(t)\sin\phi(t) - F_y(t)\cos\phi(t)$$
$$= m\left(\vec{a}_x(t)\sin\phi(t) - \vec{a}_y(t)\cos\phi(t)\right) \quad (6\text{-}1)$$

where

$F_i(t)$ = the impact force
$\phi(t)$ = the vehicular yaw angle
$F_x(t) = m\vec{a}_x(t)$ = the longitudinal component of truck impact force
$F_y(t) = m\vec{a}_y(t)$ = the horizontal component of truck impact force
m = the mass of truck

The coordinate systems for the truck and barrier are schematically shown in Figure 6.33. Equation 6-1 assumes the vehicle as a single rigid body for the purpose of calculating the impact force.

Data obtained from the truck-mounted accelerometer were analyzed, and the results are presented in Figure 6.34. As shown in Figure 6.34(a) and (b), the maximum 50 msec average longitudinal and lateral accelerations were –6.5 *g* and 15.7 *g*, respectively. The change in yaw angle with respect to time is shown in Figure 6.34(c). Using Equation 6-1, the acceleration–time histories shown in Figures 6.34(a) and (b), and the yaw angle–time history, the resultant impact force was computed as a function of time as shown in Figure 6.34(d). The maximum 50 msec average resultant impact force was calculated to be 371.3 kN (83.5 kips) at a time of 0.062 sec.

The maximum 50 msec average acceleration of the barrier, as measured by the accelerometer at the top of the barrier, is shown in Figure 6.35(a). The barrier acceleration oscillated in

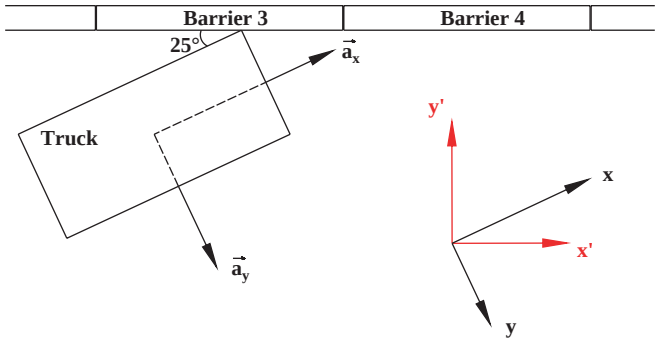

Figure 6.33. Coordinate system for vehicle and barrier.

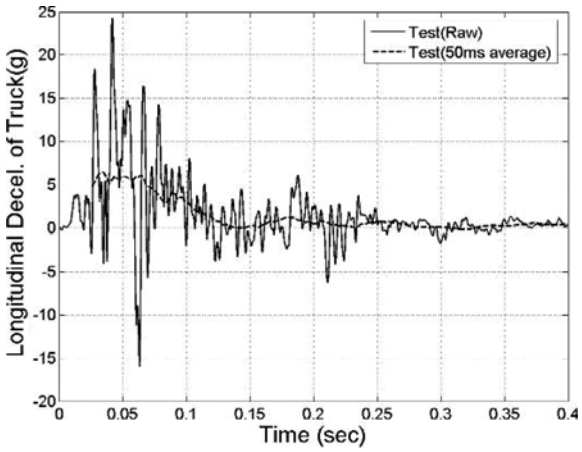

(a) Longitudinal deceleration

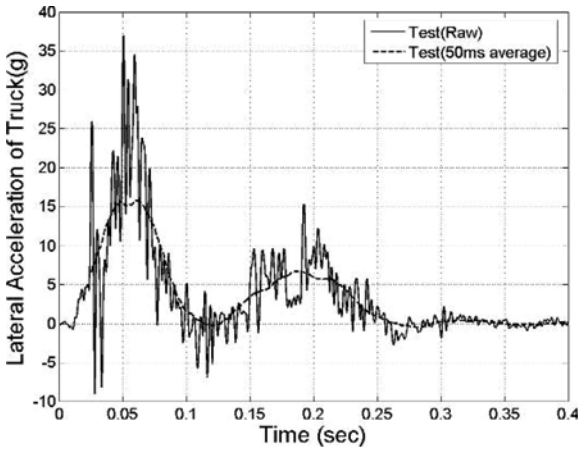

(b) Lateral acceleration

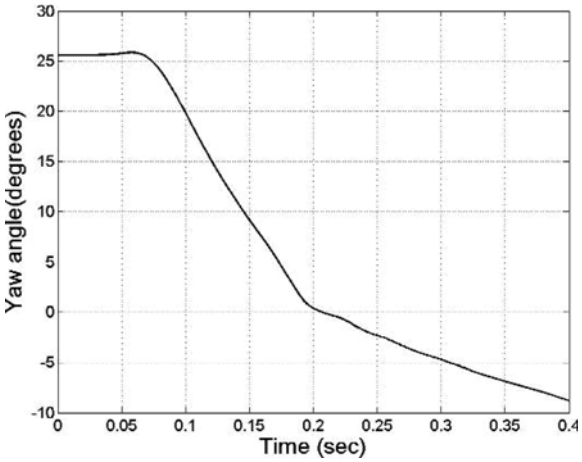

(c) Yaw angle with respect to the barrier

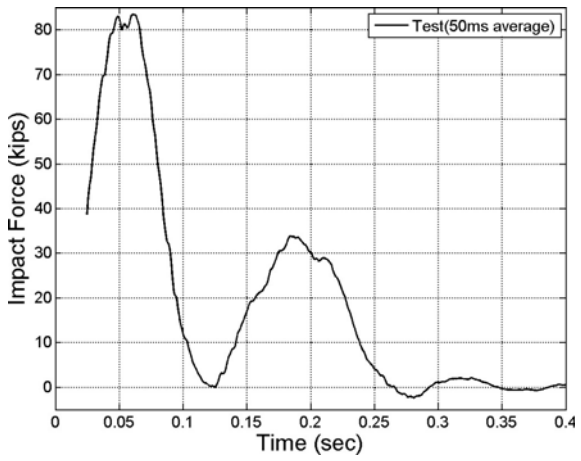

(d) Impact force

Figure 6.34. Acceleration, impact force, and yaw angle of truck.

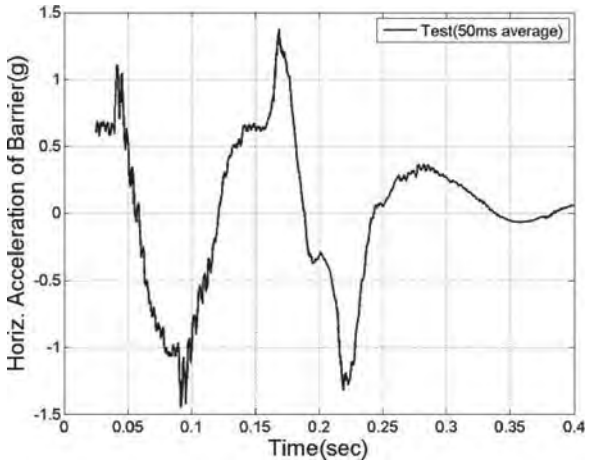

(a) Acceleration

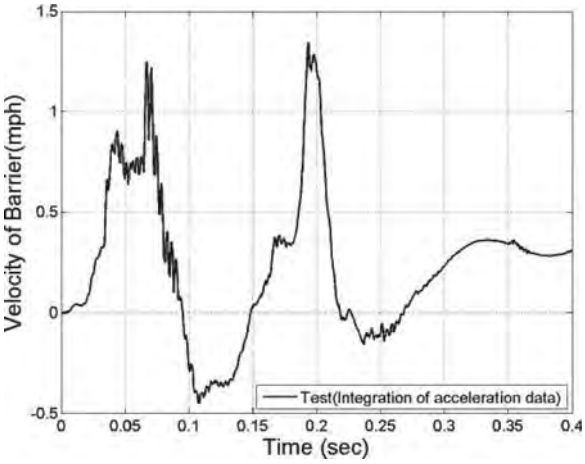

(b) Velocity

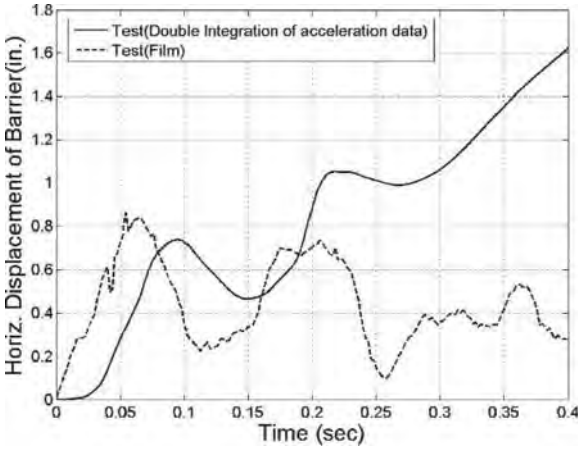

(c) Displacement

Figure 6.35. Acceleration, velocity, and displacement of barrier.

the range of 1.5 to −1.5 *g*. Examination of the impact events helps explain the barrier acceleration–time history. The barrier initially accelerated toward the field side of the installation as a result of the initial impact. As the vehicle was redirecting, the barrier began to rebound and accelerate back toward the traffic side. The back slap impact of the rear of the vehicle once again resulted in an acceleration of the barrier toward the field side, followed by the barrier rebounding and accelerating back toward the traffic side.

The velocity–time history of the barrier, as calculated by integration of the raw acceleration data, is shown in Figure 6.35(b). Some error in this time history is evident, given that the velocity did not return to zero at the end of the test. This error is magnified in the displacement–time history obtained from integration of the velocity history. Figure 6.35(c) presents displacement–time history from both double integration of the acceleration data and from analysis of the high-speed film, which is considered to be more accurate.

The maximum 50 msec average acceleration of the moment slab is shown in Figure 6.36(a). The velocity–time and vertical displacement–time histories of the moment slab are shown in Figure 6.36(b) and (c), respectively. The velocity–time history and displacement–time histories were calculated by integration of the acceleration data.

6.3.8 Photographic Instrumentation

Targets affixed to the displacement bars attached to the top and bottom of the barrier–coping section (see Figures 6.23 and 6.37) were used as reference points to determine angular and translational displacement of the barrier from analysis of high-speed video. Two distinct impacts are evident in the displacement data corresponding to the front and rear vehicle-barrier

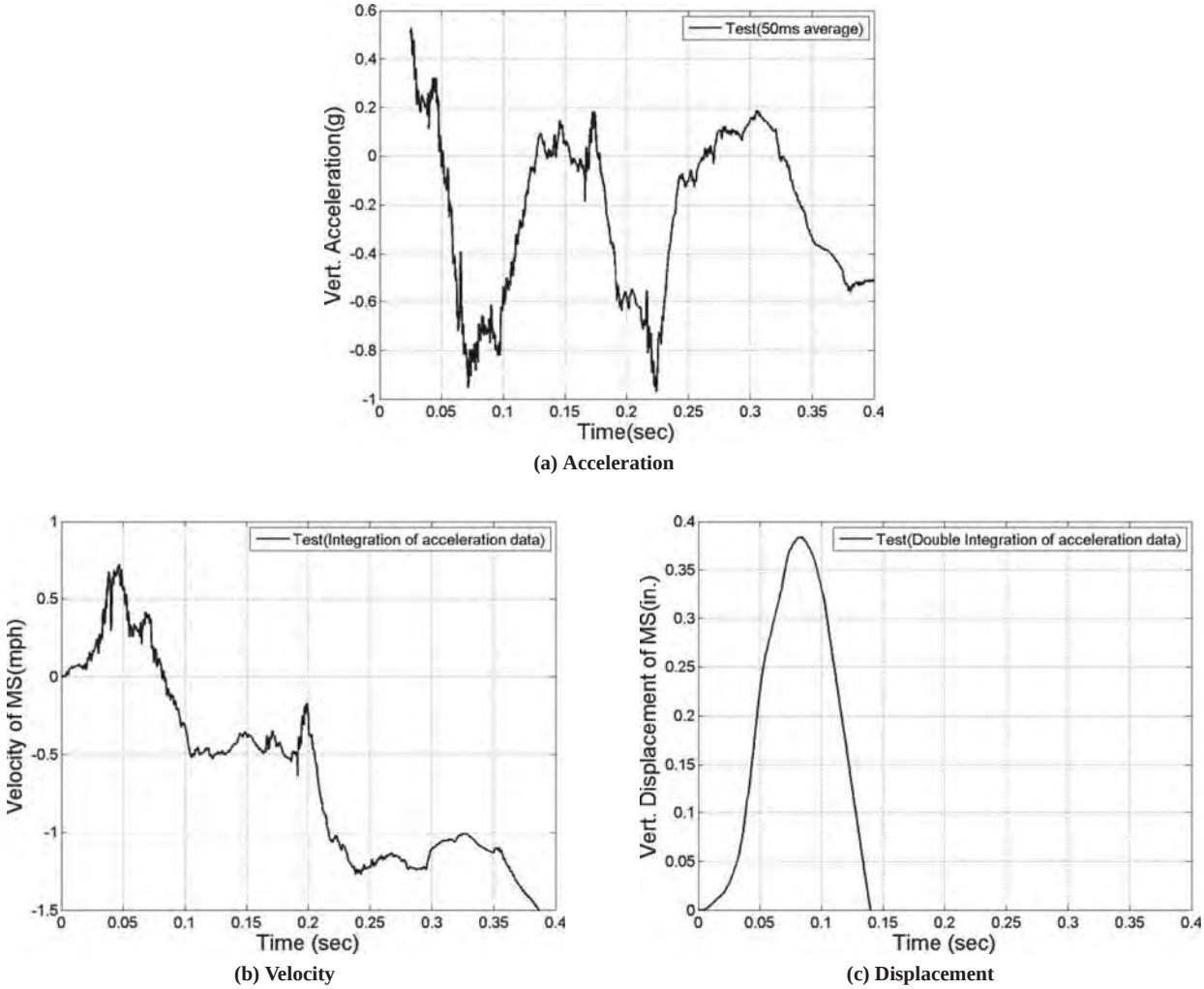

(a) Acceleration

(b) Velocity

(c) Displacement

Figure 6.36. Acceleration, velocity, and displacement of moment slab.

Figure 6.37. Location of displacement bars affixed on the barrier and panels.

contact. The dynamic displacement associated with the initial impact of the barrier was 21.3 mm (0.84 in.) at the top of the barrier and 14 mm (0.55 in.) at the bottom of the coping. After first impact, the barrier began to rebound. The subsequent rear impact (back slap) resulted in the dynamic displacements at the top of the barrier and bottom of the coping of 18.8 mm (0.74 in.) and 14 mm (0.55 in.), respectively. The permanent displacement of the barrier was 9.4 mm (0.37 in.) at the top of the barrier and 6.4 mm (0.25 in.) at the bottom of the coping. Figure 6.38 shows the displacement–time history of the barrier and panel.

Three additional targets affixed to the displacement bars attached to the wall panel at locations corresponding to these layers of wall reinforcement were used to determine angular and translational displacement of the panel from analysis of high-speed film. From the film analysis, the maximum dynamic displacement of the panel was 10.7 mm (0.42 in.) at the uppermost layer of reinforcement. The permanent displacement of the panel was 6.1 mm (0.24 in.) at the upper reinforcement layer. Less than 0.5 in. movement was measured at the second and third reinforcement layers.

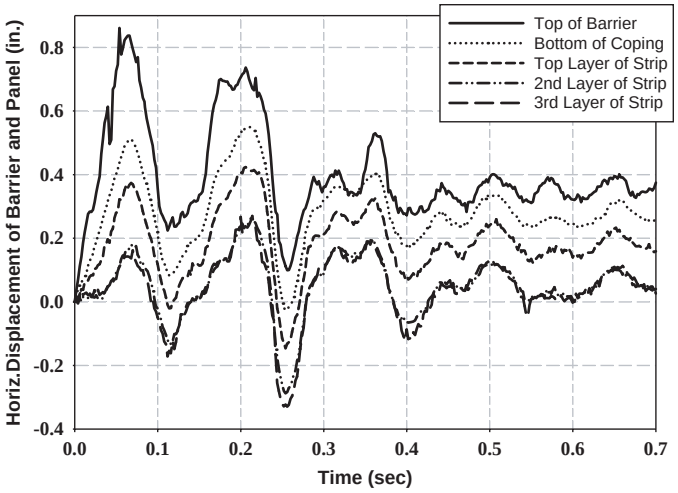

Figure 6.38. Horizontal displacement of barrier and panel (Film).

6.3.9 Load on the Strip from Strain Gages

A total of seven wall-reinforcement strips were instrumented with two strain gages (top and bottom) to capture the tensile forces transmitted into the reinforcement during vehicle impact. To enable comparison of forces and displacements, barriers and selected strip locations have been assigned alphanumeric designators that describe their horizontal position and vertical reinforcement layer. For example, strip B4-F-1st is positioned beneath the downstream end of the fourth barrier in the first (i.e., upper) layer of reinforcement as shown in Figure 6.39.

Raw data obtained from the strain gages on the strips were analyzed, and the results are presented in Figure 6.40. The 50 msec average of the raw data was analyzed to obtain design loads for the strips, and the results are presented in Figure 6.41. A summary of the maximum dynamic loads measured in the strips is shown in Table 6.3.

The static load in the strips was measured during the construction to allow computation of the total load in the strips during impact. The average static load in the uppermost layer of reinforcement was 3.34 kN (0.75 kips) and the average

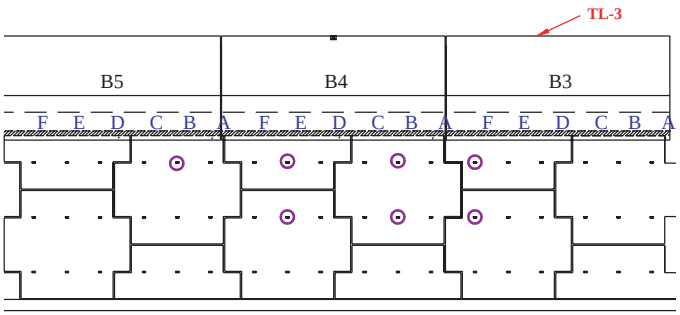

Figure 6.39. Location indicators for strain gages on the strips.

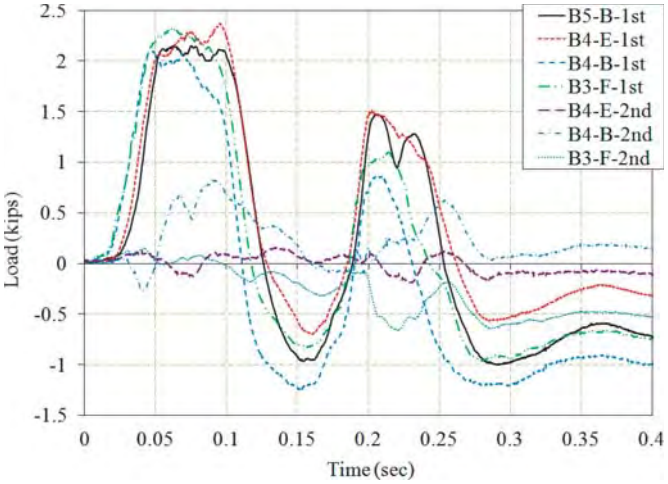

Figure 6.40. Dynamic load on the strips (raw data).

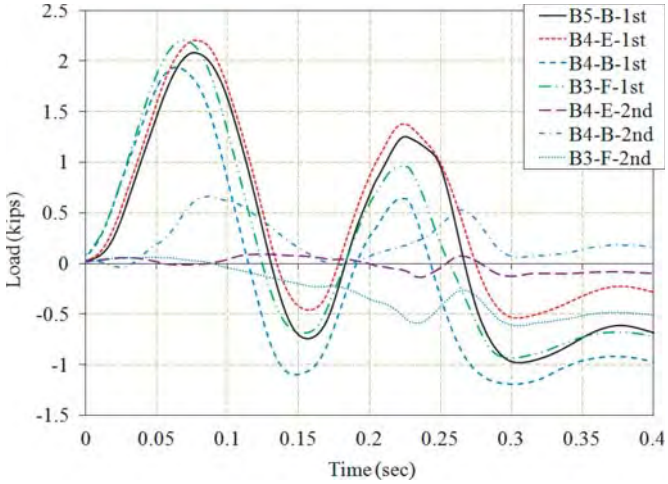

Figure 6.41. Dynamic load on the strips (50 msec avg.).

static load in the second layer of reinforcement was 8.23 kN (1.85 kips). A comparison of the measured static loads with those calculated by AASHTO LRFD is shown in Table 6.4.

Table 6.5 shows the total measured load (measured static load + measured dynamic load) in the reinforcement strips in comparison to the calculated resistance of the strips using the AASHTO LRFD Equation 11.10.6.3.2-1. The pullout resistance of the strip was calculated to be 6.623 kN (1.489 kips) at the uppermost layer of strips and 11.821 kN (2.658 kips) at the second layer.

Table 6.3. Dynamic loads on the wall reinforcement.

	Top Layer (kips)			
	B5-B-1st	**B4-E-1st**	**B4-B-1st**	**B3-F-1st**
Maximum load from raw data	2.15	2.37	2.10	2.32
Maximum 50 msec avg. load	2.08	2.21	1.94	2.20
	Second Layer (kips)			
		B4-E-2nd	**B4-B-2nd**	**B3-F-2nd**
Maximum load from raw data		0.16	0.83	0.15
Maximum 50 msec avg. load		0.09	0.66	0.06

Table 6.4. Static loads on the wall reinforcement.

	Static Load Measured (kips)	Static Load by AASHTO (kips)
Top Layer	0.75	0.688
Second Layer	1.85	1.205

Table 6.5. Total loads on the wall reinforcement.

	Static Load Measured (kips)	Dynamic Load* Measured (kips)	Total Loads (kips)	Resistance By AASHTO** (kips)
Top Layer	0.75	2.20	2.95	2.052
Second Layer	1.85	0.66	2.51	3.413

* Maximum 50 msec average load from the four tests.
** AASHTO LRFD Equation 11.10.6.3.2-1

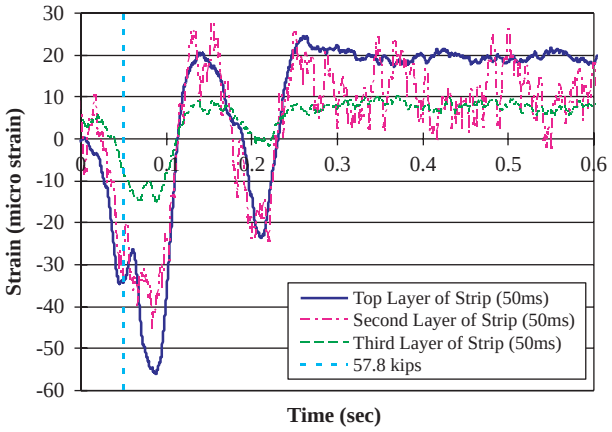

Figure 6.42. Strain on the panel.

6.3.10 Panel Analysis

The wall panel was instrumented with three strain gages to capture the strains in the panel at points corresponding to the three layers of wall reinforcement. Figure 6.42 shows the 50 msec average strain–time history of the panel at each reinforcement layer. The maximum strain in the panel occurred at a point corresponding to the upper layer of reinforcement and had a magnitude of 55.3 micro strain.

6.3.11 Other Instrumentations

String lines located 1.08 m (3.54 ft) from the face of wall panels were used to measure the permanent deflection of the barriers and panels after vehicle impact at different elevations. After vehicle impact, the permanent deflection ranged from 13 mm (0.51 in.) at the top of barrier segment B4 to 1 mm (0.04 in.) at the bottom of the coping on barrier segment B5 as shown in Figure 6.43. The maximum residual displacement occurred at the joint of barrier segment B3 and B4. The permanent deflection obtained from the film analysis, which tracked targets affixed to the barrier–coping section, was 9.4 mm (0.37 in.) at the top of the barrier and 6.4 mm (0.25 in.) at the bottom of the coping. Note that the location of the target is the centerline of the panel (B5-H6).

The permanent defection of the wall panels ranged from 5 mm (0.20 in.) to 1 mm (0.04 in.) as shown in Figure 6.43. Note that negative values indicate movement toward the traffic side of the barrier. Such movement may be the result of the panel being loaded eccentrically and rotating. The contact switch placed on the top edge of the level-up concrete on top of the wall panels inside the coping recess indicated that the coping did not contact the wall panel.

6.3.12 Damage of Moment Slab after Test

After the crash test, the overburden soil was removed to permit inspection of the moment slab and the connection between the coping and moment slab. Thin cracks were found on top of the moment slab between Barrier 3 and 4 as shown in Figure 6.44.

6.4 Conclusions

The roadside barrier mounted on the edge of the MSE wall performed acceptably according to the evaluation criteria specified for MASH test designation 3-11, as shown in Table 6.6.

The roadside barrier on the MSE wall contained and redirected the 2270P vehicle. The vehicle did not penetrate, underride, or override the installation. No lateral movement of the barrier was noted. No detached elements, fragments, or other debris was present to penetrate or show potential for penetrating the occupant compartment, or to present hazard to others in the area. Maximum occupant compartment deformation was 53.3 mm (2.1 in.) in the lateral area across the cab. The 2270P vehicle remained upright during and after the collision event. Maximum roll was 39 degrees. Occupant risk factors were within the limits specified in MASH.

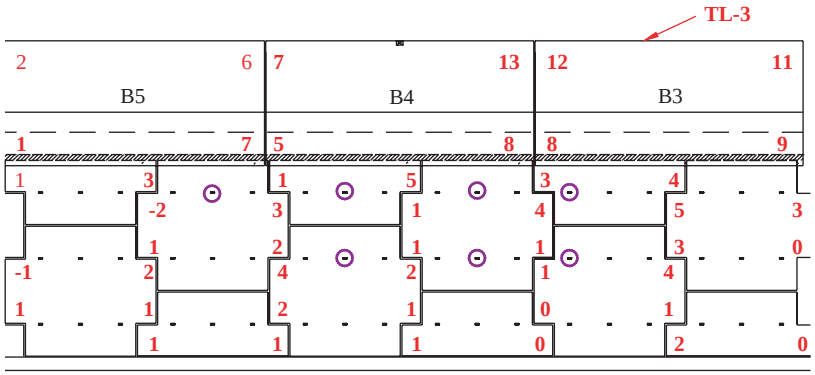

Figure 6.43. Permanent deflection of barrier and panels (units: mm).

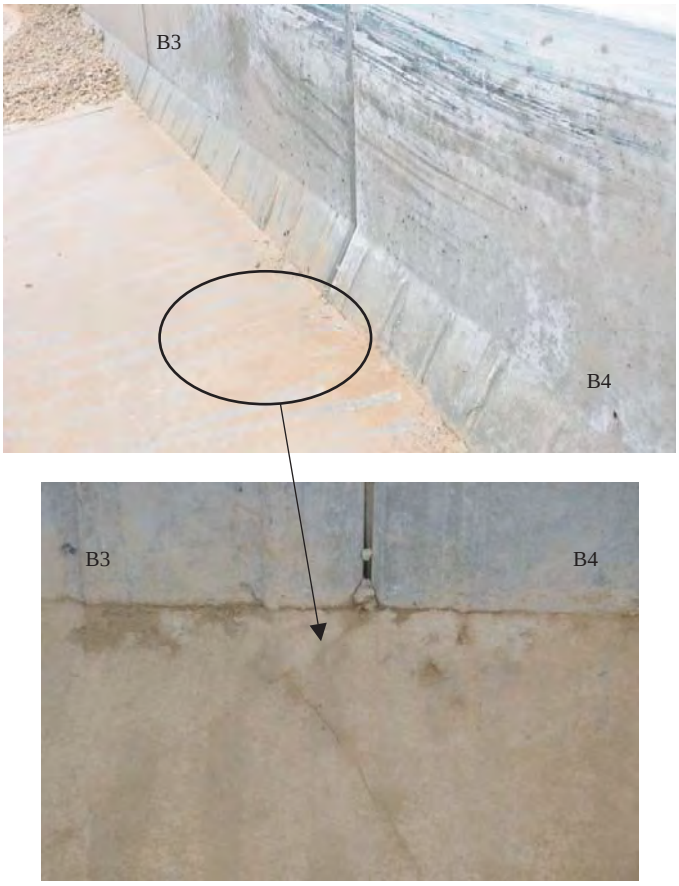

Figure 6.44. Cracks on the moment slab after test.

6.5 Comparison of Test and Simulation

A comparison between the results of the TL-3 test and the numerical simulations was conducted to establish confidence in the simulation for use in the guideline development process. Because the numerical simulation was modeled prior to performing the TL-3 test, the differences between the TL-3 test and simulation are listed below. These items may explain some of differences observed between test and numerical simulation.

1. While a 27.43 m (90 ft) long MSE wall was constructed for the test, an 18.28 m (60 ft) long MSE wall was modeled to reduce computational costs of the simulation.
2. While the wall was two full panels high [3.05 m (10 ft)] in the simulation, the test used a wall that was one and half panels high [2.29 m (7.5 ft)], as shown in Figure 6.45. However, the simulation results indicate that the load in the fourth layer of strips was negligible.
3. The simulation model had a density of three strips per layer per panel in the first layer and two strips per layer per panel in the other layers. In the test, all layers of reinforcement had a density of three strips per layer per panel.
4. The panel orientation at the location of impact (see circle in Figure 6.45) was different in simulation and test. However, this should not affect the loads in the strips.
5. The C2500 pickup truck model (reflective of *NCHRP Report 350*) used in the simulation has different characteristics than the 2270P truck (reflective of MASH) used in the TL-3 test as shown in Figure 6.46.
6. The coping detail of the barrier differed between model and test installation, as shown in Figure 6.47. Although field practice varies, the 254 mm (10 in.) coping depth and 101.6 mm (4 in.) high leveling pad used in the simulation is considered to be a typical detail. However, because the test barrier sections were cast using forms developed for a concrete pavement application, the depth of the recess had to be adjusted for the asphalt concrete application to provide the necessary strength in the coping section.

Sequential images from the simulation and TL-3 test are shown in Figure 6.48. The correlation is considered reasonable given the difference in pickup-truck body styles. In addition, the maximum 50 msec average impact loads from the accelerometer data on the truck were 439 kN (98.7 kips) in the simulation and 371.3 kN (83.5 kips) in the TL-3 test, as shown in Figure 6.49. The vehicle–barrier contact definition was used to measure the impact force on the barrier as shown in Figure 6.49. The maximum 50 msec average impact force from the contact definition was 248.21 kN (55.8 kips). The displacement of barrier is shown in Figure 6.50. The simulation overpredicts the displacement at the top of the barrier.

The strip load in the simulation includes the static load due to earth pressure and the dynamic load due to the barrier impact. Therefore, the measured average static load in the reinforcement (Table 6.4) was subtracted from the simulated strip load to provide a simulated dynamic impact load to the measured dynamic impact load (Table 6.7). The simulation overpredicted the maximum strip load in the upper layer of reinforcement but captured the trends in the load–time history of the strip [Figure 6.51(a)]. The simulation underpredicted the maximum strip load in the second layer of reinforcement but captured the trends in the load–time history of the strip [Figure 6.51(b)].

The strain on the wall panel was evaluated as shown in Figure 6.52. The maximum compressive strain was about 60 micro strain at 0.08 sec in the test and about 18 micro strain at 0.065 sec in the simulation. In the simulation, the impact occurred above a half panel rather than a full-height panel, so the estimated panel strain was smaller than in the test.

As can be seen in the comparison, the simulation is close to the results of TL-3 test. This simulation and test were evaluated to support the verification of design guidelines.

Table 6.6. Performance evaluation summary for MASH Test 3-11 on the MSE wall.

Test Agency: Texas Transportation Institute | Test No.: 475350-1 | Test Date: 2008-09-25

MASH Evaluation Criteria	Test Results	Assessment
Structural Adequacy		
A. *Test article should contain and redirect the vehicle or bring the vehicle to a controlled stop; the vehicle should not penetrate, underride, or override the installation although controlled lateral deflection of the test article is acceptable.*	The roadside barrier on the MSE wall contained and redirected the 2270P vehicle. The vehicle did not penetrate, underride, or override the installation. No lateral movement of the barrier was noted.	Pass
Occupant Risk		
D. *Detached elements, fragments, or other debris from the test article should not penetrate or show potential for penetrating the occupant compartment, or present an undue hazard to other traffic, pedestrians, or personnel in a work zone.*	No detached elements, fragments, or other debris was present to penetrate or show potential for penetrating the occupant compartment, or to present hazard to others in the area.	Pass
Deformations of, or intrusions into, the occupant compartment should not exceed limits set forth in Section 5.3 and Appendix E of MASH.	Maximum occupant compartment deformation was 2.1 in. in the lateral area across the cab.	Pass
F. *The vehicle should remain upright during and after collision. The maximum roll and pitch angles are not to exceed 75 degrees.*	The 2270P vehicle remained upright during and after the collision event. Maximum roll was 39 degrees.	Pass
H. *Longitudinal and lateral occupant impact velocities should fall below the preferred value of 9.1 m/s (30 ft/s), or at least below the maximum allowable value of 12.2 m/s (40 ft/s).*	Longitudinal occupant impact velocity was 12.8 ft/s, and lateral occupant impact velocity was 29.2 ft/s.	Pass
I. *Longitudinal and lateral occupant ridedown accelerations should fall below the preferred value of 15.0 g, or at least below the maximum allowable value of 20.49 g.*	Longitudinal ridedown acceleration was –4.4 *g*, and lateral ridedown acceleration was 9.2 *g*.	Pass
Vehicle Trajectory		
For redirective devices, the vehicle shall exit the barrier within the exit box.	The 2270P vehicle did not cross the exit box.	

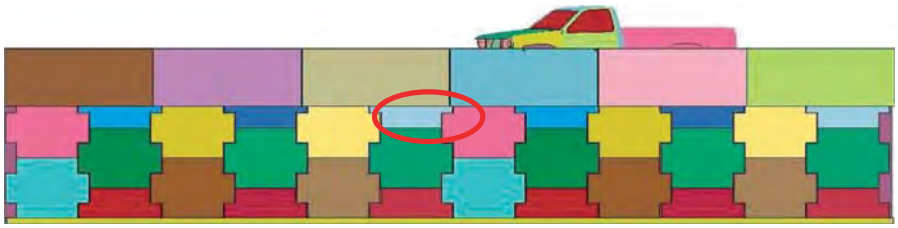

(a) Simulation

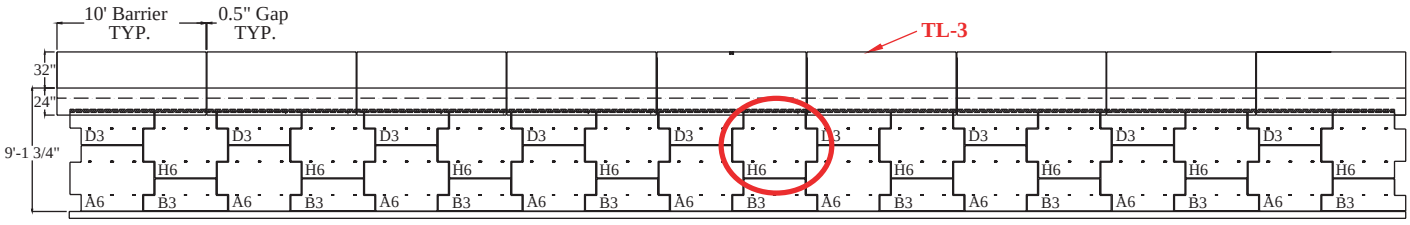

(b) TL-3 Test

Figure 6.45. Difference of wall panel details.

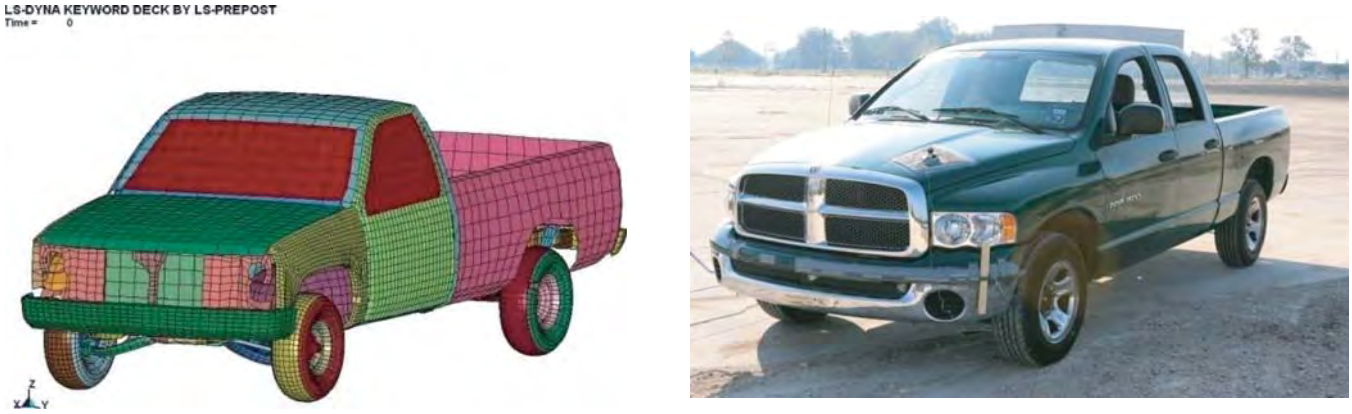

Figure 6.46. Comparison of truck of (a) simulation and (b) TL-3 test.

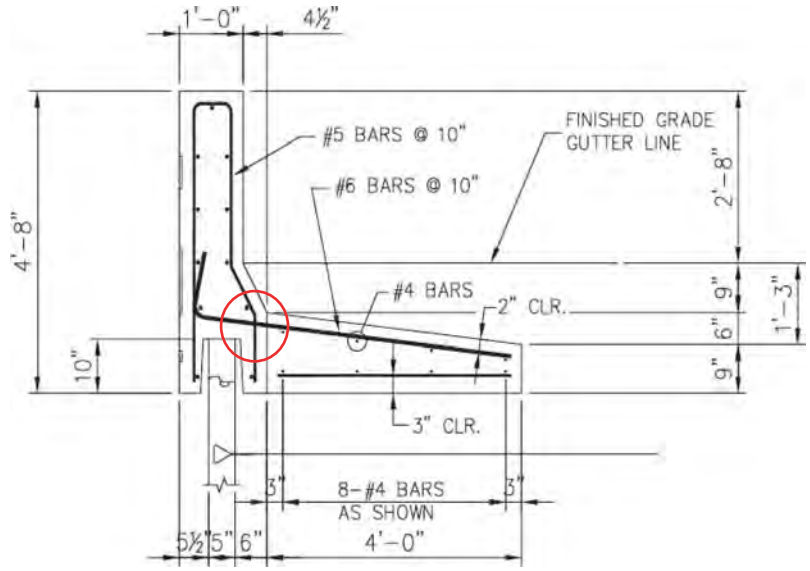

(a) Simulation

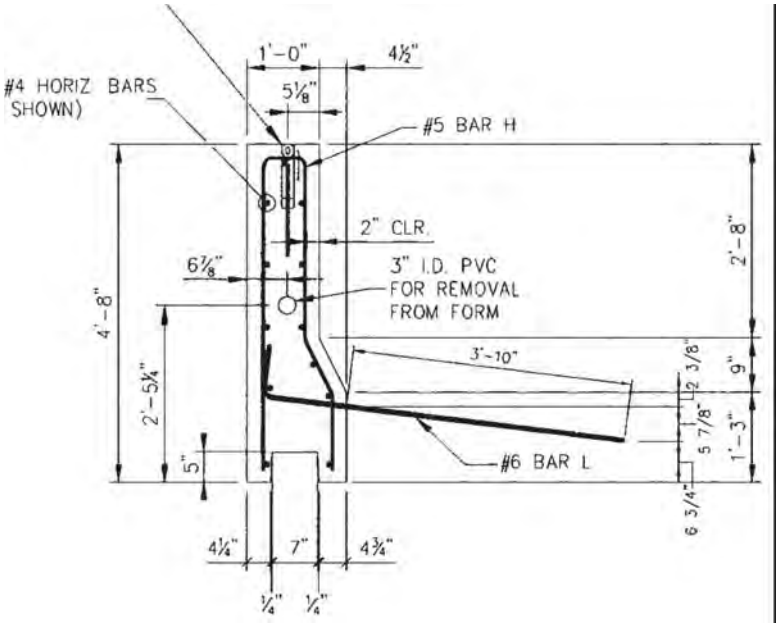

(b) TL-3 Test

Figure 6.47. Difference of barrier details.

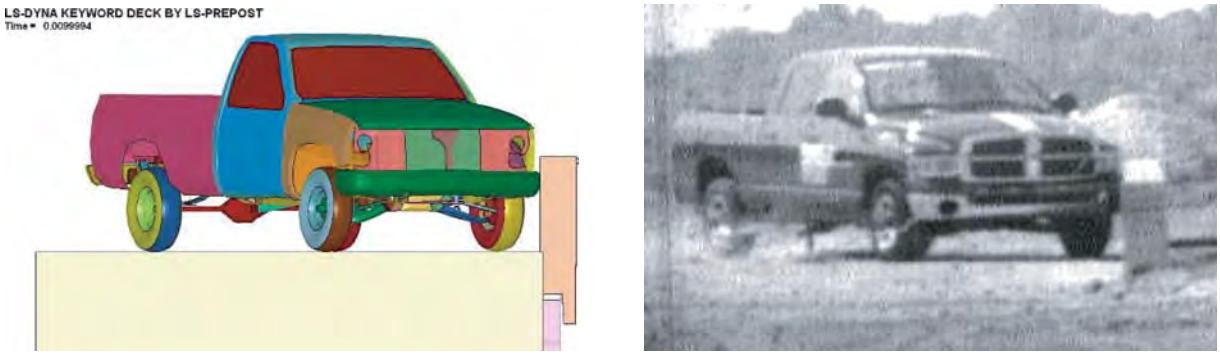

(a) 0 sec

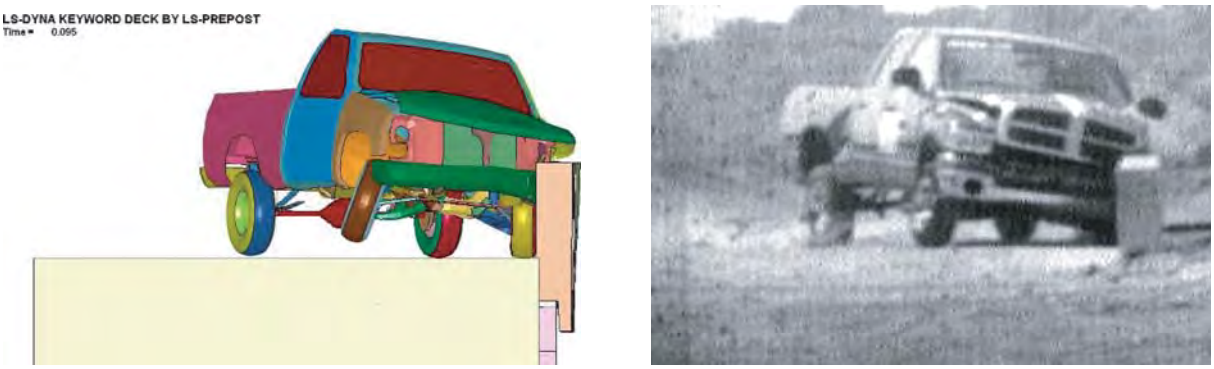

(b) 0.085 sec

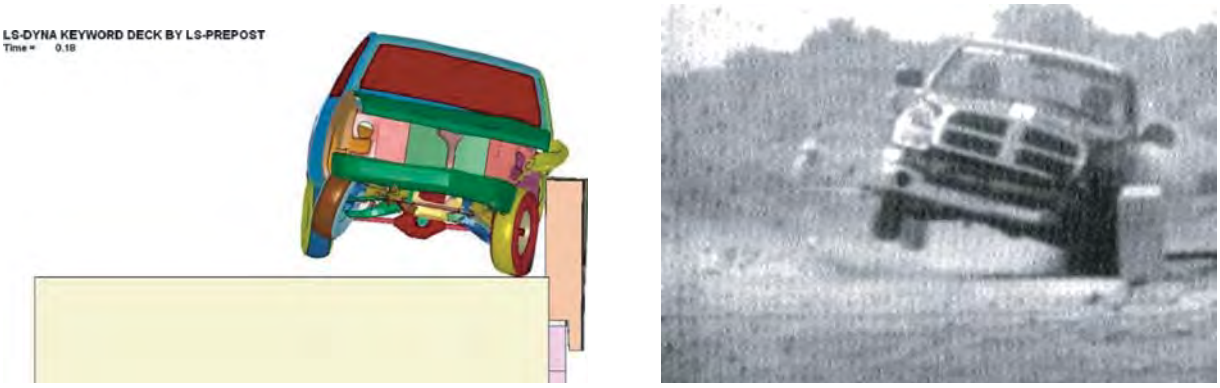

(c) 0.17 sec

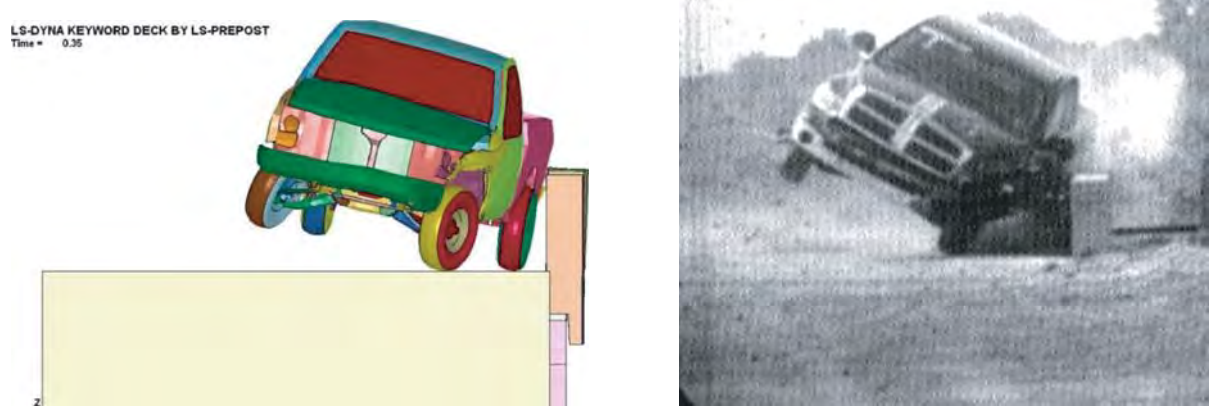

(d) 0.34 sec

Figure 6.48. Comparison of sequential photos.

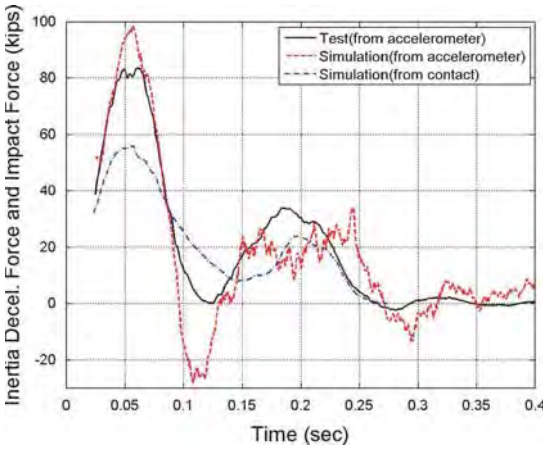

Figure 6.49. Inertia deceleration force and impact force on the barrier.

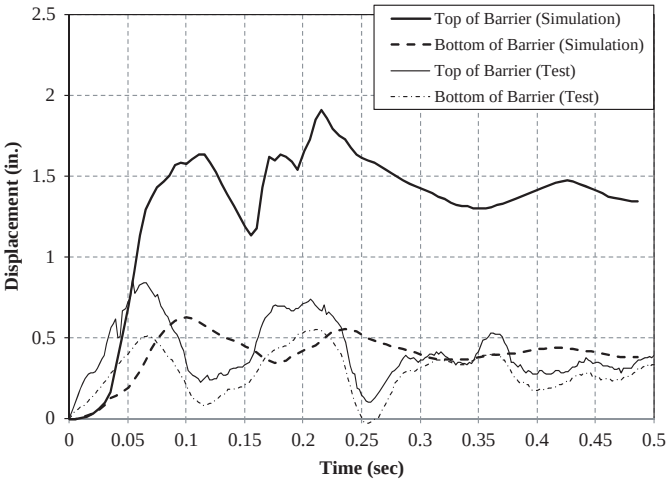

Figure 6.50. Displacement of barrier.

Table 6.7. Total loads on the wall reinforcement.

Layer	Measured Static Load (kips)	Measured Dynamic Load (kips)	Simulated Dynamic Load (kips)
Top	0.75	2.20	3.39
Second	1.85	0.66	–0.09

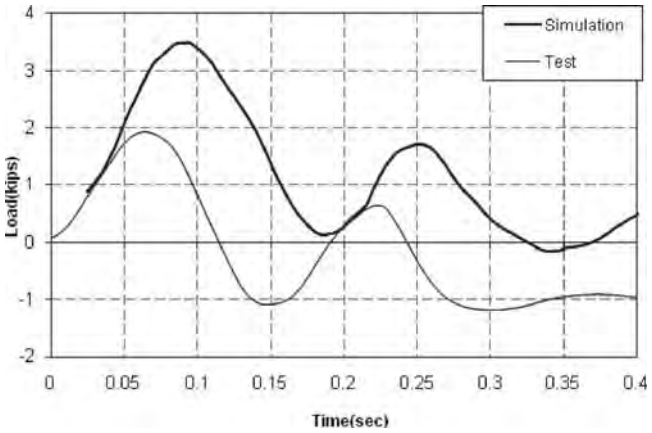

(a) First layer of strip

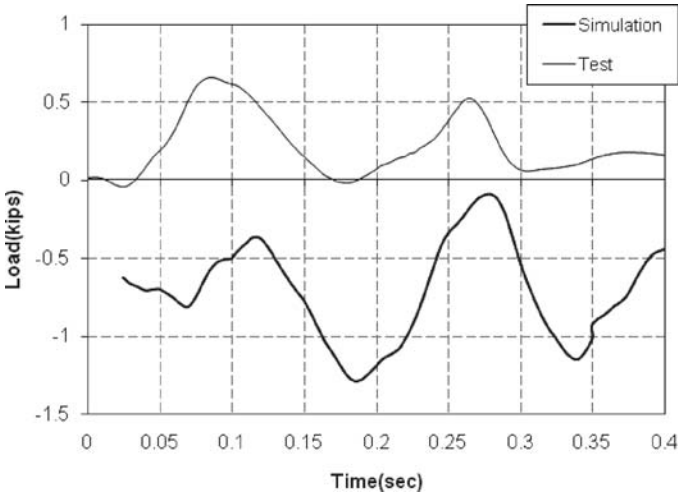

(b) Second layer of strip

Figure 6.51. Comparison of 50 msec average data of dynamic load on the strip.

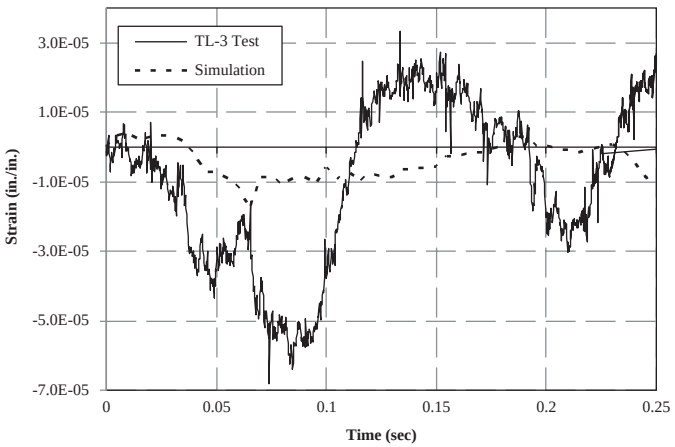

Figure 6.52. Comparison of panel strain at B4-A1.

CHAPTER 7

Design Guidelines

Design guidelines were developed as part of this project for three components:

- The barrier–moment slab system
- The MSE wall reinforcement
- The wall panel

The guidelines are set in terms of AASHTO LRFD practice. The AASHTO LRFD format version of the design guidelines is shown in Appendix I. An example of the application of the design guidelines for the TL-3 crash test MSE wall is presented in Appendix J.

Depending on the design, two points of rotation are possible as shown in Figure 7.1. The point of rotation should be determined based on the interaction between the barrier coping and top of the wall panel. With reference to Figure 7.1, the point of rotation should be taken as Point A if the top of the wall panel is isolated from contact with the coping by presence of an air gap or sufficiently compressible material. The point of rotation should be taken as Point B if there is direct bearing between the bottom of the coping and the top of the wall panel or level-up concrete.

7.1 Guidelines for the Barrier

The barrier, coping, and moment slab should be safe against structural failure. A barrier should be designed according to AASHTO LRFD Chapter 13 (*2*). Any section along the coping and moment slab should not fail in bending when the barrier is subjected to a design impact load. Two modes of stability failure are possible in addition to structural failure of the barrier system. They are sliding and overturning of the barrier–moment slab system.

7.1.1 Sliding of the Barrier

The factored static resistance (ϕ P) to sliding of the barrier–moment slab system along its base should be greater than or equal to the factored equivalent static load (γ L_s) due to the dynamic impact force (Figure 7.2).

$$\phi P \geq \gamma L_s \tag{7-1}$$

[For the load level TL-3, L_s is 44.48 kN (10 kips), ϕ resistance factor is 0.8 (AASHTO Table 10.5.5-1), and γ load factor is 1.0 (extreme event).]

The static force (P) should be calculated as:

$$P = W \tan\phi_r \tag{7-2}$$

where

W = weight of the monolithic section of barrier and moment slab plus any material laying on top of the moment slab
ϕ_r = friction angle of the soil–moment slab interface.

The factored equivalent static load should be applied to the length of the moment slab between joints. Any coupling between adjacent moment slabs or friction that may exist between free edges of the moment slab and the surrounding soil should be neglected. If the soil–moment slab interface is rough, ϕ_r is equal to the friction angle of the soil ϕ_s (cast in place). If the soil–moment slab interface is smooth, ϕ_r should be reduced accordingly $\left(\frac{2}{3}\tan\phi_s\right)$ (precast).

7.1.2 Overturning of the Barrier

The factored static moment resistance (ϕM) to overturning of the barrier–moment slab system should be greater than or equal to the factored static load (γL_s) due to the impact force times the moment arm (h_A or h_B) taken as the vertical distance from the point of impact due to the dynamic force to the point of rotation A or B (Figure 7.2).

$$\phi M \geq \gamma L_s \left(h_A \text{ or } h_B\right) \tag{7-3}$$

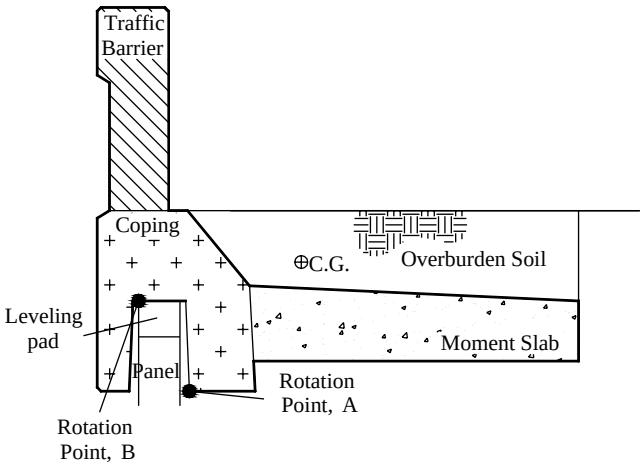

Figure 7.1. Barrier–moment slab system for design guideline.

[For the load level TL-3, L_s is 44.48 kN (10 kips), ϕ resistance factor is 0.9, and γ load factor is 1.0 (extreme event).]

M should be calculated as:

$$M = W(l_A \text{ or } l_B) \tag{7-4}$$

where

W = weight of the monolithic section of barrier and moment slab plus any material laying on top of the moment slab

l_A or l_B = horizontal distance from the center of gravity of the weight (W) to the point of rotation A or B.

The moment contribution due to any coupling between adjacent moment slabs, shear strength of the overburden soil, or friction that may exist between the backside of the moment slab and the surrounding soil should be neglected.

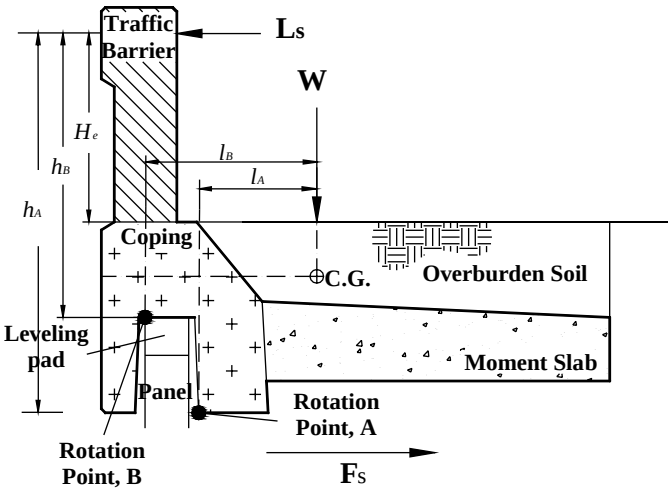

H_e = effective height of the impact force (*AASHTO LRFD Bridge Design Specifications,* Figure A13.2-1).

Figure 7.2. Barrier–moment slab system for barrier design guideline (sliding and overturning).

7.1.3 Rupture of the Coping in Bending

The critical section of the coping must be designed to resist the applicable impact load conditions for the appropriate test level as defined in *AASHTO LRFD Bridge Design Specifications* (Figure 7.3).

7.2 Guidelines for the Wall Reinforcement

The reinforcement guidelines should ensure that the reinforcement does not pull out or break during a barrier impact with the chosen design vehicle. The connection between the reinforcement and the wall panel should be able to resist the pullout load or breaking load, whichever controls.

7.2.1 Pullout of the Wall Reinforcement

Pressure Distribution Approach

The capacity of the reinforcement calculated by common static methods should be compared to the dynamic impact loads because no significant difference was found between the static capacity and the dynamic capacity of the reinforcement.

The factored static resistance (ϕ P) to pullout of the reinforcement should be greater than or equal to the sum of the factored static load ($\gamma_s F_s$) due to the earth pressure and the factored dynamic load ($\gamma_d F_d$) due to the impact. The static load (F_s) should be obtained from the static earth pressure (p_s) times the tributary area (A_t) of the reinforcement unit. The dynamic load (F_d) should be obtained from the pressure (p_d) of the pressure distribution (Figure 7.4) times the tributary area (A_t) of the reinforcement unit.

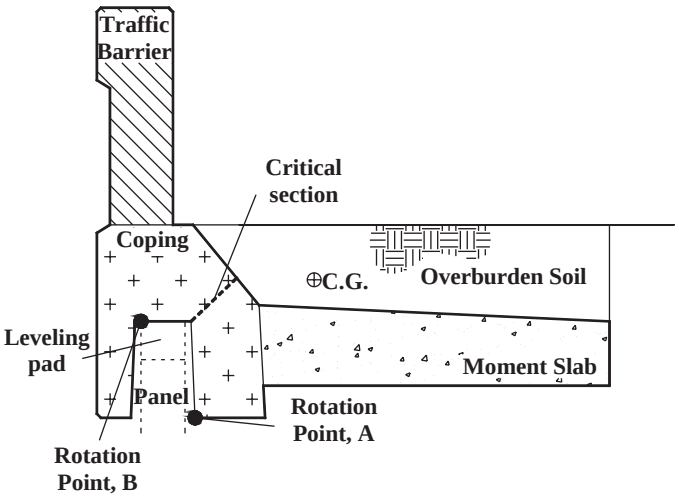

Figure 7.3. Coping and possible weakest section.

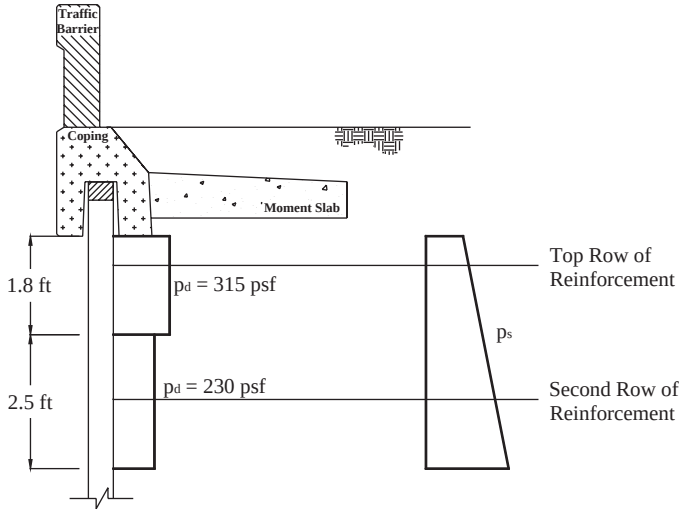

Figure 7.4. Pressure distribution (p_d) for reinforcement pullout.

$$\phi P \geq \gamma_s F_s + \gamma_d F_d \quad (7\text{-}5)$$

$$\phi P \geq \gamma_s p_s A_t + \gamma_d p_d A_t \quad (7\text{-}6)$$

(For the load level TL-3, p_d is given by the pressure distribution shown in Figure 7.4, ϕ resistance factor is 1.0, γ_d load factor is 1.0, and γ_s load factor is 1.0.)

The reinforcement resistance (P) for strips should be calculated as (AASHTO LRFD Equation 11.10.6.3.2-1):

$$P = F^* \sigma_v 2b L \quad (7\text{-}7)$$

where

F* = resistance factor (sliding plus bearing)
σ_v = vertical effective stress on the reinforcement
b = width of the strip
L = full length of the reinforcement

The value of F* should be obtained from the current AASHTO guidelines (Figure 7.5).

The reinforcement resistance (P) for bar mats should be calculated as:

$$P = F^* \sigma_v \pi D n L \quad (7\text{-}8)$$

where

D = diameter of the bar mats
N = number of longitudinal bars

Line Load Approach

The factored static resistance (ϕ P) to pullout of the reinforcement should be greater than or equal to the sum of the factored static load ($\gamma_s F_s$) due to the earth pressure and the factored dynamic load ($\gamma_d F_d$) due to the impact. The static load (F_s) should be obtained from the static earth pressure (p_s) times the tributary area (A_t) of the reinforcement unit. The dynamic impact load (F_d) should be obtained from the line load (Q_d) (Figure 7.6) times the longitudinal spacing (S_L) of the reinforcement.

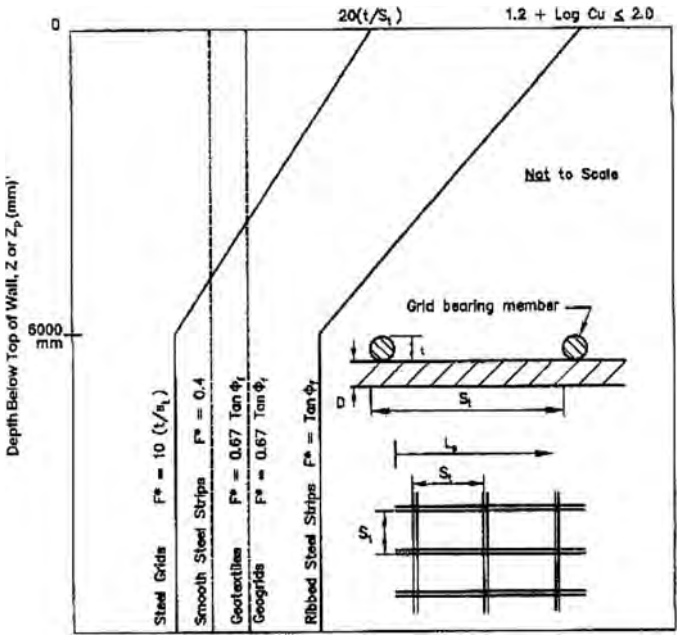

Source: AASHTO LRFD Figure 11.10.6.3.2-1

Figure 7.5. Default values for the pullout friction factor (F*).

$$\phi P \geq \gamma_s F_s + \gamma_d F_d \quad (7\text{-}9)$$

$$\phi P \geq \gamma_s p_s A_t + \gamma_d Q_d S_L \quad (7\text{-}10)$$

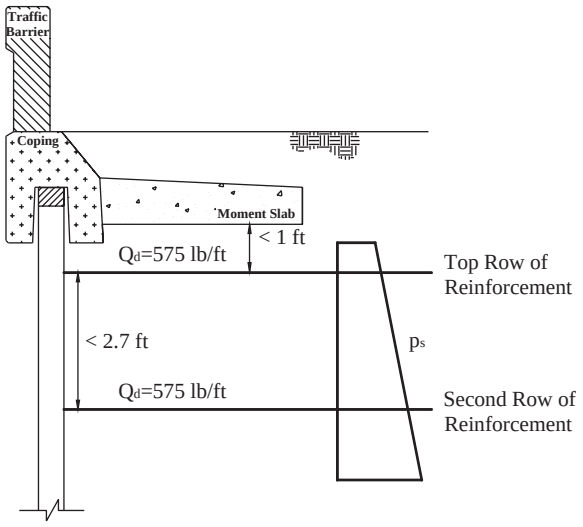

Figure 7.6. Line load (Q_d) for reinforcement pullout.

(For the load level TL-3, Q_d is given by the line load shown in Figure 7.6, ϕ resistance factor is 1.0, γ_d load factor is 1.0, and γ_s load factor is 1.0.)

The reinforcement resistance (P) for strips should be calculated as (based on AASHTO LRFD Equation 11.10.6.3.2-1):

$$P = F^* \sigma_v \, 2b \, L \tag{7-11}$$

where

F^* = resistance factor (sliding plus bearing)
σ_v = vertical effective stress on the reinforcement
b = width of the strip
L = full length of the reinforcement

The value of F^* should be obtained from the current AASHTO guidelines (Figure 7.5).

The reinforcement resistance (P) for bar mats should be calculated as:

$$P = F^* \sigma_v \pi \, D \, n \, L \tag{7-12}$$

where

D = diameter of the bar mats
n = number of longitudinal bars.

7.2.2 Rupture of the Wall Reinforcement

Pressure Distribution Approach

The factored resistance (ϕ R) to rupture of the reinforcement should be greater than or equal to the sum of factored static load ($\gamma_s F_s$) due to the earth pressure and the factored dynamic load ($\gamma_d F_d$) due to the impact. The static load (F_s) should be obtained from the static earth pressure (p_s) times the tributary area (A_t) of the reinforcement unit. The dynamic load (F_d) should be obtained from the dynamic pressure (p_d) of the pressure distribution (Figure 7.7) times the tributary area (A_t) of the reinforcement unit.

$$\phi R \geq \gamma_s F_s + \gamma_d F_d \tag{7-13}$$

$$\phi R \geq \gamma_s p_s A_t + \gamma_d p_d A_t \tag{7-14}$$

(For the load level TL-3, p_d is given by the pressure distribution shown in Figure 7.7, ϕ resistance factor is 1.0, γ_d load factor is 1.0, and γ_s load factor is 1.0.)

The reinforcement resistance (R) for strips or bar mats should be calculated as:

$$R = \sigma_t \, A_s \tag{7-15}$$

where

σ_t = tensile strength of the reinforcement
A_s = cross-section area of the reinforcement.

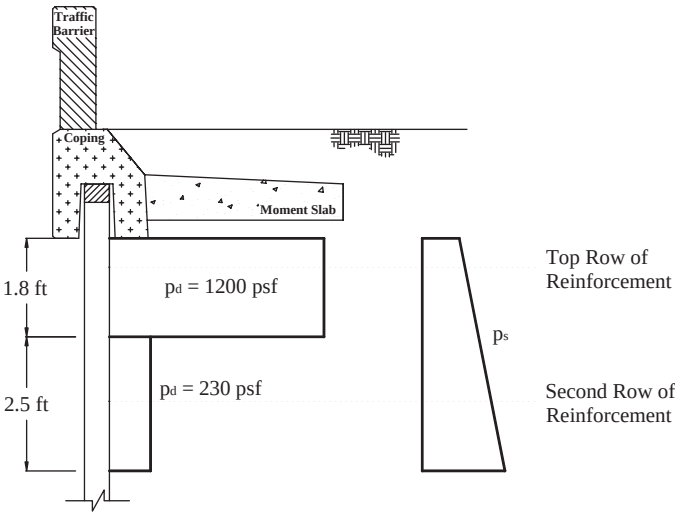

Figure 7.7. Pressure distribution (p_d) for reinforcement rupture.

$$A_s = b \times E_c \text{ for strip} \tag{7-16}$$

where E_c is the strip thickness corrected for corrosion loss. (AASHTO LRFD Figure 11.10.6.4.1-1)

$$A_s = \frac{\pi D^{*2}}{4} \text{ for bar mats} \tag{7-17}$$

where D^* is the diameter of bar or wire corrected for corrosion loss. (AASHTO LRFD Figure 11.10.6.4.1-1)

Line Load Approach

The factored resistance (ϕ R) to rupture of the reinforcement should be greater than or equal to the sum of factored static load ($\gamma_s F_s$) due to the earth pressure and the factored dynamic load ($\gamma_d F_d$) due to the impact. The static load (F_s) should be obtained from the static earth pressure (p_s) times the tributary area (A_t) of the reinforcement unit. The dynamic load (F_d) should be obtained from the line load (Q_d) (Figure 7.8) times the longitudinal spacing (S_L) of the reinforcement.

$$\phi R \geq \gamma_s F_s + \gamma_d F_d \tag{7-18}$$

$$\phi R \geq \gamma_s p_s A_t + \gamma_d Q_d S_L \tag{7-19}$$

(For the load level TL-3, Q_d is given by the line load shown in Figure 7.8, ϕ resistance factor is 1.0, γ_d load factor is 1.0, and γ_s load factor is 1.0.)

The reinforcement resistance (R) for strips or bar mats should be calculated as:

$$R = \sigma_t \, A_s \tag{7-20}$$

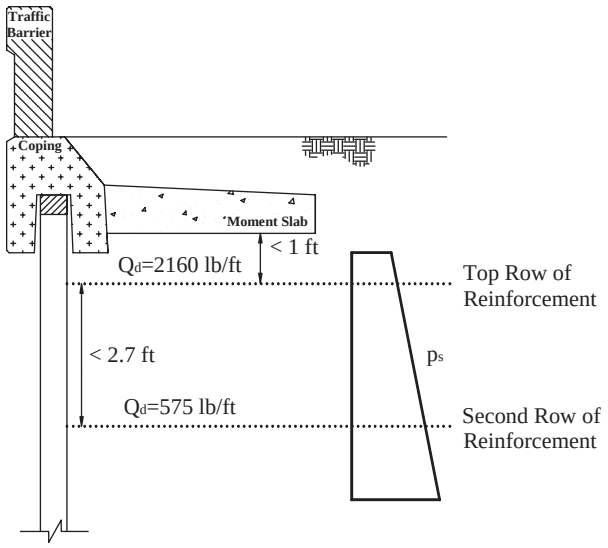

Figure 7.8. Line load (Q_d) for reinforcement rupture.

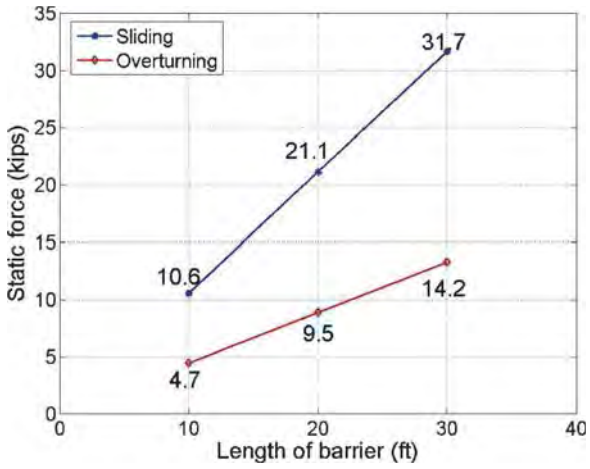

Figure 7.9. Static load by analytical solution (point of rotation A).

where

σ_t = tensile strength of the reinforcement
A_s = cross-section area of the reinforcement.

$$A_s = b \times E_c \text{ for strip} \quad (7\text{-}21)$$

where E_c is the strip thickness corrected for corrosion loss. (AASHTO LRFD Figure 11.10.6.4.1-1)

$$A_s = \frac{\pi D^{*2}}{4} \text{ for bar mats} \quad (7\text{-}22)$$

where D* is the diameter of bar or wire corrected for corrosion loss. (AASHTO LRFD Figure 11.10.6.4.1-1)

7.3 Guidelines for the Wall Panel

The wall panels must be designed to resist the dynamic pressure distributions defined in Figure 7.7. The wall panel should have sufficient structural capacity to resist the maximum design rupture load for the wall reinforcement. The static load is not included because it is not located at panel connection.

7.4 Data to Back Up Guidelines

7.4.1 Barrier

The guidelines were developed based on analysis and testing of N.J. profile and vertical-wall concrete barriers. However, the results should apply to other common barrier types.

Note that the calculations indicate that a 1.37 m (4.5 ft) wide, 9.14 m (30 ft) long moment slab without the shear strength of soil on top of it is the minimum required to satisfy the above requirements. The researchers also found that the overturning mode occurs before the sliding mode and is, therefore, the controlling mechanism.

The proposed design guidelines are based on the evidence presented below. Note that a decision was made to aim for a barrier–moment slab design that would generate 25.4 mm (1 in.) movement during impact. This 25.4 mm (1 in.) movement was considered acceptable as it would likely require little or no repair of the underlying MSE wall and should not affect the impact performance of the barrier system.

The static analysis for sliding and overturning is conducted using equilibrium equations as described in Section 3.2.1. Two points of rotation were considered for sliding and overturning as shown in Figures 7.9 and 7.10. Also the coefficient

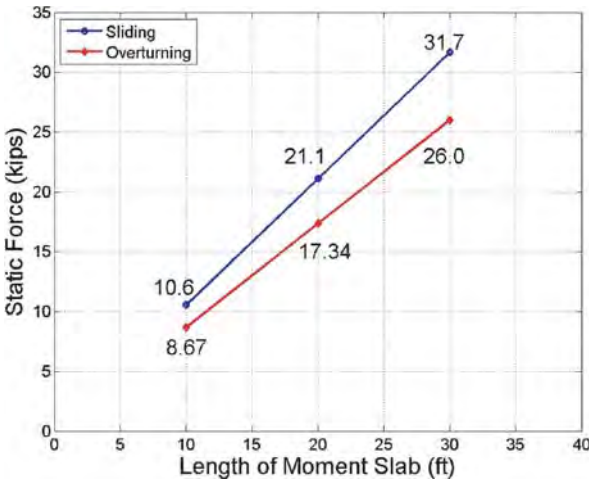

Figure 7.10. Static load by analytical solution (point of rotation B).

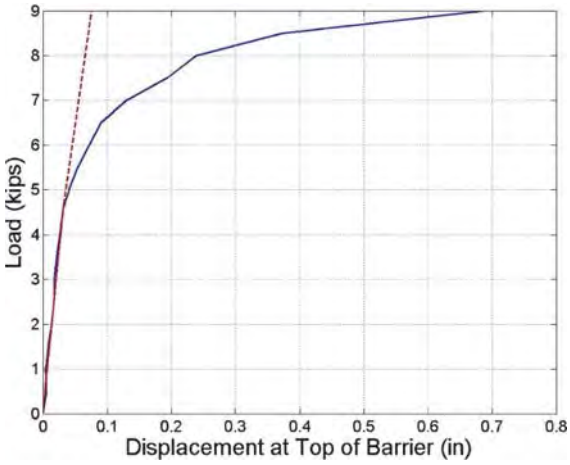

Figure 7.11. Static test data at the top of barrier.

of friction for the soil–moment slab interface was taken as equal to the coefficient of friction of the soil. These figures show the barrier force that a 1.37 m (4.5 ft) wide moment slab of varying length can resist when discounting the shear strength of the soil on top of it. As can be seen, the overturning mode develops less resistance than the sliding mode for both points of rotation. Thus, in this case, the overturning mode controls design. This is not to say that sliding could not control and that the barrier does not slide during impact. It did slide slightly during both the static and the dynamic test, but the majority of the movement was due to rotation. Evaluation of sliding should be part of the design process.

Figure 7.11 shows part of the results of the static test on the 1.37 m (4.5 ft) wide, 3.05 m (10 ft) long barrier–moment slab. As can be seen, a maximum load of 9 kips was reached. Furthermore at 22.24 kN (5 kips), the load–displacement relationship becomes nonlinear, typical of soil behavior. This behavior indicates that the load resisted by the barrier due only to the dead weight is 22.24 kN (5 kips) leaving 17.8 kN (4 kips) of soil resistance along the moment slab perimeter. Figure 7.12 shows the distribution of the soil resistance along the perimeter for the 1.37 m (4.5 ft) wide, 3.05 m (10 ft) long moment slab that was used in static test.

By extrapolation, a 1.37 m (4.5 ft) wide, 6.1 m (20 ft) long moment slab–barrier assembly would resist 44.48 kN (10 kips) without soil on its periphery and 71.17 kN (16 kips) with peripheral soil. As the length of moment slab increases, the friction associated with the side soil would be neglected. Therefore, by further extrapolation, a 1.37 m (4.5 ft) wide and $n \times$ 3.05 m (10 ft) long moment slab barrier assembly would resist $n \times$ 22.24 kN (5 kips) without soil on its periphery and $n \times$ 31.14 kN (7 kips) with peripheral soil. Table 7.1 shows the values of the static resistance developed by a barrier with a 1.37 m (4.5 ft) wide moment slab of varying length. The

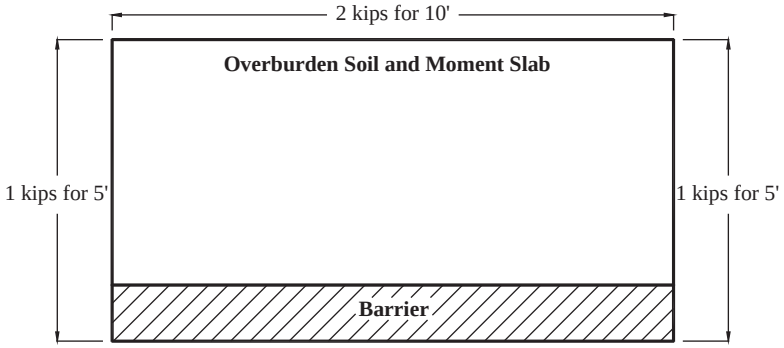

Figure 7.12. Soil resistance along the perimeter of the barrier–moment slab system.

Table 7.1. Total static load with respect to the length of the barrier.

Length of Moment Slab (ft)	**(1)** Resistance from Moment Slab and Overburden (kips)	**(2)** Soil Resistance (kips)	**(3) = (1)+(2)** Total Static Load (kips)	**(3) / (1)** Ratio
10	5	2	7	1.4
:	:	:	:	:
10 × *n*	5 × *n*	2 × *n*	7 × *n*	1.4

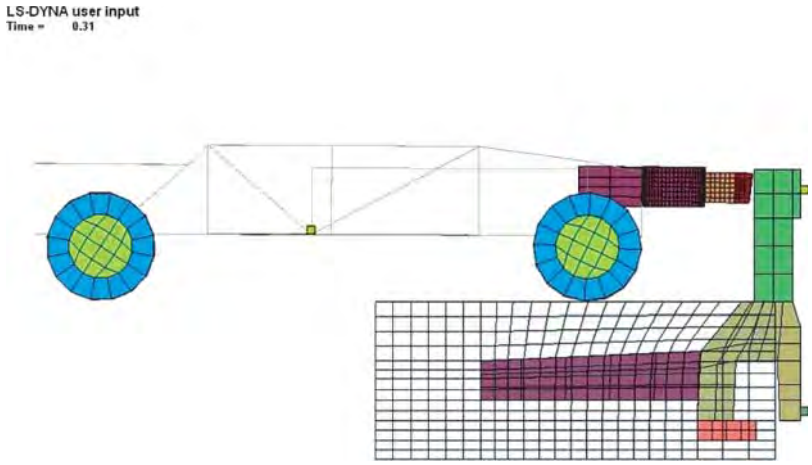

Figure 7.13. Finite element model for dynamic analysis.

resistance is split in two parts: the load due to dead weight and the load due to soil friction along the back edge of the moment slab (i.e., resistance contributed by the soil on the sides of the moment slab is neglected).

A dynamic impact test was performed with a bogie on the same 1.37 m (4.5 ft) wide, 3.05 m (10 ft) long barrier–moment slab system. At 20.9 km/h (13 mph), the bogie generated a maximum 50 msec average impact force of 193.05 kN (43.4 kips), and moved the top of the barrier 89 mm (3.5 in.). The numerical simulation was used to predict and compare the dynamic test as shown in Figure 7.13. The numerical simulation gave 204.62 kN (46 kips) and 89 mm (3.5 in.). Table 7.2 shows the maximum 50 msec average impact load and the corresponding displacement at the top of the barrier according to the numerical simulations of bogie vehicle impacts into a 3.05 m (10 ft) long barrier–moment slab system at different speeds. Figure 7.14 is a comparison between the static load test results (load–deflection curve), the numerical simulations (peak impact force and corresponding displacement), and the result of the two dynamic bogie tests [20.9 km/h (13 mph) and 28.97 km/h (18 mph)]. This comparison shows the amplification due to the inertia force with the increase in velocity at impact. This comparison gave credibility to the numerical simulations. Numerical simulation was then used to find what peak dynamic load would generate a peak displacement of the top of the barrier of 25.4 mm (1 in.) for different lengths of the 1.37 m (4.5 ft) wide moment slab.

It was found that a bogie impact at 20.9 km/h (13 mph) on a 6.1 m (20 ft) long moment slab would generate a dynamic force of 227.75 kN (51.2 kips) at 25 mm (0.98 in.) of movement, and that the same 6.1 m (20 ft) long moment slab would resist 43.59 kN (9.8 kips) statically without counting on the shear strength of the soil on top of it as shown in Figure 7.15. Another numerical simulation indicated that a bogie impact at 28.97 km/h (18 mph) on a 9.14 m (30 ft) long moment slab would generate a dynamic force of 384.74 kN (78.4 kips) at 24 mm (0.96 in.) of movement, and that the same 9.14 m (30 ft) long moment slab would resist 65.39 kN (14.7 kips) statically without counting on the shear strength of the soil on top of it.

These data indicate that a 240 kN (54 kips) dynamic load associated with 25.4 mm (1 in.) movement is approximately equivalent to a 44.48 kN (10 kips) static load when the shear strength of the soil above the moment slab is discounted. These data further indicate that a 9.14 m (30 ft) moment slab gives a

Table 7.2. Impact loads with various velocities of bogie on 10 ft barrier system.

Velocity of Bogie (mph)	Maximum Displacement of Barrier (in.)	Impact Force (kips)
2	0.14	6.79
5	0.97	23.33
8	1.73	34.35
10	2.35	39.95
13	3.56	46.00

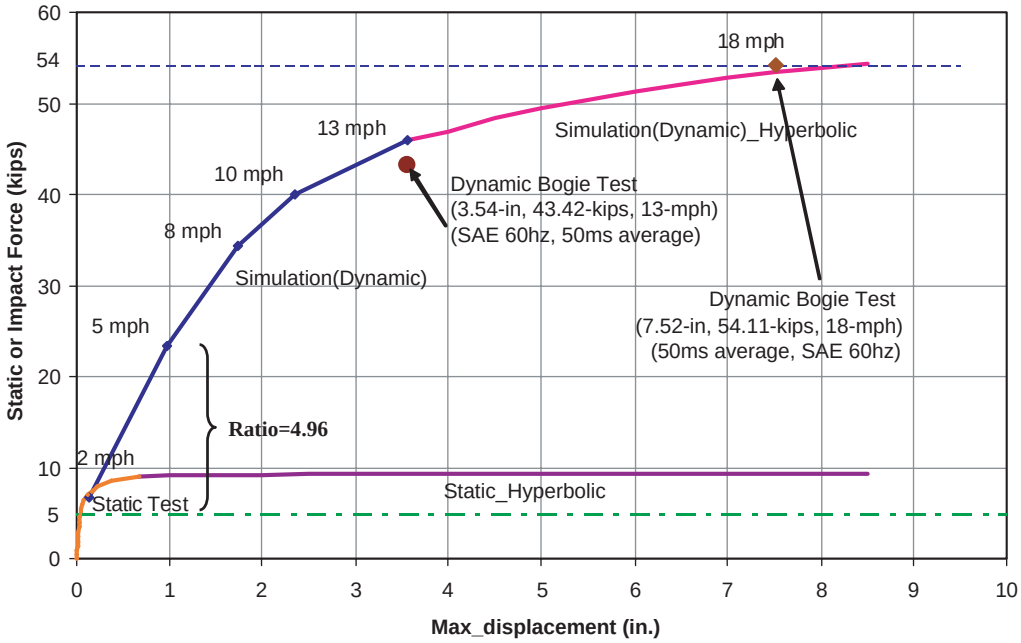

Figure 7.14. Comparison of static test and dynamic test and finite element model of 10 ft barrier–moment slab system.

factor of safety of 1.5 against the 240 kN (54 kips) dynamic design load for a 25.4 mm (1 in.) movement and a 1.5 factor of safety against a 44.48 kN (10 kips) static design load.

Figure 7.16 shows the ratio of the dynamic force over the static force (with shear resistance) as a function of the length of the 1.37 m (4.5 ft) wide moment slab. Note that for the 9.14 m (30 ft) barrier, the ratio is very close to 5.4, which is equal to 240.2 kN/44.48 kN (54 kips/10 kips).

7.4.2 Wall Reinforcement

Four bogie tests were conducted to develop the design guidelines for a barrier system on top of an MSE wall. The impact speeds varied from 32.5 km/h (20.19 mph) to 35.1 km/h (21.8 mph). The maximum load on the barrier (50 msec average) varied from 286.47 kN (64.4 kips) to 326.5 kN (73.4 kips). To capture the tensile forces transmitted into the reinforcement

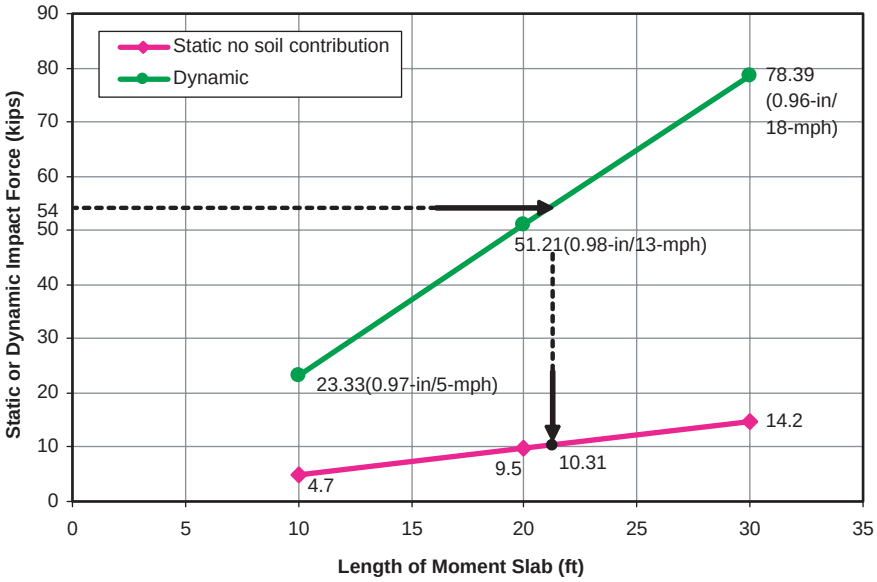

Figure 7.15. Comparison of static and dynamic impact force in 1 in. maximum displacement.

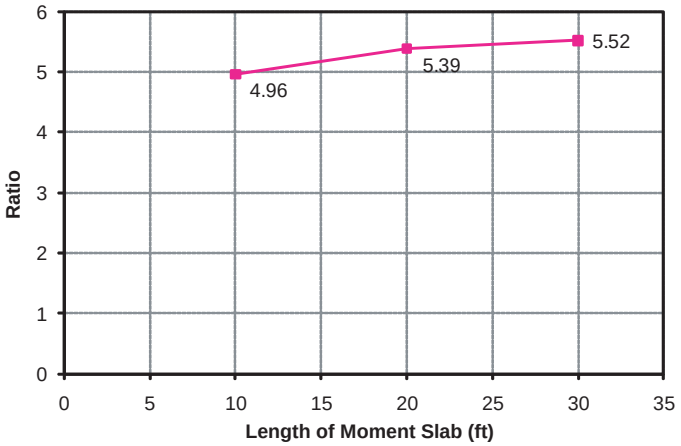

Figure 7.16. Ratio of static load and dynamic impact load.

during the dynamic impact, strain gages were installed. The placement of these strain gages was selected to measure the maximum tensile load in each layer of reinforcement as well as give an indication of the distribution of forces in the lateral, longitudinal, and vertical directions.

The maximum dynamic loads in the reinforcement in excess of the static load measured during the impact varied from 9.47 kN (2.13 kips) to 33.18 kN (7.46 kips) in the uppermost layer. The load used is the one corresponding to the location where two strain gages (top and bottom of the strip) were available to get an average value. Higher loads were registered at locations where only one gage was available. However, it appears that significant bending occurred, which made the single–strain gage readings doubtful and unreliable.

The maximum load in the strip closest to the impact (uppermost layer) in excess of the static load was 33.18 kN (7.46 kips) for the 4.88 m (16 ft) long strips under the vertical wall (Test 4) and 31.98 kN (7.19 kips) for the 4.88 m (16 ft) long strips under the N.J. barrier (Test 1). Assuming the increase in strip load is proportional to the barrier impact load, the design strip loads corresponding to a design impact load of 240 kN (54 kips) can be estimated to be 27.8 kN (6.25 kips) and 23.53 kN (5.29 kips), respectively.

For the 2.44 m (8 ft) long strips case, the maximum load in the strip closest to the impact (top layer) in excess of the static load was 9.47 kN (2.13 kips) under the vertical wall (Test 3). The design strip load in excess of static corresponding to a design impact load of 240 kN (54 kips) can be estimated to be 7.3 kN (1.64 kips).

The maximum load in excess of static in the single bar closest to the impact load (uppermost layer) in the bar mat, which was 2.44 m (8 ft) long, was 6.85 kN (1.54 kips) (Test 2). The design strip load in excess of static corresponding to a design impact load of 240 kN (54 kips) can be estimated to be 5.6 kN (1.26 kips).

Even though the reinforcement appears to have reached its maximum pullout resistance during impact, the overall performance of the wall was very satisfactory in all four tests. Therefore it was decided that having the reinforcement working at maximum pullout resistance would be acceptable. The design recommendations were based on a pressure diagram approach to be resisted by the reinforcement while using the design loads in excess of static recorded in the tests.

Pullout of the Wall Reinforcement

The pullout tests in the laboratory were performed at rates varying from quasi-static rates all the way to rates approaching impact loading rates. Because no consistent rate effect was found, the recommended design guidelines require the pullout resistance of the reinforcement to be calculated according to common static methods and sized to resist the full dynamic loads.

The design strip load in excess of static in Test 3, which is for a 2.44 m (8 ft) long strip, was used to develop the design guideline for pullout of the reinforcement. This test was selected because the wall performed well during that impact. During Test 4 with strips that were 4.88 m (16 ft) long, the strips developed a higher load because the system was stiffer. As a result, the wall panel developed a crack during impact. Therefore the stiffer 16 ft long strips are not acceptable in this case.

The resistance (P) for the 8 ft long strips was calculated to be 6.58 kN (1.48 kips) for the uppermost layer and 12.02 kN (2.7 kips) for the second layer using Equation 2-1 in Chapter 2. The pullout friction factor (F*) was 1.837 for the uppermost layer and 1.674 for the second layer.

The dynamic maximum design load (50 msec average) in excess of static in the strip at the uppermost layer was measured and then interpolated back to the 240 kN (54 kips) impact load to be 7.295 kN (1.64 kips). The static load at the uppermost layer was calculated to be 2.53 kN (0.569 kips) by AASHTO LRFD. The total design load was thus calculated to be 9.799 kN (2.203 kips) at the uppermost layer. Because this measured total design load [9.799 kN (2.203 kips)] in the strip was higher than the resistance [6.595 kN (1.483 kips)], the resistance was used to obtain the dynamic design load in excess of static at the uppermost layer. The controlling design load in excess of the static due to static earth pressures was calculated to be 4.066 kN (0.914 kips). This represents a static load, equivalent to a dynamic load, which would indicate that an 8 ft long strip would perform well in the case of a TL-3 impact. The value of 4.066 kN (0.914 kips) was found by calculating the total resistance of the 8 ft strip at the depth of the

Table 7.3. Test results and calculation of design strip load for pullout design.

Layer	(1) Measured Dynamic Load* (kips)	(2) Static** (kips)	(3)=(1) + (2) Total (kips)	(4) Calculated Resistance** (kips)	Controlling Design Dynamic Load (kips)
Top	1.64	0.569	2.209	1.483	(4)-(2) = 0.914
Second	0.92	1.095	2.015	2.702	0.92

* Adjusted for 54 kips design impact load
** Calculated from AASHTO LRFD Sections 11.10.6.2–11.10.6.3

first layer [6.595 kN (1.483 kips)] minus the calculated load due to static earth pressures from AASHTO LRFD [2.53 kN (0.569 kips)].

At the second layer, the same process was followed. The measured dynamic load in excess of static was 4.092 kN (0.92 kips). The static earth pressure load for the second layer was calculated to be 4.87 kN (1.095 kips) by AASHTO LRFD. The total load was therefore calculated to be 8.963 kN (2.015 kips), which is less than the calculated pullout load at that depth [12.019 kN (2.702 kips)]. Therefore, the measured dynamic load in excess of static was used as the controlling dynamic load in excess of static for pullout design. Table 7.3 shows the measured dynamic load, calculated static load, total load, resistance, and the controlling load for pullout design.

The dynamic pressure per strip was calculated as shown in Table 7.4. For the 2.44 m (8 ft) long strip with a density of 3 strips per panel per layer, the tributary area was 0.27 m^2 (2.92 ft^2 = 4.87 ft × 1.8 ft/3 strips per panel) for the top layer and the tributary area was 0.37 m^2 (3.94 ft^2 = 4.87 ft × 2.43 ft/3 strips per panel) for the second layer. The dynamic design pressure was calculated as shown in Table 7.4. The dynamic design pressure in excess of the static earth pressure for pullout is recommended to be 15.08 kPa (315 psf) for the uppermost layer and 11.012 kPa (230 psf) for the second layer as shown in Figure 7.4.

Table 7.4. Dynamic design load on the strip for pullout design.

Layer	Total Design Pressure (psf)
Top	0.914 kips / 2.92 ft^2 * = **313 psf**
Second	0.92 kips / 3.94 ft^2 ** = **234 psf**

* Tributary area of a panel for the top layer (2.92 ft^2 = 4.87 ft × 1.8 ft / 3 strips per panel)
** Tributary area of a panel for the second layer (3.94 ft^2 = 4.87 ft × 2.43 ft / 3 strips per panel)

Rupture of the Wall Reinforcement

The Reinforcement resistance to rupture (R) for a strip was calculated as:

$$R = \sigma_t A_s \quad (7\text{-}23)$$

where

σ_t = tensile strength of the reinforcement [ASTM Grade 60, therefore, 414 MPa (60 ksi)]
A_s = cross-section area of the reinforcement.

$$A_s = b \times E_c \quad (7\text{-}24)$$

where E_c is the strip thickness corrected for corrosion loss. (AASHTO LRFD Figure 11.10.6.4.1-1) (E_c = 1.984 mm = 0.078 in. for 100-year design life)

$$A_s = 50\ mm \times 1.984\ mm = 99.2\ mm^2 = 0.154\ in^2 \quad (7\text{-}25)$$

The reinforcement resistance to rupture (R) was calculated to be 41.037 kN (9.226 kips).

To develop the design guideline against rupture of the reinforcement, the highest design load on the strip measured in the test was used. The maximum dynamic 50 msec average load on the strip located in the uppermost layer for Test 1 was 23.531 kN (5.29 kips). In the second layer, the measured maximum dynamic load was 4.092 kN (0.92 kips). Therefore, the controlling design strip load for rupture of the reinforcement was 23.531 kN (5.29 kips) for the uppermost layer and 4.092 kN (0.92 kips) for the second layer.

The dynamic pressure per strip for rupture of the reinforcement was calculated as shown in Table 7.5. For 2.44 m (8 ft)

Table 7.5. Test results and calculation of design strip load for breaking design.

Layer	(1) Measured Dynamic Load* (kips)		(2) Static** (kips)		(1)+(2)=(3) Total (kips)		(4) Calculated Resistance** (kips)		Controlling Design Dynamic Load (kips)
	8 ft	16 ft	8 ft	16 ft	8 ft	16 ft	8 ft	16 ft	
Top	1.64	5.29	0.569	0.853	2.209	6.143	9.23†	9.23	5.29
Second	0.92	0.06	1.095	1.642	2.015	1.702	9.23	9.23	0.92

* Adjusted for 54 kips design impact load
** Calculated from AASHTO Section 11.10.6.4.3
† Reinforcing steel is ASTM Grade 60.

long strip with a density of three strips per panel per layer, the tributary area was 0.37 m^2 (3.94 ft^2 = 4.87 ft × 2.43 ft/3 strips per panel). For 4.88 m (16 ft) long strip with a density of two strips per panel per layer, the tributary area was 0.41 m^2 (4.38 ft^2 = 4.87 ft × 1.8 ft/2 strips per panel). The dynamic design pressure in excess of static earth pressure to consider in the design against rupture of the reinforcement was calculated as shown in Table 7.6. The dynamic design pressure for rupture of the reinforcement is recommended to be 57.456 kPa (1,200 psf) for the uppermost layer and 11.01 kPa (230 psf) for the second layer as show in Figure 7.7.

Table 7.6. Design load on the strip for breaking design.

Layer	Total Design Pressure, *p* (psf)
Top	5.29 kips / 4.38 ft^2 * = **1,208 psf**
Second	0.92 kips / 3.94 ft^2 ** = **224 psf**

* Tributary area of a panel for the top layer (4.38 ft^2 = 4.87 ft × 1.8 ft / 2 strips per panel)
** Tributary area of a panel for the second layer (3.94 ft^2 = 4.87 ft × 2.43 ft / 3 strips per panel)

CHAPTER 8

Summary and Conclusions

8.1 Summary of Studies and Tests

8.1.1 Study of Barrier Stability

A set of static and dynamic analytical calculations representing increasing levels of complexity were developed. One static load test and two impact tests were performed on a full-scale barrier. Comparison between the analytical results and the results of the three full-scale barrier tests show good agreement. In this study, overturning occurred before sliding. This outcome was shown analytically and confirmed by the full-scale static and dynamic test results. However, both criteria should be checked.

There is a significant ratio between the static load and the dynamic load that the barrier can resist. For the 3.05 m (10 ft) barrier tested, the ultimate static load was 40.5 kN (9.1 kips). For the same barrier, the maximum dynamic load in a 20.9 km/h (13 mph) impact test was 189 kN (42.5 kips), which gives a dynamic to static ratio of 4.7. The maximum dynamic load in an 18 mph impact test was 240 kN (54 kips) for a dynamic to static ratio of 5.9. This ratio is due to the inertial resistance of the system.

These ratios use a static load and a dynamic load that do not correspond to the same amount of displacement. If a tolerable barrier displacement of 25 mm (1 in.) is targeted, then the static load is still 40.5 kN (9.1 kips) but the dynamic load drops to 170 kN (38.2 kips) for the 13 mph impact test (dynamic to static ratio of 4.2) and to 210 kN (47.2 kips) for the 18 mph impact test (dynamic to static ratio of 5.2).

The static load resisted by the dead weight (excluding soil shear strength) of the 3.05 m (10 ft) long barrier is 22.8 kN (5.1 kips). Therefore, for a barrier to resist an equivalent static design load of 44.5 kN (10 kips) with a factor of safety of 1.5, it needs to be at least 9.15 m (30 ft) long.

8.1.2 Pullout Tests on the Reinforcement

A series of pullout tests were performed to evaluate the influence of rate effect on the pullout capacity of the reinforcement. Ten tests were conducted: seven on steel reinforcement strips and three on steel bar mats.

A load–displacement curve was obtained for each test. The data indicate that there is no particular trend in the effect of the rate of loading. The pullout resistance at the fastest rate is often equal to the resistance at slower rates. Therefore, these tests are an indication that there is no reason to take into account any rate effect on the pullout capacity of the reinforcement during a barrier impact event.

The present AASHTO recommendations for calculating the resistance of MSE wall reinforcement to static loading lead to a predicted reinforcement resistance smaller or equal to the actual reinforcement resistance under impact loading (safe condition). On the basis of these few tests, it is suggested that the current AASHTO recommendations be used as-is to calculate the resistance of the reinforcement to impact loads.

8.1.3 Study of 5 ft MSE Wall and Barrier

Four reference tests were conducted as summarized in Table 8.1. The impact speeds of the bogie vehicle varied from 32.5 km/h (20.2 mph) to 35.08 km/h (21.8 mph). The barrier types used were an 812.8 mm (32 in.) tall N.J. shape barrier (Test 1) and a 685.8 mm (27 in.) tall vertical wall barrier (Tests 2 through 4). Wall reinforcement types included 4.88 m (16 ft) steel strips at a density of four per panel (Tests 1 and 4), 2.43 m (8 ft) bar mat (Test 2), and 2.43 m (8 ft) steel strips at a density of six per panel (Test 3).

The maximum 50 msec average impact load on the barriers varied from 286.55 kN (64.42 kips) to 326.5 kN (73.4 kips) and are all higher than the 240 kN (54 kips) dynamic force associated with the design of barriers for AASHTO TL-3 and TL-4 levels.

Table 8.1 presents the dynamic and permanent deflection at the top and bottom of the barrier and at the upper and lower layer of reinforcement. Even though the wall systems were subjected to loads higher than design conditions, all movements were considered acceptable from a performance point

Table 8.1. Bogie test and TL-3 test results.

		Stability Test 1	Stability Test 2	Bogie Test 1	Bogie Test 2	Bogie Test 3	Bogie Test 4	TL-3
Test Installation	Barrier Type	27 in. tall Vertical Wall	27 in. tall Vertical Wall	32 in. tall New Jersey	27 in. tall Vertical Wall	27 in. tall Vertical Wall	27 in. tall Vertical Wall	32 in. tall Vertical Wall
	Reinforcement	NA	NA	16 ft long Strip (4 per panel)	8 ft long Bar Mat	8 ft long Strip (6 per panel)	16 ft long Strip (4 per panel)	10 ft long Strip (6 per panel)
	Speed of Bogie	13 mph	18 mph	21.8 mph	20.3 mph	20.19 mph	20.19 mph	63.2 mph
Test Results								
Peak Acceleration	Bogie or Truck	-8.5 g	-10.9 g	-14.45 g	-13 g	-13.82g	-12.69 g	-6.5 g (long.) 15.67 g (lateral)
	Barrier	2.8 g	2.5 g	7.36 g	10.71 g	10.16 g	13.04 g	1.5 g
	Moment Slab	2.2 g	3.9 g	1.84 g	N/A	1 g	N/A	0.52 g
Impact Force		42.5 kips	54.1 kips	73.4 kips	66.1 kips	70.17 kips	64.42 kips	83.3 kips
Displacement Top of Barrier								
	Dynamic	4.9 in.	7.81 in.	6.14 in.	6.04 in.	5.17 in.	6.02 in.	0.86 in.
	Permanent	2.4 in.	4.02 in.	3.0 in.	4.0 in.	2.5 in.	3.0 in.	0.37 in.
	Bottom of Coping							
	Dynamic	0.3 in.	0.32 in.	1.12 in.	0.93 in.	1.16 in.	0.69 in.	0.55 in.
	Permanent	0 in.	0.1in.	0.55 in.	0.5 in.	0.6 in.	0.22 in.	0.68 in.
	Panel (Upper Layer)							
	Dynamic	N/A	N/A	0.63 in.	0.37 in.	0.92 in.	0.3 in.	0.42 in.
	Permanent	N/A	N/A	0.24 in.	0.2 in.	0.55 in.	0.07 in.	0.16 in.
	Panel (Second Layer)							
	Dynamic	N/A	N/A	0.0 in.	0.1 in.	0.19 in.	0.07 in.	0.26 in.
	Permanent	N/A	N/A	0.0 in.	0.02 in.	0.18 in.	0.0 in.	0.04 in.
Loads in Strip Upper Layer								
	Max. 50-msec	N/A	N/A	7.19 kips	1.54 kips	2.13 kips	7.46 kips	1.94 kips
	Design Load	N/A	N/A	5.29 kips	1.68 kips	1.64 kips	6.25 kips	N/A
	Design Load (kip/ft)	N/A	N/A	2.15 kip/ft	1.023 kip/ft	1.01 kip/ft	2.57 kip/ft	N/A
	Second Layer							
	Max. 50-msec	N/A	N/A	-1.2 kips	0.08 kips	1.19 kips	0.15 kips	0.66 kips
	Design Load	N/A	N/A	-0.88 kips	0.083 kips	0.92 kips	0.13 kips	N/A
	Design Load (kip/ft)	N/A	N/A	-0.36 kip/ft	0.05 kips/ft	0.57 kips/ft	0.05 kips/ft	N/A

of view. The wall system with the 2.44 m (8 ft) strip reinforcement (Test 3) had the highest panel movements, while the lowest movements were recorded for the configuration that incorporated 4.88 m (16 ft) strips and the vertical wall barrier (Test 4). However, the Test 4 configuration also had the most extensive panel damage. In this test, the top panel exhibited a horizontal flexure crack along a line corresponding to the location of the top layer of reinforcement.

8.1.4 Study of 10 ft MSE Wall and Barrier

The roadside barrier mounted on the edge of the MSE wall performed acceptably according to the evaluation criteria specified for MASH test designation 3-11. The roadside barrier on the MSE wall contained and redirected the 2270P vehicle. The vehicle did not penetrate, underride, or override the installation. No lateral movement of the barrier was noted. No detached elements, fragments, or other debris was present to penetrate or show potential for penetrating the occupant compartment or to present a hazard to others in the area. Maximum occupant compartment deformation was 53.3 mm (2.1 in.) in the lateral area across the cab. The 2270P vehicle remained upright during and after the collision. Maximum roll was 39 degrees. Occupant risk factors were within the limits specified in MASH. Test results are presented in Table 8.1.

8.2 Conclusions

Traffic barriers that can resist vehicle impact without being tied to a structure are needed at the top of MSE walls. These barriers are usually constructed in an L shape so that the impact load on the vertical part of the L can be resisted by the inertia force required to uplift the horizontal part of the L. The design load for such barriers has changed from 44.5 kN (10 kips) to 240 kN (54 kips) over the last decade. This jump has created concern about which load should be used.

A design procedure was developed for roadside barrier systems mounted on the edge of a MSE wall. Three components of the structural system are addressed in the design procedure: the barrier–moment slab system, the wall reinforcement, and the wall panel. The stability of the barrier system was investigated using static and dynamic analytical solutions, full-scale

static and dynamic impact load tests, and numerical modeling. It was determined that barrier stability can be satisfied using static equilibrium analyses with an equivalent static load of 44.5 kN (10 kips). Using the dynamic barrier load of 240 kN (54 kips) is appropriate for the strength design of the barrier but will result in an overly conservative design of the moment slab.

Guidelines for MSE wall reinforcement subject to a barrier impact were desired from reinforcement pullout tests, full-scale impacts of barrier systems mounted on an MSE test wall, and numerical modeling. No influence of rate effects was found in the reinforcement pullout tests. Therefore, conventional reinforcement design procedures are appropriate for determining the dynamic pullout resistance of the wall reinforcement. In the dynamic bogie vehicle impact tests, the barrier systems were loaded to failure. While the barriers sustained significant damage, the overall behavior of the wall was satisfactory. The displacements of the wall panels were acceptable, and there was no panel damage observed except for a longitudinal failure crack in one panel at the upper layer of reinforcement in one of the test configurations with 4.88 m (16 ft) long strips. The loads measured in the reinforcement indicate that the reinforcement was brought to its ultimate pullout capacity. However, because the impact duration was so short and the displacements were within tolerable limits, this is considered acceptable. The measured maximum dynamic loads in the strips were found to be 3 to 5 times higher than the calculated maximum static loads by AASHTO LRFD guidelines. The measured loads were therefore factored to coincide with current design practice. Pressure diagrams and line loads were developed for the dynamic loads that should be considered in the reinforcement.

The full-scale dynamic bogie impact tests and dynamic impact simulations were used to develop design guidelines for the wall panels to resist the moment applied during a barrier impact. The guidelines define recommended design loads due to the increased load in the reinforcement and the contact forces transmitted into the wall panel from direct bearing of the barrier–coping system as appropriate.

A full-scale vehicle crash test into a vertical wall barrier mounted on the edge of a 2.74 m (9 ft) tall MSE wall was performed to verify the guidelines. The barrier system performed acceptably and met the evaluation criteria of MASH. Damage and displacement of the barrier system and underlying MSE wall were minimal.

The resulting guidelines are presented in Chapter 7 of this report. They were developed following AASHTO LRFD design practices and consider two different points of bearing and rotation of the barrier system. One point of rotation is applicable if the wall panels are isolated from contact with the coping by presence of a suitable air gap or sufficiently compressible material. The other point of rotation addresses the scenario of direct bearing of the barrier–coping system on top of the wall panels.

The design procedures for the barrier system address sliding, overturning, and structural adequacy of the coping and wall panel. The reinforcement design procedure considers pullout and rupture of the reinforcement. The dynamic design loads are specified using both a pressure distribution approach and a line load approach.

References

1. *Standard Specifications for Highway Bridges,* 17th Edition. American Association of State Highway and Transportation Officials, Washington, D.C., 2002.
2. *AASHTO LRFD Bridge Design Specifications,* Third Edition. American Association of State Highway and Transportation Officials, Washington, D.C., 2004.
3. Ross, H. E., D. L. Sicking, R. A. Zimmer, and J. D. Michie, *NCHRP Report 350: Recommended Procedures for the Safety Performance Evaluation of Highway Features.* Transportation Research Board, Washington, D.C., 1993.
4. Elias, Victor, Barry R. Christopher, and Ryan R. Berg, *Mechanically Stabilized Earth Walls and Reinforced Soil Slopes Design and Construction Guidelines.* Ryan R. Berg & Associates, Inc., Woodbury, Minn.; National Highway Institute, Federal Highway Administration, U.S. Department of Transportation, Washington, D.C., 2001.
5. Committee on Guardrails and Guide Posts, "Proposed Full-Scale Testing Procedures for Guardrails," *Highway Research Correlation Service Circular 482.* Highway Research Board, Washington, D.C., 1962.
6. Bronstad, M. E., and J. D. Michie, *NCHRP Report 153: Recommended Procedures for Vehicle Crash Testing of Highway Appurtenances.* Transportation Research Board, National Research Council, Washington, D.C., 1974.
7. *Transportation Research Circular 191: Recommended Procedures for Vehicle Crash Testing of Highway Appurtenances.* Transportation Research Board, National Research Council, Washington, D.C., 1978.
8. Michie, J. D., *NCHRP Report 230: Recommended Procedures for the Safety Performance Evaluation of Highway Appurtenances.* Transportation Research Board, National Research Council, Washington, D.C., 1981.
9. Improvement of Procedures for Safety-Performance Evaluation of Roadside Features, American Association of State Highway and Transportation Officials, Washington, D.C., 2008.
10. *Manual for Assessing Safety Hardware.* American Association of State Highway and Transportation Officials, Washington, D.C., 2009.
11. *Standard Specifications for Highway Bridges,* Ninth Edition. American Association of State Highway and Transportation Officials, Washington, D.C., 1965.
12. Noel, J. S., T. J. Hirsch, C. E. Buth, and A. Arnold, "Loads on Bridge Railings," *Transportation Research Record 796.* Transportation Research Board, National Research Council, Washington, D.C., 1981, pp. 31–35.
13. Beason, W. L., and T. J. Hirsch, *Measurement of Heavy Vehicle Impact Forces and Inertia Properties,* Research Report. Texas Transportation Institute, College Station, Tex., 1989.
14. *AASHTO Guide Specifications for Bridge Railings,* American Association of State Highway and Transportation Officials, Washington, D.C., 1989.
15. Buth, C. E., A. Arnold, W. L. Camprise, T. J. Hirsch, D. L. Ivey, and J. S. Noel, *Safer Bridge Railings, Volume 1: Summary Report,* Report No. FHWA/RD-82/072. Federal Highway Administration, U.S. Department of Transportation, Washington, D.C., 1984.
16. *AASHTO LRFD Bridge Design Specifications,* First Edition. American Association of State Highway and Transportation Officials, Washington, D.C., 1996.
17. Alberson, D. C., W. F. Williams, W. L. Menges, and R. R. Haug, *Testing and Evaluation of the Florida Jersey Safety Shaped Bridge Rail,* Research Report 9-8132-1. Texas Transportation Institute, College Station, Tex., 2004.
18. *Crash Testing of a Precast Traffic Barrier Atop a Reinforced Earth Wall: Technical Bulletin: MSE-8,* The Reinforced Earth Company, 1995.
19. *Standard Specifications for Highway Bridges,* 15th Edition. American Association of State Highway and Transportation Officials, Washington, D.C., 1992.
20. Hallquist, J. O., *LS-DYNA: Keyword User's Manual, Version 971,* Livermore Software Technology Corporation (LSTC), Livermore, Calif., 2007.
21. Beer, F. P., and E. R. Johnston, *Vector Mechanics for Engineers: Dynamics,* Seventh Edition. McGraw-Hill, New York, 2004.
22. Lee, H. S., and A. Bobet, *Design of MSE Walls for Fully Saturated Conditions.* Report No. FHWA-IN-JTRP-2002/13 for the Joint Transportation Research Program, Washington, D.C., 2002.
23. *Apparent Coefficient of Friction, f* to be Used in the Design of Reinforced Earth Structures: Technical Bulletin: MSE-6,* The Reinforced Earth Company, 1995.
24. Murray, Y. D., *Users Manual for LS-DYNA Concrete Material Model 159,* Publication FHWA-HRT-05-062. Federal Highway Administration, U.S. Department of Transportation, 2007
25. Desai, D. S., and H. J. Siriwardane, *Constitutive Laws for Engineering Materials with Emphasis on Geologic Materials.* Prentice-Hall, Inc., N.J., 1984.
26. Chen, W. F., and E. Mizuno, *Nonlinear Analysis in Soil Mechanics, Theory and Implementation.* Elsevier, 1990.

27. Hofstetter, G., J. C. Simo, and R. L. Taylor, "A Modified Cap Model: Closest Point Solution Algorithms," *Computers & Structures,* Vol. 46, No. 2, 1993, pp. 203–214.
28. Wu, J. T. H., K. Z. Z. Lee, S. B. Helwany, and K. Ketchart, *NCHRP Report 556: Design and Construction Guidelines for Geosynthetic-Reinforced Soil Bridge Abutments with a Flexible Facing.* Transportation Research Board of the National Academies, Washington, D.C., 2006.
29. ACI 318-08: Building Code Requirements for Structural Concrete and Commentary, American Concrete Institute, 2008.
30. *Standard Specifications for Construction and Maintenance of Highways, Streets, and Bridges,* Texas Department of Transportation, 2004.
31. Briaud, J.-L., Y. Li , and K. Rhee, "BCD: A Soil Modulus Device for Compaction Control," *Journal of Geotechnical and Geoenvironmental Engineering,* Vol. 132, No. 1, 2006.

APPENDICES A THROUGH H

Appendices A through H are available on the *NCHRP Report 663* summary web page on the TRB website. To find them, go to www.trb.org and search for "NCHRP Report 663". Titles of Appendices A through H are as follows:

Appendix A: Design of MSE Wall
Appendix B: State-of-Practice Survey
Appendix C: Detailed Drawing of MSE Wall for Bogie Test
Appendix D: Bogie Test MSE Wall Construction Procedure
Appendix E: Detailed Drawing of MSE Wall for TL-3 Test
Appendix F: TL-3 MSE Wall Construction Procedure
Appendix G: Crash Test Vehicle Properties and Information
Appendix H: Crash Test Sequential Photographs

APPENDIX I

AASHTO LRFD Format Design Guideline

SECTION 1

DESIGN GUIDELINES

1.1 SCOPE

This section provides guidelines to design three components: the barrier–moment slab, the MSE wall reinforcement, and the wall panel.

The guidelines are applicable for TL-3 and TL-4 criteria as defined in Section 13 of AASHTO LRFD *Bridge Design Specifications*, and for inextensible MSE wall reinforcement (e.g., strips, bar mats)

Depending on the design, two points of rotation are possible as shown in Figure 1.1. The point of rotation should be determined based on the interaction between the barrier coping and top of the wall panel. With reference to Figure 1.1, the point of rotation should be taken as Point A if the top of the wall panel is isolated from contact with the coping by the presence of an air gap or a sufficiently compressible material. The point of rotation should be taken as Point B if there is direct bearing between the bottom of the coping and the top of the wall panel or level-up concrete.

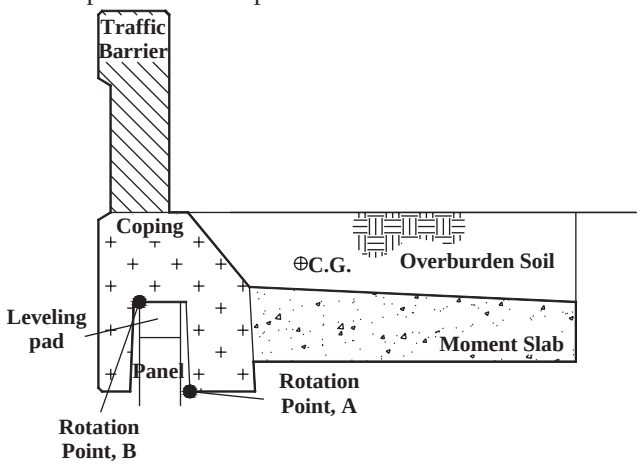

Figure 1.1. Barrier–moment slab system for design guideline.

1.2 DEFINITIONS

Rotation Point A—The rotation point of a barrier–moment slab system if the top of the wall panel is isolated from contact with the coping by the presence of an air gap or a sufficiently compressible material as shown in Figure 1.1.

Rotation Point B—The rotation point of a barrier–moment slab system if there is direct bearing between the bottom of the coping and the top of the wall panel or level-up concrete as shown in Figure 1.1.

1.3 NOTATION

H = horizontal shear load on top of the panel (kips)
h_a = moment arm taken as the vertical distance between the point of impact of the dynamic force and the point of rotation A (ft)
h_b = moment arm taken as the vertical distance between the point of impact of the dynamic force and the point of rotation B (ft)
h_c = moment arm taken as the vertical distance between the point of impact of the dynamic force and the middle of the weakest section of the coping (ft)
L_d = dynamic load (kips)
L_s = static load equivalent to the dynamic impact force (kips)
l = vertical distance from the top of the panel to the uppermost reinforcement layer (ft)
l_A = horizontal distance from the center of gravity of the weight to the point of rotation A (ft).
l_B = horizontal distance from the center of gravity of the weight to the point of rotation B (ft).
M = static moment resistance to overturning of the barrier–moment slab system (kips-ft)
M_d = Ultimate moment resistance of the coping of the barrier–moment slab system in bending (kips-ft)
M_i = moment applied to the panel during impact (kips-ft)
M_u = ultimate moment resistance of the wall panel (kips-ft)
P = static resistance to sliding of the barrier–moment slab system (kips)
P_r = static resistance to pullout of the reinforcement (kips)
p_d = dynamic pressure diagram for pullout or rupture of the reinforcement (psf)
Q_d = dynamic line load diagram for pullout or rupture of the reinforcement (lb/ft)
R = resistance for rupture of the reinforcement (kips)
t = thickness of the panel (ft)
V = vertical load transferred from the barrier to the panel during the impact (kips)
W = weight of the monolithic section of barrier and moment slab between joints plus any material laying on top of the moment slab (kips)
γ = load factors
ϕ = resistance factors
ϕ_r = friction angle of the soil–moment slab interface (°)
ϕ_s = friction angle of the soil (°)
σ_v = vertical soil stress (ksf)

1.4 GUIDELINES FOR THE BARRIER

1.4.1 General

The barrier, the coping, and moment slab should be safe against structural failure. Any section along the coping and moment slab should not fail in bending when the barrier is subjected to the design impact load. Two modes of stability failure are possible in addition to structural failure of the barrier system. They are sliding and overturning of the barrier–moment slab system.

The equivalent static load defined in this section should be used for sizing the moment slab. The design for structural capacity of the barrier, coping, and moment slab should follow the design recommended in Section 13 of *AASHTO LRFD Bridge Design Specifications* including the loads.

Width of moment slabs should range between 4.5 ft to 10 ft. Length of moment slabs should range between 20 ft to 60 ft. Dimensions outside these ranges can be used provided it is shown that sufficiently rigid body behavior is achieved.

C1.4.1

Much of the knowledge and experience with MSE structures and traffic barriers have been with design as specified in Sections 11 and 13 of *AASHTO LRFD Bridge Design Specifications*.

In these recommendations it is assumed that a barrier–moment slab design would generate 1 in. movement or less at the top of the barrier during impact. This 1 in. dynamic movement is considered acceptable as it would likely require little or no repair and should not affect the impact performance of the barrier system.

1.4.2 Sliding of the Barrier

The factored static resistance (ϕP) to sliding of the barrier–moment slab system along its base should satisfy the following condition (Figure 1.4.1):

$$\phi P \geq \gamma L_s \qquad (1.4.2\text{-}1)$$

L_s = equivalent static load (10 kips)

ϕ = resistance factor (0.8) (*AASHTO LRFD Bridge Design Specifications* Table 10.5.5-1)

γ = load factor (1.0) [extreme event]

P = static resistance (kips)

The static force (P) should satisfy the following condition:

$$P = W \tan \phi_r \qquad (1.4.2\text{-}2)$$

where:

W = weight of the monolithic section of barrier and moment slab between joints (with an upper limit of 60 ft) plus any material laying on top of the moment slab

ϕ_r = friction angle of the soil–moment slab interface (°)

C1.4.2

The equivalent static load should be applied to the length of the moment slab between joints. Any coupling between adjacent moment slabs or friction that may exist between free edges of the moment slab and the surrounding soil should be neglected.

If the soil–moment slab interface is rough (e.g., cast in place), ϕ_r is equal to the friction angle of the soil ϕ_s. If the soil–moment slab interface is smooth (e.g., precast), ϕ_r should be reduced accordingly $\left(\frac{2}{3}\tan\phi_s\right)$.

1.4.3 Overturning of the Barrier

The factored static moment resistance (ϕ M) of the barrier–moment slab system to overturning should satisfy the following condition (Figure 1.4.1):

$$\phi M \geq \gamma L_s (h_A \text{ or } h_B) \quad (1.4.3\text{-}3)$$

where:

L_s = equivalent static load (10 kips)

ϕ = resistance factor (0.9)

γ = load factor (1.0) [extreme event]

h_a = moment arm taken as the vertical distance from the point of impact due to the dynamic force to the point of rotation A

h_b = moment arm taken as the vertical distance from the point of impact due to the dynamic force to the point of rotation B

M = static moment resistance (kips-ft)

M should be calculated as:

$$M = W (l_A \text{ or } l_B) \quad (1.4.3\text{-}4)$$

where:

W = weight of the monolithic section of barrier and moment slab plus any material laying on top of the moment slab

l_A = horizontal distance from the center of gravity of the weight W to the point of rotation A

l_B = horizontal distance from the center of gravity of the weight W to the point of rotation B

1.4.4 Design of the Coping

The critical section of the coping must be designed to resist the applicable impact load conditions for the appropriate test level as defined in Section 13 of *AASHTO LRFD Bridge Design Specifications* (Figure 1.4.2).

The moment contribution due to any coupling between adjacent moment slabs, shear strength of the overburden soil, or friction which may exist between the backside of the moment slab and the surrounding soil should be neglected.

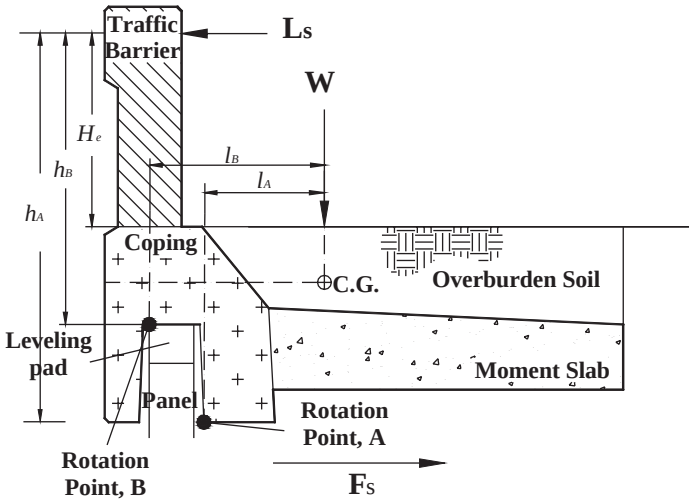

H_e = effective height of the impact force (*AASHTO LRFD Bridge Design Specifications Figure A13.2-1).*

Figure 1.4.1. Barrier–moment slab system for barrier design guideline (sliding and overturning).

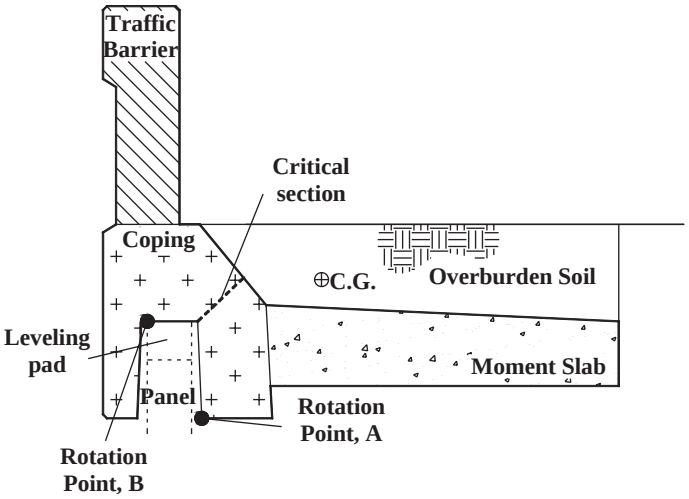

Figure 1.4.2. Coping and possible critical section.

1.5 GUIDELINES FOR THE SOIL REINFORCEMENT

1.5.1 General

The reinforcement guidelines should ensure that the reinforcement does not pullout or break during the impact of the chosen vehicle.

C1.5.1

In this section, the recommendations for the load in the reinforcement due to the impact are based on a pressure diagram and line load diagram back calculated by using the design loads in excess of static earth pressure loads recorded in the tests.

The design load for pullout is different from the design load for rupture. The reason is that the design load for pullout is an equivalent static load while the design load for rupture is a measured dynamic load.

1.5.2 Pullout of the Soil Reinforcement

1.5.2.1 Pressure distribution approach

The factored ultimate static resistance (ϕP_r) to pullout of the reinforcement should satisfy the following condition:

$$\phi P_r \geq \gamma_s p_s A_t + \gamma_d p_d A_t \qquad (1.5.2\text{-}1)$$

where,

ϕ = resistance factor (1.0)

γ_s = load factor for static load (1.0)

p_s = static earth pressure

A_t = the tributary area of the reinforcement unit

p_d = dynamic pressure distribution to pullout of the reinforcement (Figure 1.5.1)

γ_d = load factor for dynamic load (1.0)

C1.5.2.1

The reinforcement resistance (P_r) should be calculated by the equation shown in AASHTO LRFD Section 11.10.6.3.2.

The traffic surcharge should not be added as it is already included in the measured load during the experiments.

1.5.2.2 Line load approach

The factored static resistance (ϕP_r) to pullout of the reinforcement should satisfy the following condition:

$$\phi P_r \geq \gamma_s p_s A_t + \gamma_d Q_d S_L \qquad (1.5.2\text{-}2)$$

where,

ϕ = resistance factor (1.0)

γ_s = load factor for static load (1.0)

p_s = static earth pressure

A_t = the tributary area of the reinforcement unit

C1.5.2.2

The reinforcement resistance (P_r) should be calculated by the equation shown in AASHTO LRFD Section 11.10.6.3.2.

γ_d = load factor for dynamic load (1.0)

Q_d = dynamic line load to pull out of the reinforcement (Figure 1.5.2)

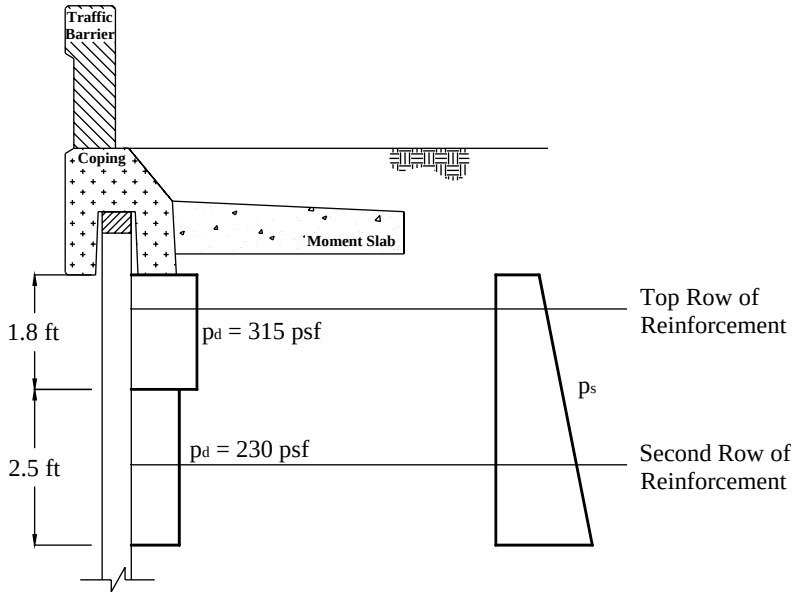

Figure 1.5.1. Pressure distribution (p_d) for reinforcement pullout.

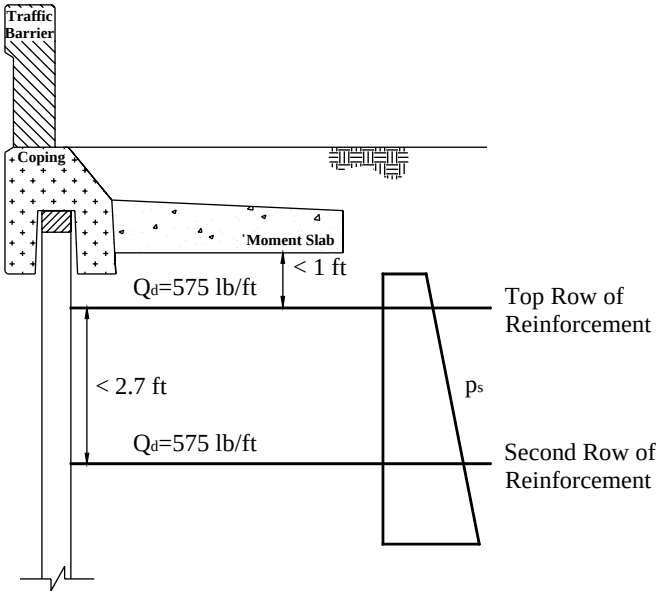

Figure 1.5.2. Line load (p_d) for reinforcement pullout.

1.5.3 Rupture of the Soil Reinforcement

C1.5.3

In this section, the recommendations for the load in the reinforcement due to the impact are based on a pressure diagram and line load diagram back calculated by using the design loads in excess of static earth pressure loads recorded in the tests.

1.5.3.1 Pressure distribution approach

C1.5.3.1

The factored resistance (ϕR) to rupture of the reinforcement should satisfy the following condition:

The factored resistance (ϕR) to rupture of the reinforcement is specified in Article 11.10.6.4.

The cross section of the reinforcement can be subject to corrosion in the long term, depending on the expected time of burial and the composition of the soil, sand, or aggregate. (AASHTO LRFD Section 11.10.6.4.2).

$$\phi R \geq \gamma_s p_s A_t + \gamma_d p_d A_t + \gamma_{LL} p_{LL} A_t \quad (1.5.3\text{-}1)$$

where,

ϕ = resistance factor (1.0)

γ_s = load factor for static load (1.0)

p_s = static earth pressure

A_t = the tributary area of the reinforcement unit

p_d = dynamic pressure distribution to rupture of the reinforcement (Figure 1.5.3)

γ_d = load factor for dynamic load (1.0)

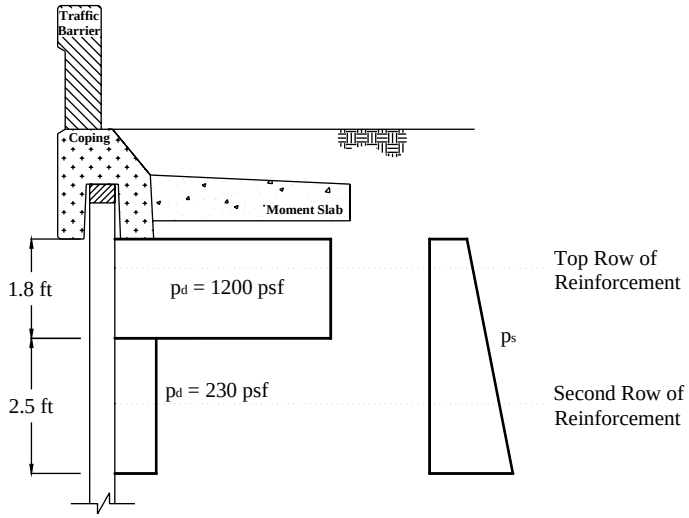

Figure 1.5.3. Pressure diagram (p_d) for reinforcement rupture.

1.5.3.1 Line load approach

C1.5.3.2

The factored resistance (ϕR) to rupture of the reinforcement should satisfy the following condition:

The resistance (ϕR) to rupture of the reinforcement should be calculated by the equation shown in AASHTO LRFD Section 11.10.6.4.

The cross section of the reinforcement can be subject to corrosion in the long term, depending on the

$$\phi R \geq \gamma_s p_s A_t + \gamma_d Q_d S_L + \gamma_{LL} p_{LL} A_t \quad (1.5.3\text{-}2)$$

where,

ϕ = resistance factor (1.0)

γ_s = load factor for static load (1.0)

p_s = static earth pressure

A_t = the tributary area of the reinforcement unit

γ_d = load factor for dynamic load (1.0)

Q_d = dynamic line load to rupture of the reinforcement (Figure 1.5.4)

S_L = longitudinal spacing of the reinforcement unit

expected time of burial and the composition of the soil, sand, or aggregate. (AASHTO LRFD Section 11.10.6.4.2).

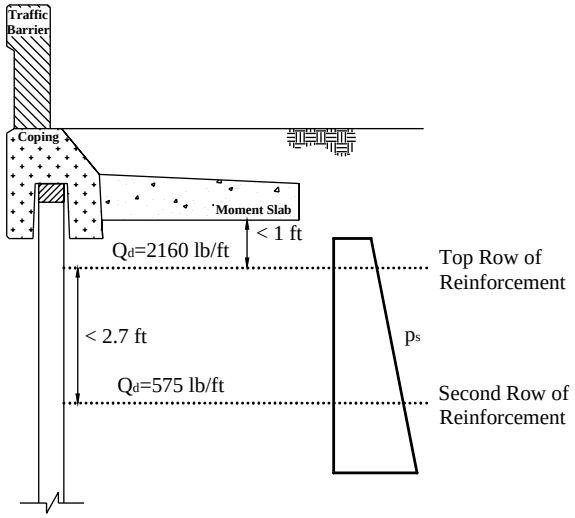

Figure 1.5.4. Line load (Q_d) for reinforcement rupture.

1.6 GUIDELINES FOR THE WALL PANEL

The wall panels must be designed to resist the dynamic pressure distributions defined in Figure 1.5.3, Section 1.5.3.1.

The wall panel should have sufficient structural capacity to resist the maximum design rupture load for the wall reinforcement.

The static load is not included because it is not located at the panel connection.

APPENDIX J

Example of Design Guideline

Design guideline for 10 ft high MSE wall with 10 ft long strips design

1. Guidelines for the barrier

1.1. Sliding

$\phi P \geq \gamma L_s$ → 25.91 kips > 10 kips → **OK**

$\gamma L_s = 1 \times 10$ kips = 10 kips
$P = W \tan \phi_r = 32.39$ kips → $\phi P = 0.8 \times 32.39$ kips = 25.91 kips

W = 56.1 kips for three 10 ft long barrier and one 30 ft long moment slab and overburden soil.
$\phi_r = 30$ assumed this is the same as retained fill → $\tan \phi_r = 0.58$

In order to obtain the weight of 30 ft long barrier-moment slab system, the detail calculation was conducted below.

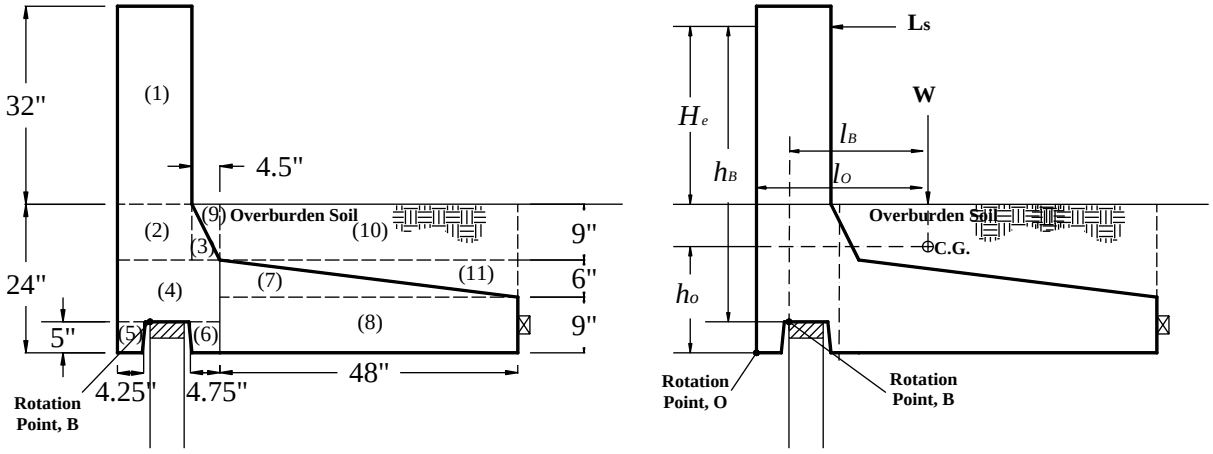

Figure J.1. Section of a barrier-moment slab system for calculation of sliding

Table J.1. Calculation of barrier-moment slab system weight

	Section	Longitudinal distance, x	Vertical distance, y	Area (in^2)	weight (k)	x from O	y from O	y*weight	x*weight
Barrier and Coping	1	12.00	32.00	384.0	12.00	6.00	40.00	480.00	72.00
	2	12.00	9.00	108.0	3.38	6.00	19.50	65.81	20.25
	3	4.50	9.00	20.25	0.63	13.50	18.00	11.39	8.54
	4	16.50	10.00	165.0	5.16	8.25	10.00	51.56	42.54
	5	4.25	5.00	21.25	0.66	2.13	2.50	1.66	1.41
	6	4.75	5.00	23.75	0.74	14.13	2.50	1.86	10.48
Moment Slab	7	48.00	6.00	144.0	4.50	32.50	11.00	49.50	146.25
	8	48.00	9.00	432.0	13.50	40.50	4.50	60.75	546.75
Soil	9	4.50	9.00	20.25	0.53	15.00	21.00	11.07	7.91
	10	48.00	9.00	432.0	11.25	40.50	19.50	219.38	455.63
	11	48.00	6.00	144.0	3.75	48.50	13.00	48.75	181.88
	Total			1894.5	56.10			1001.73	1493.64
	h_o and l_o =							17.86	26.63

1.2. Overturning

$\phi M \geq \gamma L_s h_B$ → 88.88 kips-ft > 35.83 kips-ft → **OK**

l_O = 17.86 in. and h_O = 26.63 in. from Table J-1 → l_B = 21.13 in. and h_B = 43.0 in.

$\gamma L_s h_B$ = 1 × 10 kips × 43 in. = 430 kips-in. = 35.83 kips-ft

M = W l_B = 56.1 kips × 21.13 in. = 1185.1 kips-in. = 98.76 kips-ft
ϕ M = 0.9 × 98.76 kips = 88.88 kips-ft

1.3 Rupture of the coping in bending (referred from AASHTO LRFD Section 5)

f_y = 60 ksi, f_c' = 4 ksi

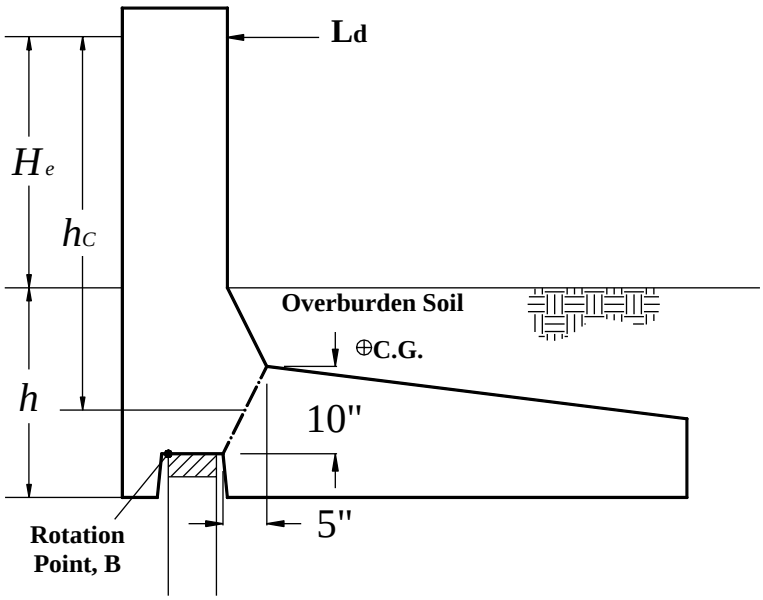

Figure J.2. A barrier-moment slab system for calculation of rupture of the coping in bending

$\phi M_{ult} \geq \gamma M_{impact}$ → 205.41 kip-ft > 171 kips-ft → **OK**

$\gamma M_{impact} = \gamma \times L_d \times h_c = 1 \times 54$ kips $\times$ 38 in. = 2052 kip-in. = 171 kips-ft

$\phi M_{ult} = \phi \left[A_s f_y d \left(1 - \frac{k}{2}\right)\right] = 0.9 \times [5.3 \text{ in}^2 \times 60 \text{ ksi} \times 9 \text{ in.} (1\text{-}0.08662/2)] = 2464.9$ kips-in.
= 205.41 kips-ft

$$k = \frac{A_s f_y}{0.85 f'_c bd} \quad \frac{5.3 \text{ in}^2 \times 60 \text{ ksi}}{0.85 \times 4 \text{ ksi} \times 10 \text{ ft} \times 9 \text{ in.}} = 0.08662$$

The thickness of the critical section on the coping = 11.18 in.
Use No. 6 bars at 10 in. o.c.

$d_b = 0.75$ in., $A_b = 0.44$ in^2, d = 11.18 in. -2 in. -0.38 in. = 8.81 in.
Therefore, use d = 9 in.

Impact is resisted by the 10 ft length of a barrier unit at the moment slab
A_s = 10 ft / 0.83 ft per bar $\times$ 0.44 in^2 = 5.3 in^2

2. Guidelines for the soil reinforcement

The traffic live load has been neglected in this example.
Please refer to Appendix A, Example 3 (pages A-15 to A-23) for detailed calculations of p_s (static earth pressure)

2.1. Pullout of the soil reinforcement

$\phi P \geq \gamma_s p_s A_t + \gamma_d p_d A_t + \gamma_{LL} p_{LL} A_t$

1) Top layer of reinforcement
$\phi P = 1 \times 2b \times L \times \sigma_v \times F^* = 2.052$ kips

$p_s A_t = 0.688$ kips (See Appendix A, Example 3)
$p_d A_t = 313$ psf $\times$ 2.92 ft^2 = 0.914 kips (using pressure diagram)
$\gamma_s p_s A_t + \gamma_d p_d A_t = 1 \times 0.688$ kips + 1×0.914 kips = 1.602 kips

$\phi P \geq \gamma_s p_s A_t + \gamma_d p_d A_t$ → 2.05 kips > 1.60 kips → **OK**

2) Second layer of reinforcement
$\phi P = 1 \times 2b \times L \times \sigma_v \times F^* = 3.413$ kips

$p_s A_t = 1.205$ kips (See Appendix A, Example 3)
$p_d A_t = 230$ psf $\times$ 3.993 ft^2 = 0.918 kips (using pressure diagram)
$\gamma_s p_s A_t + \gamma_d p_d A_t = 1 \times 1.205$ kips + 1×0.918 kips = 2.123 kips

$\phi P \geq \gamma_s p_s A_t + \gamma_d p_d A_t$ → 3.413 kips > 2.12 kips → **OK**

2.2. Rupture of the soil reinforcement

$\phi R \geq \gamma_s p_s A_t + \gamma_d p_d A_t + \gamma_{LL} p_{LL} A_t$

1) Top layer of reinforcement

$\phi R = \sigma_t A_s = \sigma_t \times b \times Ec = 60$ ksi $\times$ 50 mm $\times$ 1.984 mm = 9.226 kips
for 100 year corrosion

$p_s A_t = 0.688$ kips (See Appendix A, Example 3)
$p_d A_t = 1200$ psf $\times$ 3.993 ft^2 = 4.792 kips (using pressure diagram)
$\gamma_s p_s A_t + \gamma_d p_d A_t = 1 \times 0.688$ kips + 1×4.792 kips = 6.566 kips

$\phi R \geq \gamma_s p_s A_t + \gamma_d p_d A_t$ → 9.226 kips > 6.566 kips → **OK**

2) Second layer of reinforcement

$\phi R = \sigma_t A_s = \sigma_t \times b \times Ec = 60$ ksi $\times$ 50 mm $\times$ 1.984 mm = 9.226 kips
for 100 year corrosion

$p_s A_t = 1.205$ kips (See Appendix A, Example 3)
$p_d A_t = 230$ psf $\times$ 3.993 ft^2 = 0.918 kips (using pressure diagram)
$\gamma_s p_s A_t + \gamma_d p_d A_t = 1 \times 1.205$ kips + 1×0.918 kips = 2.123 kips

$\phi R \geq \gamma_s p_s A_t + \gamma_d p_d A_t$ → 9.226 kips > 2.123 kips → **OK**

3. Guidelines for the wall panels

3.1. Check Moment Stability

$\phi M_u \geq \gamma M_i$

3.1.1 Find M_u

b = 12 in. (unit length) $f_y = 60000$ psi h = 5.5 in.
$E_y = 29000000$ psi $f'_c = 4000$ psi d = 2.75 in.
$A_s = 0.22$ in^2

1) Cracking

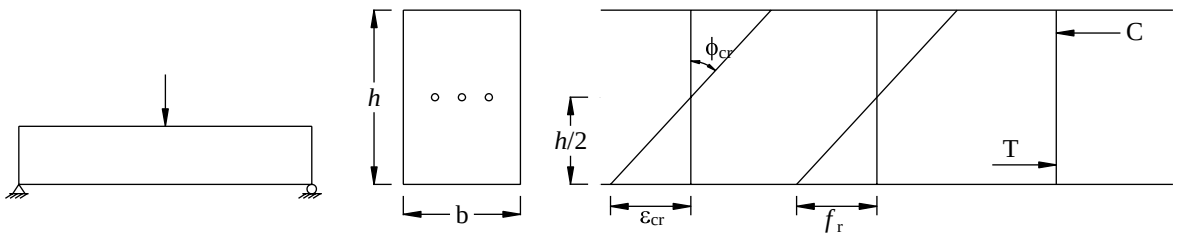

$M_{cr} = \frac{I_g f_r}{c_b} = \frac{166.38 \text{ in}^4 \times 474.34 \text{ psi}}{2.75 \text{ in.}} = 28697.67$ lbs-in/ft = 2.39 kips-ft/ft

I_g (2nd moment of area) = $bh^3/12 = 166.38$ in^4

$c_b = h/2 = 2.75$ in. $f_r = 7.5\sqrt{f'_c} = 474.34$ psi

$E_{cr} = 57000\sqrt{f'_c} = 3605$ ksi

$\varepsilon_{cr} = f_r/E_{cr} = 0.000132$ strain → $\phi_{cr} = \varepsilon_{cr}/c_b = 0.000574$ strain/ft

2) Yield

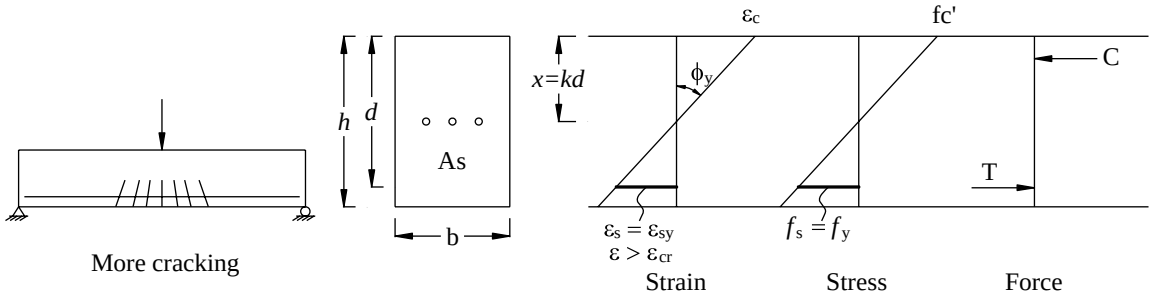

$M_n = A_s f_y d\left(1-\frac{k}{3}\right)$ = 0.22 in^2 × 60 ksi × 2.75 in × (1-0.21/3) = 33803.62 lbs-in/ft

= 2.82 kips-ft/ft

$\rho = A_s/A_c = 0.333\%$

$n = E_s/E_c = 8.04$ → $\rho n = 0.027$

$\kappa = \sqrt{(\rho n)^2 + 2\rho n} - \rho n = 0.21$

$\varepsilon_{cr} = f_r/E_s = 0.00207$ strain

$\phi_{cr} = \varepsilon_{cr}/(d - \kappa d) = 0.0114$ strain/ft

3) Ultimate

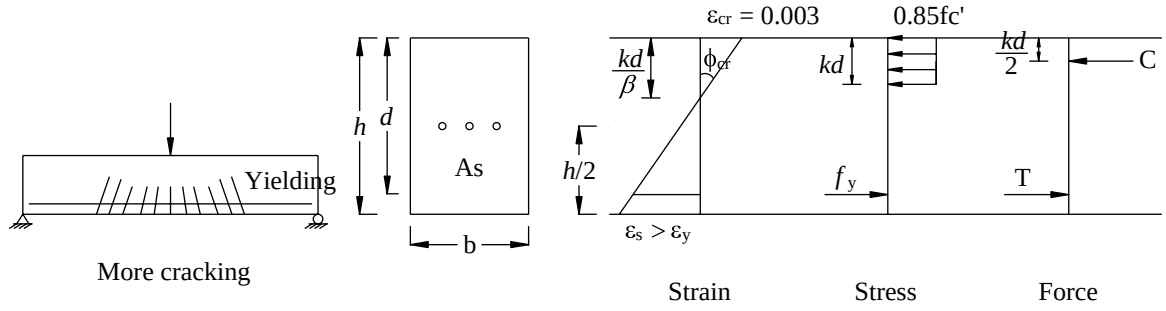

$M_n = A_s f_y d\left(1-\frac{k}{3}\right)$ = 0.22 in^2 × 60 ksi × 2.75 in × (1-0.1176/2) = 34,164.7 lbs-in/ft

= 2.85 kips-ft/ft

$$\kappa = \frac{A_s f_y}{0.85 f_c' bd} = \frac{0.22\ in^2 \times 60 ksi}{0.85 \times 4 ksi \times 12\ in. \times 2.75\ in.} = 0.1176$$

$\varepsilon_u = 0.003$ strain

$\beta_1 = 0.85$ → $\phi_u = \varepsilon_{cr}/(\kappa d/\beta_1) = 0.0946$ strain/ft

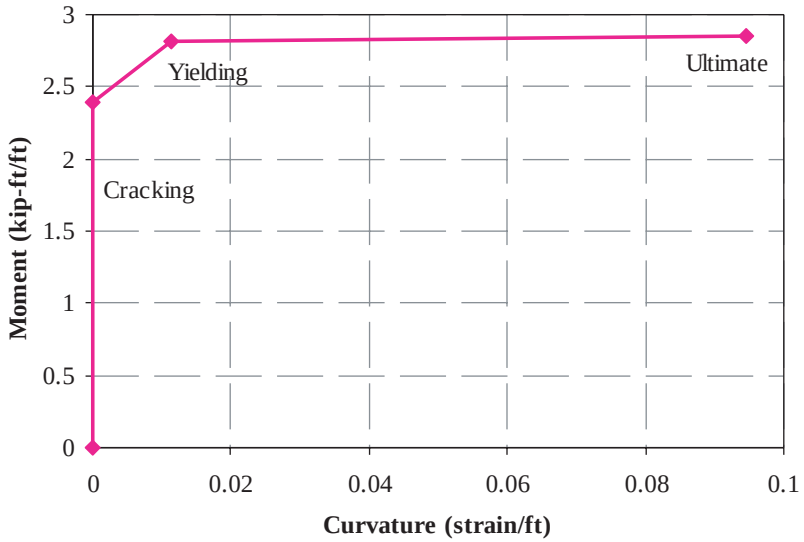

Figure J.3. Moment and curvature relationship for a wall panel

$\phi M_u = 0.9 \times 2.85$ kip-ft/ft = 2.56 kip-ft/ft

3.1.2 Find M_i

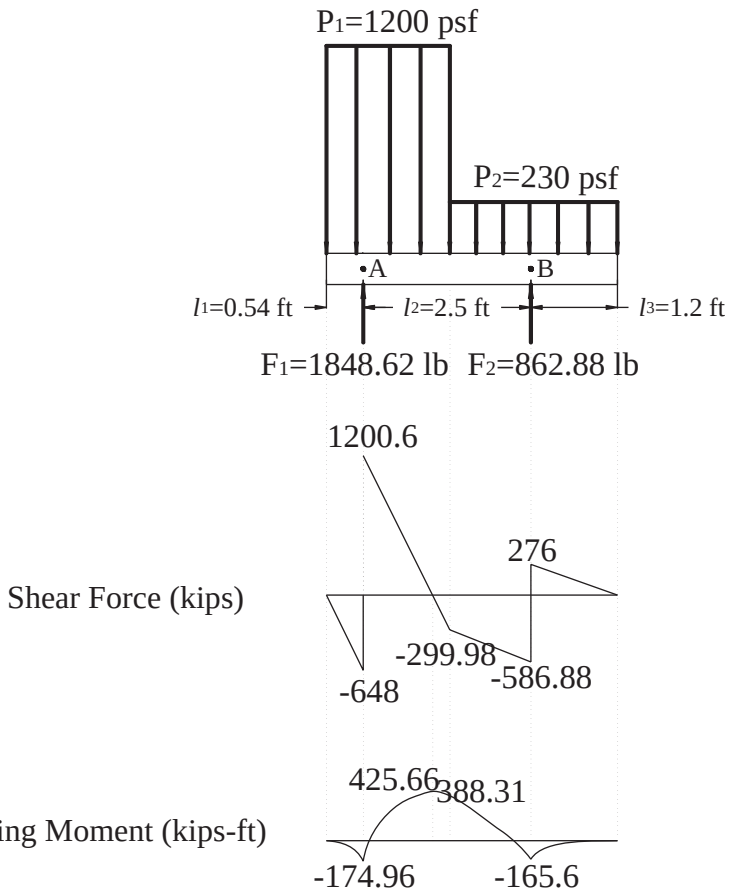

M_i has been selected maximum positive moment.

$\gamma M_i = 1 \times 0.43$ kips-ft/ft = 0.43 kip-ft/ft

$\phi M_u \geq \gamma M_i$ → 2.56 kip-ft/ft > 0.43 kip-ft/ft → **OK**

3.2. Check Shear Stability

$1/2\ \phi V_{ult} \geq V_{impact}$

$\phi V_{ult} = \phi 2\sqrt{f_c'} b_w d = 0.9 \times 2 \times 63.25 \times 12 \times 2.75 = 3756.79$ lbs = 3.76 kips

$1/2\ \phi V_{ult} = 1.88$ kips > $V_{impact} = 1.2$ kip → **OK**

Abbreviations and acronyms used without definitions in TRB publications:

AAAE	American Association of Airport Executives
AASHO	American Association of State Highway Officials
AASHTO	American Association of State Highway and Transportation Officials
ACI–NA	Airports Council International–North America
ACRP	Airport Cooperative Research Program
ADA	Americans with Disabilities Act
APTA	American Public Transportation Association
ASCE	American Society of Civil Engineers
ASME	American Society of Mechanical Engineers
ASTM	American Society for Testing and Materials
ATA	Air Transport Association
ATA	American Trucking Associations
CTAA	Community Transportation Association of America
CTBSSP	Commercial Truck and Bus Safety Synthesis Program
DHS	Department of Homeland Security
DOE	Department of Energy
EPA	Environmental Protection Agency
FAA	Federal Aviation Administration
FHWA	Federal Highway Administration
FMCSA	Federal Motor Carrier Safety Administration
FRA	Federal Railroad Administration
FTA	Federal Transit Administration
HMCRP	Hazardous Materials Cooperative Research Program
IEEE	Institute of Electrical and Electronics Engineers
ISTEA	Intermodal Surface Transportation Efficiency Act of 1991
ITE	Institute of Transportation Engineers
NASA	National Aeronautics and Space Administration
NASAO	National Association of State Aviation Officials
NCFRP	National Cooperative Freight Research Program
NCHRP	National Cooperative Highway Research Program
NHTSA	National Highway Traffic Safety Administration
NTSB	National Transportation Safety Board
PHMSA	Pipeline and Hazardous Materials Safety Administration
RITA	Research and Innovative Technology Administration
SAE	Society of Automotive Engineers
SAFETEA-LU	Safe, Accountable, Flexible, Efficient Transportation Equity Act: A Legacy for Users (2005)
TCRP	Transit Cooperative Research Program
TEA-21	Transportation Equity Act for the 21st Century (1998)
TRB	Transportation Research Board
TSA	Transportation Security Administration
U.S.DOT	United States Department of Transportation